GEOPHYSICAL
T R A N S A C T I O N S
EÖTVÖS LORÁND GEOPHYSICAL INSTITUTE OF HUNGARY

CONTENTS

TARTALOMJEGYZÉK

Inverzió

Editorial Note

Most of the papers here were presented at the Second Workshop on Inversion organized by the Geophysics Department of the University of Miskolc, hold in June 2002 in honour of the 70th birthday of Professor Ferenc Steiner.

Analysis of inversion of secondary EM field obtained by 'casing-surface electrodes' source

Ernő TAKÁCS[*]

An electromagnetic field's secondary components are highly informative in the geological mapping of lateral changes. They are especially useful when certain components are missing from the primary field of the source and the anomalous — secondary — part of the field can be measured directly. Consequently it is also worth while — besides the possibility of indicating the lateral changes — to be concerned with the inversion of the secondary components, which means determining the subsurface charge-, or dipole-distribution linked with the inhomogeneities.

On the one hand the paper examines the peculiar influences that the charges and dipoles have in creating the secondary components; on the other hand, it tests by simulated data D. Patella's procedure elaborated originally for the inversion of SP data.

Keywords: electrical sounding, borehole casing electrode, electromagnetic field, secondary components, charge distribution, inversion

1. Introduction

Secondary electromagnetic fields caused by geological inhomogeneities are capable of perceptibly modifying the more stronger primary field of the source only at a rather large separation. Therefore considerable spacings are needed for deep prospecting. The situation is quite different when some components of the primary field are missing. In such a case the weak secondary field becomes measurable and will indicate deep inhomogeneities even at small separations [TAKÁCS, HARSTON 2000]. Consequently it is worth while to be concerned with the inversion of the secondary components.

This paper intends to outline a train of thought using examples gained by an excitation mode, whose primary field is peculiar. On the one hand we examine the roles of the charges and dipoles in creating the secondary

* University of Miskolc, Geophysics Department, H–3515 Miskolc–Egyetemváros
Manuscript received: 4 November, 2002.

components, on the other hand we test a possible inversion procedure by simulated data.

The selected method uses for current injection a steel borehole casing and surface electrodes circularly grounded around it. The principles of the geometric and frequency sounding with this kind of source were elaborated in the framework of OTKA (Hungarian Scientific Research Fund) Project 2383 beginning from 1990 [TAKÁCS et al. 1995]. Later the Domestic Research Division of the Hungarian Oil and Gas Company (MOL Rt) provided support to carry out experimental measurements and numerical simulation [TAKÁCS et al. 2001].

It is mentioned that instead of the casing a central surface electrode can also be used, as in the case of the vertical electric current transient sounding, which is based on the same principles [MOGILATOV, BALASKOV 1996].

The 'casing-surface electrodes' source can be regarded as a sequence of vertical electric dipoles (VED) connected in series. The primary field of such a source has at the surface only one component, namely the radial electric one [TAKÁCS 1995]. Along a radial profile the tangential electric EFI (perpendicular to the profile) and all of the magnetic components (radial HR, tangential HFI, vertical HZ) are caused solely by subsurface inhomogeneities. The primary currents are concentrated in much smaller volume compared with the traditional sources. Therefore this method is especially suitable for investigating local, 3-D structures. Because the casing injects current into the deeper horizons, too, the depth of investigation at a given separation is larger than in the case of traditional current-sources. At the same time the layering appears in the sounding curves unusually owing to the VED character of the 'casing-surface electrodes' configuration.

2. Origin and features of secondary components

The model presented in *Fig. 1* will be investigated several times. The lateral inhomogeneities are prisms elongated towards N–S. The lower one is a horst of the basement — with a height of 300 m, a width of 1000 m, a length of 1400 m — and its top is located at a depth of 1450 m. The upper prism is created by a local downward thickening of a layer of 300–350 m and covers the lower one. The casing penetrates the prisms asymmetrically.
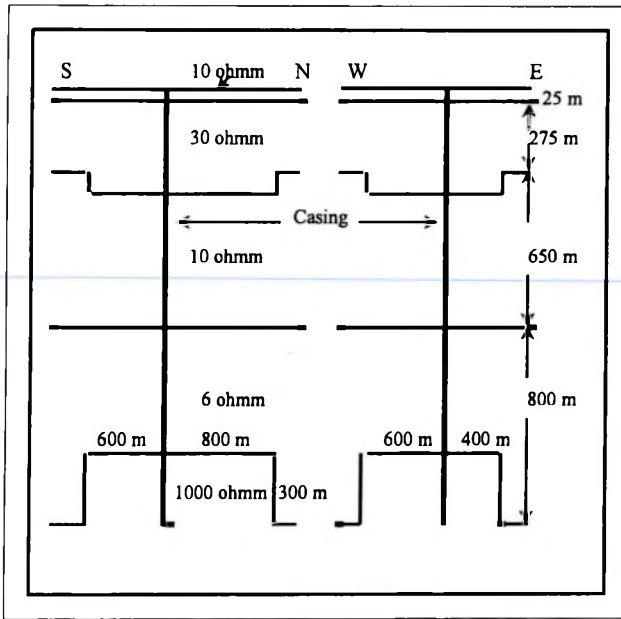
Fig. 1. Side view of 3-D inhomogeneity model penetrated by the casing

1. ábra. A béléscsővel harántolt laterális inhomogenitások modelljének oldalnézeti vetületei

Let us examine first the case when the horst of the basement is the only inhomogeneity. The current emitted from the casing accumulates electrical charge on the surface of the prism, as is seen in *Fig. 2*. Charges on the top and side faces are shown from above. This charge distribution can be substituted by point-sources distribution, which produces the secondary electric field components at the earth's surface. The maxima of the charge distribution can be found on the side faces where they are closest to the casing and on the top and bottom face around the casing. On the top and bottom faces the signs of the charges are opposite, they act against each other thereby reducing the effects of the horizontal planes.

Extreme values of the *secondary radial electric field* isolines reflect the horst contour rather well (*Fig. 3*). However, this component itself cannot be measured because it is superposed on the primary field of the source.
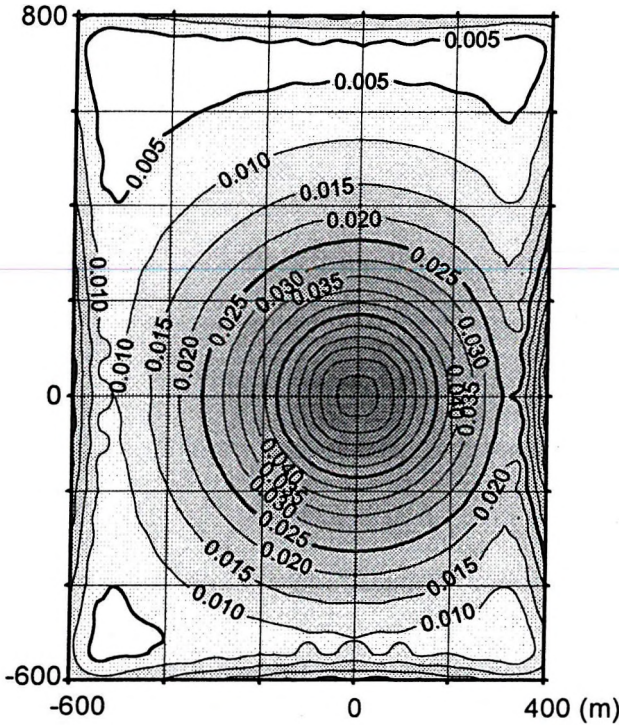
Fig. 2. 'Current intensity' distribution on the upper and side faces of the lower inhomogeneity in Fig. 1.

2. ábra. „Áramerősség" eloszlás az 1. ábra alsó inhomogenitásának felső és oldalsó lapjain

Fig. 3. Contour map of anomalous radial electric component caused by the lower inhomogeneity

3. ábra. Az alsó inhomogenitástól származó anomális radiális elektromos összetevő felszíni izovonalai
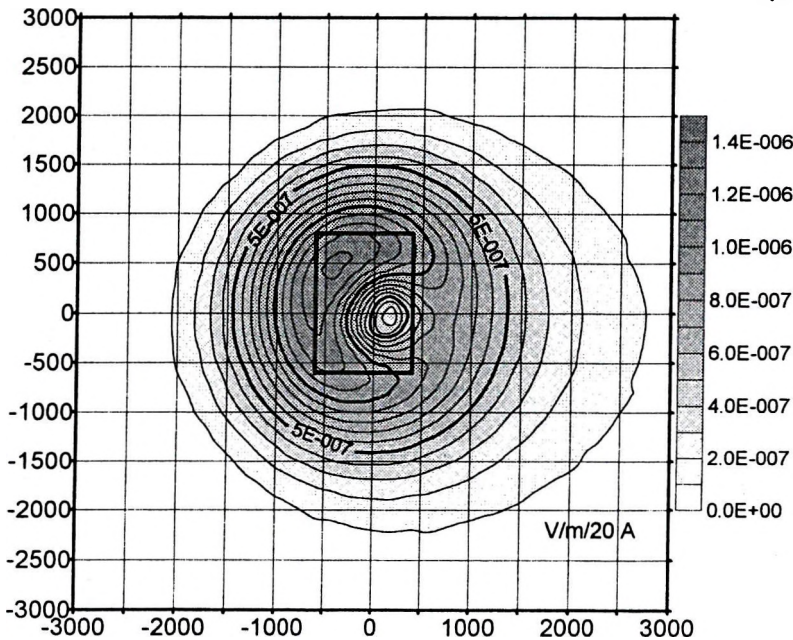
Apparent resistivities calculated from the total radial electric field — the sum of the primary and secondary fields — already reflect less clearly the shape of the inhomogeneity (*Fig. 4*). It should be noted that the resistive basement — in consequence of the VED behaviour of the source — will diminish the apparent resistivity until separation occurs. The nearly circular strip of the somewhat reduced apparent resistivity values at about 1600 m separation — ROA< 9.7 ohmm — appears outwards from the contour of the horst. Clear conclusions on the asymmetrical position and on the orientation of the horst can be drawn on the deformation of the isolines only at rather large separation.
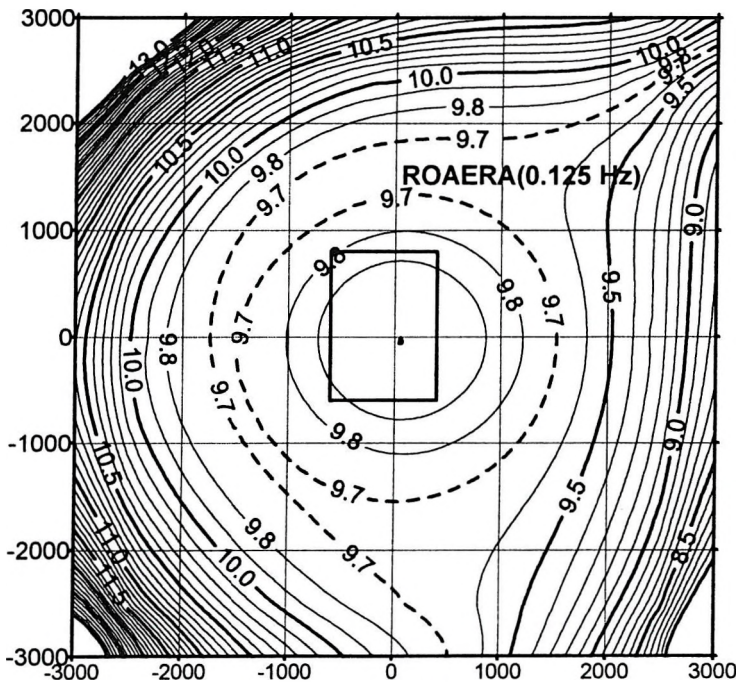
Fig. 4. Effect of lower inhomogeneity on the apparent resistivity contour map calculated from radial electric amplitude

4. ábra. Az alsó inhomogenitás hatása a radiális elektromos összetevőből számított látszólagos fajlagos ellenállás izovonalaira

The tangential electric component will appear only when the charge distribution has an asymmetry relating to the radial profile of the observation. Therefore on the contour map of its isolines — in *Fig. 5* — there is a sector with very small values which is in the east nearly perpen-
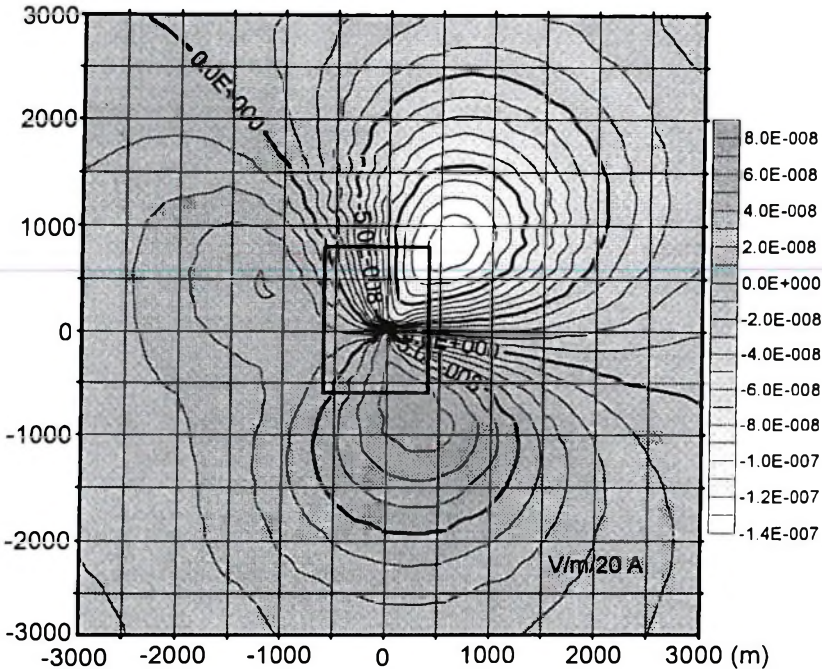
Fig. 5. Contour map of tangential electric amplitude caused by the lower inhomogeneity

5. ábra. Az alsó inhomogenitástól származó tangenciális elektromos összetevő felszíni izovonalai

dicular to the side face, where the charge values have their maximum. Extreme values are located very near to the eastern boundary of the horst. The sharp zone with minimum values — from where, looking towards the casing, there is a symmetry in the charge distribution — turns out to be a reliable indicator of a lineamentum near to the borehole. As a result of the asymmetrical position of the horst the minimum zone passes over it in a curved manner. The pattern of isolines looks like one over a horizontal dipole with a bent axis. It should be noted that the tangential electric component could not exist without lateral inhomogeneities and its source is exclusively the charge accumulation on the surface of the horst. Owing to that, if the current density at the depth of the inhomogeneity is strong enough, its presence can be detected at small separation, even in the vicinity of the source.

Secondary magnetic components are caused by currents flowing inside the inhomogeneity to maintain the charge distribution on its surface. These currents, in addition to the horizontal one, will have a vertical

component, too. However, the magnetic fields caused by the vertical currents vanish at the earth's surface [KAUFMAN 1992] consequently the secondary magnetic components observed at the earth's surface are caused only by the horizontal currents; in other words, by the multitude of horizontal electric dipoles distributed inside the inhomogeneity. *Figure 6* shows the momentum distribution of the horizontal electric dipoles inside the horst. The length of the arrows is proportional to the resultant momentum in the volume-element of 100 m x 100 m x 300 m. Because the 'casing-surface electrodes' source has no primary magnetic field component at the surface, the observed magnetic field components will be connected — based on their own individual behaviour — to the resultant current filament flowing along the minimum zone of the tangential electric field (Fig. 5). In *Fig. 7* the vertical magnetic field is given as an example.

stack(N,M)
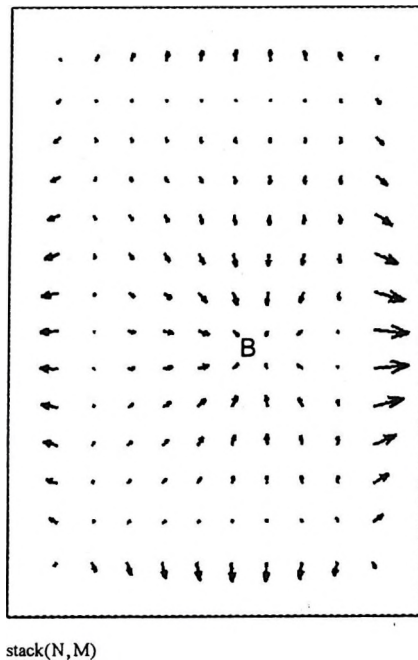
Fig. 6. Momentum distribution of horizontal electric dipoles inside the volume-elements of the lower inhomogeneity

*6. ábra.* A térfogatelemenkénti vízszintes elektromos dipólusok momentumainak eloszlása az alsó inhomogenitáson belül
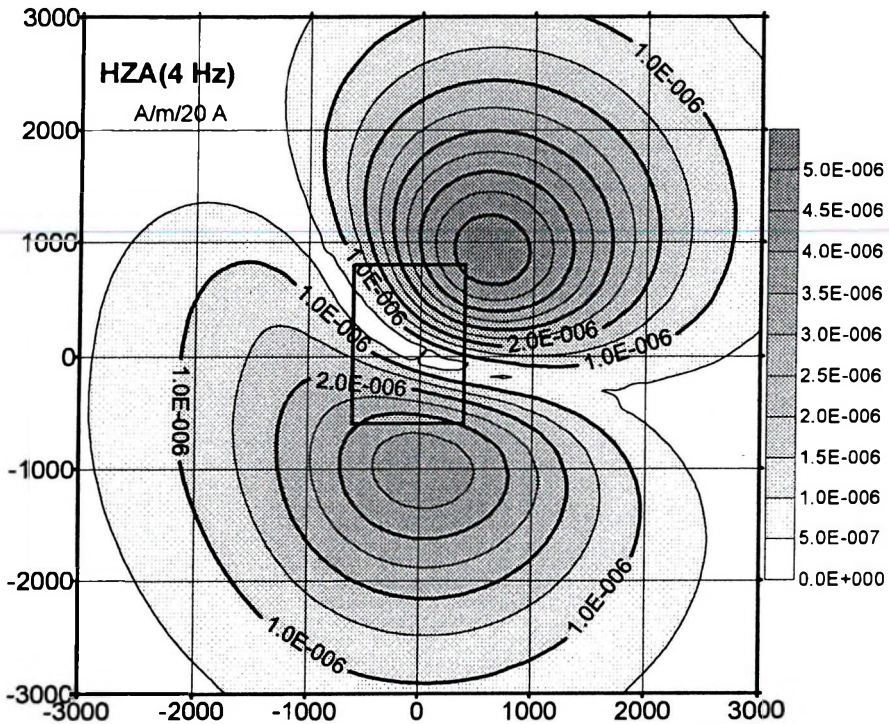
Fig. 7. Contour map of vertical magnetic amplitude caused by the lower inhomogeneity
7. ábra. Az alsó inhomogenitástól származó vertikális mágneses összetevő felszíni izovonalai

3. Role of subsurface horizontal electric dipoles in the inversion of the secondary components

Analysis of the secondary components has shown that

—in the inversion of the secondary electric components we have to determine the location of surface charges, or horizontal and vertical electric dipoles inside the inhomogeneities,

—in the inversion of the secondary magnetic components we have to determine the locations of horizontal electric dipoles inside the inhomogeneity.

We can conclude that the dominant effects on the secondary components are caused — in the case of prismatic inhomogeneities — by the extreme values of the charge, or dipole distribution on the nearest part

of the side walls to the casing (Figs. 2, 6). With the increase of the elongation this dominance will be more and more pronounced and the patterns due to a single horizontal electric dipole will appear. This means, however, that by inversion the depth can be deduced more reliably than the contour.

Taking into account the leading role of the horizontal electric dipoles in the creation of the secondary components, let us now consider the behaviour of their field components at the earth's surface. Tangential electric, tangential and vertical magnetic amplitude curves caused by a subsurface horizontal electric dipole — normalized to their own maximum — are shown in *Fig. 8* as a function of the 'separation/depth' quotient along a profile perpendicularly oriented to the dipole axis. Characteristic points can be selected — e.g. maximum, null-crossing, half value, etc. — for the depth estimation, which in my experience is quite reliable for a single inhomogeneity.

Inversion needs the solution of the direct problem. Simple expressions exist for calculating the stationary field components caused by the subsurface charges and dipoles in the uniform halfspace. After the men-
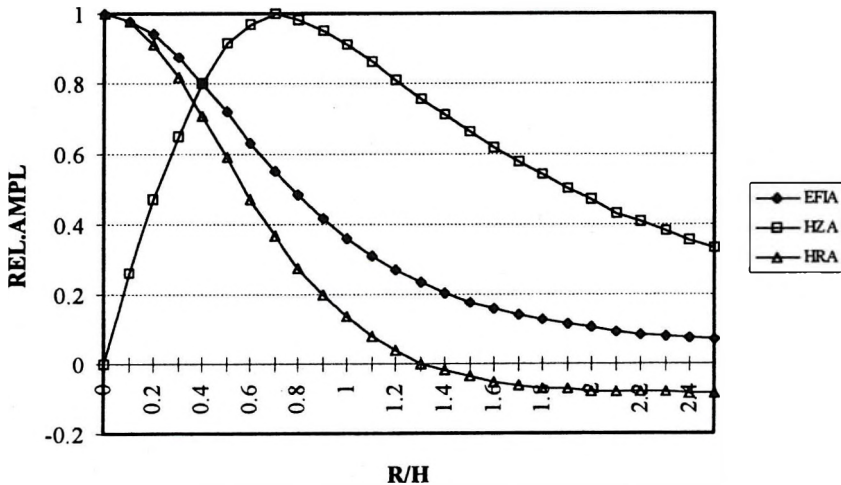
Fig. 8. Normalized to their maximum amplitude curves of the tangential electric (EFI), radial (HR) and vertical magnetic (HZ) components due to a buried electric dipole as a function of 'separation/depth' quotient

8. ábra. A mélybeli horizontális elektromos dipólus tangenciális elektromos (EFI), radiális (HR), és vertikális mágneses (HZ) térerősségének maximumukra normált értékei a felszíni, a dipólus irányára merőleges szelvényen a távolság és mélység hányadosának függvényében

tioned normalization, they contain only geometrical data. Equations of the electric field above layered earth are already rather complicated. At the same time, formulae of the stationary magnetic fields are independent of layering. Moreover, they remain valid up to a frequency limit. To get some information in this respect the position of the vertical magnetic field amplitude maximum was studied as a function of the 'conductivity × frequency' product for dipoles of different depth (*Fig'. 9*). We can see that at 2.5 Hz and at a dipole-depth of 1000 m the shift of the maximum is within 10 %. Theoretically, a correction is possible, too.
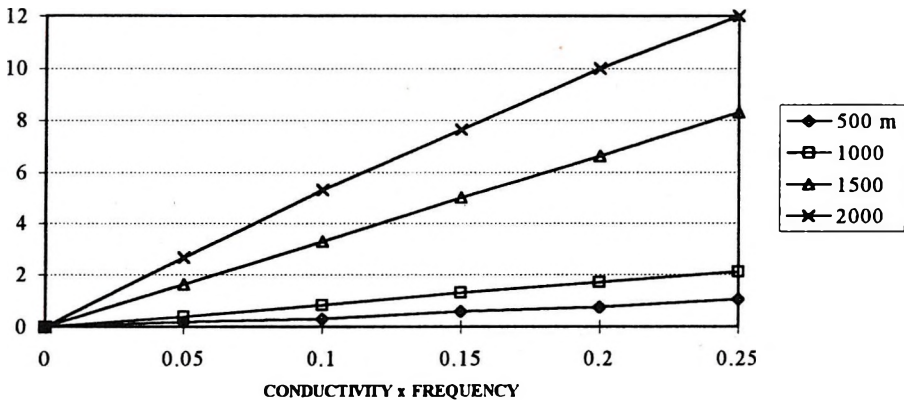
Fig. 9. Relative shift — caused by the frequency increase — of the vertical magnetic maxima due to a buried, horizontal direct current dipole and low frequency electric dipoles at different depths as a function of the conductivity × frequency product

9. ábra. A különböző mélységű felszin alatti, egyenáramú és kis frekvenciás, vízszintes elektromos dipólusok vertikális mágneses térerőssége maximumainak relatív eltolódása a frekvencia növekedése miatt a fajlagos vezetőképesség és a frekvencia szorzatának függvényében

4. Inversion attempt with Patella's method

It was mentioned above that the aim of the inversion of the secondary components is some kind of reconstruction of the subsurface electric charge-, or dipole-distribution. Inversion of the observed SP data has the same task. However, analogies could be found with the inversion procedures for gravity and magnetism, too.

For my first attempt I selected Patella's method [MAURIELLO et al. 1998, PATELLA 1997] elaborated initially for the inversion of SP data and later for DC vertical electric sounding. For simplicity my first attempt was

limited to a 2-D cross-cut inversion used for the synthetic data of the numerical simulation treated above. The selected SW–NE profile passes through the extreme values in the presence of both the upper and the lower inhomogeneity.

Patella's method consists of scanning the vertical section through the profile along the regular grid by a unit-strength charge, or dipole. For each point of the grid field-strength components are calculated to the obser-vation point of the profile. These calculated field data are cross-correlated with the observed values. Then, at each point of the grid charge or dipole occurrence, probability values are calculated from the cross-correlation data. Expressions for the steps of the inversion are shown in *Fig. 10*. The meanings of the symbols are as follows:

x — observation point coordinate along the profile,

x_q, h_q — coordinates of the continuously displaced unit source,

$E_x(x)$ — secondary radial *electric* field, or instead of it any observed field component,

$I_x(x_q, h_q)$ — scanning function depending on the type of source and the measured component, it contains only x_q, h_q coordinates,

C — normalization factor, which includes normalization by the total power of the field component recorded at the earth's surface,

$\eta(x_q, h_q)$ — charge , or dipole occurrence probability.

$$\eta(x_q, h_q) := C \cdot \int_{-\infty}^{\infty} E_x(x) \cdot I_x(x - x_q, h_q)\, dx$$

$$C := \left[\int_{-\infty}^{\infty} [E_x(x)]^2\, dx \cdot \int_{-\infty}^{-\infty} [I_x(x - x_q, h_q)]^2\, dx \right]^{-0.5}$$
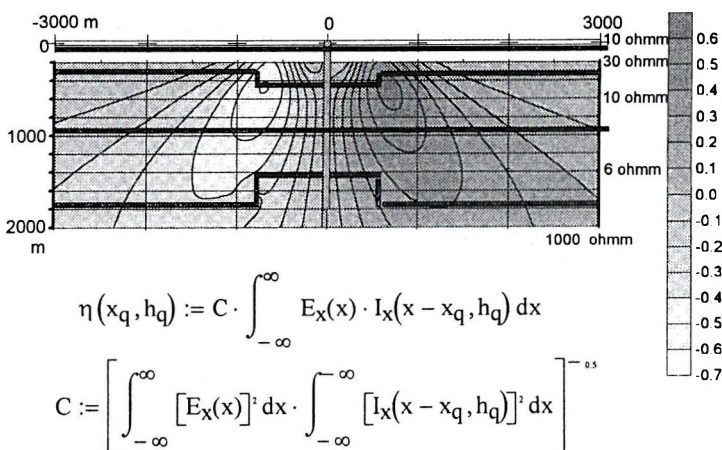
Fig. 10. Charge occurrence probability section calculated from anomalous radial electric amplitude along the SW–NE profile

10. ábra. Az anomális radiális elektromos térerősségből számított töltés-előfordulási valószinűség metszete a DNY–ÉK szelvényre

The complete set of calculated grid values of $\eta(x_q, h_q)$ is used to draw a contoured section in order to single out the zones of highest probability of concentration.

Figure 10 shows the result of the secondary radial electric field inversion. The location of the side walls of the upper prism are marked out quite well. The presence of the lower prism can only be guessed from the elongation of isolines downwards. The reason for this is that in the electric component — especially at small separation — the signal from the lower inhomogeneity is comparatively insignificant. However, the main problem with this component is rather the elimination of the primary field from the observed total field. Furthermore, in principle a scanning function valid for the layered section should have been used.

The situation is more favourable for magnetic components. In this case
—the primary field is missing at the earth's surface,
—stationary magnetic components do not depend on layering: this means scanning functions remain even in very simple expressions,
—the effect of inhomogeneities near to the surface is less dominant than in the electric field.

For example, the vertical magnetic component reflects the horst of the basement, as *Fig. 11* shows. The image is rather smoothed owing to the

Fig. 11. Horizontal electric dipole occurrence probability section calculated from the vertical magnetic amplitude due to the lower inhomogeneity along the SW–NE profile
11. ábra. A vertikális mágneses térerősségből számított dipólus-előfordulási valószinűség metszete az alsó inhomogenitás esetében a DNY–ÉK szelvény alatt

great depth, and it is shifted upwards. The upper and lower inhomogeneities have distinct indications in *Fig. 12*. The exact positions of the maxima along the vertical axis under the observation points are marked by triangles. Asymmetry between the eastern and western side becomes more accentuated. Above the side of larger extension of inhomogeneities — where the field strength is also larger — the superposition of effects gives rise to distortion in the position of the probability maximum. Omitting values at small separation between −600 and +600 m (where the effect of the upper inhomogeneity is the strongest) the result — marked by circles — will be somewhat better.

It is to be noted that 2-D inversion suffers from several ambiguities. Very characteristic patterns of the contour maps are not taken into account The real areal subsurface charge- or dipole-distribution — which is asymmetrical to the profile with dynamically changing strength and orientation — is substituted by dipoles perpendicular to the profile. Therefore, it is reasonable anyway to investigate the efficiency of the 3-D version.
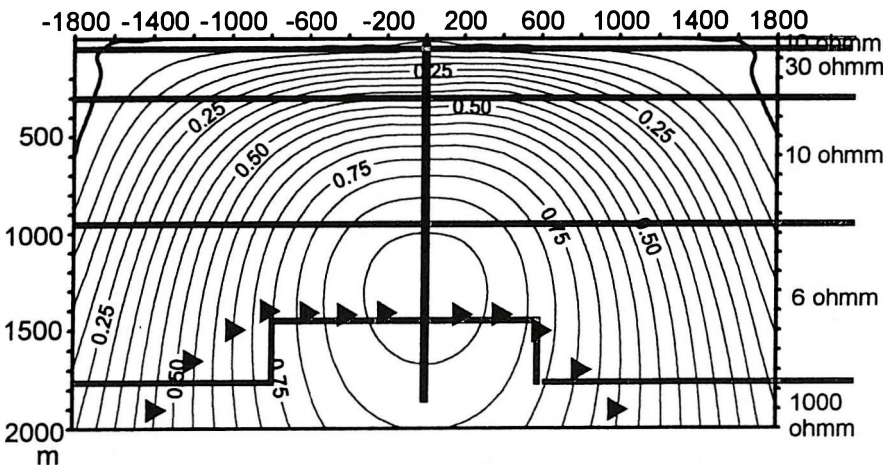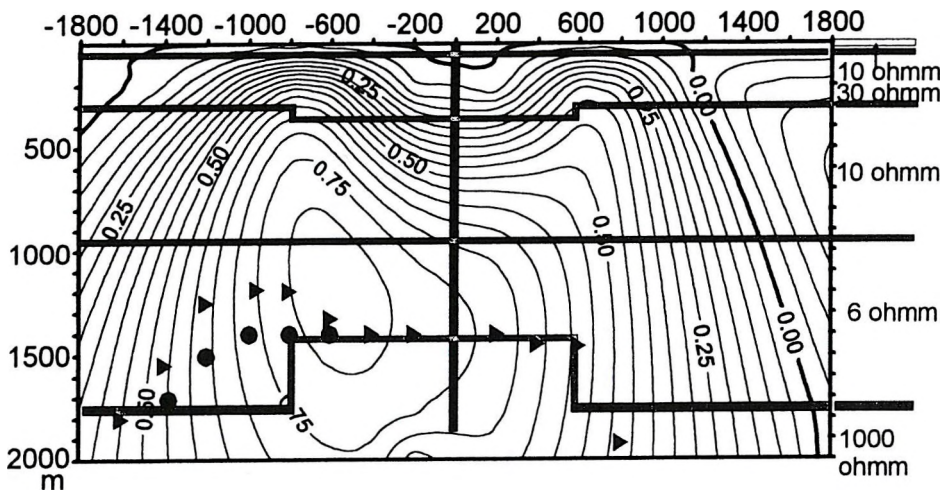

Fig. 12. Horizontal electric dipole occurrence probability section calculated from the vertical magnetic component due to the upper and lower inhomogeneities along the SW–NE profile

12. ábra. A vertikális mágneses térerősségből számított dipólus-előfordulási valószínűség a felső és alsó inhomogenitás esetére a DNY–ÉK szelvény alatt

5. Information gained by frequency sounding

Rather large separations are required to detect deep inhomogeneities by geometrical sounding. The resolving capability and reliability of the data gained by geometrical sounding will become worse with the increase of the separation and depth. Therefore I investigated what kind of information abundance can be gained by frequency sounding especially in the resolving capability of deep inhomogeneities at shorter separations.

Figure 13 shows a separation–frequency section of the vertical magnetic amplitude for the lower inhomogeneity along the N–E profile through the maximum. At each frequency a single, isolated maximum indicates the uplift of the basement. This maximum due to the eastern border of the horst grows and moves outwards as the frequency decreases, this means that the depth of the penetration increases. In this case — as was mentioned earlier — the depth of the inhomogeneity can be quite well estimated from the separation dependence of the stationary field strength.
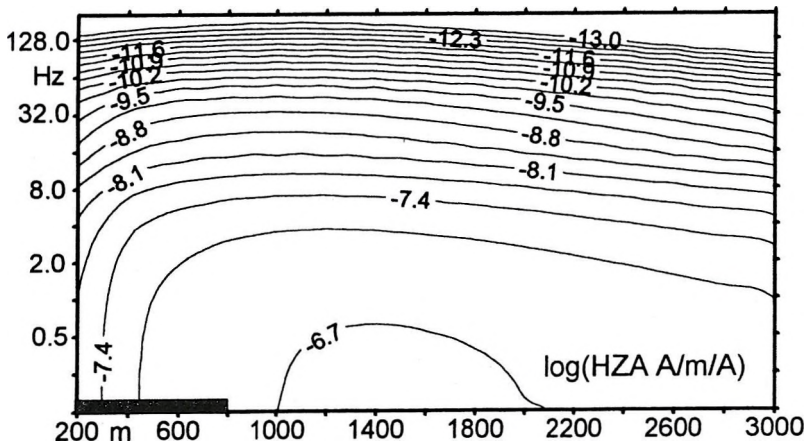
Fig. 13. Separation–frequency section of the vertical magnetic amplitude due to the lower inhomogeneity along the profile through the maxima in Fig. 7.

13. ábra. A vertikális mágneses térerősség távolság–frekvencia metszete az alsó inhomogenitás esetében a 7. ábra maximumain átmenő szelvényre

As far as the model with two inhomogeneities is concerned, we found that the superposition of the secondary fields generated by the two subsurface sources results in a rather surprising pattern (*Fig. 14*). The upper prism appears with a distinct maximum at 4–32 Hz. The field
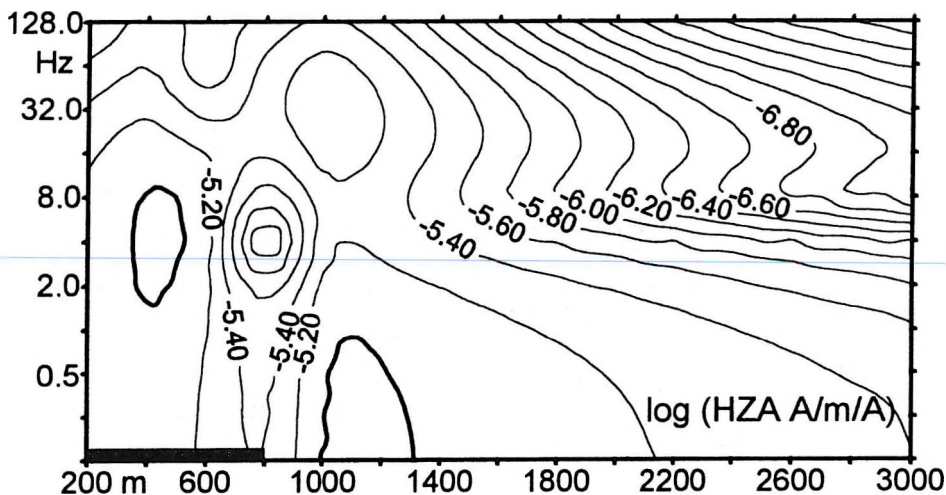
Fig. 14. Separation–frequency section of the vertical magnetic amplitude due to the upper and lower inhomogeneities along the profile through the maxima

14. ábra. A vertikális mágneses térerősség távolság–frekvencia metszete a felső és alsó inhomogenitás esetére a maximumokon átmenő szelvényen

strength has been increased significantly and its separation dependence — at least in the region close to the casing — is basically determined by the upper inhomogeneity. The lower inhomogeneity is indicated at 0.1– 0.5 Hz by a second, separated maximum. It is noteworthy that the frequency dependence of the amplitude shows, even at stations near to the casing, the presence of the two prisms. In the case of geometrical sounding the trend change — caused by the lower inhomogeneity in the separation dependence of the amplitude — would appear clearly only at much larger separations.

Moving outwards along the profile on the separation–frequency section — as well as in the frequency sounding curves (*Fig. 15*) — a well correlated sharp minimum zone takes shape — in the frequency-range 4–8 Hz — between the indications of the two prisms. To avoid false interpretation it is important to emphasize that this pattern of the separation–frequency section — and of the frequency sounding curves — of the secondary fields is caused by inhomogeneities in the vicinity of the casing and does not indicate local layering.

The sharp local extreme values and the surprising variability found in the frequency dependence of the secondary components hint at new
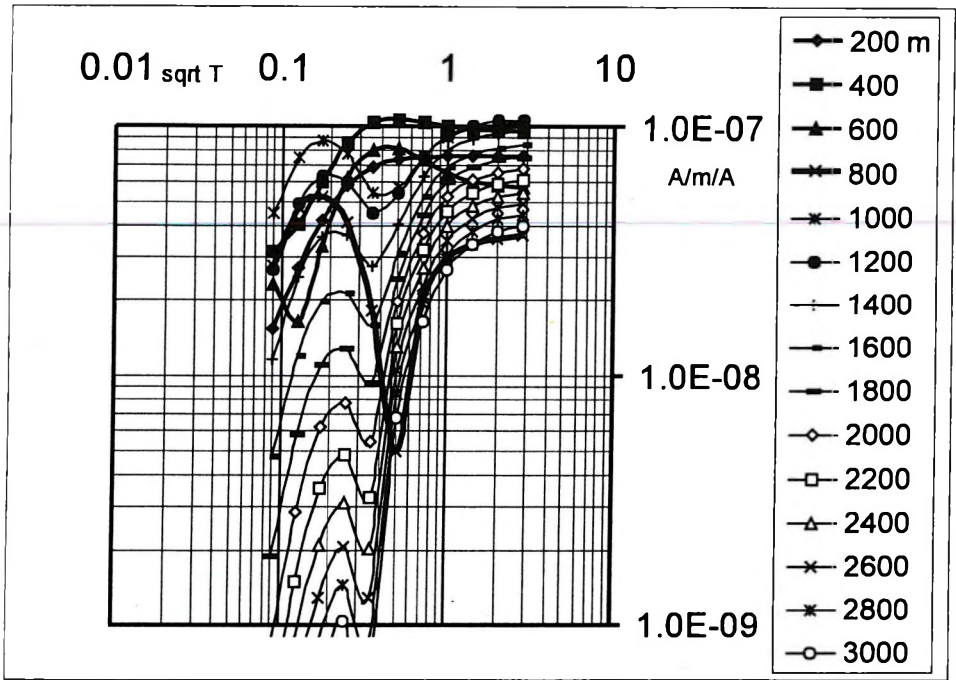
Fig. 15. Vertical magnetic amplitude frequency sounding curves along the profile through the maxima

15. ábra. A vertikális mágneses összetevő frekvencia-szondázási görbéi a maximumon átmenő szelvényen

possibilities in the lateral and vertical delineation of inhomogeneities. Besides, it seems quite reasonable that much shorter profiles are needed using frequency sounding than with the geometrical one. However, we have to add that there is a need for a thorough study of the features of the indications because they depend strongly on the shape of the inhomogeneity and on the orientation of the profile.

6. Conclusions

Based on the above analysis we can conclude that the secondary electromagnetic components have very characteristic, very dynamic and — for the interpretation — very useful indications of the lateral inhomogeneities. At the same time very detailed measurements are needed to

detect all their local peculiarities. Perfect inversion could be realised only by 3-D inversion taking into account the changeable areal distribution of the field-strength and the amount of data.

*

The paper was read at the 3rd Inversion Seminar in 2002. My intention was to use it as a means of greeting Professor Dr. Ferenc Steiner on his 70th birthday, motivated by our nearly 50-years' friendship and common work.

Acknowledgements

REFERENCES

KAUFMAN A. A. 1992: Geophysical Field Theory and Method, Part A, Academic Press, 459 p.
MAURIELLO P., MONNA D., PATELLA D. 1998: 3-D geoelectric tomography and archeological applications. Geophysical Prospecting 46, pp. 543–570
MOGILATOV V., BALASKOV D. 1996: A new method of geoelectrical prospecting by vertical electric current soundings. Journal of Applied Geophysics 36, pp. 31–44
PATELLA D. 1997: Introduction to ground surface self-potential tomography. Geophysical Prospecting 45, pp. 653–681
TAKÁCS E., SZARKA L., VARGA M. 1995: Vertical steel casing as a monopole transmitter antenna for electromagnetic prospecting. Magyar Geofizika 36, OKA különszám, pp. 60–64
TAKÁCS E. 1995: The normal surface electric field of an E-field excited steel-casing. Acta Geodaet., Geophys. Hung. 30, pp. 331–341
TAKÁCS E., HARSTON G. 2000: Three-dimensional inhomogeneity indications in the secondary components of the electromagnetic field generated by the steel-casing electrode. Magyar Geofizika 41, 3, pp. 108–114
TAKÁCS E., NAGY Z., FERENCZY L. 2001: Experiences obtained with the first use of the frequency sounding by casing pipe excitation. Geosciences, Publ. of the Univ.of Miskolc, Ser.A, Mining 59, pp. 153–190

Az anomális elektromágneses összetevők inverziós szempontú elemzése

TAKÁCS Ernő

A laterális földtani változások határvonalának felderítéséhez az elektromágneses tér anomális komponensei kedvező sajátságúak. Ez a tény különösen akkor hasnzálható ki, ha a tér forrásának primér térerősségében hiányzik valamelyik összetevő és így a megfelelő anomális komponens közvetlenül mérhető. Emiatt a határvonalak indikálásának lehetőségén túllépve érdemes az anomális összetevők inverziójával foglalkozni, ami forrásuk — a hozzájuk kötődő elektromos töltések, illetve dipólusok — felszín alatti eloszlásának meghatározását jelenti.

A tanulmány egyrészt azt vizsgálja, hogy a töltéseknek és dipólusoknak milyen eltérő sajátságai vannak az anomális elektromos és mágneses komponensek létrehozásában. Másrészt szimulált adatokon teszteli Patellának eredetileg a természetes potenciál adatok inverziójára kidolgozott eljárását.

ABOUT THE AUTHOR

Ernő Takács (1927) graduated from the Technical University of Heavy Industry — Sopron/Miskolc — as a mining engineer specialized in prospecting. In 1951 he joined the Department of Geophysics that had been founded that year. He was head of the Department from 1983 to 1991. He is now a professor emeritus. During the years 1956–59 he worked as telluric party-chief of the Chinese–Hungarian Geophysical Expedition.

His main scientific interest is in the development of electromagnetic methods. He was a pioneer in introducing tellurics, magnetotellurics, and several modifications of dipole frequency sounding in Hungary. He is honorary member of the Association of Hungarian Geophysicists and served two terms as chairman of the Scientific Committee of Geophysics of the Hungarian Academy of Sciences.

Homoeopathic method to increase the accuracy of inversion results

Ferenc STEINER[*]

The basic principle of the surplus-error method is given and its effectiveness is demonstrated on the basis of a microgravimetric example.

The algorithm presented below supposes that an adequate model is given for inversion.

The basic principle of the method of surplus errors may be explained as follows: *If a surplus error series of considerable number is superposed on the measured data, even though in each case the increase in the error of the model parameters is likely, it may be that the medians of the model parameters (or the median of medians after some kind of reasonable grouping of the parameters) are significantly more accurate than the results of direct inversion based on the original measured data.*

A comprehensive example is given in STEINER [2002] for the application and for the possible effectiveness of the surplus-error method. The 2-D model given below was defined by 6 parameters: two horizontal cylinder-shaped cavities of unknown depth, diameter and horizontal position. The actual values for the two cavities were: depth — 7.5 m and 6.5 m; diameters — 3 m and 3 m; horizontal position — 5 m and 13 m. Along the profile exactly calculated 19 g_i gravimetric values with error of statistical type using $S = 4$ as parameter of scale were superposed as the semi-intersextile range Q equals 2.2 µGal in this case (see STEINER [1990] page 52 for $a=5$ which defines the statistical probability distribution), the scatter amounts to 2.8 µGal in full accordance with the well known fact that the er-

[*] University of Miskolc, Geophysics Department, H–3515 Miskolc–Egyetemváros
Manuscript received: 4 November, 2002.

ror of microgravimetric measurements cannot be less than 2–3 μGal. The chosen type was based on DUTTER [1986–87]: the occurrence of such a type is most probable in geostatistics.

Denoted by h_i the random numbers obtained according to the above mentioned way, regarding them as 'natural errors', the 'measured' values can be calculated obviously as $g_i^{measured} = g_i + h_i$ ($I = 0, 1, \ldots. 18$).

Inversion needs to determine the six model parameter values on the basis of these 19 measured data. Aptly, the P-norm of the deviations (see STEINER (ed) [1997] p. 20.) can be chosen to minimize the deviations because this procedure gives, with sufficient accuracy, the S parameter of scale, too, which — in practice — is not a priori known. This S-value of the measuring ('natural') error is chosen as the S-value of the surplus errors, too.

In STEINER [2002], 21 surplus-error series were superimposed 21 times on the measured microgravimetric values; for all six model parameters the median of the 21 medians was accepted (i.e. 441 inversions were carried out).

Was this amount of calculation really worth while? The answer is given in STEINER [2002]: 'Yes' in all ten investigated cases (see the comprehensive Tables for all six model parameters in the cited article). Here, however, a much shorter way should be used.

The points in *Fig. 1* correspond to the $g_i^{measured}$ values. The thin line demonstrates the direct P-fitting results, the thick line corresponds to the six parameter-values which were obtained after the above-mentioned procedure (with 441 inversions). The fitting quality of both curves seems to be (judged on the face of it) quite the same — the chief meaning of these parameter values, however, is not in the fitting of the measured values, but in the final definition of the investigated model as model parameters. The two thin line circles in Fig. 1 correspond to one single inversion; they are fully unacceptable in relation to the true situation (see the data after the formulation of the basic principle: e.g. both true diameters are the same). On the other hand, the model obtained using the surplus-error method (these circles are drawn by thick lines in Fig. 1), is near to the true case.

It seems to be necessary to characterize quantitatively the model distances (instead of using the qualitative expressions 'near' or 'far'). In our case the following formula should be used as the 'relative model distance':
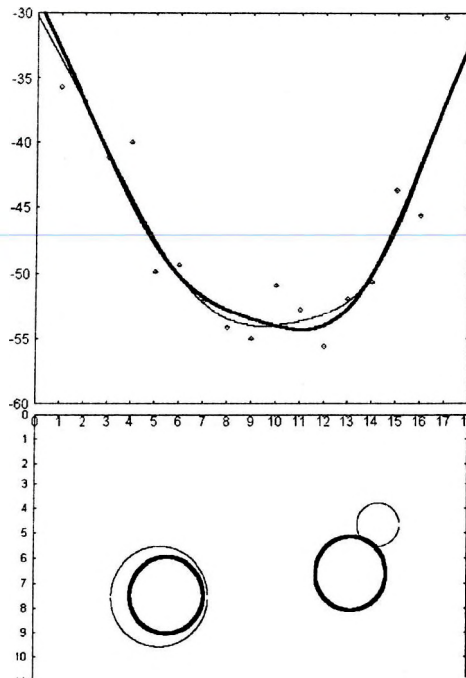
Fig. 1. Two thin line circles show that the results of one single step of inversion based on the measured points may be fully unacceptable whereas both thick line circles — which are the results of the surplus-error method — are acceptably near to the true model (see the true values of the model parameters after the formulation of the basic principle)

1. ábra. A mérési pontok alapján végrehajtott egyetlen inverziós lépés a két, vékony vonallal rajzolt körkeresztmetszetre vezet, amely teljesen elfogadhatatlan eredmény. Ezzel szemben a többlethiba-módszer a vastag vonallal rajzolt köröket szolgáltatja, amelyeknek adatai a (módszerdefiníció után számszerűen megadott) helyes értékekhez nagyon közel állnak

$$\delta = 100 \cdot \sqrt{\frac{1}{6} \sum_{j=1}^{6} \left(\frac{p_j^{calculated} - p_j^{true}}{p_j^{true}} \right)^2}$$

If one single inversion is carried out, δ is denoted by δ_0; on the other hand, if the six $p_j^{calculated}$ model parameters are the results of the surplus-error method, the model-distance is denoted by $\delta_{surplus}$. The cases in Fig. 1 result in the values $\delta_0 = 34.4\%$ and $\delta_{surplus} = 5.2\%$. The latter value as

δ_0 could be achieved only if the error of the microgravimetric values would be 0.4–0.6 μGals; this is, however, in the near (or even in the predictable) future not realizable.

One single example is perhaps not convincing enough (although in STEINER [2002] ten examples were comprehensively investigated) and the question arises, too, whether really many hundreds of inversions are needed to achieve a significant decrease in the relative model distance.

In HAJAGOS and STEINER [2003] one hundred 'natural' error-series of statistical type were generated (otherwise speaking: 100 measured data sets were given) but only 5 surplus-error sets were superimposed on each measured data set and 6 medians of the model parameters determined. The whole procedure was repeated 9 times and finally the median of the 9 medians was accepted for all six model parameters as a result of the surplus-error method (i.e. only 45 inversions were carried out for all 100 cases). Calculating both $\delta_{surplus}$ and δ_0 for all hundred cases, the values of $\delta_{surplus}$ and also those of $\delta_{surplus}$ were ordered, consequently 'empirical distribution functions' could be constructed for both types of model distances. *Figure 2* shows these functions, demonstrating that 45 surplus-error superpositions and inversions are enough to halve the δ_0 model distances which belong to one single inversion.
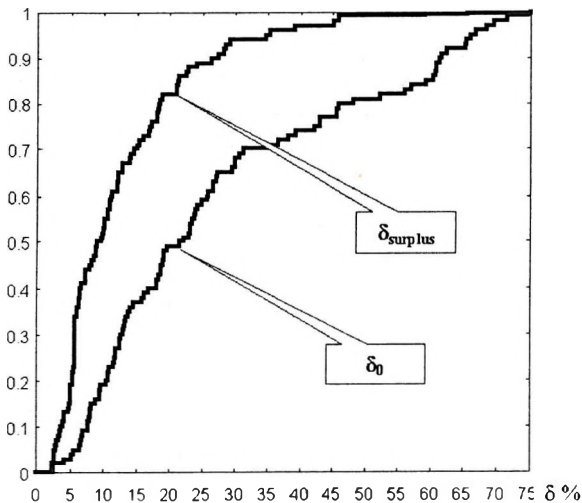
Fig. 2. Empirical distribution functions of model distances from the true situation of two kinds: δ_0 concerns the results of one single inversion step, $\delta_{surplus}$ concerns the results of the surplus-error method using 45 superpositions. The natural error was of statistical type

2. ábra. A valódi hatótól mért kétféle modelltávolság empirikus eloszlásfüggvényei: δ_0 az egyetlen inverziós lépéssel, $\delta_{surplus}$ a 45 szuperpozíciót alkalmazó többlethiba-módszerrel adódó eredményekre vonatkozik. A természetes hiba statisztikus típusú volt mind a száz esetben
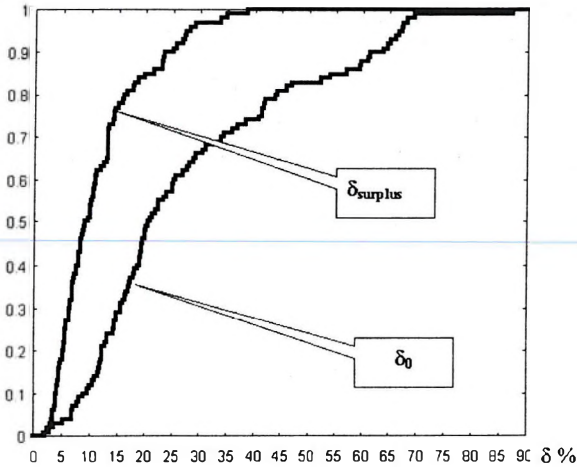
Fig. 3. Empirical distribution functions of model distances from the true situation of two kinds: δ_0 concerns the results of one single inversion step, $\delta_{surplus}$ concerns the results of the surplus-error method using 45 superpositions. The natural error was of Laplace type

3. ábra. A valódi hatótól mért kétféle modelltávolság empirikus eloszlásfüggvényei: δ_0 az egyetlen inverziós lépéssel, $\delta_{surplus}$ a 45 szuperpozíciót alkalmazó többlethiba-módszerrel adódó eredményekre vonatkozik. A természetes hiba Laplace típusú volt mind a száz esetben

Similar halving is shown in *Fig. 3* although the natural errors here are of Laplace type (but are characterized naturally by the same semi-intersextile range of $Q=2.2$), consequently it seems that the procedure is insensitive to the 'natural' error-types. Even if the natural error is of Cauchy-type and characterized by $Q=2.2$ (see *Fig. 4*), the $\delta_{surplus}$-curve hardly differs from the $\delta_{surplus}$-curves of Figs. 2 and 3. In contrast, the δ_0-curve of Fig. 4 is more elongated than the δ_0-curves in Figs. 2 and 3.
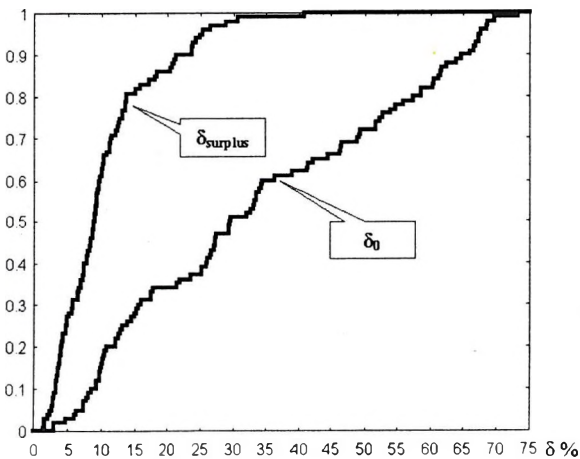
Fig. 4. Empirical distribution functions of model distances from the true situation of two kinds: δ_0 concerns the results of one single inversion step, $\delta_{surplus}$ concerns the results of the surplus-error method using 45 superpositions. The natural error was of Cauchy type

4. ábra. A valódi hatótól mért kétféle modelltávolság empirikus eloszlásfüggvényei: δ_0 az egyetlen inverziós lépéssel, $\delta_{surplus}$ a 45 szuperpozíciót alkalmazó többlethiba-módszerrel adódó eredményekre vonatkozik. A természetes hiba Cauchy típusú volt mind a száz esetben

Even so, it should be recalled that TARANTOLA [1987] mentioned that the Cauchy-type ab ovo contains some amount of outliers and this circumstance can cause this elongation of the δ_0-curve. It seems (astonishingly enough) that the surplus-error procedure is able to eliminate this effect, too: see once more the similarity of the three $\delta_{surplus}$-curves in Figs 2, 3, and 4.

REFERENCES

DUTTER R. 1986–87: Mathematische Methoden in der Montangeologie. Vorlesungsnotizen, Manuscript, Leoben

HAJAGOS B., STEINER F. 2003: War against error using the method of surplus errors. Acta Geod., Geoph. Acad. Sci. Hung. **38**, 4

STEINER F. 1990: Introduction to Geostatistics (in Hungarian). Tankönyvkiadó, Budapest, 357 p

STEINER F. (ed.) 1997: Optimum Methods in Statistics. Akadémiai Kiadó, Budapest, 370 p.

STEINER F. 2002: Decrease in the error of information yielded by measured data from the method of 'surplus errors' (in Hungarian). Magyar Geofizika, **43**, 2

TARANTOLA A. 1987: Inverse problem theory. Elsevier, Amsterdam 613 p.

Homeopatikus módszer az inverzió eredményeinek pontosítására

STEINER Ferenc

A dolgozat megadja a többlethiba-módszer alapelvét, hatékonyságát pedig egy mikrogravitációs példán mutatja be.

ABOUT THE AUTHOR

Ferenc Steiner was born in 1932; he received his diploma in physics in 1954 at the University of Science in Szeged. He started teaching and scientific work in 1954 and has continued this till now at the Geophysics Department of the University of Miskolc. He was qualified as D.Sc. in 1975 (awarded by the Hungarian Academy of Sciences). He is a member of the Editorial Board of Acta Geod. Geophys. Mont. Acad. Sci. Hung., and a member of the Scientific Commission for Geophysics of the Hungarian Academy of Sciences. The author is an Academic Prize winner and his award of the silver medallion of the President of the Hungarian Republic was personally presented by Á. Göncz in 1999. In 2001 he was elected an honorary member of the Association of Hungarian Geophysicists.

Applicability of Poisson's relation to gravity and vertical magnetic anomalies

Károly KIS[*], Géza WITTMANN[**]

Poisson's relation expresses the general link between gravity and magnetic anomalies. The applicability of this relation is investigated by means of eight Hungarian field examples. The Bouguer and vertical magnetic anomalies of the eight prospecting areas are digitized at the same point with a sampling interval of 1 km. Poisson's relation can be written in the form of a linear inverse problem which requires determination of the derivatives with respect to the variables x, y, and z of the Bouguer anomalies. The inverse problem is solved using an iterative procedure. The result of this procedure is the magnetization vector (i.e. its declination and inclination) of the anomaly source. The vertical magnetic anomalies can be reduced to the pole if the declination and inclination are known. Theoretically the vertical magnetic anomalies reduced to the pole are correlated to the derivative with respect to variable z of the Bouguer anomalies. The correlation coefficient may be taken as the measure of applicability of Poisson's relation. In that two prospecting areas show a higher correlation coefficient, they can be regarded as cases where Poisson's relation can be applied.

Keywords: gravity anomalies, magnetic anomalies, Poisson's relation, inverse problem, dihesion

1. Poisson's relation

Poisson's relation links gravitational potential V and magnetic scalar potential W in the 3-D Cartesian coordinate system, and is given by

$$W(x,y,z)=\frac{\mu_0}{4\pi G}\frac{\mathbf{J}}{\rho}\frac{\partial}{\partial s}V(x,y,z) \quad ,$$

(1)

where μ_0 is the permeability of a vacuum, G is Newton's gravitational constant, $\mathbf{J}$ and ρ are uniform magnetization and density of the 3-D source, respectively [BLAKELY 1995]. The direction of uniform magnetization is

* Research Group of Geophysics and Environmental Physics of the Hungarian Academy of Sciences, H–1117 Budapest Pázmány Péter sétány 1/C.
** MOL Hungarian Oil and Gas Co. Geophysical Operations H–1039 Budapest Batthyány u. 45.

given by unit vector **s**. A direction derivative in the previous equation can be expressed as

$$\frac{\partial}{\partial s} = \mathbf{i}\, L \frac{\partial}{\partial x} + \mathbf{j}\, M \frac{\partial}{\partial y} + \mathbf{k}\, N \frac{\partial}{\partial z}\,, \qquad (2)$$

where **i**, **j**, and **k** are unit vectors along the x, y, and z axes; L, M, and N are the direction cosines, given by the equations: $L = \cos\alpha \cos\beta$, $M = \cos\alpha \sin\beta$, $N = \sin\alpha$; α is the magnetic inclination, and β is the magnetic declination of magnetization if the x-axis and the y-axis are respectively directed north and east, and the z-axis points vertically downward. The direction of magnetization is the resultant of the remanent and induced magnetization. Induced magnetization is generally well known, and its amplitude can be determined if the susceptibility of the sources is also known — though this information is generally not available.

It should be emphasized that Poisson's relation is valid if the boundaries of the gravitational and magnetic sources are the same and the magnetization and density are uniform [BLAKELY 1995]. These strict conditions will be investigated in terms of the applicability of the Poisson's relation to further calculations.

Poisson's relation will be applied to the vertical magnetic anomaly field Z; that is: the derivative of equation (1) with respect to variable z. From this it follows that

$$Z = \frac{\mu_0}{4\pi G}\left(\frac{J}{\rho} L \frac{\partial}{\partial x} g_z + \frac{J}{\rho} M \frac{\partial}{\partial y} g_z + \frac{J}{\rho} N \frac{\partial}{\partial z} g_z \right), \qquad (3)$$

where g_z is the vertical component of gravity. Vertical magnetic anomaly field Z and the derivatives of the vertical component of gravity with respect to variables x, y, and z are determined at the same point, respectively. The new variables p_1, p_2, and p_3 respectively indicate the x, y, and z components of the $\mathbf{J}/\rho$ vector,. They are

$$p_1 = \frac{J}{\rho} L, \quad p_2 = \frac{J}{\rho} M, \quad p_3 = \frac{J}{\rho} N, \qquad (4)$$

and the constant $\mu_0/4\pi G$ will be indicated by C. The derivatives in equation (3), determined numerically at the identical point to the vertical magnetic anomalies are indicated by the subscripts x, y, and z. The method for

determining the derivatives will be discussed elsewhere. In this way we obtain

$$Z = C\left(p_1 g_{zx} + p_2 g_{zy} + p_3 g_{zz}\right)$$ (5)

The variables J/ρ, α, and β can be expressed by the formulae

$$J/\rho = \left(p_1^2 + p_2^2 + p_3^2\right)^{1/2}, \quad \alpha = \sin^{-1}\frac{p_3}{J/\rho}, \quad \beta = \tan^{-1}\frac{p_2}{p_1}.$$ (6)

The parameters p_1, p_2, and p_3 will be determined by solving a weighted linear inverse problem. If the conditions included in the Poisson's relation are valid, the values for α and β can be used to reduce the vertical magnetic anomalies to the magnetic pole.

Poisson's relation can be utilized for the joint interpretation of the gravity and magnetic anomalies if the necessary conditions apply.

KANSEWICH and AGARWAL [1970] applied Poisson's relation to obtain a combined analysis of gravity and magnetic anomalies. One of their results was the distribution of the ratio J/ρ for the prospecting area, and they analysed the wavelength of the J/ρ ratio. In addition to the coherency of the observed magnetic data reduced to the pole, the theoretically calculated field using gravity data was determined. The high coherency wavelength of J/ρ was an indication that the magnetic and gravity anomalies are probably from the same rock units.

WILSON [1970] showed that the ratio of the magnetization and density, and the direction of magnetization were required for the interpretation when anomalies arise from different sources. When the magnetization and density are not uniform, the source can be regarded as results for anomalies from different sources, but a knowledge of rock properties helps the successful interpretation of these anomalies.

Poisson's relation was also used by CORDELL and TAYLOR [1971] for the joint interpretation of gravity and magnetic anomalies of the North Atlantic Gilliss seamount. The position of the Cretaceous virtual magnetic pole was also determined from the magnetic direction obtained from their calculations.

In order to separate the individual anomalies CHANDLER et al. [1981] applied a moving-window. Their intention was to avoid interference from the neighbouring anomalies. A linear regression of the anomalies reduced to the pole, and the vertical gradient of the Bouguer anomalies are

determined. Distribution of the J/ρ ratio was obtained from the linear regression.

2. Linear inverse problem

The general solution of the overdetermined linear inverse problem is widely discussed [e.g. by MENKE 1989, HJELT 1992]. The general equation for the weighted least squares case is

$$\Delta p^{est} = \left[A^T W_e A\right]^{-1} A^T W_e d,\tag{7}$$

where Δp^{est} is the estimated model parameter vector; matrix A is called the data kernel; matrix W_e defines the weighting matrix; d is the measured data vector. Superscript T represents the transpose. Model parameters are represented by a vector Δp which is of length m; n measured data are available, they are the elements of vector d of length n. In this way, matrix A has n rows and m columns, matrix W has the dimension $n \times n$. Equation (7) will be specialized for the processed problem later.

3. Application of the linear inverse problem

If the parameters are to be determined by solving a linear inverse problem; it requires the linearizing of equation (3). Linearizing can be done by expanding equation (3) using Taylor's theorem as follows

$$Z(p_1, p_2, p_3) \approx Z(p_{10}, p_{20}, p_{30}) + \frac{\partial Z}{\partial p_1}\Delta p_1 + \frac{\partial Z}{\partial p_2}\Delta p_2 + \frac{\partial Z}{\partial p_3}\Delta p_3,\tag{8}$$

where the second and higher orders of the expansion are ignored [AL–CHALABI 1970, MENKE 1998].

If n data are available the parameter vector $p(p_1, p_2, p_3)$ will be determined from the solution of an extremum problem:

$$\Phi = \sum_{i=1}^{n}\left(Z_i^{measured} - \left(Z_i(p_{10}, p_{20}, p_{30}) + \frac{\partial Z_i}{\partial p_1}\Delta p_1 + \frac{\partial Z_i}{\partial p_2}\Delta p_2 + \frac{\partial Z_i}{\partial p_3}\Delta p_3\right)\right)^2 = min.$$

$$\tag{9}$$

The above least squares minimum problem will be solved by an iterative procedure. In equation (9), p_{10}, p_{20}, and p_{30} offer an initial estimate of the parameters.

The present application of the weighted linear inverse problem requires the specialization of the variables given in equation (7). As previously discussed, vector Δp has three elements. Matrix A has n rows (number of measurements) and m columns (number of parameters, in the present case $m=3$); its elements are given by the equations

$$a_{i1} = \frac{\partial Z_i}{\partial p_1} = C g_{zxi}, \quad a_{i2} = \frac{\partial Z_i}{\partial p_2} = C g_{zyi}, \quad \text{and} \quad a_{i3} = \frac{\partial Z_i}{\partial p_3} = C g_{zzi}, \quad (10)$$

where $i=1,\ldots,n$. Vector d has n elements, its ith element is as follows,

$$d_i = Z_i^{measured} - Z_i(p_1, p_2, p_3). \tag{11}$$

The elements of parameter vector p will be determined by an iterative procedure, and each step of the iteration is indicated by k, where $k=0,1,\ldots,$ K. This means that the linear inverse problem will be solved K times. An initial value means the 0th step of the iteration. In this way the elements of matrix A and the elements of vector d are determined for p_{1k}, p_{2k}, and p_{3k} ($k=0$ for the initial guess of the parameters), $Z_i(p_{1k}, p_{2k}, p_{3k})$ is determined by utilizing equation (8), where subscript I indicates the ith measurements of Z, g_{zx}, g_{zy}, and g_{zz}. The solution of the linear inverse problem gives Δp_{10}, Δp_{20}, and Δp_{30} for the 0th step. The parameter values will be given by the sum of the vector components $p_{10} + \Delta p_{10}$, $p_{20} + \Delta p_{20}$, and $p_{30} + \Delta p_{30}$.

In general, for the kth iterative step the parameters are determined by $p_{1k}=p_{1\ k-1}+\Delta p_{1\ k-1}$, $p_{2k}=p_{2\ k-1}+\Delta p_{2\ k-1}$, and $p_{3k}=p_{3\ k-1}+\Delta p_{3\ k-1}$ ($k \neq 0$). Termination of the iterative process is when the sum of $\Delta p^2_{1k}+ \Delta p^2_{2k}+ \Delta p^2_{3k}$ is less than a given limit. The values of J/ρ, α, and β are determined by equation (6).

4. Weight matrix W of the linear inversion

Weight matrix W is a diagonal matrix in the present case. These elements of matrix W will be determined by the procedure suggested by STEINER [1988, 1990]. Diagonal elements w_{ii} are determined by

$$w_{ii} = \frac{\varepsilon_k^2}{\varepsilon_k^2 + l_i^2}, \tag{12}$$

where

$$l_i = Z_i - C\left(p_{1i}g_{zxi} + p_{2i}g_{zyi} + p_{3i}g_{zzi}\right) \qquad (13)$$

and $i=1,\ldots,n$. ε_k means the dihesion (initiated by STEINER [1988, 1990]), subscript k indicates the kth iterative step. Dihesion is also determined in an iterative way: it is calculated by

$$\varepsilon_k^2 = \frac{3\sum_{i=1}^{N}\dfrac{l_i^2}{\left(\varepsilon_{k-1}^2 + l_i^2\right)^2}}{\sum_{i=1}^{N}\dfrac{1}{\left(\varepsilon_{k-1}^2 + l_i^2\right)^2}} \qquad \text{if } k \neq 0 . \qquad (14)$$

The initial value of the dihesion (for $k=0$) is given by the equation

$$\varepsilon_0 \leq \frac{\sqrt{3}}{2}\left(\max(Z_i) - \min(Z_i)\right). \qquad (15)$$

5. Reduction to the pole

In the case of a uniform magnetized source the transfer function $S(f_x, f_y)$ for reduction to the magnetic pole anomaly is defined by

$$\left(f_x, f_y\right) = \frac{\left(f_x^2 + f_y^2\right)^{1/2}}{N\left(f_x^2 + f_y^2\right)^{1/2} + j\left(Lf_x + Mf_y\right)} \qquad , \qquad (16)$$

where f_x and f_y are the spatial frequencies measured along the x and y axes, respectively; j means the imaginary unit. If angles α and β are known (they are determined by the above discussed procedure) the reduction of vertical magnetic anomalies can be determined. Z_p will indicate the vertical magnetic anomaly reduced to the magnetic pole.

Realization of the conditions included in Poisson's relation can be investigated in the following way. The reduced magnetic anomaly should be correlated with the derivative of vertical gravity with respect to variable z. The correlation coefficient can be regarded as a measure of realization of the conditions included in Poisson's relation. The correlation coefficient r and its 99% confidence interval (r_1, r_2) are determined by the equations:

$$r = \frac{\sum_i \sum_j \left(Z_{pij} - Z_p^m\right)\left(g_{zzij} - g_{zz}^m\right)}{\left(\sum_i \sum_j \left(Z_{pij} - Z_p^m\right)^2 \sum_i \sum_j \left(g_{zzij} - g_{zz}^m\right)^2\right)^{1/2}} \qquad (17)$$

and

$$r_1 = \frac{(1+r)\exp\left(\sqrt{\dfrac{32}{n-3}}\right) - 1 + r}{(1+r)\exp\left(\sqrt{\dfrac{32}{n-3}}\right) + 1 - r} \quad \text{and} \quad r_2 = \frac{(1+r)\exp\left(-\sqrt{\dfrac{32}{n-3}}\right) - 1 + r}{(1+r)\exp\left(-\sqrt{\dfrac{32}{n-3}}\right) + 1 - r},$$

$$(18)$$

where Z_p and g_{zz}^m are the mean values of Z_{pij} and g_{zzij}. Those data defined by the inner frame are taken into consideration for determining the correlation coefficient.

6. Error of the parameters

The parameters that are determined rely on a linear least–squares procedure. Error analysis will be done by the method of CLIFFORD [1973]. If the linear least–squares calculation has been done, then the matrix $P=[A^T WA]^{-1}$ will already have been calculated by equation (7). Variance $\sigma(p_i)$ of the ith parameter and correlation $r(p_i, p_j)$ of the parameters p_i and p_j are expressed by

$$\sigma(p_i) = \sigma(P_{ii})^{1/2}, \qquad (19)$$

and

$$r(p_i, p_j) = \frac{P_{ij}}{\left[P_{ii} P_{jj}\right]^{1/2}}, \qquad (20)$$

where P_{ij} indicates the element of matrix P. The value σ is obtained by

$$\sigma = \left(\frac{d^T W d}{N - M}\right)^{1/2}, \qquad (21)$$

where vector **d** is determined by equation (11). The standard error of the estimate is given by the ± three sigma (equation 19) rule.

7. Interpretation of field data

The applicability of Poisson's relation is investigated in eight Hungarian prospecting areas (Balmazújváros–Ny, Egyek, Kunszentmárton, Nagykörű, Nova, Ölbő, Pusztamonostor, Vése). The location of these areas is shown in *Fig. 1*. Bouguer and vertical magnetic anomalies were digitized in the same grid pattern with a sampling interval of 1 km.

The Bouguer anomalies of the prospecting areas were recorded by ELGI (Eötvös Loránd Geophysical Institute of Hungary). The gravity stations were distributed randomly, with the average sampling distance being 500 m. The surface density of the stations was approximately 1 station/km^2. The accuracy of the digitized data was ±0.1 mGal . The range of the Bouguer anomalies exceeds the noise level.

The vertical magnetic anomalies of the prospecting areas were also recorded by ELGI. The magnetic stations were distributed randomly with an

Fig. 1. Location of the eight prospecting areas
1. ábra. A nyolc kutatási terület elhelyezkedése

average sampling distance of 1000–1500 m, their surface density was approximately 0.5 station/km². The accuracy of the digitized data was ± 3 nT, the error of the derivatives of the Bouguer anomalies with respect to the variables *x, y,* and *z* is ±1 Eötvös.

Those data that we used to determine parameters p_1, p_2, and p_3 are selected by an appropriate 2-D window. One of the aims of using the 2-D window is to select those anomalies that are probably produced by the same sources. The extension of the 2-D window (indicated by an inner frame in these anomaly maps) is determined by trial and error.

The other significant phase of the application of the iterative procedure is for tracing convergence when iteration started from different initial estimates. If the result of these iterations is the same, it is accepted as a stable convergence. Convergence of the iterative process takes place in 5–7 iterative steps. The applied weight factor, the dihesion, supports the effective convergence.

Balmazújváros–Ny prospecting area

Balmazújváros–Ny prospecting area is located in the Szolnok flysch zone. It extends from Szolnok (Hungary) to Nagykároly (Romania) and is approximately 150 km in length and about 20–30 km wide. Its strike is in the SW–NE direction. Judging from seismic measurements this zone has a

Fig. 2. Bouguer and vertical magnetic anomalies over the Balmazújváros–Ny prospecting area, anomalies are given in mGal and nT units, respectively. Inner frame indicates the position of the 2-D window

2. ábra. A Balmazújváros–Ny kutatási terület Bouguer- és vertikális mágneses anomália térképe, az anomáliák egysége: mGal, illetve nT. Belső keret jelöli a kétdimenziós ablak helyzetét

thickness of 1000–1500 m, consisting of four different layers: Upper Cretaceous, Upper Paleocene, Middle–Upper Eocene, and Upper Oligocene. The flysch is superpositioned on some Mesozoic napes. It creates the basement of the Pannonian layers. The thickness of the Neogene overlaying beds varies between 2 and 3 km. The flysch complex was reached by drilled wells or the wells ended in some Tortonian volcanic complex.

Figure 2 shows the Bouguer and vertical magnetic anomalies. The derivatives with respect to variables *x, y,* and z are presented in *Fig. 3*. The estimated values of the parameters and their errors are as follows, $J/\rho = (0.0025\pm0.0008)$ Am^2/kg, $\alpha=-65.22°\pm21.54°$, and $\beta=32.02°\pm11.6°$. Parameter J/ρ shows relatively high negative correlation (–0.49) with parameter α (Eq. 20). The other elements of

Derivative with respect to the variable x

Derivative with respect to the variable y

Derivative with respect to the variable z

Fig. 3. Derivative of the Bouguer anomalies of Balmazújváros–Ny prospecting area with respect to variables *x, y,* and z; anomalies contoured in Eötvös units. Inner frame indicates the position of the 2-D window

3. ábra. A Balmazújváros–Ny kutatási terület Bouguer-anomáliainak *x, y,* és z változó szerinti deriváltja, az anomáliák eötvös egységben adottak. Belső keret jelöli a kétdimenziós ablak helyzetét

the correlation matrix are minor ones (between 0.07 and 0.1). The correlation coefficient between the vertical magnetic anomalies reduced to the pole and the derivative with respect to variable z of the Bouguer anomalies is 0.189, and its 99% level confidence interval extends from 0.063 to 0.31 (Eqs. 17 and 18). The value of the parameters summarized above leads to the conclusion that the anomalies are produced by different sources.

Egyek prospecting area

The Egyek prospecting area is to be found in the Jászság basin, which is one of the sub-basins of the Great Hungarian Plain. This particular sub-basin is filled with the Újfalui formation (Neogene complex) whose thickness is of 1400 m.

Figure 4 illustrates the Bouguer and the vertical magnetic anomalies. The derivatives with respect to variables x, y, and z of the Bouguer anomalies are presented in *Fig. 5*. The estimated values of the parameters and their errors are as follows, $J/\rho = (0.000404 \pm 0.00046)$ Am^2/kg, $\alpha=-23.9°\pm44.6°$, and $\beta=293.1°\pm140.9°$. Parameter J/ρ shows significant

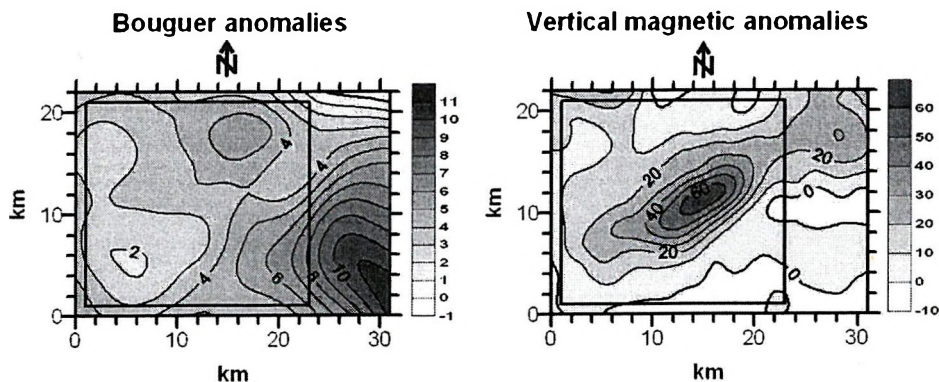*Fig. 4.* Bouguer and vertical magnetic anomalies over the Egyek prospecting area, anomalies are given in mGal and nT units, respectively. Inner frame indicates the position of the 2-D window

4. ábra. Az Egyek kutatási terület Bouguer- és vertikális mágneses anomália térképe, az anomáliák egysége: mGal, illetve nT. Belső keret jelöli a kétdimenziós ablak helyzetét

**Derivative with respect
to the variable x**

**Derivative with respect
to the variable y**

**Derivative with respect
to the variable z**

anti-correlation (−0.75) with parameter α (Eq. 20). The other elements of the correlation matrix show some correlation between 0.07 and 0.38. The correlation coefficient between the vertical magnetic anomalies reduced to the pole and the derivative with respect to variable z of the Bouguer anomalies is 0.0187, and its 99% level confidence interval extends from −0.089 to 0.26 (Eqs. 17 and 18). The high errors of the estimated parameters and the low correlation coefficients express certain discrepancies between the sources of the Bouguer and vertical magnetic anomalies.

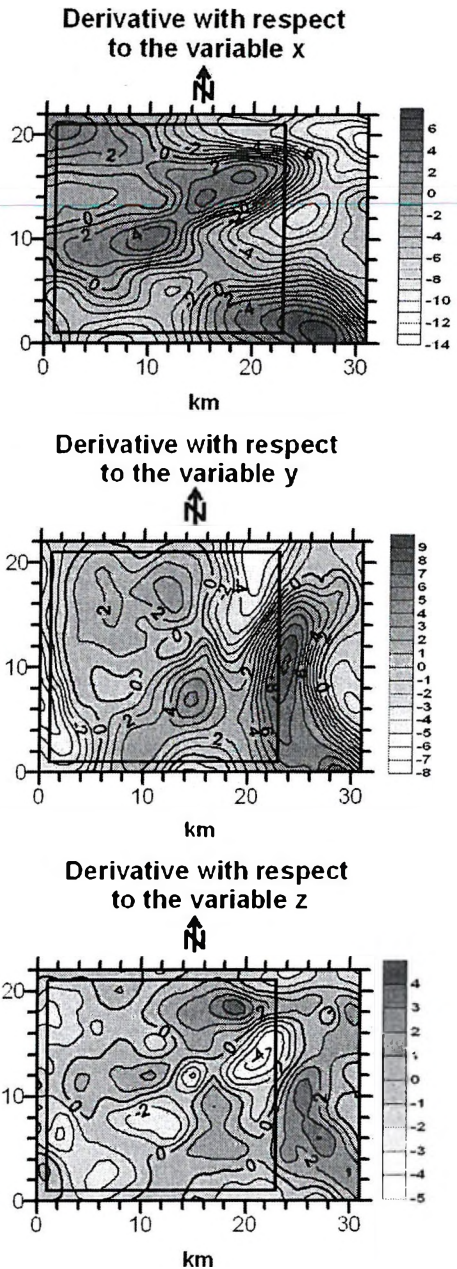*Fig. 5.* Derivative of the Bouguer anomalies of Egyek prospecting area with respect to variables x, y, and z; anomalies contoured in Eötvös units. Inner frame indicates the position of the 2-D window

5. ábra. Az Egyek kutatási terület Bouguer-anomáliainak x, y, és z változó szerinti deriváltja, az anomáliák eötvös egységben adottak. Belső keret jelöli a kétdimenziós ablak helyzetét

Kunszentmárton prospecting area

The Kunszentmárton prospecting area is located in the middle part of the Great Hungarian Plain. It belongs to the Mecsek zone of the Tisza unit. The basement consists of Valanginian–Barremian volcanic and volcanic–sediments of Mecsek type. In addition to the volcanic layers the basement also contains marl, marl–clay, and limestone. The characteristic formation of the area is Hidasvölgyi marl complex.

The Bouguer and the vertical magnetic anomalies of the prospecting area can be seen in *Fig. 6*. The derivatives with respect to variables x, y, and z of the Bouguer anomalies are contoured in *Fig. 7*. The estimated values of the parameters and their errors are as follows, $J/\rho = (0.0146\pm0.00315)$ Am^2/kg, $\alpha=81.1°\pm5.1°$, and $\beta=35.4°\pm21.23°$. The elements of the correlation matrix show minor values (0.1–0.2) (Eq. 20). The correlation coefficient between the vertical magnetic anomalies reduced to the pole and the vertical derivative of the Bouguer anomalies is 0.61, and its 99% level confidence interval extends from 0.48 to 0.7 (Eqs. 17 and 18). The estimated value of the parameters and the correlation coefficient support
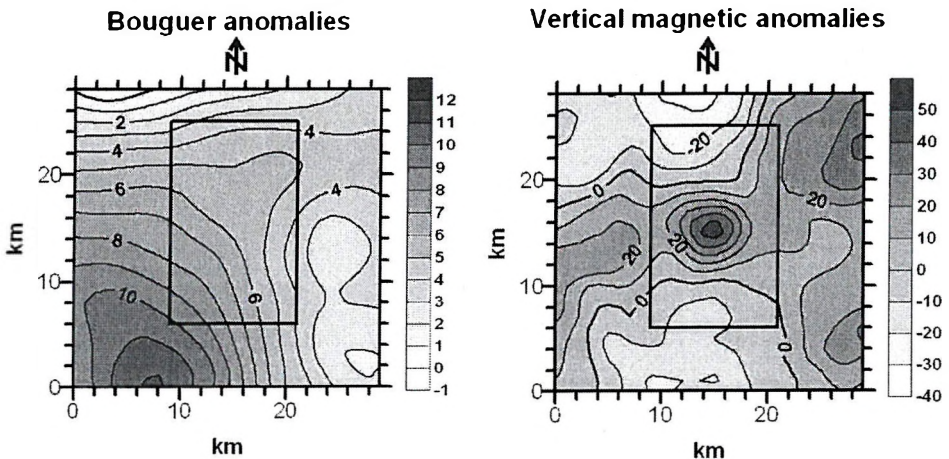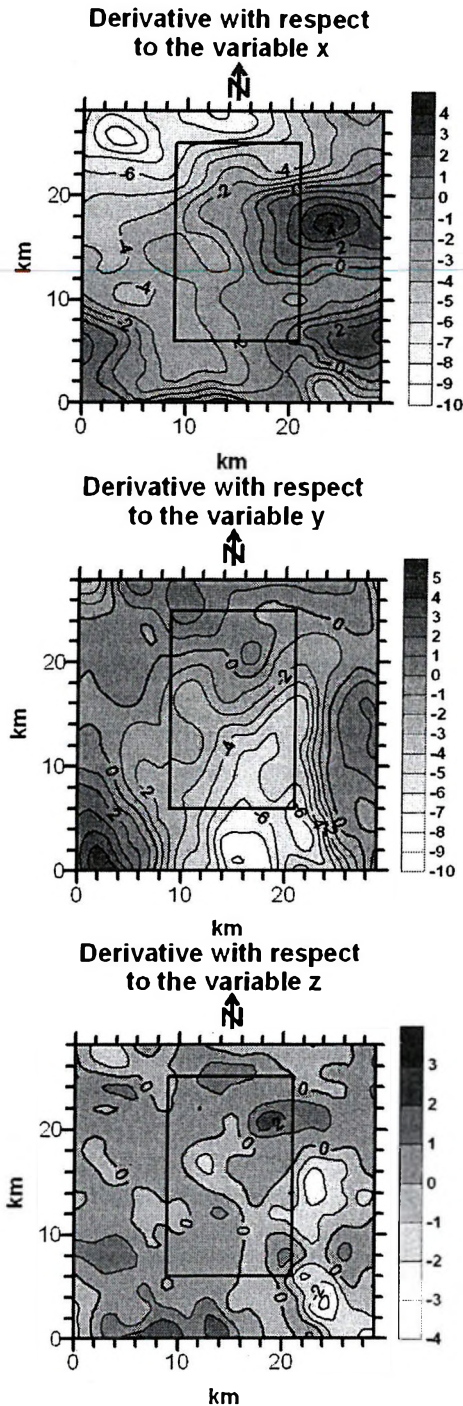

Fig. 6. Bouguer and vertical magnetic anomalies over the Kunszentmárton prospecting area, anomalies are given in mGal and nT units, respectively. Inner frame indicates the position of the 2-D window

6. ábra. A Kunszentmárton kutatási terület Bouguer- és vertikális mágneses anomália térképe, az anomáliák egysége: mGal, illetve nT. Belső keret jelöli a kétdimenziós ablak helyzetét

**Derivative with respect
to the variable x**

**Derivative with respect
to the variable y**

**Derivative with respect
to the variable z**

the applicability of Poisson's relation. The Bouguer and vertical magnetic anomalies certainly have some common source.

Nagykörű prospecting area

The Nagykörű prospecting area also belongs to the Szolnok flysch zone. Its geologic structure is similar to the Balmaz-újváros–Ny area. The prospecting wells discovered thick Upper Paleocene and Lower Eocene layers.

The Bouguer and the vertical magnetic anomalies of the prospecting area are presented in *Fig. 8*. The derivatives with respect to variables x, y, and z of the Bouguer anomalies can be seen in *Fig. 9*. The estimated values of the parameters and their errors are as follows, $J/\rho = (0.0095\pm0.00153)$ Am^2/kg, $\alpha = 10.4°\pm19.5°$, and $\beta = 92.5°\pm39.5°$. The elements of the correlation matrix are between 0.15 and 0.3

Fig. 7. Derivative of the Bouguer anomalies of Kunszentmárton prospecting area with respect to variables x, y, and z; anomalies contoured in Eötvös units. Inner frame indicates the position of the 2-D window

7. ábra. A Kunszentmárton kutatási terület Bouguer-anomáliainak x, y, és z változó szerinti deriváltja, az anomáliák eötvös egységben adottak. Belső keret jelöli a kétdimenziós ablak helyzetét

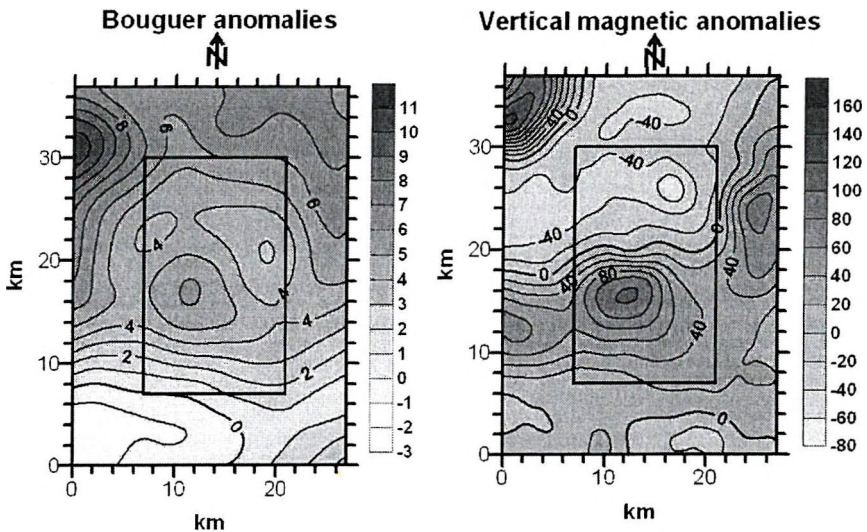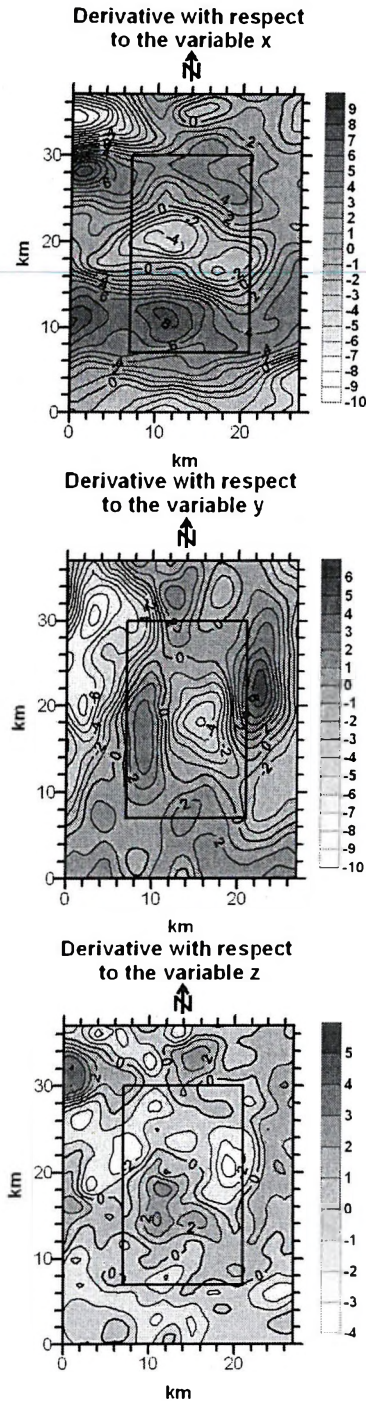**Bouguer anomalies**   **Vertical magnetic anomalies**
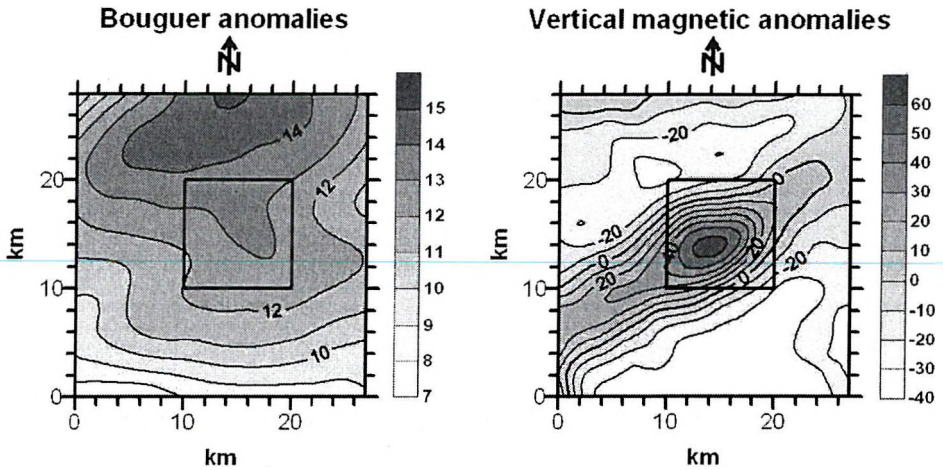
Fig. 8. Bouguer and vertical magnetic anomalies over the Nagykörű prospecting area, anomalies are given in mGal and nT units, respectively. Inner frame indicates the position of the 2-D window

8. ábra. A Nagykörű kutatási terület Bouguer- és vertikális mágneses anomália térképe, az anomáliák egysége: mGal, illetve nT. Belső keret jelöli a kétdimenziós ablak helyzetét

(Eq. 20). The correlation coefficient of the vertical anomalies reduced to the pole and the vertical derivative of the Bouguer anomalies is 0.23, and its 99% level confidence interval is −0.062 and −0.46 (Eqs. 17 and 18). From the results it can be interpreted that there is no certainty of there being any coincidence of the gravity and magnetic anomalies.

Nova prospecting area

The Nova prospecting area is located in the southwest part of Hungary. Its pre-Neogene basement consists of two main structural units: the Balaton crystalline swell and the central mountain facies belt.

The elements of the Balaton crystalline swell are detected in the southern part of Nova. Mica-schist, granite, granodiorite, quartz–porphyrites were cored by exploration wells. The age of these rocks may be Precambrian, but the main mass is Paleozoic: Ordovician–Silurian metamorphic rocks, Carboniferous granite, and Permian quartz-porphyrite. These rocks are located in an east–west emergent ridge in the Orta-háza–Pusztaederics–Kilimán line. They subsided to greater depths along to the north and south, as well as to the west from Ortaháza.
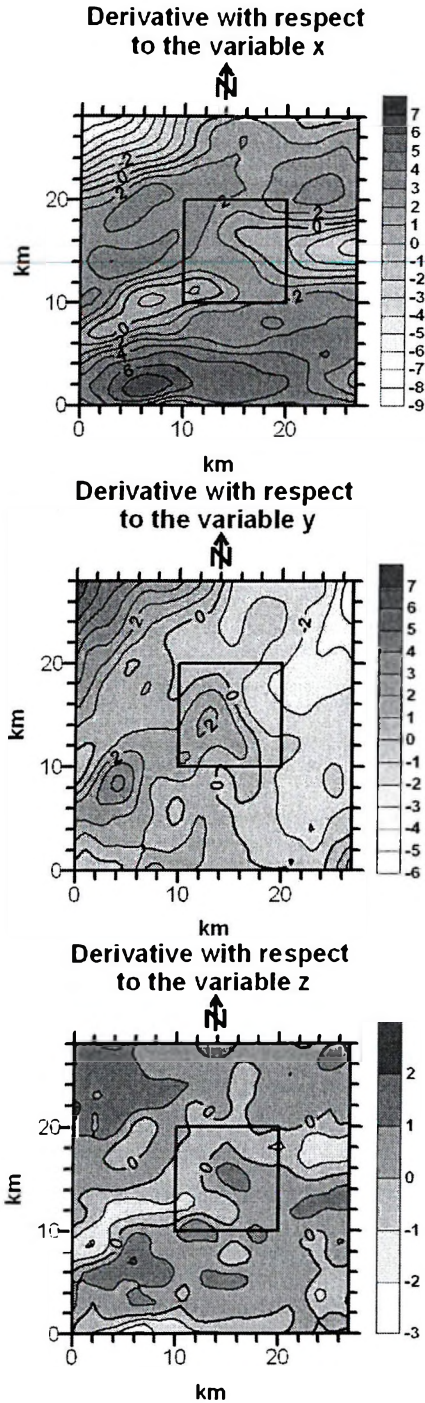
The rocks of the central mountain facies belt can be found north of the crystalline swell. Large amounts of sediments were deposited in the late Paleozoic–Mesozoic cycle. The products of exploration wells indicate that Permian rocks are probably located south of Dióskál. Triassic Dachstein limestone and dolomite formation can be detected in the entire area. Jurassic detritus is found in the northeast–southeast direction in the vicinity of Bárszentmihályfa and Kehida. The limestone formation of Ugod and the marl formation of Polány are the products of Upper Cretaceous sedimentation.

Eocene series are superimposed on the eroded surface of Mesozoic rocks with angular unconformity. Middle and Upper Eocene sediments were deposited simultaneously with subsidence of the basin. The deepest part of the basin is in the central zone of the area. This east–west trench of Zalatánok contains more than 1000 m of the sedimentary complex.

Fig. 9. Derivative of the Bouguer anomalies of Nagykörű prospecting area with respect to variables *x*, *y*, and *z;* anomalies contoured in Eötvös units. Inner frame indicates the position of the 2-D window

9. ábra. A Nagykörű kutatási terület Bouguer-anomáliainak *x*, *y*, és *z* változó szerinti deriváltja, az anomáliák eötvös egységben adottak. Belső keret jelöli a kétdimenziós ablak helyzetét

An erosion period was dominant from the Eocene to the Miocene. Sedimentation started probably in Badenian, and it continued with short hiatuses in Sarmatian as well as in Pannonian. The Badenian–Sarmatian transgression period turned into a regressional filling cycle (Lower Pannonian) and terrestrial sediments were deposited as the last stage of the basin evolution.

Figure 10 shows the Bouguer and the vertical magnetic anomalies of the prospecting area. The derivatives with respect to variables x, y, and z of the Bouguer anomalies are presented in *Fig. 11*. The estimated values of the parameters and their errors are as follows, $J/\rho = (0.0025 \pm 0.000369)$ Am^2/kg, $\alpha = -45.2° \pm 8.3°$, and $\beta = 277.0° \pm 6.8°$. Parameter J/ρ shows a high negative correlation of -0.69 with parameter α (Eq. 20). Other elements of the correlation matrix vary between -0.24 and 0.12. The correlation coefficient of the vertical magnetic anomalies and the vertical gradient of the Bouguer anomalies is -0.21, its 99% level confidence interval extends from -0.37 to -0.035 (Eqs. 17 and 18). The geological structure of the Nova prospecting area is rather complex. It is very probable that the gravity and magnetic sources are different.

Fig. 10. Bouguer and vertical magnetic anomalies over the Nova prospecting area, anomalies are given in mGal and nT units, respectively. Inner frame indicates the position of the 2-D window

10. ábra. A Nova kutatási terület Bouguer- és vertikális mágneses anomália térképe, az anomáliák egysége: mGal, illetve nT. Belső keret jelöli a kétdimenziós ablak helyzetét

Derivative with respect
to the variable x

Derivative with respect
to the variable y

Derivative with respect
to the variable z

Fig. 11. Derivative of the Bouguer
anomalies of Nova prospecting area
with respect to variables *x*, *y*, and *z;*
anomalies contoured in Eötvös
units. Inner frame indicates the
position of the 2-D window

11. ábra. A Nova kutatási terület
Bouguer-anomáliainak *x, y,* és *z*
változó szerinti deriváltja, az
anomáliák eötvös egységben
adottak. Belső keret jelöli a
kétdimenziós ablak helyzetét

Ölbő prospecting area

The Ölbő prospecting area is located on the northwest side of the Rába tectonic line. The area belongs to the east Alp type napes which consists of Rába type metamorphic complex or Graz type Paleozoic (Silurian–Devonian) complex. The metamorphic complex has different formations: sericite-schists, sandstone-schists, metamorphic dolomites, quartz-phyllites, and metasandstones. The metamorphic complex is covered by Miocene (Upper Badenian) sediments. The basement of Miocene sediments belongs to the Rákosi Limestone formation. They superpositioned, with discordances, to the Paleozoic basement.

Figure 12 shows the Bouguer and the vertical magnetic anomalies of the prospecting area. The derivatives with respect to variables x, y, and z of the Bouguer anomalies are presented in *Fig. 13*. The estimated values of the parameters and their errors are as follows, $J/\rho = ($ 0.00508±0.00042$)$ Am^2/kg, α=32.7°±21.3°, and β=35.1°±8.5°. The elements of the correlation matrix vary between 0.35 and 0.04 (Eq. 20). The correlation coefficient of the vertical magnetic anomalies reduced to the pole and the vertical gradient of the Bouguer anomalies is –0.167 and its 99% confidence interval extends from –0.270 to –0.0605 (Eqs. 17 and 18). The anti-correlation of the two anomalies and the values of the estimated parameters express the concept that the gravity and magnetic anomalies have different sources.
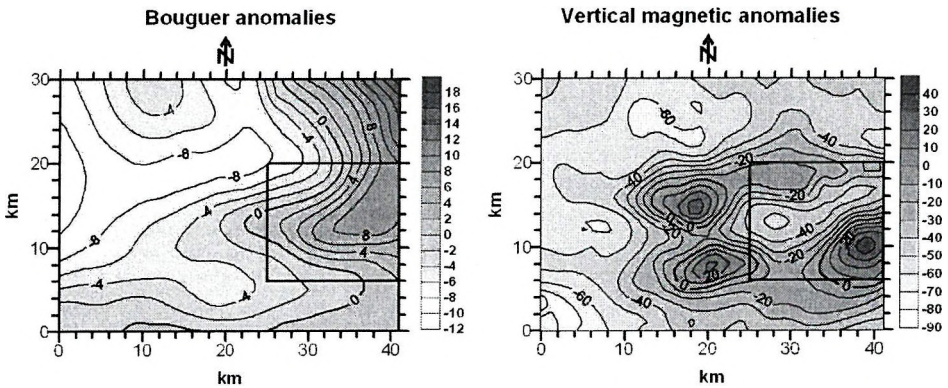

Fig. 12. Bouguer and vertical magnetic anomalies over the Ölbő prospecting area, anomalies are given in mGal and nT units, respectively. Inner frame indicates the position of the 2-D window

12. ábra. Az Ölbő kutatási terület Bouguer- és vertikális mágneses anomália térképe, az anomáliák egysége: mGal, illetve nT. Belső keret jelöli a kétdimenziós ablak helyzetét
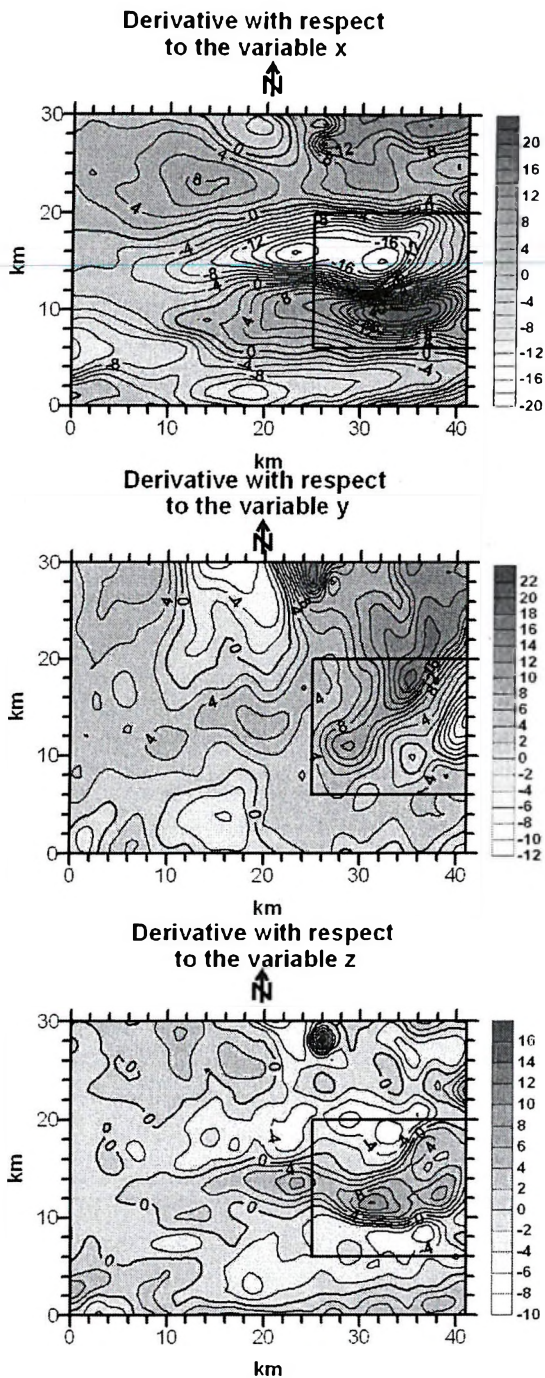
Derivative with respect to the variable x

Derivative with respect to the variable y

Derivative with respect to the variable z

Fig. 13. Derivative of the Bouguer anomalies of Ölbő prospecting area with respect to variables x, y, and z; anomalies contoured in Eötvös units. Inner frame indicates the position of the 2-D window

13. ábra. Az Ölbő kutatási terület Bouguer-anomáliainak x, y, és z változó szerinti deriváltja, az anomáliák eötvös egységben adottak. Belső keret jelöli a kétdimenziós ablak helyzetét

Pusztamonostor prospecting area

The Pusztamonostor prospecting area is part of the Alp type Bükk unit. The basement consists of Paleozoic and Mesozoic metamorphic complex. Middle and Upper Triassic carbonate rocks are also detected and Jurassic Szarvaskő diabase formation can be found in the basement. Because of the lack of wells the sources of anomalies cannot be determined.

Figure 14 shows the Bouguer and the vertical magnetic anomalies. The derivatives with respect to variables x, y, and z of the Bouguer anomalies are presented in *Fig. 15*. The estimated values of the parameters and their errors are as follows, $J/\rho = (0.003 \pm 0.00024)$ Am^2/kg, $\alpha=9.2°\pm25.8°$, and $\beta=348.7°\pm18.6°$. Parameter J/ρ shows 0.51 and 0.54 correlation with parameters α and β, respectively (Eq. 20). The correlation coefficient of the vertical magnetic anomalies and the vertical gradient of the gravity anomalies is -0.052 and its 99% level confidence interval extends from -0.235 to 0.133 (Eqs. 17 and 18). The low correlation coefficient and the value of the estimated parameters show that the source of the gravity and magnetic anomalies is not common.

Bouguer anomalies **Vertical magnetic anomalies**
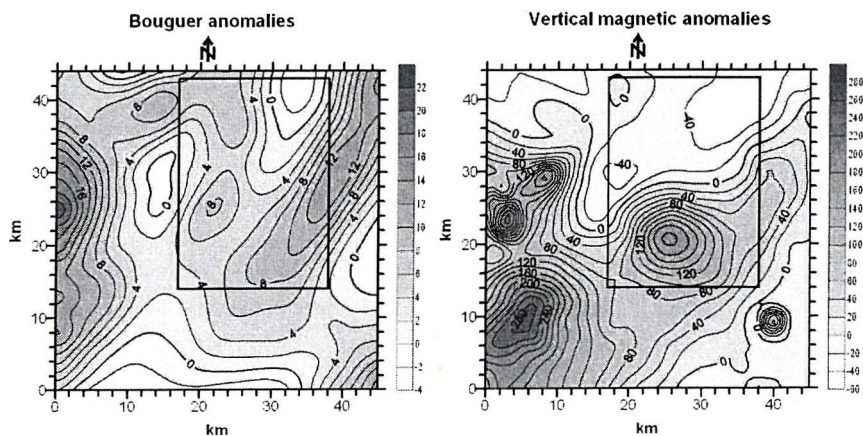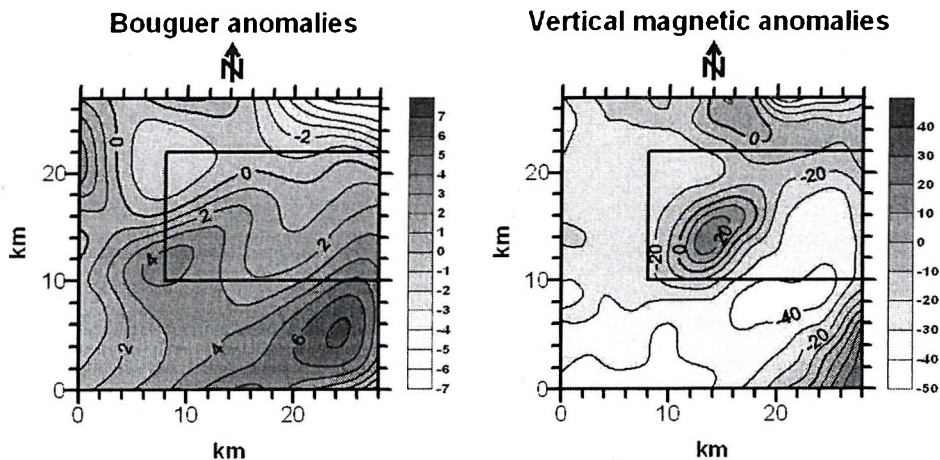
Fig. 14. Bouguer and vertical magnetic anomalies over the Pusztamonostor prospecting area, anomalies are given in mGal and nT units, respectively. Inner frame indicates the position of the 2-D window

14. ábra. A Pusztamonostor kutatási terület Bouguer- és vertikális mágneses anomália térképe, az anomáliák egysége: mGal, illetve nT. Belső keret jelöli a kétdimenziós ablak helyzetét

Derivative with respect
to the variable x

Derivative with respect
to the variable y

Derivative with respect
to the variable z

Fig. 15. Derivative of the Bouguer anomalies of Pusztamonostor prospecting area with respect to variables *x*, *y*, and *z;* anomalies countoured in Eötvös units. Inner frame indicates the position of the 2-D window

15. ábra. A Pusztamonostor kutatási terület Bouguer-anomáliainak *x, y,* és *z* változó szerinti deriváltja, az anomáliák eötvös egységben adottak. Belső keret jelöli a kétdimenziós ablak helyzetét

Vése prospecting area

The Vése prospecting area is a part of the Alp type Middle Transdanubian unit. The basement probably consists of a Paleozoic and Mesozoic metamorphic complex.

Figure 16 shows the Bouguer and the vertical magnetic anomalies. The derivatives with respect to variables x, y, and z of the Bouguer anomalies are presented in *Fig. 17*. The estimated values of the parameters and their errors are as follows, $J/\rho = (\ 0.00101\pm0.000273)\ Am^2/kg$, $\alpha=41.2°\pm64.8°$, and $\beta=76.6°\pm24.9°$. The elements of the correlation matrix vary between -0.28 and 0.1 (Eq. 20). The correlation coefficient of the vertical magnetic anomalies reduced to the pole and the vertical gradient of the Bouguer anomalies is 0.251 and its 99% level confidence interval extends from 0.00139 to 0.471 (Eqs. 17 and 18). The correlation coefficient and the estimated parameters support the concept that the gravity and magnetic anomalies have a common source.
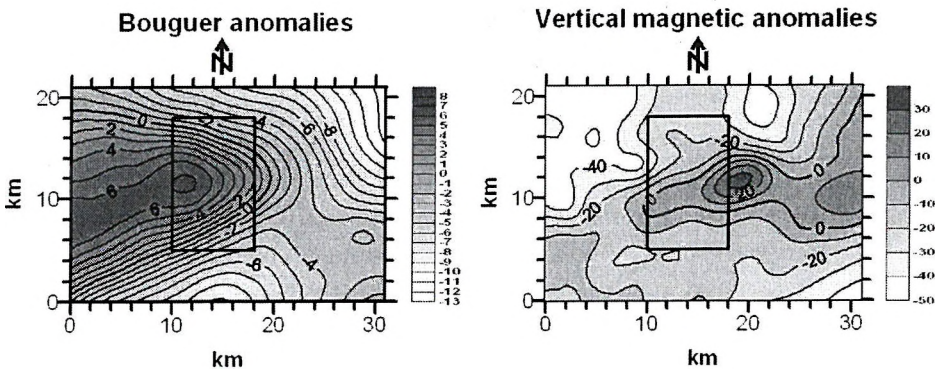
Fig. 16. Bouguer and vertical magnetic anomalies over the Vése prospecting area, anomalies are given in mGal and nT units, respectively. Inner frame indicates the position of the 2-D window

16. ábra. A Vése kutatási terület Bouguer- és vertikális mágneses anomália térképe, az anomáliák egysége: mGal, illetve nT. Belső keret jelöli a kétdimenziós ablak helyzetét
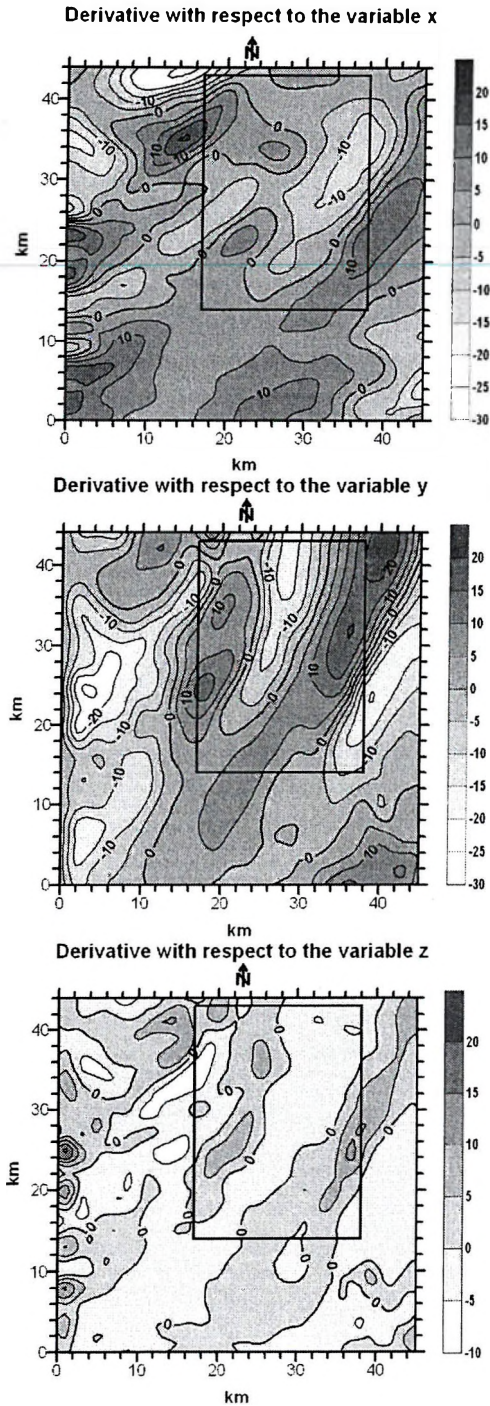
Derivative with respect to the variable x

Derivative with respect to the variable y

Derivative with respect to the variable z
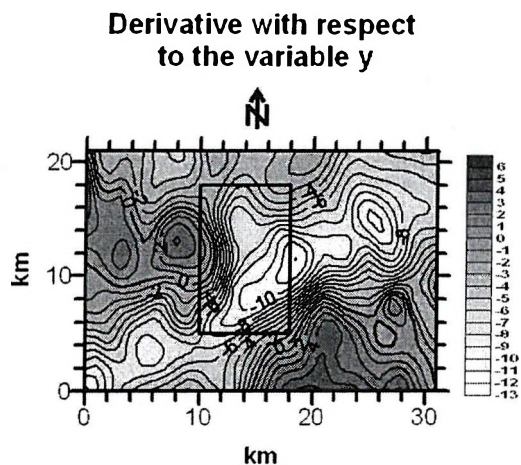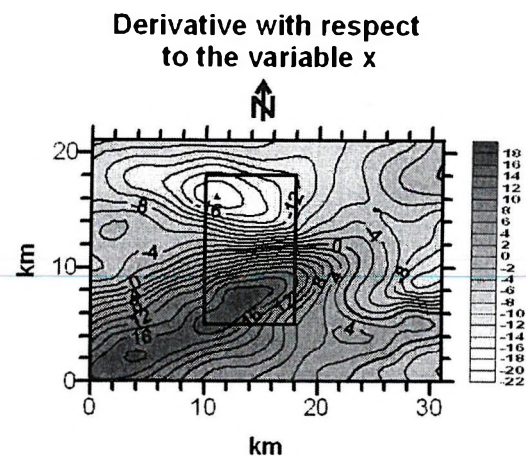
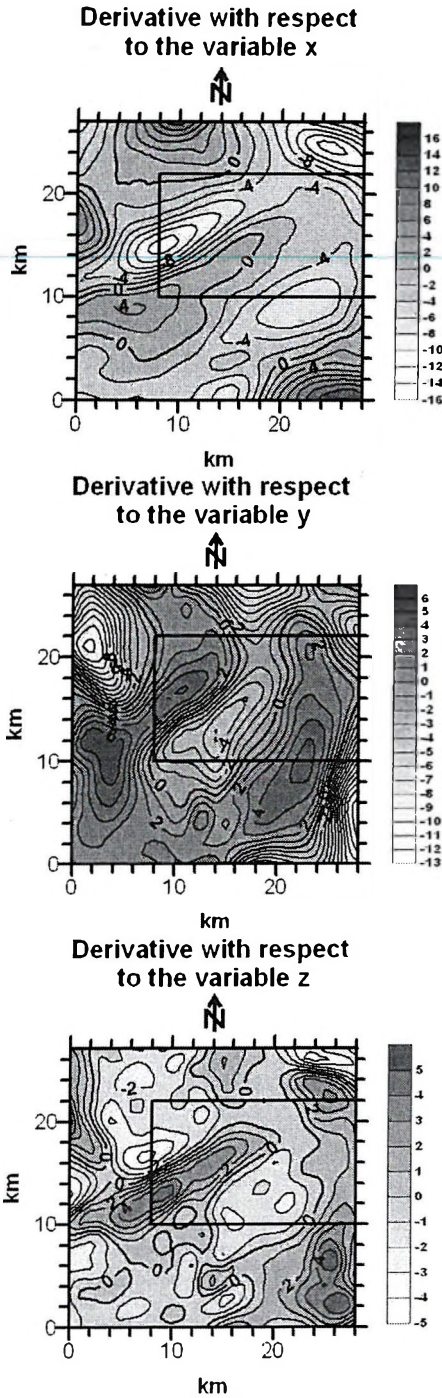*Fig. 17.* Derivative of the Bouguer anomalies of Vése prospecting area with respect to variables *x, y,* and *z;* anomalies contoured in Eötvös units. Inner frame indicates the position of the 2-D window

17. ábra. A Vése kutatási terület Bouguer-anomáliainak *x, y, és z* változó szerinti deriváltja, az anomáliák eötvös egységben adottak. Belső keret jelöli a kétdimenziós ablak helyzetét

Acknowledgement

REFERENCES

AL–CHALABI M. 1970: Interpretation of two-dimensional magnetic profiles by non-linear optimization. Bollettino di Geofisica Teorica ed Applicata **12**, pp. 3–20

BLAKELY R. J. 1995: Potential theory in gravity and magnetic applications. Cambridge University Press, 441 p.

CHANDLER V. W., KOSKI J. S., HINZE, W. J., BRAILES L. W. 1981: Analysis of multisource gravity and magnetic anomaly data sets by moving-window application of Poisson's theorem. Geophysics **46**, pp. 30–39

CLIFFORD A. A. 1973: Multivariate error analysis. Applied Science Publishers, London.

CORDELL L., TAYLOR P. T. 1971: Investigation of magnetization and density of a north Atlantic seamount using Poisson's theorem. Geophysics **36**, pp. 919–937

HJELT S-E. 1992: Pragmatic inversion of geophysical data. Springer Verlag, Berlin

KANASEWICH E. R., AGARWAL R. G., 1970: Analysis of combined gravity and magnetic fields in wave number domain. Journal of Geophysical Research **75**, pp. 5702–5712

MENKE W. 1989: Geophysical data analysis: Discrete inverse theory. Academic Press, London, 289 p.

STEINER F. 1988: Most frequent value procedures (a short monograph). Geophysical Transactions **34**, pp. 139–260

STEINER F. 1990: Fundamentals of geostatistics (in Hungarian). Tankönyvkiadó, Budapest, 363 p.

WILSON C. D. V. 1970: The use of Poisson relationship for separating the anomalies due to neighbouring bodies, and for recognizing inhomogeneities and structural deformation. Bollettino di Geofisica Teorica ed Applicata **12**, pp. 158–182

A gravitációs és a földmágneses anomáliák együttes értelmezhetősége

KIS Károly és WITTMANN Géza

A Poisson-féle összefüggés általános kapcsolatot fejez ki a gravitációs és földmágneses anomáliák között. A Poisson-féle összefüggés alkalmazhatósága nyolc magyarországi kutatási területen került vizsgálatra. A kutatási területek Bouguer és ver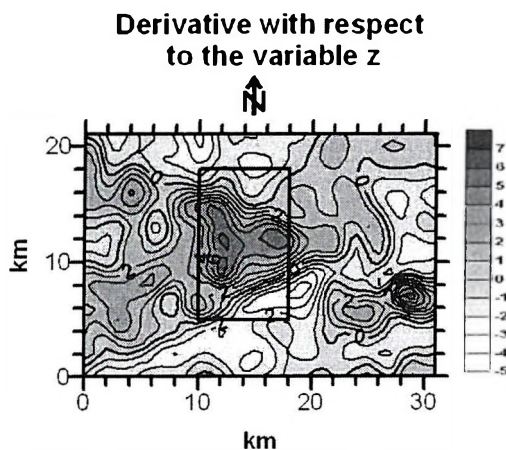tikális mágneses anomália térképei 1 km-es mintavételi távolsággal kerültek digitalzálásra identikus pontokban. A Poisson-féle összefüggés lineáris inverz feladat formájában is felírható. A lineáris inverz feladat a Bouguer-anomáliák x-, y- és z-változók szerinti deriváltjainak meghatározását teszi szükségessé. Az inverz feladat megoldása iterációval történik. Az inverz feladat megoldásának eredménye az eredő mágnesezettség vektor (annak deklinációja és inklinációja). A vertikális mágneses anomáliák a mágnesezettség deklinációjának és inklinációjának ismeretében északi földmágneses pólusra

redukálhatók. A Poisson-féle összefüggésből következik, hogy az északi földmágneses pólusra redukált mágneses anomáliák a Bouguer-anomáliák vertikális deriváltjával fognak korrelálódni. A korrelációs együttható a Poisson-féle összefüggés alkalmazhatóságának mértéke lehet. Két kutatási terület rendelkezik nagyobb korrelációs együtthatóval, ahol a Poisson-féle összefüggés teljesültnek tekinthető.

ABOUT THE AUTHORS

Károly Kis received his M.Sc. (1969) and Ph.D. (1972) in geophysics from the Eötvös Loránd University, and in 1969 joined its Geophysics Department. Since 1964 he has been a member of the Research Group of Geophysics and Environmental Physics of the Hungarian Academy of Sciences, and in 1984 he became a Senior Research Associate. In 1985 he was awarded the title of Honorary Associate Professor of Geophysics by the Eötvös Loránd University. His main interests lie in the data processing and interpretation of measurements done by satellites; and inversion of gravity and magnetic anomalies.

Géza Wittmann received his M.Sc. (1991) in geophysics from the Eötvös Loránd University. In 1991 he joined Geophysical Services Ltd. Budapest, as a seismic 2-D/3-D data processor. Since 1995 he has been working as processing supervisor at the MOL Hungarian Oil and Gas Co. Division of E&P, Budapest. He is a member of the Association of Hungarian Geophysicists.

Quality management for electrical and penetration soundings (VES & EGPS)

Péter SALÁT[*] and Dezső DRAHOS[*]

The possibilities of utilizing Quality Control (QC) and Quality Assessment (QA) in the inversion of the Engineering Geophysical Penetration Sounding and in the inversion of Vertical Electrical Sounding methods are dealt with. The possible geological targets and their models, and the parameters to be determined are described. The general elements and operations of the quality controlled geophysical technology are shown. Lithology classification, quantitative evaluation, and mixed qualitative-quantitative evaluation are utilized. Field examples are used to demonstrate the evaluation results.

Keywords: geoelectrics, penetration soundings, quality management, VES, EGPS

1. Introduction

The Vertical Electrical Sounding (VES) and the Engineering Geophysical Penetration Sounding (EGPS) methods are widely used in Hungary for investigating loose sediments. Determination of the quality (reliability and/or accuracy) of their data acquisition capability and their data inversion is not only an important part of geophysical methodology, but it has recently become a strict requirement for standardizing geophysical activities too. These general technical standards relate to both the accreditation of the field data acquisition (ISO/IEC 17025: 1999) and the quality control of the inversion of the measured sounding data (ISO 5725-1: 1994/Cor. 1:1998).

The key aspects of our work are quality control (QC) and quality assessment (QA), which together will hereafter be referred to as quality management (QM). It is a very simple engineering and scientific axiom that a measured quantity without error estimation amounts to nothing. Thus

every geophysical prospecting technology should be accompanied by reliability and/or accuracy analysis. This is a general requirement for standardization. Special planning, data acquisition and inversion techniques are needed to solve the qualification problems of the engineering geophysical exploration by VES and EGPS. The paper presents the results of methodological research work for assessing some important quality managing (QM) problems concerning the mentioned geophysical sounding methods.

At present there are no standardized quality management rules for geophysical activities, but trends can be found especially in hydrocarbon well logging. The Schlumberger, the Baker Atlas, and the Halliburton companies have worked out QC log acquisition and QC log evaluation procedures on the basis of quality controlling technology [see BATEMAN 1985] and on the basis of mathematical statistical inversion theory [see SERRA 1986]. They have been applying them since the 1980's. In their log evaluation algorithms and in software packages the quality of the output results is measured quantitatively by the Reduced Incoherence function [Schlumberger: MAYER, SIBBIT 1980; Halliburton: ALBERTY, HASHMY 1984], or by the Weighted Sum of Squared Error (WSSE) function [Baker Atlas: RODRIGUEZ et al. 1989] and by other quality indicators.

In order to determine the quality of the geophysical output results, one needs to know the data acquisition errors and the errors when modelling the inversion. For most evaluation algorithms the characteristics of the input errors are formulated as the sum of variances of two components, viz. the dispersion of the observational errors and the dispersion of the modelling errors. Qualification of the whole geophysical procedure — which includes measurement planning, execution of measurement, and data inversion — can be done by applying sophisticated modelling and mathematical statistical estimations.

2. Characterization of the examined objects

2.1. Geological targets and characteristics of the target model to be determined

VES and the EGPS are shallow penetrating methods. They are effective for the examination of young sedimentary structures, mainly loose

sediments. The objects targeted by our suggested measurement and inversion technology are objects which are equally important in environment protection, water management, and engineering:

— riverine water resources and flood areas;
— sub-soil of waste deposits;
— sub-soil around mud dumps;
— other clayey, sandy and gravelly sedimentary structures;
— river banks and dams and their geological basement;
— earth dams around refuse dumps and their neighbourhood;
— dikes similar to the previous ones, e.g. barrages and their neighbourhood.

The target bodies show mainly stratified structure. The task of geophysical soundings is to give a reliable qualitative classification of the soil layers and quantitative estimation of the layer parameters with a prescribed accuracy. Let us denote the unknown characteristics of the model object by the symbol x.

a) For qualitative classification ν is the particular variable of x so that there are N unknown discrete classes with the codes $\nu = 1, 2, ..., N$. For instance when the task is to determine the type of a given soil, the classes and codes can be for $N = 4$: clay ($\nu = 1$), sandy clay ($\nu = 2$), clayey sand ($\nu = 3$) and sand ($\nu = 4$).

b) For quantitative estimation x is replaced by the parameter vector $p(p_1, p_2, ..., p_l)$. A typical problem is the VES inversion, when the components of p are the resistivities ρ_m and the thicknesses d_m of a one-dimensional layer model:

$$p = p(\rho_1, d_1, \rho_2, d_2, ..., \rho_m, d_m, ..., \rho_{M-1}, d_{M-1}, \rho_M) \qquad (1)$$

In the quantitative inversion of EGPS data the following models are applied, their parameter vectors are:

$$p = p\left(V_{sd}, V_{cl}, \phi\right) \qquad (2)$$

and

$$p = p\left(V_{sd}, V_{cl}, \phi, S_w\right) \qquad (3)$$

where

V_{sd} is the amount of sand,
V_{cl} is the amount of clay,
ϕ is the porosity and
S_w is the water saturation.

c) For simultaneous qualitative-quantitative estimation, when the unknowns are both the $v = 1, 2, \ldots, N$ possible classes, and for a given v the continuous p_v variables too, the particular realization of the symbol x is the parameter vector $p_v(p_{v1}, p_{v2}, \ldots, p_{vl})$. For example, the unknowns of VES can be the number M of the layers and the resistivities and thicknesses of the layers:

$v = 1$, if $M = 2$ and $p_1 = p_1(\rho_{11}, d_{11}, \rho_{12})$,

$v = 2$, if $M = 3$ and $p_2 = p_2(\rho_{21}, d_{21}, \rho_{22}, d_{22}, \rho_{23})$,

$v = 3$, if $M = 4$ and $p_3 = p_3(\rho_{31}, d_{31}, \rho_{32}, d_{32}, \rho_{33}, d_{33}, \rho_{34})$.

Another example is when EGPS measurements are inverted: the codes v relate to the class of composition of the soil and the components of p_v vector are determined by the volumetric ratios of the elementary compounds:

$v = 1$, if there are sand, clay, water and air, $p_1 = p_1(V_{sd}, V_{cl}, \phi, S_w)$,

$v = 2$, if there are sand, clay, water, hydrocarbon and air, $p_2 = p_2(V_{sd}, V_{cl}, \phi, S_w, S_{CH})$, where S_{CH} is the hydrocarbon saturation.

For our quality controlled interpretation problems the models a), b) and c) are applied.

2.2. Measured data and the corresponding theoretical responses

During the measuring activity one gets the measured data which will be denoted by y_k, for $k = 1, 2, \ldots, K$, where K is the total number of measurements.

The other types of quantities are the computed or theoretical tool responses denoted by $f_k(x)$, which are the counterparts of the observed data. Other notations of measured and theoretical quantities are the superscripts (M) and (T) respectively.

The group of experimentally observed quantities for VES contains the results of geoelectric sounding measurements, with the usual arrangements or with any arbitrary electrode configurations. The data vector for the measured $\rho_a^{(M)}(K_i^{(M)})$ apparent resistivity values is:

$$y = y\left(\rho_a^{(M)}(K_1^{(M)}), \rho_a^{(M)}(K_2^{(M)}), \ldots, \rho_a^{(M)}(K_I^{(M)})\right) , \qquad (4)$$

where $K_i^{(M)}$ is the experimental coefficient of the ith arrangement.

The second group of quantities contains the computed model responses. The theoretical $\rho_a^{(T)}(p, K_i^T)$ apparent resistivity values for parameter vector p given by Eq. (1) is:

$$f(p) = f\left(\rho_a^{(T)}(p, K_1^{(T)}), \rho_a^{(T)}(p, K_2^{(T)}), \ldots, \rho_a^{(T)}(p, K_I^{(T)})\right) \qquad (5)$$

where $K_i^{(T)}$ is the theoretical coefficient of the ith arrangement. All geoelectric sounding theoretical values are deduced from the well-known integral of Stefanesco and can be computed by digital filtering [see SALÁT, DRAHOS 1974 and DRAHOS, SALÁT 1975].

For EPGS the first group of quantities contains the field results of penetration soundings. Cone resistance ($RCPT^{(M)}$) and electrical resistivity ($RES^{(M)}$) are measured during penetration. Natural gamma ray ($GR^{(M)}$), density ($RHOB^{(M)}$), and neutron porosity ($NPHI^{(M)}$) are measured in the penetration steel tube after it has reached its maximum depth. The symbolic data vector for EGPS is:

$$y = y\left(RCPT^{(M)}, GR^{(M)}, RHOB^{(M)}, NPHI^{(M)}, RES^{(M)}\right) \qquad . \qquad (6)$$

The second group of quantities contains the corresponding tool response functions. The theoretical values of $f_k(p)$ logs at p parameter vector given by Eq. (2) or Eq. (3) form the vector:

$$f(p) = f\left(RCPT^{(T)}(p), GR^{(T)}(p), RHOB^{(T)}(p), NPHI^{(T)}(p), RES^{(T)}(p)\right) \qquad (7)$$

These two types of quantities relate to a depth point or they are the representative values for a preselected layer.

For quantitative inversion the theoretical tool response functions are [see SERRA 1986]:

$$GR^{(T)}(V_{cl}) = GR_{sd} + V_{cl}(GR_{cl} - GR_{sd}) \quad , \qquad (8)$$

$$RHOB^{(T)}(V_{sd}, V_{cl}, \phi, S_w) = \phi\, S_w \rho_w + V_{cl}\rho_{cl} + (1 - \phi - V_{cl})\rho_{sd} \quad , \qquad (9)$$

$$NPHI^{(T)}(V_{cl}, \phi, S_w) = \phi\, S_w + V_{cl}\phi_{Ncl} \qquad (10)$$

and

$$R_t^{(T)}(V_{cl},\phi,S_w) = \frac{1}{(\phi+V_{cl})^m}\left(\frac{\phi+V_{cl}}{\phi\,S_w+V_{cl}}\right)^2 \frac{1}{\dfrac{V_{cl}}{\phi\,S_w+V_{cl}}\dfrac{1}{R_{cl}}+\dfrac{\phi\,S_w}{\phi\,S_w+V_{cl}}\dfrac{1}{R_w}} \qquad (11)$$

is the theoretical resistivity of the soil.

In the above equations the so-called zone parameters are as follows:

GR_{sd}:	gamma ray activity of sand,
GR_{cl}:	gamma ray activity of clay,
ρ_w:	density of pore water,
ρ_{cl}:	density of clay,
ρ_{sd}:	density of sand,
ϕ_{Ncl}:	neutron porosity of clay,
R_w:	resistivity of pore water,
R_{cl}:	resistivity of clay,
m:	cementation exponent.

3. Basic principles of quality controlled geophysical technologies

3.1. Elements and operations of geophysical activity

Following the inversion theory of GOLZMAN [1971, 1982], ZVEREV [1974, 1979], and TARANTOLA [1987] the essential elements of any geophysical exploration are:

— q => the sources of the field data, i.e. the environment and the transmitter and the noises;

— y_k => the data set registered by the kth measuring configuration;

— x =>the unknown that is searched for or some appropriate environmental target model;

— $\hat{x}$ => the approximate solution for the unknown x or the final result or conclusion;

— $d(x,\hat{x})$=> the difference between the exact unknown x and the approximate solution $\hat{x}$.

The basic operations or transformations between the above-mentioned elements are:

— A => the field measurement or the data acquisition process;

— B => the data processing or the inversion;

— **C** => the purpose or the modelling of the environmental target or regularization. The **C** operation selects or defines the most wanted unknowns x of the sought target object q.

In that $x = Cq$ and $y = Aq$ and $\hat{x} = By = B(Aq)$, the theoretical formula for the actual individual error of the final result is:

$$d(x,\hat{x}) = d\{[Cq, B(Aq)]\} \tag{12}$$

An important requirement to be satisfied by the whole geophysical procedure is that it should provide minimal average errors of the conclusions. This formula has an important role in measurement planning and in the inversion.

Figure 1 outlines the above geophysical exploration processes.

$$d(x,\hat{x}) = d(Cq, By) = d(Cq, B(Aq))$$
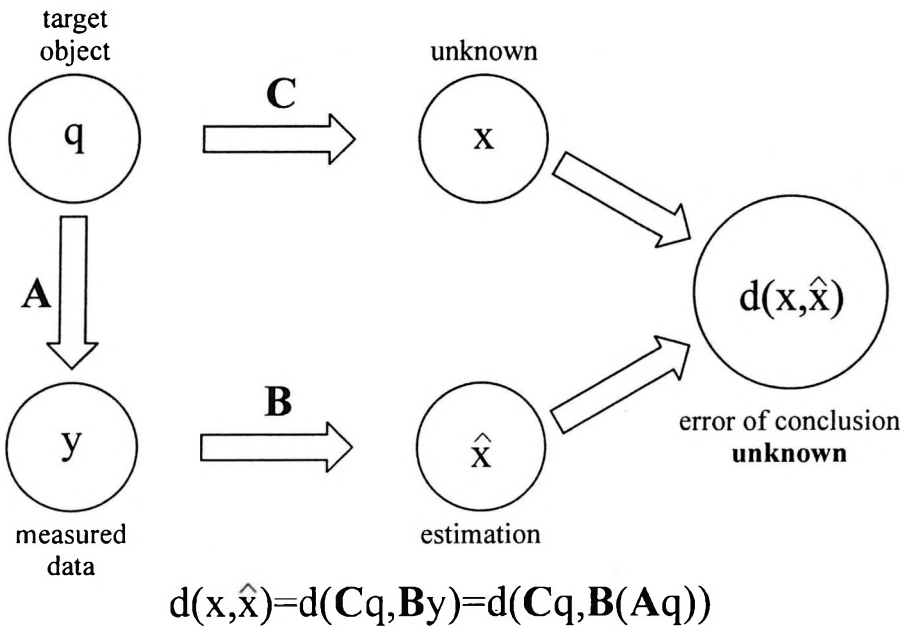
Fig. 1. Outline of geophysical exploration processes (modified scheme of ZVEREV [1974])
1. ábra. A geofizikai vizsgálatok folyamatábrája
(ZVEREV [1974] sémájának módosított változata)

3.2. Mathematical bases of quality management

The mathematical background of quality management of geophysical exploration can be found in GOLZMAN [1971, 1981, 1982], MENKE [1984, 1989] and TARANTOLA [1987]. The essence of these investigations is the

determination of the extremum of a statistical objective function. Such a function may be the

— $prd(x \mid y)$ posterior probability function, or the
— $prd(y \mid x)$ likelihood function, and the very often applied
— *WSSE* (Weighted sum of squared error) function, which has the form of:

$$WSSE(p) = \sum_k \frac{[y_k - f_k(p)]^2}{\sigma_k^2} = \min \Rightarrow \hat{p} \quad . \quad (13)$$

In this formula the variance σ_k^2 is the sum of the variances $(\sigma_k^{obs})^2$ and $(\sigma_k^{mdl})^2$ which variances respectively represent the error of the observation and the error of modelling, if they are uncorrelated:

$$\sigma_k^2 = \left(\sigma_k^{obs}\right)^2 + \left(\sigma_k^{mdl}\right)^2 \quad . \quad (14)$$

The covariance matrix $\mathbf{Cov}(\hat{p})$ of the results is the inverse of the so called Fisher-information matrix $\mathbf{Info}(\hat{p})$:

$$\mathbf{Cov}(\hat{p}) = \mathbf{Info}(\hat{p})^{-1} \quad (15)$$

The (I, j) elements of the information matrix in our case are given by:

$$Info_{i,j} = \sum_k \left[\left(\frac{\partial f_k(p)}{\partial p_i} \right) \cdot \frac{1}{\sigma_k^2} \cdot \left(\frac{\partial f_k(p)}{\partial p_j} \right) \right]_{p=\hat{p}} \quad . \quad (16)$$

The $\mathbf{Cov}(\hat{p})$ covariance matrix characterizes the accuracy of the results $\hat{p}$, its (i, j) element is $\sigma_i \sigma_j r_{ij}$. σ_i is the dispersion of the ith estimated parameter: the smaller its value, the greater the accuracy of the estimate. r_{ij} is the correlation coefficient which measures the level of the dependence between the ith and jth estimates.

4. Qualification of the data–modelling connection between VES and EGPS

4.1. Qualification for VES based on results of EGPS

The purpose of qualifying the data–model connection is to determine the magnitude of the dispersions σ_k. The direct method of determination is

experimental testing. It means that geophysical measurements are carried out on sites where the underground structure is well known from other investigations. The results of the other surveys should be at least one order more accurate than that of the geophysical method to be applied. *Figure 2* shows the scheme for qualifying the data–model connection of the geophysical exploration processes.
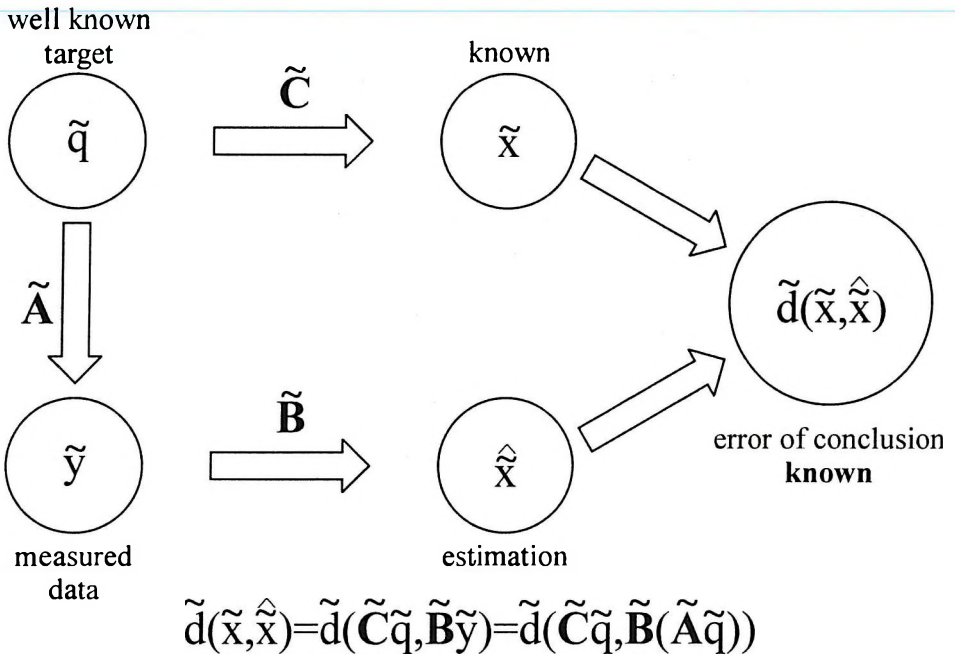
Fig. 2. Outline of the qualification analysis of the data–model connection of geophysical prospecting (modified scheme of ZVEREV [1974])

2. *ábra.* A geofizikai vizsgálatokban szereplő adat–modell viszony minősítés analízisének folyamatábrája (ZVEREV [1974] sémájának módosított változata)

With VES measurements the EGPS results can be used. From the EGPS measurements layer thicknesses and resistivities can directly be read. From these data VES theoretical apparent resistivities are computed and compared with the measured ones, and the statistics of the differences determine σ_k. Another known method for VES inversion on logarithmic scale is to assume that $\sigma_k = \sigma_0$ for $k = 1, 2, ..., N$. The common σ_0 can then be computed from the residuals.

4.2. Qualification of EGPS based on results of drillings

With regard to EGPS, the results of laboratory measurements on soil samples may form the basis for qualifying both qualitative and quantitative interpretations.

Table I contains the results of processing some 850 m penetration logs of RCPT, GR and RHOB. The soil samples were classified into the four lithological classes (clay ($v = 1$), sandy clay ($v = 2$), clayey sand ($v = 3$) and sand ($v = 4$)) after their visual inspection, and then the empirical means and dispersions of the corresponding log readings were calculated.

v (LITHO CLASS)	Number of samples	RCPT mean (bar)	RCPT dispersion (bar)	GR mean (cpm)	GR dispersion (cpm)	RHOB mean (g/cm^3)	RHOB dispersion (g/cm^3)
1	2707	27.4	21.4	1660	282	1.93	0.11
2	1358	56.4	26.4	1096	199	1.93	0.08
3	2014	79.2	30.7	828	150	1.96	0.08
4	2491	128.4	41.5	742	162	2.03	0.09

Table I. Empirical means and dispersions of RCPT, GR and RHOB penetration logs for different four lithological classes

I. táblázat. RCPT, GR és RHOB penetrációs mérésekre vontakozó empirikus várható értékek és szórások négy litológiai osztály esetén

Table II contains the first approximations of the dispersions for quantitative EGPS inversion which were determined in a similar manner to the dispersions of Table I.

Measurement	σ_k Dispersion	Unit
Gamma Ray	0.2 – 0.3	$GR_{cl}-GR_{sd}$
Density	0.05 – 0.1	g/cm^3
Specific resistivity	0.3 – 0.4	On log scale
Neutron porosity	0.05 – 0.1	On decimal scale

Table II. The σ_k dispersion intervals for different EGPS logs related to three component soil model

II. táblázat. A három komponensből álló talajmodellre vonatkozó σ_k diszperziós értéktartományok

The next step is taking into account these σ_k's in the evaluation and to compare the evaluated results with the original ones, i.e. the determination of the actual values of quantity $\tilde{d}(\tilde{x},\hat{x})$. If these values are not small

enough, there are various ways to intervene: changing the aim **C**, applying different measurement configuration **A**, or the algorithm **B** of evaluation can also be changed.

5. Examples for interpretation

5.1. Soil classification on the basis of EGPS logging data

The measured data were registered at a young alluvial region and the task was to classify the layers into the varieties in accordance with the model defined in section 2 (model a). The classification was done on the basis of the RCPT and GR logs. *Figure 3* shows the result of the classification.

The quality of the results of the classification was tested on more than 800 m length of penetration. Based on these studies the reliability of the classification was found to be 82 %.

5.2. Quality controlled quantitative evaluation of EGPS logs

A previous investigation [DRAHOS 2004] showed that the penetration electric log $RES^{(M)}$ holds real information about the soil resistivity, therefore in the following it is regarded as the measured value of the true resistivity $(R_t^{(M)})$ of the soil and it is combined with the measuring complex which now consists of the gamma ray $(GR^{(M)})$, the density $(RHOB^{(M)})$, the neutron porosity $(NPHI^{(M)})$, and the resistivity($R_t^{(M)}$).

Quality controlled formation evaluation of the measured penetration logs y_k was applied, which is widely used now in quantitative well log analysis, see MAYER, SIBBIT [1980], ALBERTY. HASHMY [1984], RODRIGUEZ et al. [1989] and CSEREPES et al. [1994a, 1994b]. The principle of quality controlled log evaluation is briefly described in section 3.2.

The measured values y_k of four different logs at a particular depth point or the representative ones for a preselected layer are $GR^{(M)}$, $RHOB^{(M)}$, $NPHI^{(M)}$, $R_t^{(M)}$. Their theoretical counterpart values computed for a soil model characterized by model parameters $p = p(V_{sd},\ V_{cl},\ \phi)$ (see formula (2)) are the theoretical tool response functions given by formula (8) for
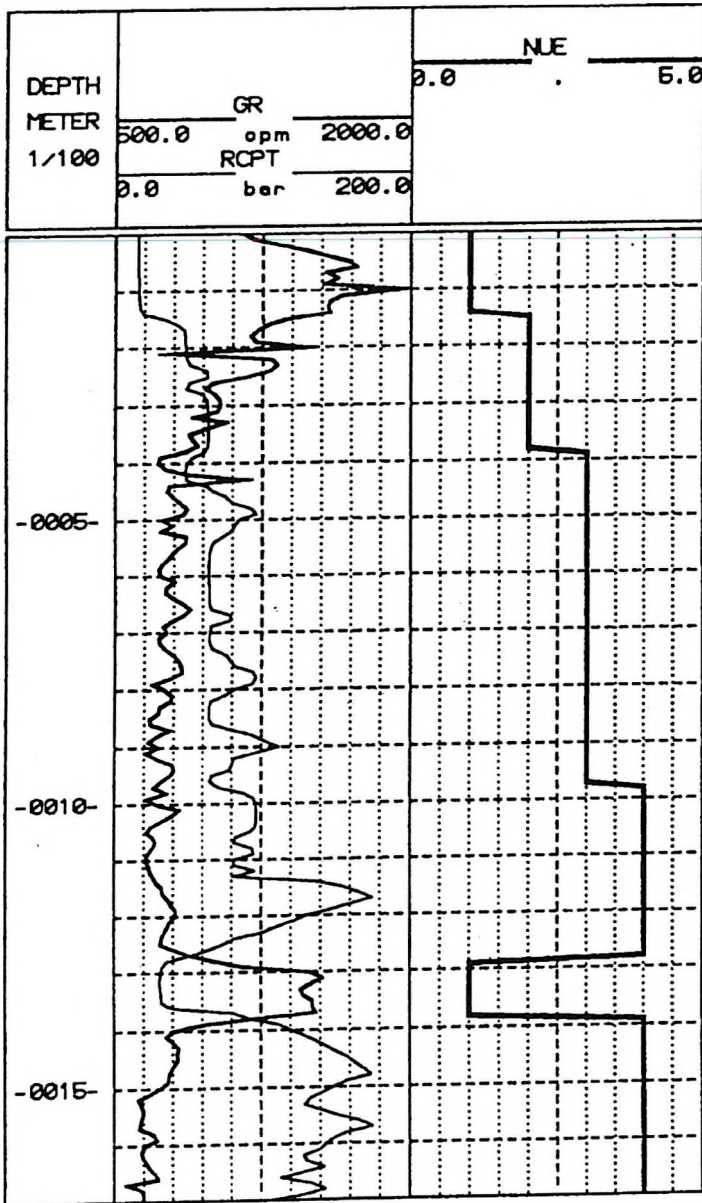
Fig. 3. Results of soil classification (NUE) based on gamma ray (GR) and cone resistance (RCPT) penetration logs (see Table I.)

3. ábra. A talajrétegek NUE minőségi osztályba sorolása természetes gamma (GR) és csúcsellenállás (RCPT) szelvények alapján az I. táblázat szerint

$GR^{(T)}(V_{cl})$, by formula (9) for $RHOB^{(T)}(V_{sd}, V_{cl}, \phi, S_w)$, by formula (10) for $NPHI^{(T)}(V_{cl}, \phi, S_w)$, and formula (11) for $R_t^{(T)}(V_{cl}, \phi, S_w)$.

Assuming normal probability distribution for the differences of the measured values y_k and the theoretical tool responses $f_k(p)$ with diagonal covariance matrix and applying the maximum likelihood estimator, one arrives at the weighted least squares criteria of (16), where σ_k^2 represents the variances relating to differences $\varepsilon_k = [y_k - f_k(p)]$ in the criterion function $WSSE(p)$:

$$WSSE(p) = \tag{17}$$

$$= \frac{[GR^{(M)} - GR^{(T)}(p)]^2}{\sigma_{GR}^2} + \frac{[RHOB^{(M)} - RHOB^{(T)}(p)]^2}{\sigma_{RHOB}^2} +$$

$$+ \frac{[NPHI^{(M)} - NPHI^{(T)}(p)]^2}{\sigma_{NPHI}^2} + \frac{[R_t^{(M)} - R_t^{(T)}(p)]^2}{\sigma_{RES}^2} =$$

$$= \min.$$

The soil model consists of sand and gravel (V_{sd}), of clay (V_{cl}), and of pore space (ϕ) saturated with water ($S_w = 1$). The following identity holds for them:

$$V_{sd} + V_{cl} + \phi = 1 \quad , \tag{18}$$

which means that there are only two unknowns ($p_1 = V_{cl}, p_2 = \phi$), and V_{sd} is calculated from (18). The applied theoretical tool response functions are the well-known formulae (8), (9), (10) and the resistivity equation of DeWitte's shaly sand model (11).

Fulfilling the condition (17) one gets the estimated values of the model parameters. The covariance matrix can also be determined by formulae (15) and (16):

$$\tag{19}$$

where
$$\mathbf{Cov}(\hat{p}) = \left(\mathbf{A}^{TRP} \mathbf{Cov}(\varepsilon)^{-1} \mathbf{A} \right)^{1}$$

$$A_{ki} = \left[\frac{\partial f_k(p)}{\partial p_i} \right]_{p=\hat{p}} \tag{20}$$

and $\mathbf{Cov}(\varepsilon)$ is the covariance matrix of the differences $\varepsilon_k = [y_k - f_k(p)]$:

$$\mathbf{Cov}(\varepsilon) \; = \; \begin{pmatrix} \sigma^2_{GR} & 0 & 0 & 0 \\ 0 & \sigma^2_{RHOB} & 0 & 0 \\ 0 & 0 & \sigma^2_{NPHI} & 0 \\ 0 & 0 & 0 & \sigma^2_{RES} \end{pmatrix} \qquad (21)$$

With regard to the determination of the dispersions σ_{AR}, σ_{RHOB}, σ_{NPHI}, σ_{RES} see Table II in section 4.2. Quality control is the reduced incoherence (RINC) proposed by MAYER, SIBBIT [1980]. The results of the quality controlled formation evaluation of engineering geophysical penetration sounding logs are shown in *Figs. 4* and *5*.
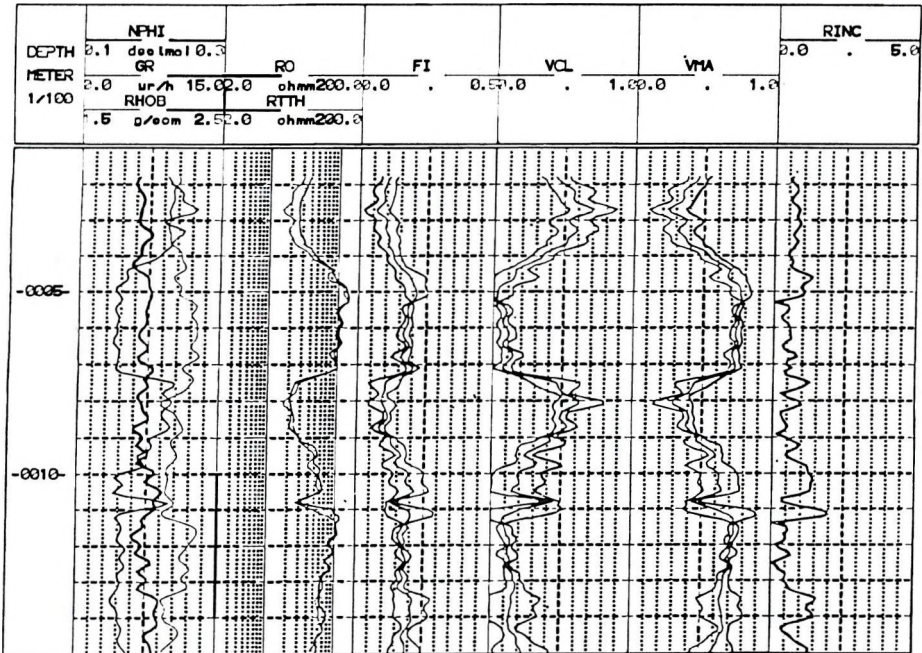
Fig. 4. Quantitative evaluation of gamma ray (GR), neutron (NPHI), density (RHOB) and resistivity (RO) EGPS logs. The volumetric ratio results are the porosity (FI), clay content (VCL) and sand content (VMA) with their plus-minus dispersion logs. The dimensionless RINC measures the overall quality of the evaluation

4. ábra. MGSZ szelvények (természetes gamma (GR), neutron porozitás (NPHI), sűrűség (RHOB) és fajlagos ellenállás (RO) adatsorainak) kvantitatív kiértékelése. Az eredmények a porozitás (FI), az agyagtartalom (VCL) és a homoktartalom (VMA) szelvények, plusz-minusz egyszeres szórásokkal együtt ábrázolva. A dimenziótlan RINC szelvény a formáció kiértékelés általános minősítésére szolgáló szelvény
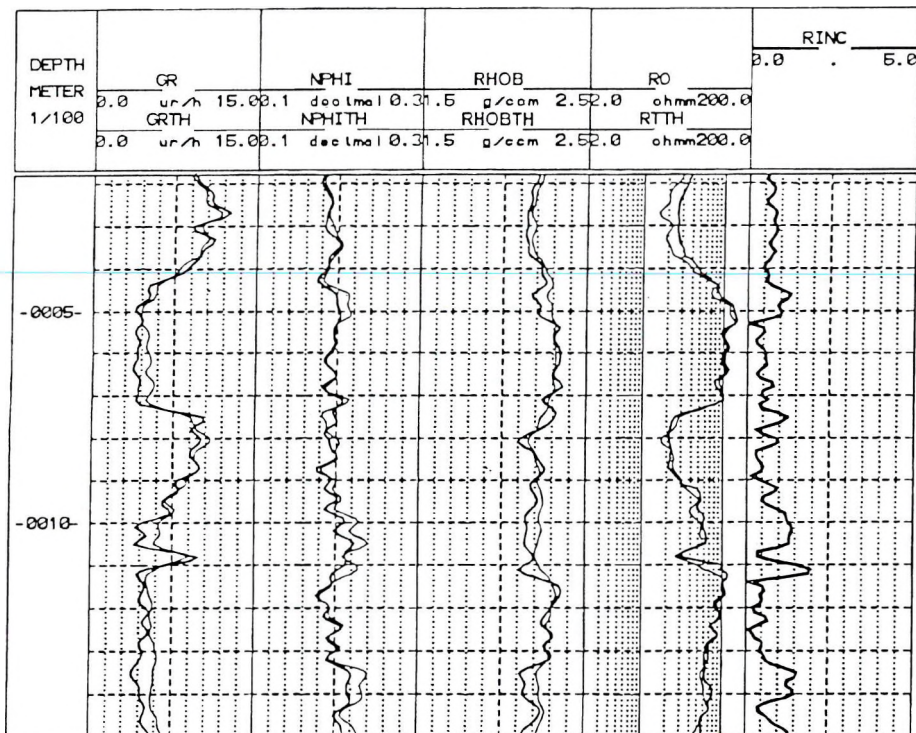
Fig. 5. Comparison of measured gamma ray (GR), neutron (NPHI), density (RHOB) and resistivity (RO) logs with the corresponding theoretical logs GRTH, NPHITH, RHOBTH and RTTH respectively

5. ábra. A mért GR, NPHI, RHOB, és RO szelvények összehasonlítása az elméleti GRTH, NPHITH, RHOBTH és RTTH szelvényekkel

5.3. Simultaneous qualitative–quantitative VES evaluation

The model which was applied is described in section 2.1 (model c) where, besides the layer parameters, the number of layers N belongs also to the unknowns. The statistical evaluation method was proposed by the authors SALÁT, DRAHOS [1974].

In *Fig. 6* there are evaluation results for two, three and four layer models for the same measured data. When the number of layers is increasing, the overall fitting between the measured and theoretical curves is decreasing. But on the contrary, the average uncertainty of the estimated parameters is increasing together with the highest correlation coefficients. The best result was achieved for the four layer model when a priori

One horizontal layer over basement

Deviation of fitting: **4.97%**

Results of the quality controlled inversion

$\hat{\rho}_1 = 20.9 \pm 0.35\ \Omega m\ (1.67\%)$

$\hat{\rho}_2 = 52 \pm 1.13\ \Omega m\ (2.17\%)$

$\hat{d}_1 = 3.7 \pm 0.24\ m\ (6.48\%)$

Average uncertainty: 3.44%

Highest correlation (between ρ_1 and d_1):   0.622

Two horizontal layers over basement

Deviation of fitting: **2.53%**

Results of the quality controlled inversion

$\hat{\rho}_1 = 25.4 \pm 1.34\ \Omega m\ (5.27\%)$

$\hat{\rho}_2 = 17.5 \pm 0.86\ \Omega m\ (4.91\%)$

$\hat{\rho}_3 = 51.3 \pm 0.55\ \Omega m\ (1.07\%)$

$\hat{d}_1 = 0.51 \pm 0.13\ m\ (25.5\%)$

$\hat{d}_2 = 2.41 \pm 0.29\ m\ (12\%)$

Average uncertainty: 9.75%

Highest correlation (between ρ_3 and d_2):   0.97

Three horizontal layers over basement

Deviation of fitting: **1.2%**

Results of the quality controlled inversion

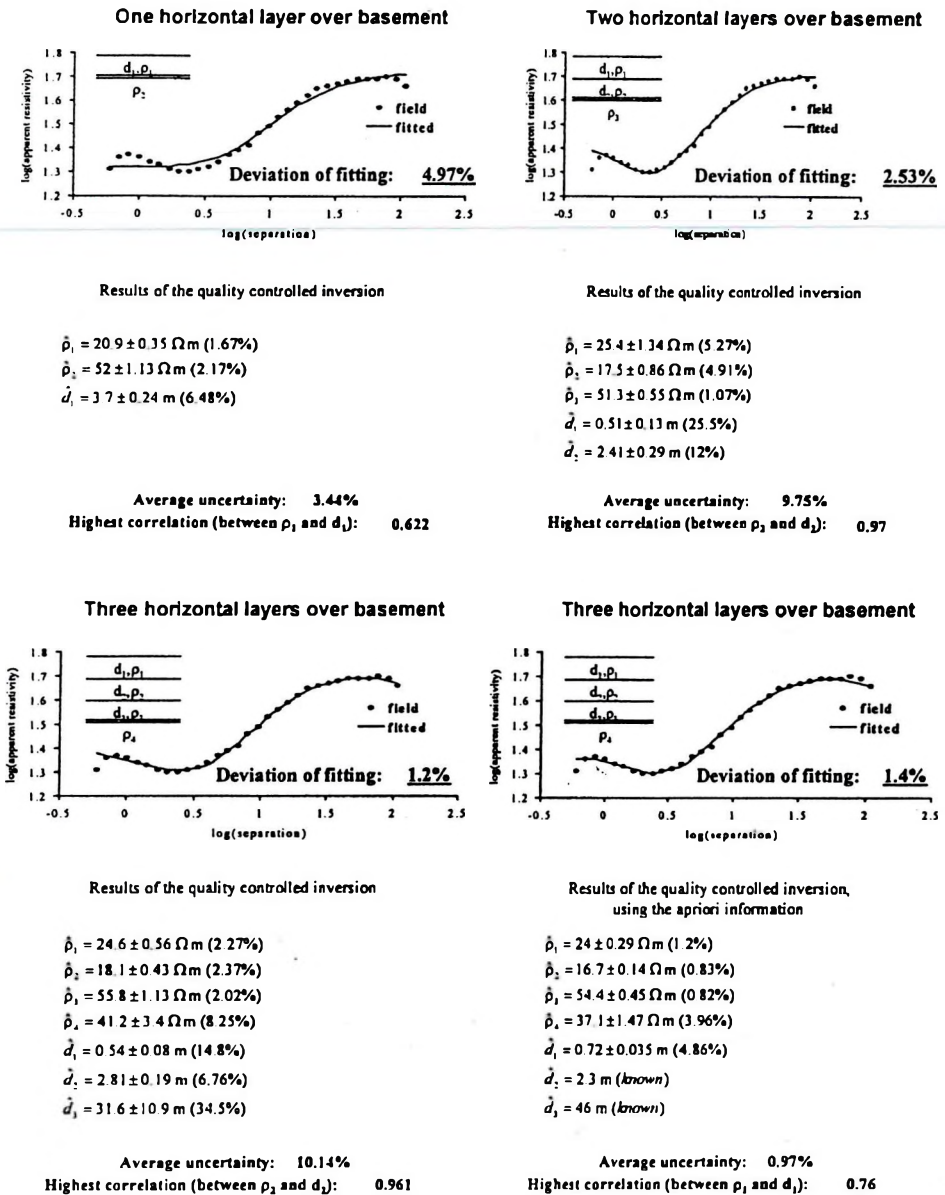$\hat{\rho}_1 = 24.6 \pm 0.56\ \Omega m\ (2.27\%)$

$\hat{\rho}_2 = 18.1 \pm 0.43\ \Omega m\ (2.37\%)$

$\hat{\rho}_3 = 55.8 \pm 1.13\ \Omega m\ (2.02\%)$

$\hat{\rho}_4 = 41.2 \pm 3.4\ \Omega m\ (8.25\%)$

$\hat{d}_1 = 0.54 \pm 0.08\ m\ (14.8\%)$

$\hat{d}_2 = 2.81 \pm 0.19\ m\ (6.76\%)$

$\hat{d}_3 = 31.6 \pm 10.9\ m\ (34.5\%)$

Average uncertainty: 10.14%

Highest correlation (between ρ_3 and d_3):   0.961

Three horizontal layers over basement

Deviation of fitting: **1.4%**

Results of the quality controlled inversion, using the apriori information

$\hat{\rho}_1 = 24 \pm 0.29\ \Omega m\ (1.2\%)$

$\hat{\rho}_2 = 16.7 \pm 0.14\ \Omega m\ (0.83\%)$

$\hat{\rho}_3 = 54.4 \pm 0.45\ \Omega m\ (0.82\%)$

$\hat{\rho}_4 = 37.1 \pm 1.47\ \Omega m\ (3.96\%)$

$\hat{d}_1 = 0.72 \pm 0.035\ m\ (4.86\%)$

$\hat{d}_2 = 2.3\ m\ (known)$

$\hat{d}_3 = 46\ m\ (known)$

Average uncertainty: 0.97%

Highest correlation (between ρ_1 and d_1):   0.76

Fig. 6. Results of simultaneous qualitative–quantitative evaluation of VES data, *field* means observed data, and *fitted* means theoretical model response

6. ábra. VES adatsorok mennyiségi–minőségi kiértékelésének eredményei, mért (*field*) és számított (*fitted*) értékek

information of d_2 and d_3 was built in, which came from EGPS measurements. In this case the average uncertainty was less than 1%, and the greatest value of the correlation coefficients was only 0.76.

Acknowledgement

REFERENCES

ALBERTY M., HASHMY K. H. 1984: Application of ULTRA to log analysis. Transactions SPWLA 25th Annual Well Logging Symposium, 1984.

BATEMAN R. M. 1985: Log quality control. IHRDC Publishers, Boston, 398 p.

CSEREPES L., DRAHOS D., SALÁT P. 1994a: Quality controlled log evaluation technique for water well logs in clastic sediments. Transaction of International Symposium on Well Logging 94' Xian, pp. 253–278

CSEREPES L., DRAHOS D., SALÁT P. 1994b: Quality controlled evaluation of well logs when prospecting for water. Hidrológiai Közlöny **74**, 4, pp. 233–245

DRAHOS D. 2004: On penetration electric sounding. Geophysical Transactions, this issue

DRAHOS D., SALÁT P. 1975: Applications of the linear filter theory in the direct and indirect interpretation of geoelectrical and well log measurements. Annales Univ. Sci. Budapest. R. Eötvös, Sec. Geologica **XVII**, pp. 113–132

GOLZMAN F. M. 1971: Statisticheskie modeli interpretacii. Izdat. Nauka, Moszkva, 327 pp.

GOLZMAN F. M. (editor) 1981: Statisticheszkaja interpretacija geofizicheskikh dannykh. Izdat. Leningrad. Univer., Leningrad, 255 p.

GOLZMAN, F. M. 1982: Fizicheskijj experiment I statisticheskie vyvodi. Izdat. Leningrad Univer., Leningrad, 191 p.

ISO 5725-1: 1994/Cor. 1. 1998: Accuracy (trueness and precision) of measurement methods and results. Part 1: General principles and definitions. European Standard, European Committee for Standardization, Brussels, 1994, 1998

ISO/IEC 17025. 1999: General requirements for the competence of testing and calibration laboratories, European Standard, European Committee for Standardization, Brussels, 1999

MAYER C., SIBBIT A. 1980: GLOBAL, a new approach to computer-processed log interpretation. SPE of AIME 55th Conference, Dallas, Paper No. 9341, pp. 1–12

MENKE W. 1984: Geophysical Data Analysis: Discrete Inverse Theory. Academic Press Inc., Orlando, 260 p.

MENKE W. 1989: Geophysical Data Analysis: Discrete Inverse Theory. Academic Press Inc., San Diego, 289 p.

RODRIGUEZ A., MEZZATESTA A., TERZLAFF D. 1989: Determination of statistical confidence intervals for petrophysical formation properties. Transactions, Log Analysis Software

Evaluation and Review (LASER) symposium, SPWLA London Chapter, 1989, paper 23, pp. 1–16

SALÁT P., DRAHOS, D. 1974: The strategy for the interpretation of surface and borehole electromagnetic soundings based on the information theory and the linear filter theory. Contributions, 19th Geophysical Symposium, Torun, 1974

SERRA O. 1986: Fundamentals of well-log interpretation, 2. The interpretation of logging data. Elsevier, Amsterdam, 684 p.

TARANTOLA A. 1987: Inverse Problem Theory, Methods for Data Fitting and Model Parameter Estimation. Elsevier, Amsterdam, 599 p.

ZVEREV G. N. 1974: K obobschennoj teorii obrabotki nabljudenij. Neftepromyslovaja Geofizika, Ufa, Vyp. 4, pp. 3–50

ZVEREV G. N. 1979: The theory of log interpretation. Transactions, SPWLA 20th Annual Logging Symposium, Paper C, pp. 1–31

Elektromos és penetrációs szondázások minőségellenőrzése

SALÁT Péter és DRAHOS Dezső

A dolgozat a minőségellenőrzés (QC) és minőségbiztosítás (QA) geofizikai alkalmazhatóságát vizsgálja mérnökgeofizikai szondázás és vertikális elektromos szondázás kutatómódszerek esetében. Ismerteti a minőségellenőrzés geofizikai technológiájának elveit, módszereit. Bemutatja a kutatandó objektumok modelljeit és a meghatározandó modell-paramétereket. Az alkalmazott kiértékelési módszerek: minőségi osztályozás, mennyiségi kiértékelés és összetett minőségi-mennyiségi kiértékelés.

ABOUT THE AUTHORS

Péter Salát is a geophysicist and an associate professor at Eötvös Loránd University at the Department of Geophysics. Since his graduation from the Eötvös Loránd University in 1962, he has been employed at the Department of Geophysics of Eötvös University. His Ph.D. degree is from Leningrad State University (1975). He lectures on 'Electrical Prospecting', 'Geophysical Inversion Theory', 'Engineering Geophysics', and 'Geophysics for Environmental Exploration'. His research activities include forward and inverse modelling in geophysics, measurements of penetration soundings, and the development and application of quality-controlled software for environmental and engineering geophysics.

Dezső Drahos, for a photograph and biography, see this issue, p. 220.

On penetration electric sounding

Dezső DRAHOS[*]

A comparison is made of a penetration resistivity log with a resistivity log measured in a drilled hole. From natural gamma ray and neutron porosity logs, clay content and porosity were estimated and then true resistivity was calculated on the basis of De Witte's shaly sand model and the Dual Water model. The approximation of the penetration resistivity log with the simulated true resistivity logs is acceptable.

Keywords: penetration sounding, resistivity log, Dual Water model, De Witte model

1. Introduction

A penetration geophysical complex consists of measurements of natural gamma ray, gamma-gamma density, neutron porosity, and specific apparent resistivity [FEJES, JÓSA 1990]. The last is a relatively new one because several technical difficulties had to be overcome to create the penetration electric sonde. A penetration electric sonde consists of ring shaped electrodes mounted on an insulating cylinder outside the steel penetration tube. Between the current and the voltage electrode there is a spacing of 5 cm, and the return current electrode is 20 cm from the current one. The reference electrode is on the surface. The whole length of the insulating cover on the steel tube is 30 cm. It can be supposed that the steel tube has a perturbation effect on the measured apparent resistivity, which probably depends on the length of the steel tube. Although theoretical modelling has not yet been used, there is evidence that the penetration measured apparent resistivity value differs only slightly from the true one.

[*] Eötvös Loránd University, Department of Geophysics, H–1112 Budapest, Pázmány Péter sétány 1/C
Manuscript received: 12 November, 2002.

2. Comparison of penetration and borehole electric measurements

Penetration and borehole electric measurements took place in the same field: the borehole and the penetration site were some 10 m apart. The borehole was drilled with mud having an apparent resistivity of 5 ohmm. Two apparent resistivity log curves were measured in the borehole, the usual short normal and a shorter one — with spacings of 40 cm and 10 cm respectively. From these, the true resistivity curve was calculated, to eliminate the borehole effect. No processing was carried out on the penetration resistivity curve. Depth matching was necessary in order to compare the penetration and the true resistivity curves (shown in *Fig. 1*). By comparing the two curves, it is seen that the penetration resistivity curve is much more rugose than the borehole true resistivity curve, probably due to its shorter spacing. Another finding is the systematic difference between the curves: the penetration resistivity has higher values than the other one, and the difference increases with increasing depth. Nevertheless the shapes of the curves are very similar, the correlation coefficient value is 0.866. Regardless of the fact that the measurement sites were not the same but only close to each other, there are other reasons for the difference. In both cases the environment is changed but in a different manner. For borehole electrical log the invasion process may change the resistivity, during penetration the soil environment is more or less compressed in the near zone thereby causing porosity decrease and resistivity increase. Another factor is the effect of the steel tube which has not been taken into account.

3. Simulation of penetration resistivity from other logs

At another site, where the water was polluted by sodium hydroxide, several penetration soundings were performed. The measuring complex consisted of natural gamma rays, neutron porosity, and resistivity. The soil environment was modelled with fine grain components (clay and silt) and coarse grain components (sand and gravel). The remaining part of the soil is the effective pore space. The volume of the fine grain components and that of the porosity are denoted by v_{cl} and ϕ respectively. The pore space was completely saturated with polluted water up to the surface.
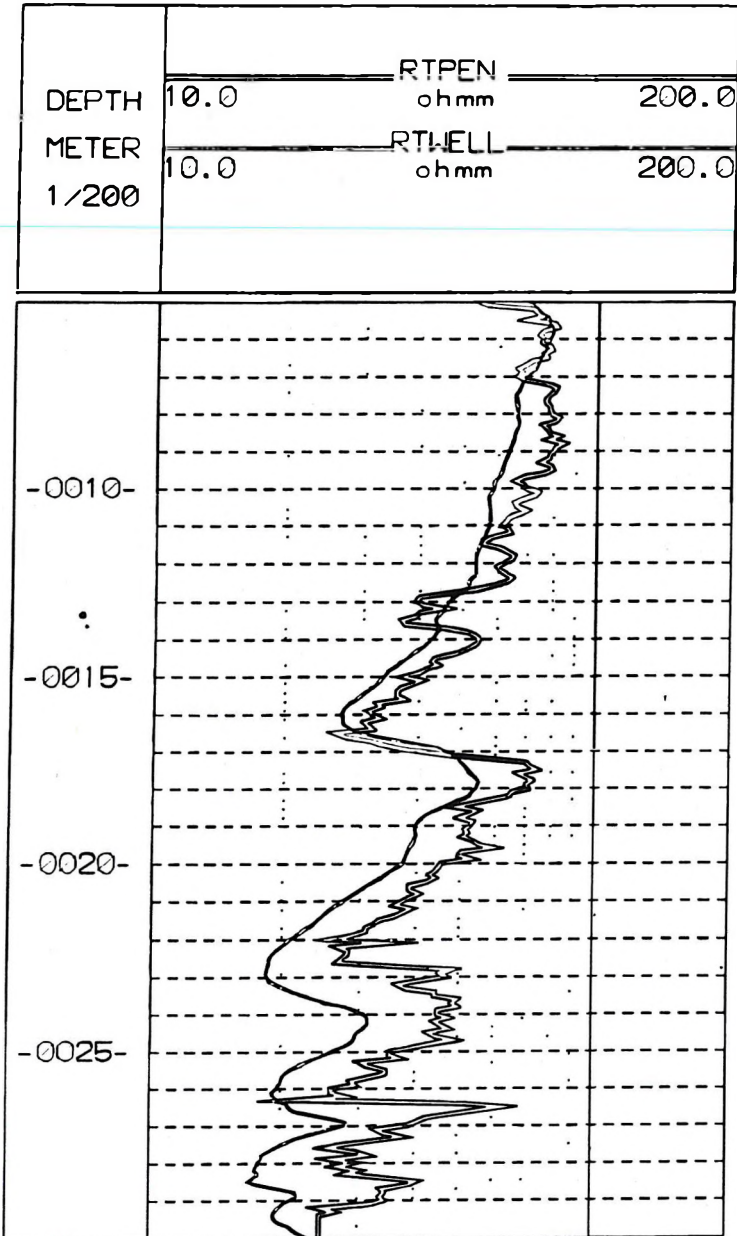
Fig. 1. Comparison of penetration (RTPEN) and borehole (RTWELL) resistivity logs
1. ábra. Penetrációs (RTPEN) és fúrásban mért (RTWELL) fajlagos ellenállás szelvények összehasonlítása

As is known, gamma ray logs are sensitive to clay, and the clay content can be estimated from gamma ray logs as follows:

$$v_{cl} = \frac{GR - GR_s}{GR_{cl} - GR_s} \tag{1}$$

where GR_{cl} and GR_s are the gamma ray activities of clay and sand respectively.

The neutron porosity (ϕ_N) log measures the soil's total hydrogen concentration, which comes from the movable free water and the bound water of clay. The neutron porosity of the clay is denoted by ϕ_{Ncl}:

$$\phi_N = \phi + v_{cl}\phi_{Ncl} \tag{2}$$

In the shaly-sand resistivity model of De Witte [SERRA 1984 p. 458] the free water and the electrically conducting clay are regarded as two components of a mixture of electrolytes that fill the generalized pore space ($\phi + v_{cl}$). From this model the following formula is deduced for the resistivity R_t of the shaly sand when the pore space is totally saturated with water:

$$R_t = F\left(\frac{q}{R_{cl}} + \frac{1-q}{R_w}\right)^{-1} \tag{3}$$

where F is Archie's formation resistivity factor relating to the generalized pore space and q the relative clay content:

$$q = \frac{v_{cl}}{\phi + v_{cl}} \quad . \tag{4}$$

R_{cl} and R_w are the resistivities of the clay and the water respectively.

The other model considered is the Dual Water shaly sand resistivity model (Schlumberger Document 1987, p.114), in which the conductance effect of the clay is taken into account as a consequence of the exchange cations close to the particle surfaces; these cations cause an increase in the conductivity of the bound water. The resulting conductivity C_{we} of the electrolyte in the pore space is the weighted average of the conductivities C_{wb} and C_w of the bound water and the free water respectively. The amount of bound water on a saturation scale is S_{wb}. By applying Archie's law and supposing that the pore space is totally saturated with water, the conductivity of the shaly sand is:

$$C_t = \phi_t^m C_{we} \tag{5}$$

where ϕ_t is the total porosity which includes the volume of bound water and free water and m is the cementation exponent. Without going into detail, the conductivity of the soil will be:

$$C_t = \phi_t^m (C_w + S_{wb}(C_{wb} - C_w)) \tag{6}$$

In order to calculate the conductivity one needs to know the values of ϕ_t, C_w, C_{wb} and S_{wb}. Neglecting the effect of the mineralogical composition of the soil on neutron measurement, as a first approximation:

$$\phi_t = \phi_N \tag{7}$$

$$C_{wb} = \phi_{Ncl}^m C_{cl} \tag{8}$$

and

$$S_{wb} = v_{cl}\phi_{Ncl} / (\phi + v_{cl}\phi_{Ncl}) \quad . \tag{9}$$

Rewriting Eq. (6) by applying Eqs. (7), (8) and (9) one arrives at:

$$R_t = C_t^{-1} = \phi_N^{-m} \left\{ \frac{1}{R_w} + \frac{v_{cl}\phi_{Ncl}}{\phi_N} \left(\frac{1}{\phi_{Ncl}^m} \frac{1}{R_{cl}} - \frac{1}{R_w} \right) \right\}^{-1} \quad . \tag{10}$$

Now there are two equations (Eq. (3) and Eq. (10)) depending on different earth models to calculate the resistivity of the soil from the neutron and the gamma ray logs. In addition to these, other quantities have to be known, viz. the constants or zone parameters. These are: GR_{cl}, GR_s, ϕ_{Ncl}, R_w, R_{cl}, R_{wb} and m. The value of R_w is known from direct electrolyte resistivity measurement, its value was 4.6 ohmm. The values of the other constants were determined first from the minimum and maximum log readings and then refined in order to reach a fairly good approximation between the synthetic and measured resistivity curves. The results are shown in *Fig. 2*. In the first track are the measured gamma ray and neutron porosity logs; the other two tracks contain the pairs of measured penetration resistivity logs and synthetic resistivity logs for the two model cases. There is a visual similarity between the synthetic and measured logs. On calculating the correlation coefficient we found the following values: 0.902 for De Witte's model and 0.884 for the Dual Water model.
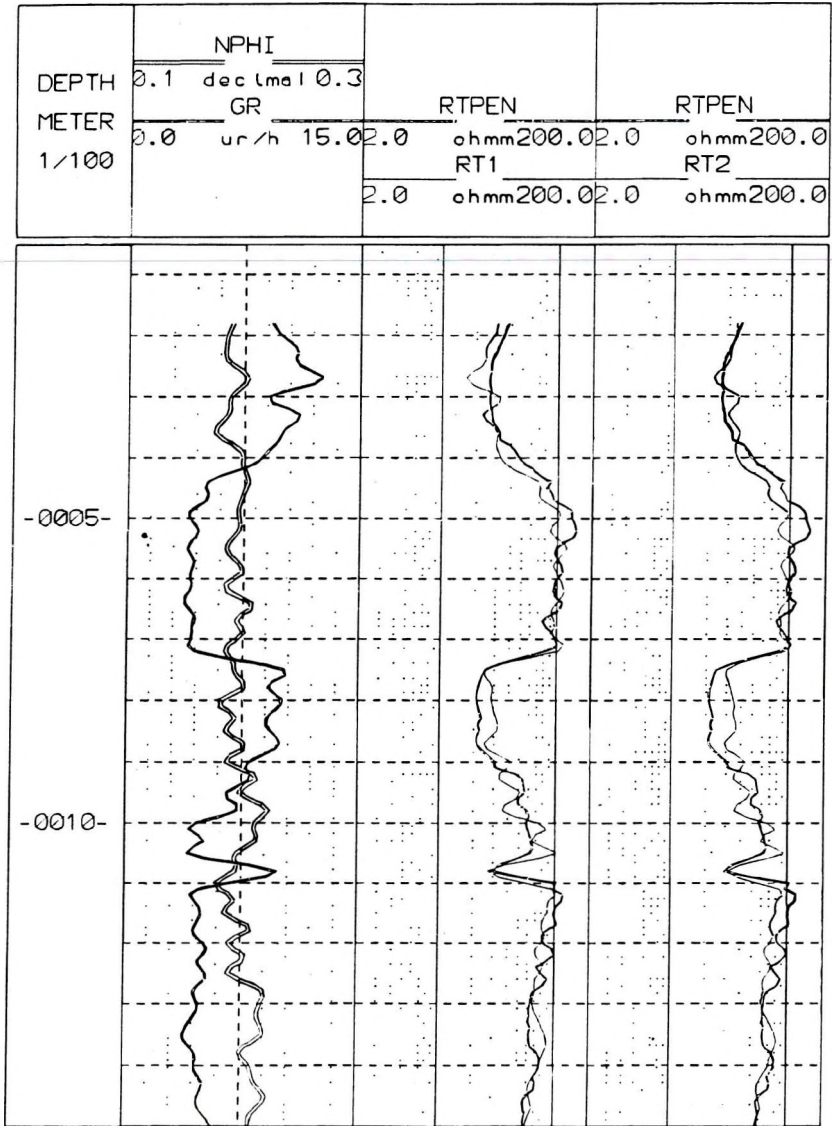
Fig. 2. Comparison of penetration resistivity (RTPEN) and simulated true resistivity logs RT1 and RT2 which were calculated from De Witte's and from the Dual Water model respectively. The other logs are neutron porosity (NPHI) and gamma ray(GR) .

2. ábra. Mért penetrációs fajlagos ellenállás szelvény (RTPEN) összehasonlítása természetes gamma (GR) és neutron (NPHI) szelvények alapján számított fajlagos ellenállás szelvényekkel. A számított szelvények:
RT1: De Witte modell alapján számított fajlagos ellenállás szelvény,
RT2: Dual Water modell alapján számított fajlagos ellenállás szelvény

4. Conclusion

Direct comparison of penetration and borehole resistivity measurements show convincing similarity, and the effect of the steel tube does not mask the effect of the soil environment. But if the magnitude of the tube effect is unknown, the answer is in theoretical modelling. The good approximation of the penetration resistivity log by shaly sand models proves their applicability in a soil environment and also proves that the penetration apparent resistivity is close to the true soil resistivity.

Acknowledgements

REFERENCES

FEJES I., JÓSA E. 1990: The engineering geophysical sounding method: Principles, instrumentation and computerized interpretation. *In:* S. H. WARD (Ed.), Geotechnical and Environmental Geophysics, Vol II: Environmental and Groundwater. Society of Exploration Geophysicists, Tulsa, OK, pp. 321–331

SERRA O. 1984: Fundamentals of Well-Log Interpretation, 1. The Acquisition of Logging Data, Elsevier, 423 p.

Schlumberger Document 1987: Log Interpretation/Applications, 198 p.

A mérnökgeofizikai elektromos szondázásokról

DRAHOS Dezső

A dolgozatban bemutatunk azonos területen fúrásban mért és penetrálás során fölvett fajlagos ellenállás szelvényeket, amelyek — kisebb eltérésektől eltekintve — hasonlóságot mutatnak. Egy másik kutatási területen a penetrációs mérés során természetes gamma szelvény és neutron-porozitás szelvény is készült, amelyekből porozitást és agyagtartalmat határoztunk meg. Ezek alapján szintetikus fajlagos ellenállás szelvényt számítottunk az agyagos homokkő modellekre vonatkozó De Witte és Dual Water modellek alapján. A szintetikusan előállított ellenállás szelvények jól megközelítik a mért penetrációs fajlagos ellenállás szelvényt.

ABOUT THE AUTHOR

Dezső Drahos graduated as a geophysicist from the Eötvös Loránd University, Budapest in 1967. He received his Ph.D. degree from the Hungarian Academy of Sciences in 1989. From 1967 to 1970 he worked as a scientific assistant at the Eötvös Loránd Geophysical Institute where he was involved in theoretical and experimental modelling of logging sondes. Since 1970 he has been at the Department of Geophysics of Eötvös Loránd University initially as a lecturer and, since 1991, as associate professor. Besides his teaching activities he is interested in geophysical inversion, well logging and petrophysics. He is a member of the Association of Hungarian Geophysicists, and also a member of SEG and SPWLA.

Bootstrap inversion of local earthquake data in the Pannonian Basin

Zoltán WÉBER[*]

Short-period waveforms of weak local earthquakes are inverted in order to retrieve the source mechanisms (moment tensors) for certain local events that occurred in the Pannonian Basin. Using the reflectivity method, synthetic Green's functions are computed for a given earth model for several hypocentral depths, and the moment tensor components are calculated by linear inversion. The shape of the source time function (STF) is also estimated. The moment tensor and event depth giving the best fit between the measured and synthetic seismograms are considered as the solution.

For the statistical validation of the results the bootstrapping technique is used. The estimated uncertainties in the resulting moment tensor components are plotted on the focal sphere in such a way that the significance of the double-couple, the compensated linear vector dipole, and the volumetric parts of the source can be assessed.

The moment tensor solutions for the selected events have an insignificant volumetric part, implying the tectonic nature of the events. The STFs are very simple, lasting 0.1–0.2 sec. The retrieved mechanisms are in agreement with the available clear readings of first-arrival P-wave polarities. The principal axes of the resulting source mechanisms also agree well with the main stress pattern published for the central part of the Pannonian Basin.

Keywords: earthquakes, waveform inversion, moment tensor, bootstrap resampling, Pannonian Basin

1. Introduction

Determination of mechanisms of weak local events is of prime interest while monitoring local seismicity, because these events reflect the stress pattern acting in the area under study and may help to map even its small-scale tectonic structure. Using analogue records, the only applicable method is to analyse the first motion polarities or, at most, the first amplitudes picked up from the seismograms. Such methods, which retrieve only a little information from the seismic records, often dominate digital data processing as well. However, digital instrumentation allows more advanced processing, aimed at earthquake source parameter retrieval, than

* Seismological Observatory of the Hungarian Academy of Sciences, H–1112 Budapest, Meredek u. 18.
Manuscript received: 25 October, 2002.

the classical methods of first arrival analysis. Provided that a structural model of the given region is available, synthetic seismograms generated by various types of source can be constructed and compared with observed records in a suitable inversion scheme.

Several methods for point source mechanism retrieval with simultaneous determination of the source time function for teleseismic events have been developed. Techniques for inverting normal-mode data [BULAND, GILBERT 1976], surface waves [McCOWAN 1976, AKI, PATTON 1978, KANAMORI, GIVEN 1981], and body waves [DZIEWONSKI et al. 1981, LANGSTON 1981, SIPKIN 1982, OLDENBURG 1982] have been presented. Some of these approaches also allow the source depth to be determined. Sophisticated source retrieval methods also exist for inverting near-source strong motion recordings [JI et al. 2002, SEKIGUCHI et al. 2002]. These approaches make use of near-source data recorded by dense accelerometer arrays.

There is a gap between the teleseismic and near-source approaches which is not tackled satisfactorily. For regional and local earthquakes the seismic network is usually not dense enough and the knowledge of the medium is not detailed enough to allow the reconstruction of a finite-source model as in near-source studies. In comparison with teleseismic waveforms, seismograms of regional and local events contain much higher frequencies thereby making the application of teleseismic approaches dubious [KOCH 1991a,b]. The use of higher frequencies requires more detailed models of inhomogeneous media for which the synthetic seismograms, specifically the Green's functions, should be computed.

This requirement was followed by SILENY et al. [1992] and MAO et al. [1994], who used the method of modal summation to compute Green's functions in a vertically inhomogeneous medium of very fine structure. To improve the results, they used dynamic relocalization of the depths of the events, i.e. they used amplitudes to relocate event depths determined from the kinematics. Their method has been successfully applied for inverting weak volcanic earthquake data [PANZA, SARAO 2000, SARAO et al. 2001].

The central part of the Pannonian Basin (mostly occupied by Hungary) can be characterized by fairly low seismicity with local earthquake magnitudes of mostly less than 3. Weak events are usually recorded at only a few stations, so reliable focal mechanism solutions can only be obtained by waveform inversion. In this study waveforms of weak local earthquakes are inverted in order to retrieve the source mechanisms (moment tensors)

and focal depths for certain events that occurred in the central part of Hungary. The method used slightly differs from that of SILENY et al. [1992] and it is capable of determining the uncertainties of the solution as well.

2. Theory

Central to any linear inversion of waveform data for the seismic source is the concept of the moment tensor. This representation was first proposed by GILBERT [1971] for studying the free oscillations of the earth. On using the moment tensor representation for body waves [AKI and RICHARDS 1980] one may write the *j*th component of the displacement field as

$$u_j(\mathbf{r},t)= \iint_S M_{kl}(\mathbf{r}',t)* G_{jk,l}(\mathbf{r},t;\mathbf{r}',0)\,\mathrm{d}S$$

where M_{kl} are the components of the moment density tensor, $G_{jk,l}$ are the elastodynamic Green's functions, $\mathbf{r}$ the position of the receiver, $\mathbf{r}'$ a point on the fault surface, and dS an element on the fault surface S. The symbol $*$ denotes temporal convolution. When considering only wavelengths for which S is effectively a point source, the entire surface may be considered as a system of couples operating at a point. The moment tensor is then defined as

$$M_{kl}(t)= \iint_S M_{kl}(\mathbf{r}',t)\,\mathrm{d}S$$

and

$$u_j(\mathbf{r},t)= M_{kl}(t)* G_{jk,l}(\mathbf{r},t;\mathbf{R}_0,0)$$

where $\mathbf{R}_0$ is the centroid of S. In general, this equation contains terms in both M_{kl} and $\dot{M}_{kl}$ (where a superscript dot denotes the time derivative) [AKI and RICHARDS 1980]. However, in view of the distance dependence of these terms and the symmetry of $\dot{M}_{kl}$, the far-field displacement can be written as

$$u_j(\mathbf{r},t)= \sum_{k=1}^{6} m_k(t)* g_{jk}(\mathbf{r},t;\mathbf{R}_0,0)$$

where $\mathbf{m}(t)$ is the vector containing the six independent elements of the moment rate tensor, i.e.

$$m_1(t) = \dot{M}_{11}(t) \qquad m_4(t) = \dot{M}_{13}(t)$$
$$m_2(t) = \dot{M}_{12}(t) \qquad m_5(t) = \dot{M}_{23}(t)$$
$$m_3(t) = \dot{M}_{22}(t) \qquad m_6(t) = \dot{M}_{33}(t)$$

and the g_{jk} are the corresponding Green's functions. This is the linear relationship upon which most inversion schemes depend.

For weak events, when the focal mechanism is considered as constant in time during the rupture process, all of the $m_k(t)$ components have the same time dependence $s(t)$. Then the far-field displacement seismogram is

$$u_j(\mathbf{r},t) = \sum_{k=1}^{6} m_k \cdot \left[s(t) * g_{jk}(\mathbf{r},t;\mathbf{R}_0,0) \right] \tag{1}$$

where **m** is the vector containing the six independent elements of the moment tensor (constants in time) and $s(t)$ is the source time function (STF).

3. The inversion procedure

According to Eq. (1) if the STF and the Green's functions (i.e. the velocity distribution and hypocentre coordinates) are known, the earthquake waveforms can be inverted for the unknown moment tensor elements by a linear procedure. However, the STF is usually unknown, and the velocity structure and hypocentre coordinates are only known with a degree of uncertainty. If, besides the moment tensor, all or some of these parameters are also treated as unknowns, the inversion problem becomes nonlinear.

In practice, routine event location techniques usually determine the epicentre coordinates acceptably well, while the hypocentre depth is usually poorly resolved. Since the Green's functions are very sensitive to the event depth, in the course of the moment tensor inversion procedure the event depth must be considered as unknown.

The velocity structure also has a strong effect on the Green's functions, so it, also should be treated as an unknown. However, the weak local events in the Pannonian Basin are usually recorded at only a few digital stations in view of which there are relatively few data. This fact simply does not allow us to increase the model space by the unknown velocity values and layer thicknesses. Moreover, variation of the velocity structure during the inversion process would require so much computer

time to continuously re-compute the Green's functions that routine application of the waveform inversion would not be economical.

Based on the above discussion, in the course of the waveform inversion procedure used in this study we carried out the following steps:

1) We estimated the source time function from the *P* form recorded at the station nearest to the event.

2) Keeping the routinely calculated epicentre coordinates as fixed parameters, we calculated Green's functions by the reflectivity method for several hypocentre depths and for all stations that recorded the event under consideration. We used the reflectivity method because it allows the entire wavefield for one-dimensional (1-D) earth models to be calculated.

3) We solved Eq. (1) for all possible depth values by a least squares linear inversion method in order to estimate the moment tensor. The best depth and moment tensor are given by the case that produces the smallest sum of squared error between the recorded waveforms and the calculated seismograms. The truncated singular value decomposition (TSVD) algorithm is used here to solve Eq. (1) [see, e.g. AKI, RICHARDS 1980, VAN DER SLUIS, VAN DER VORST 1987, XU 1998].

4) If we know the moment tensor and the Green's functions, we can again solve Eq. (1) to refine the STF.

5) We repeated steps 3 and 4 until the event depth, the STF, and the moment tensor components did not change considerably. The F-test known from statistics helps one to decide when to stop the iteration.

4. Bootstrapping

In order to determine the reliability of the solution of an inversion procedure, one must evaluate the variance of the model parameters. In many cases the model parameters are a linear function of the data, and model variance can be estimated by mapping the data variance to model space. However, estimation of data variance is a problem in itself. Because many geophysical data are non-reproducible (e.g. a certain earthquake cannot be repeated), it is not possible to verify any assumptions made with respect to the probability distribution of the data. A further difficulty in estimating model variance is that for many problems the physical relationship between data and model is nonlinear. For these cases it is often not possible

to find an analytical expression for model variance in terms of data variance.

As a means of overcoming the above mentioned difficulties it is recommended that the bootstrap resampling technique be used. This method is completely insensitive to the probability distribution of the data: the data do not have to follow a normal distribution and it is also not necessary that each item of data has equal variance. Furthermore, this technique allows evaluation of statistical properties that cannot be determined analytically. A short discussion of the mathematical basis of bootstrapping and its application to a geophysical inverse problem can be found in TICHELAAR, RUFF [1989].

A bootstrap resample is a random selection of n data out of n original data in such a way that any original item of data may be chosen more than once. This means that for an extreme case a particular resampled data set may consist of n identical observations of one of the original data items. If N bootstrapped data sets are created and all of them are inverted, we get N solutions for the model parameters. Then several statistical properties of the model parameters can be determined, such as standard deviation, mean, or median. It can also be very informative to plot the histograms of the estimated model parameters. The construction of confidence intervals is also possible.

The issue of what magnitude of N should be chosen to get a good estimate of the model variance is not settled yet. EFRON and TIBSHIRANI [1986] give rough estimates of N and show that $N\sim100$ is a reasonable value for the bootstrap estimate of the standard deviation. However, in order to estimate confidence intervals a much larger N ($O(1000)$) is required. Because the bootstrap technique requires the full inverse problem to be solved N times, it is clear that the use of this method is computationally a very demanding job, particularly when confidence intervals are desired.

In our inversion problem the model space consists of the moment tensor elements, the event depth, and the STF. After all, the relation between them and the data (waveforms) is nonlinear. Moreover, it is very difficult to estimate data uncertainty and the errors introduced by the use of an inadequate velocity model. From the above discussions it follows that the bootstrap technique appears to be the only appropriate method for estimating model uncertainties.

5. Data

The waveform data used in this study were recorded by the three-component seismological stations of the Microseismic Observation Network of Paks (MONP), maintained by Georisk Ltd. in Hungary (*Fig. 1*). The transfer functions of the velocity instruments are flat above 1 Hz. To remove low- and high-frequency numerical effects from the records, a causal bandpass filter from 1 to 5 Hz was applied to the time series after transforming them to displacement. The same filter was applied to the displacement Green's functions. The synthetic seismograms were calculated with a sampling interval of 0.024 s. As the data were originally sampled at 125 Hz, they were resampled to match the sampling interval of the Green's functions.

For the three events studied (circles in Fig. 1) the network was azimuthally well distributed. Because of the small location uncertainties of 1–2 km, the epicentre coordinates were taken from the Hungarian Earth-
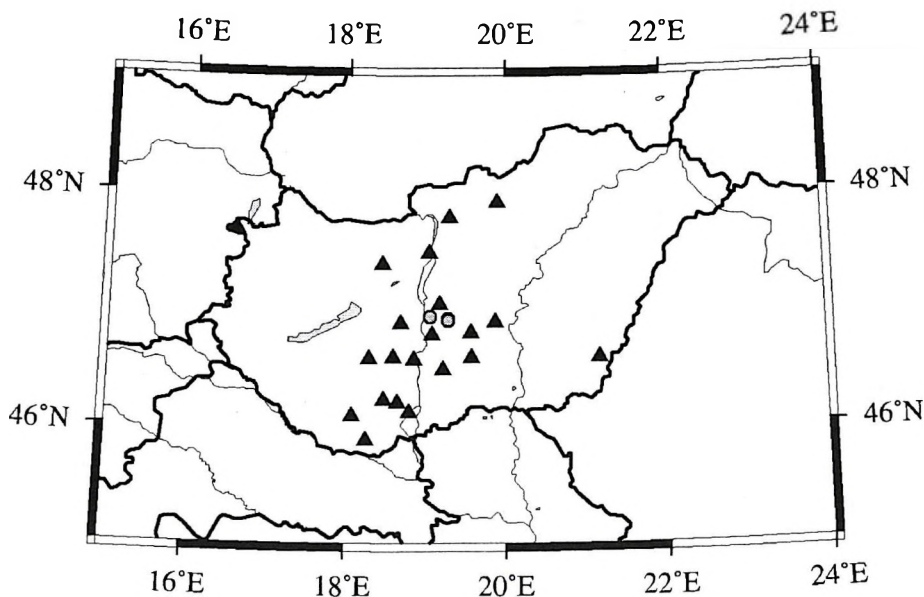
Fig. 1. Map showing the epicentres of the events (circles) selected for the present study together with the digitally equipped seismological stations. Two events occurred at practically the same epicentral coordinates

1. ábra. A jelen tanulmányban feldolgozott földrengések epicentrumai (körök) és a digitális szeizmológiai hálózat állomásai (háromszögek). Két esemény epicentruma gyakorlatilag megegyezik

quake Bulletin [TÓTH et al. 1996, 1997, 2001]. However, hypocentre depths were considered as unknown parameters to be determined by the waveform inversion process.

For generating the Green's functions, the reflectivity method [MÜLLER 1985] was used, since this allows the entire wavefield for 1-D velocity models to be calculated. It is by no means easy to construct a suitably detailed velocity function required for inverting local waveform data. For this study we derived a rather simple velocity model from measured traveltimes of local earthquakes and controlled seismic sources (*Fig. 2*).

Since epicentral distances usually range from a few tens of kilometers to 100–200 km with a wide range of event–station azimuths, if one uses the same simple velocity structure for all event–station pairs it is almost
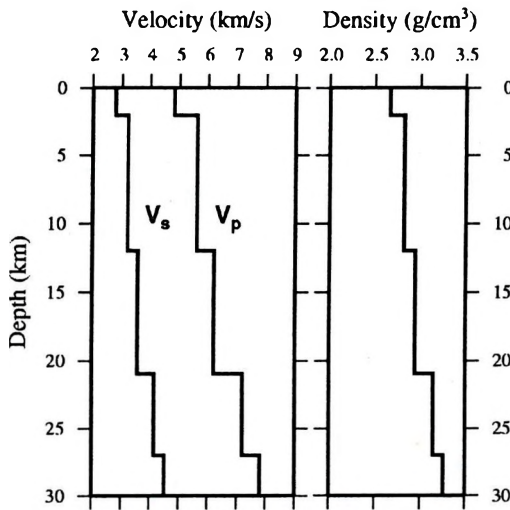
Fig. 2. 1-D earth model used for calculating Green's functions with the reflectivity method. The *P* velocities are deduced from measured traveltimes of local earthquakes and controlled seismic sources. The *S* velocity is assumed to follow v_P as $v_S = v_P/\sqrt{3}$. For density, another empirical law is used: $\rho = 1.7 + 0.2v_P$. In this study the earth model is not varied during the inversion process

2. ábra. A szintetikus Green-függvények számításához használt 1-D földmodell. A *P* hullámsebességeket lokális földrengések és felszíni robbantások első beérkezési időadatainak felhasználásával határoztuk meg. Az *S* hullámsebességekről feltételeztük, hogy a $v_S = v_P/\sqrt{3}$ összefüggés szerint követik v_P-t. A sűrűség meghatározásához szintén egy empirikus összefüggést használtunk: $\rho = 1.7 + 0.2v_P$. A földmodellt ismertnek tételeztük fel az inverzió során

inevitable that inconsistencies will be introduced. The effects of inadequacies of the structural models were investigated by SILENY et al. [1992] and KRAVANJA et al. [1999]. They proved, by synthetic tests, that a poorly known velocity structure: (1) introduces apparent non-double-couple components in the moment tensor solutions; (2) contaminates particularly the CLVD, which may be as large as 40 per cent; (3) maintains the orientation of the double-couple within ±10°; and (4) leads to spurious peaks in the source time function [KRAVANJA et al. 1999].

An inadequate velocity structure is certainly not capable of predicting the reflected and converted waves arriving between the first *P*- and *S*-waves. So, in order to reduce the above-mentioned effects on the inversion results, only the first *P*- and/or *S*-waveforms were inverted. The use of *S*-waves in the inversion process may be crucial when the first *P*-arrival is too small in amplitude to trigger the instrument (i.e. it is absent from the seismogram) or its signal-to-noise ratio is too small. If one includes *S*-waves in the calculations it also helps to constrain the solution.

6. Iversion results

Displacement seismograms derived from the observed velocity recordings were used to invert for the seismic moment tensors and source time functions of three local earthquakes. The epicentres of the three events were close to each other in the central part of Hungary (Fig. 1). Only waveforms with a good signal-to-noise ratio were used in the inversion process.

The inversion results for the local event that occurred on June 9, 1995 near Szabadszállás are presented in *Fig. 3*. The map depicts the position of the epicentre and the seismological stations used in the calculations. To the left of the map the observed seismograms (bold lines) and the synthetic waveforms (thin lines) computed using the inverted source parameters are compared. On the left-hand side of each seismogram the station name, component, and wave type are indicated, while to the right the epicentral distance is given in kilometers. The numbers above each waveform represent the normalized correlation (*Corr*), the normalized mean squared error (*nmse*), and the maximum amplitude in nanometers (*amp*). Since the earth model is rather uncertain, only the first *P*- and *S*-waves could be inverted successfully.
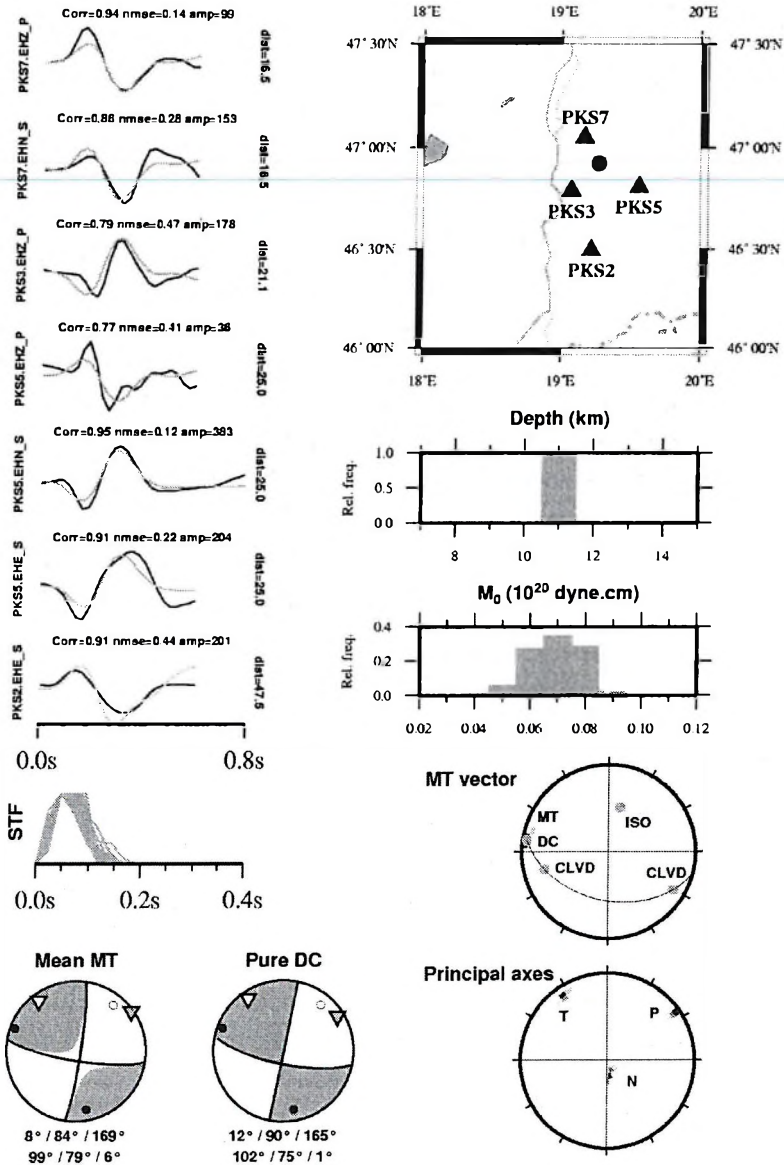
Szabadszállás [1995/06/09]

Fig. 3. Waveform comparison and moment tensor solution for the local event that occurred on June 9, 1995 near Szabadszállás, Hungary. For details, see text

3. ábra. A Szabadszállás közelében, 1995. június 9-én kipattant lokális földrengés inverziójával kapott fészekparaméterek, valamint a mért és számított hullámformák. Részleteket lásd a szövegben

For the statistical validation of the results the bootstrapping technique was used. In this study the uncertainties of the solution are estimated by inverting 300 bootstrapped data sets. The histograms of the inverted source parameters obtained after the 300 bootstrap inversions may be considered as good approximations of the corresponding confidence regions. The method of RIEDESEL and JORDAN [1989] is employed to display the histogram of the moment tensor solution. The principal vectors of a moment tensor define the tension (T), the neutral (N) and compression (P) axes, while the principal values give their magnitudes. It is a straightforward matter to construct and display the histograms of the principal axes (bottom right plot in Fig. 3). In the principal axis system, various unit vectors can be constructed using various combinations of the principal values. The vector that describes a general source mechanism is MT, a double-couple source mechanism has the vector representation DC, the vector corresponding to a purely isotropic source is the vector ISO, and two possible CLVD vectors can also be defined [JOST, HERRMANN 1989]. The histograms of the MT vectors, together with the DC, ISO, and CLVD vectors corresponding to the mean moment tensor solution are then plotted on the surface of the focal sphere. The great circle that connects the DC and CLVD vectors on the unit sphere defines the subspace on which MT must lie for a deviatoric source. The distribution of the MT solutions with respect to the DC, ISO, and CLVD vectors allows us to assess the significance of the DC, ISO, and CLVD parts of the solution.

Below the histograms of event depth and scalar moment in Fig. 3, the histograms of the MT vector and the principal axes can be seen. The histogram of the moment tensor vector (MT) contains the DC vector: thus, a pure DC may be the solution of the inversion. The tightly confined zones of the principal axes allow only a small variation of the orientation of the mechanism. The P-axis strikes NE–SW, which is in accordance with the stress field in the central part of the Pannonian Basin [BADA et al. 1998]. The plot of the 300 calculated STFs below the seismograms in Fig. 3 shows that the source time function is also well constrained and it has a simple peak with a time duration of about 0.1–0.15 s.

The beach ball representation of the mean focal mechanism is also shown in the bottom left corner of Fig. 3 (shaded area: compression; open area: dilatation; open triangle: T-axis; solid triangle: P-axis). The fault plane solution given below the beach ball corresponds to the best double-couple part of the general mechanism. Clear readings of *P*-wave

polarities are also shown (open circle: dilatation; solid circle: compression).

In order to justify the pure DC solution of the problem, the selected waveforms were also inverted with the constraint that the source be a double-couple. Since this constraint is nonlinear, a grid search algorithm was used. Using the average source time function calculated from the earlier mentioned 300, we searched for the strike, dip, and slip angles giving the best fit between the observed and synthetic seismograms. The beach ball representation of the resulting fault plane solution is given next to the beach ball of the mean MT solution in Fig. 3. The pure DC solution is very similar to the DC component of the general MT solution and there is no significant difference between the waveform misfits produced by the two solutions.

The inversion results for the local event that occurred on March 28, 1996 near Szabadszállás are presented in *Fig. 4*. The epicentral coordinates of this event are almost identical to those of the previously discussed earthquake. The structure of Fig. 4 is similar to that of Fig. 3.

The uncertainty of the solution is larger than in the previous case. The MT histogram contains the locus of deviatoric solutions and it also touches the DC vector. Thus, the DC may also represent the solution of the problem. The azimuth of the P-axis is well constrained and it strikes NE–SW, which is in accordance with the stress field in this region of Hungary [BADA et al. 1998]. The source time function has only one significant peak whose time duration is about 0.1 s. The pure DC solution of the grid search algorithm is almost identical to the DC component of the general MT solution. Since the synthetic waveforms fit the observed seismograms equally well for both solutions, the pure double-couple mechanism can be considered as justified. The apparent non-DC components in the moment tensor solution are probably due to the inconsistent velocity model used for computing the Green's functions.

The third investigated local event occurred on November 23, 2000 near Kunadacs. The inversion results for this earthquake are presented in *Fig. 5*. The structure of Fig. 5 is similar to that of Figs. 3 and 4.

The uncertainty of the solution is the largest among the three discussed in this paper. The histogram of the moment tensor vector (MT) again contains the locus of the deviatoric solutions and, particularly, the DC vector. Thus, a DC may also be acceptable as the solution of the inversion problem. The azimuth of the P-axis spreads about 30°. However, it undoubtedly
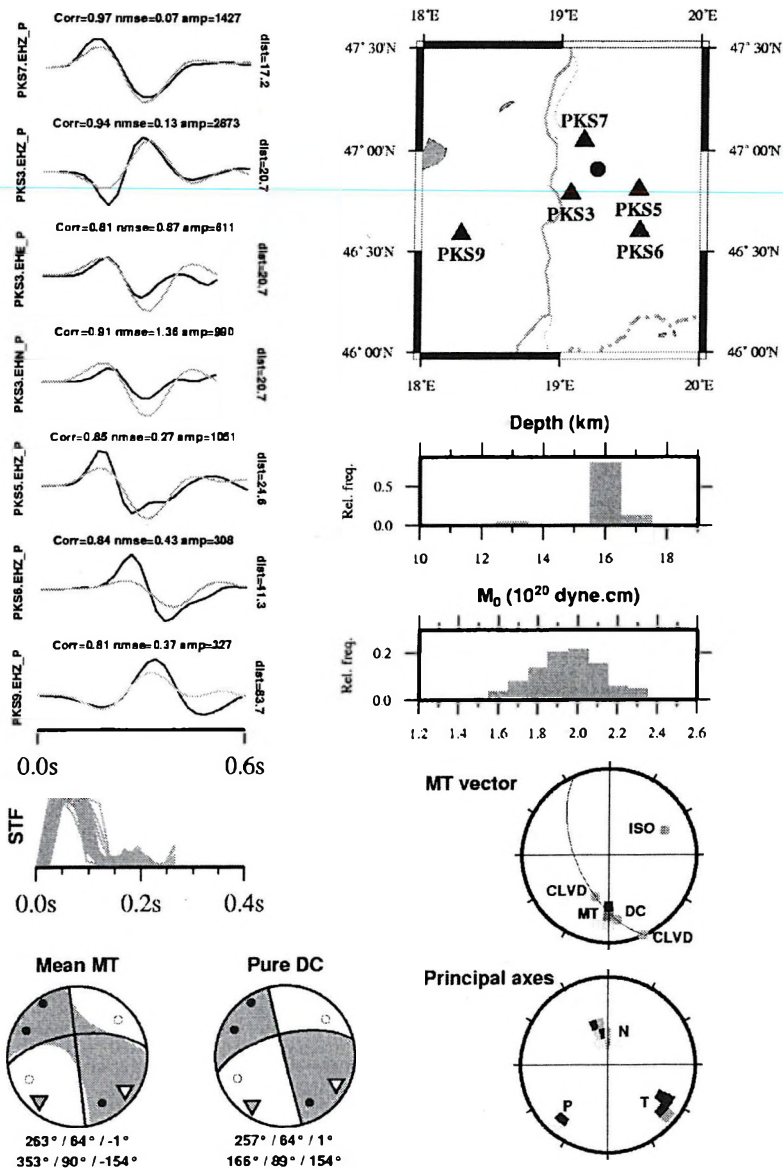
Szabadszállás [1996/03/28]

Fig. 4. Waveform comparison and moment tensor solution for the local event that occurred on March 28, 1996 near Szabadszállás, Hungary. For details, see text

4. ábra. A Szabadszállás közelében, 1996. március 28-án kipattant lokális földrengés inverziójával kapott fészekparaméterek, valamint a mért és számított hullámformák. Részleteket lásd a szövegben
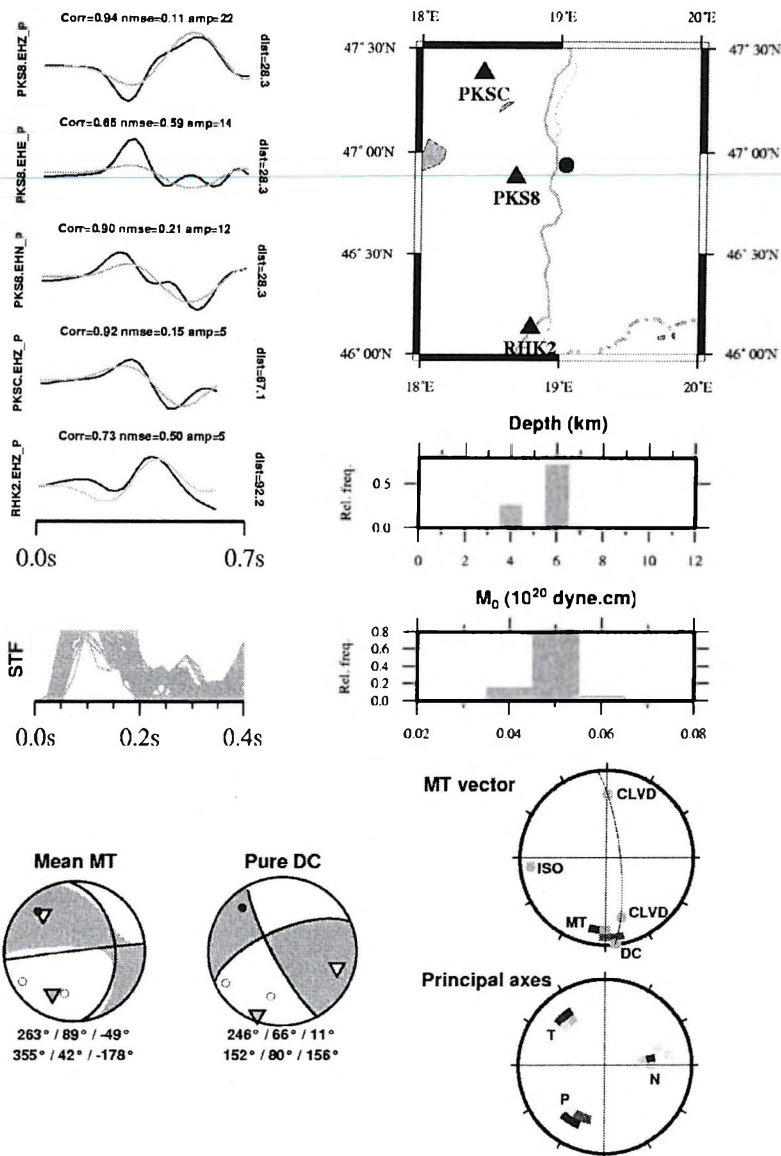
Kunadacs [2000/11/23]

Fig. 5. Waveform comparison and moment tensor solution for the local event that occurred on November 23, 2000 near Kunadacs, Hungary. For details, see text

5. ábra. A Kunadacs közelében, 2000. november 23-án kipattant lokális földrengés inverziójával kapott fészekparaméterek, valamint a mért és számított hullámformák. Részleteket lásd a szövegben

strikes NE–SW, which agrees well with the main stress pattern in this region [BADA et al. 1998]. The source time function has only one significant peak with a time duration of about 0.2 s. Although the pure DC solution of the inversion problem differs from the DC component of the general MT solution, the main features remain the same: the differences between the strike angles and the azimuths of the *P*-axes are rather small. It should also be taken into account that besides the use of the inconsistent earth model in the calculations, the main sources of the relatively large uncertainties of the solution are the irregular station coverage and the low signal-to-noise ratio. The ambient noise contaminating the low-amplitude signals is the main cause of the apparent ISO component in the moment tensor solution [SILENY et al. 1992].

7. Conclusions

The method illustrated in this paper is capable of retrieving simultaneously the hypocentral depth, the source time function, and the full seismic moment tensor of weak local earthquakes from waveform data even when the only records available are a few noisy ones. Error analysis, carried out by the bootstrap resampling technique, allows us to estimate and display the uncertainties of the event depth, scalar moment, the STF, and the moment tensor solution and its *T*-, *N*- and *P*-axes. This makes it possible to assess the significance of the DC, ISO, and CLVD parts of the solution.

The method has been applied to three local earthquakes that occurred in the central part of the Pannonian Basin. The inversion of the short-period records was successful. The non-DC components of the moment tensor solutions for the selected events are insignificant, implying the tectonic nature of the events. The source time functions obtained during the inversion process are very simple with a time duration of 0.1–0.2 seconds. The retrieved mechanisms are in agreement with the available clear readings of first-arrival *P*-wave polarities. The principal axes of the resulting source mechanisms also agree well with the main stress pattern published for the central part of the Pannonian Basin (*Fig. 6*).
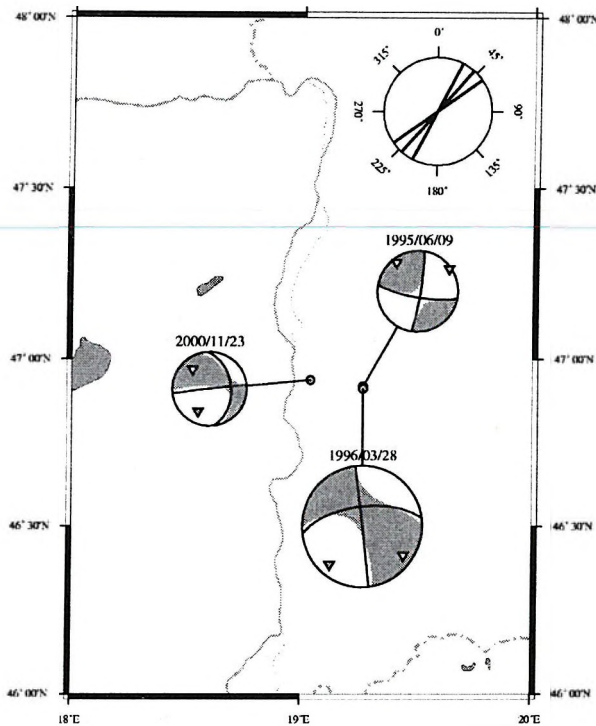
Fig. 6. Map showing the mean focal mechanisms obtained by waveform inversion. The diagram in the top-right corner of the Figure illustrates the horizontal projections of the P-axes. The azimuths of the P-axes are in good agreement with the main stress pattern published for the central part of the Pannonian Basin. Beach ball diameters are proportional to moment magnitude

6. ábra. A hullámforma inverzióval kapott átlagos fészekmechanizmusok. Az ábra jobb felső sarkában látható diagram a P tengelyek horizontális vetületét ábrázolja. A P tengelyek iránya jó egyezést mutat a szakirodalomban publikált fő feszültésgiránnyal. A "strandlabdák" átmérője arányos a momentum magnitudójával

Acknowledgments

REFERENCES

AKI K., PATTON H. 1978: Determination of seismic moment tensor using surface waves. Tectonophysics **49**, pp. 213–222

AKI K., RICHARDS P. 1980: Quantitative Seismology: Theory and Methods. Freeman, San Francisco

BADA G., CLOETHING S., GERNER P., HORVÁTH F. 1998: Sources of recent tectonic stress in the Pannonian region: inferences from finite element modelling. Geophysical Journal International **134**, pp. 87–101

BULAND R., GILBERT F. 1976: Matched filtering for seismic moment tensor. Geophysical Research Letters 3, pp. 205–206

DZIEWONSKI A. M., CHOU T.-A., WOODHOUSE J. H. 1981: Determination of earthquake source parameters from waveform data for studies of global and regional seismicity. Journal of Geophysical Research **86**, pp. 2825–2852

EFRON B., TIBSHIRANI R. 1986: Bootstrap methods for standard errors, confidence intervals, and other measurements of statistical accuracy. Stat. Sci. **1**, pp. 54–77

GILBERT F. 1971: Excitation of the normal modes of the earth by earthquake sources. Geophysical Journal of the Royal Astronomical Society **22**, pp. 223–226

JI C., WALD D. J., HELMBERGER D. V. 2002: Source description of the 1999 Hector Mine, California, earthquake, part I: Wavelet domain inversion theory and resolution analysis. Bulletin of the Seismological Society of America **92**, pp. 1192–1207

JOST M. L., HERRMANN R. B. 1989: A student's guide to and review of moment tensors. Seismological Research Letters **60**, pp. 37–57

KANAMORI H., GIVEN J. W. 1981: Use of long-period surface waves for fast determination of earthquake source parameters. Physics of the Earth and Planetary Interiors **27**, pp. 8–31

KOCH K. 1991a: Moment tensor inversion of local earthquake data. I. Investigation of the method and its numerical stability with model calculations. Geophysical Journal International **106**, pp. 305–319

KOCH K. 1991b: Moment tensor inversion of local earthquake data. II. Application to aftershocks of the May 1980 Mammoth Lakes earthquakes. Geophysical Journal International **106**, pp. 321–332

KRAVANJA S., PANZA G. F., SILENY J. 1999: Robust retrieval of seismic point source time function. Geophysical Journal International **136**, pp. 385–394

LANGSTON C. A. 1981: Source inversion of seismic waveforms: the Koyna, India, earthquakes of 13 September 1967. Bulletin of the Seismological Society of America **71**, pp. 1–24

MAO W. J., PANZA G. F., SUHADOLC P. 1994: Linearized waveform inversion of local and near-regional events for source mechanism and rupturing processes. Geophysical Journal International **116**, pp. 784–798

McCOWAN D. W. 1976: Moment tensor representation of surface waves. Geophysical Journal of the Royal Astronomical Society **44**, pp. 595–599

MÜLLER G. 1985: The reflectivity method: a tutorial. Journal of Geophysics **58**, pp. 153–174

OLDENBURG D. W. 1982: Multichannel appraisal deconvolution. Geophysical Journal of the Royal Astronomical Society **69**, pp. 405–414

PANZA G. F., SARAO A. 2000: Monitoring volcanic and geothermal areas by full seismic moment tensor inversion: are non-double-couple components always artefacts of modelling? Geophysical Journal International **143**, pp. 353–364

RIEDESEL M. A., JORDAN T. H. 1989: Display and assessment of seismic moment tensors. Bulletin of the Seismological Society of America **79**, pp. 85–100

SARAO A., PANZA G. F., PRIVITERA E., COCINA O. 2001: Non-doublecouple mechanisms in the seismicity preceding the 1991–1993 Etna volcano eruption. Geophysical Journal International **145**, pp. 319–335

SEKIGUCHI H., IRIKURA K., IWATA T. 2002: Source inversion for estimating the continuous slip distribution on a fault — introduction of Green's functions convolved with a correction function to give moving dislocation effects in subfaults. Geophysical Journal International **150**, pp. 377–391

SILENY J., PANZA G. F., CAMPUS P. 1992: Waveform inversion for point source moment tensor retrieval with variable hypocentral depth and structural model. Geophysical Journal International **109**, pp. 259–274

SIPKIN S. A. 1982: Estimation of earthquake source parameters by the inversion of waveform data: synthetic waveforms. Physics of the Earth and Planetary Interiors **30**, pp. 242–259

TICHELAAR B. W., RUFF L. J. 1989: How good are our best models? Jackknifing, bootstrapping, and earthquake depth. EOS Trans. AGU **70**, pp. 593

TÓTH L., MÓNUS P., ZSÍROS T. 1996: Hungarian Earthquake Bulletin 1995. GeoRisk Budapest 69 p.

TÓTH L., MÓNUS P., ZSÍROS T. 1997: Hungarian Earthquake Bulletin 1996. GeoRisk Budapest 67 p.

TÓTH L., MÓNUS P., ZSÍROS T., KISZELY M. 2001: Hungarian Earthquake Bulletin 2000. GeoRisk Budapest 98 p.

VAN der SLUIS A., VAN der VORST H. A. 1987: Numerical solution of large, sparse linear algebraic systems arising from tomographic problems. *In:* NOLET G. (Ed.), Seismic Tomography. Reidel, Dordrecht, pp. 49–83

WESSEL P., SMITH W. H. F. 1998: New, improved version of generic mapping tools released. EOS Trans. AGU **79**, pp. 579

XU P. 1998: Truncated SVD methods for discrete linear ill-posed problems. Geophysical Journal International **135**, pp. 505–514

Lokális földrengések bootstrap inverziója a Pannon medencében

WÉBER Zoltán

Kis erejű lokális földrengések rövid periódusú hullámformáinak inverziójával meghatároztuk néhány, a Pannon medence területén kipattant rengés forrásmechanizmusát (momentum tenzorát). A reflektivitás módszer felhasználásával — adott földmodell mellett — számos hipocentrum mélységre szintetikus Green-függvényeket számítottunk, majd a momentum tenzor komponenseit lineáris inverzióval meghatároztuk. A forrásfüggvény alakját is megbecsültük. Azt a hipocentrum mélységet és momentum tenzort fogadtuk el megoldásként, melyek mellett a számított és mért szeizmogramok a legjobban illeszkedtek egymáshoz.

Az eredmények statisztikai jellemzése érdekében a bootstrap eljárást alkalmaztuk. Az eredményül kapott momentum tenzor komponenseinek bizonytalanságát oly módon ábrázoltuk a fókuszgömbön, hogy a DC, CLVD és izotróp összetevők statisztikai jelentősége becsülhető legyen.

A kiválasztott események inverziójával kapott momentum tenzorok csupán jelentéktelen nagyságú izotróp komponenssel rendelkeznek, ami a rengések tektonikai természetére utal. A ka-

pott forrásfüggvények nagyon egyszerű lefutásúak, hosszuk mintegy 0,1–0,2 s. A kapott mechanizmusok összhangban vannak az első *P*-hullám beérkezések polaritásával. A momentum tenzorok saját tengelyeinek irányai jó egyezést mutatnak a szakirodalomban publikált feszültségiránnyal.

ABOUT THE AUTHORS

Zoltán Wéber graduated from Eötvös Loránd University, Budapest, in 1985, whereupon he became a postgraduate scholarship holder of the Hungarian Academy of Sciences (HAS) at the Geophysical Department of Eötvös University. He was awarded a C.Sc. (1991) from the HAS in earth sciences. From 1988 to 1996 he worked for the Geophysical Research Group of the HAS, Geophysical Department of Eötvös University. His main fields of interest were seismic data processing, VSP modelling and interpretation, and seismic inversion. Since 1996 he has been working at the Seismological Observatory of the Geodetic and Geophysical Research Institute of the HAS. He mainly deals with traveltime tomography and waveform inversion for focal mechanism and hypocentre coordinates. Since 1999 he has headed the Theoretical Department of the observatory. He is the national titular member of IASPEI and the ESC.

Horizontal inversion of guided wave dispersion data

Mihály DOBRÓKA[*]

Guided waves play an important role both in the investigation of near surface structures and in mining applications; channel waves are commonly used to detect and locate tectonic disturbances of coal seams. On the other hand, guided waves contain information about the structural- and material parameters of the wave-guide model, so — using the methods of geophysical inversion — these characteristics can be determined by means of frequency-dependent phase- and group velocity and absorption coefficient data. Near-surface geological structures often serve as seismic wave-guides. By inverting the frequency dependent dispersion characteristics of surface waves the model parameters of the wave-guide structure can also be determined. For laterally heterogeneous wave-guides the lateral changes of the material or geometrical parameters of the model can also be determined.

In this paper the inversion of in-situ measured surface wave data is presented. The input data of the inversion algorithm are the group traveltimes determined from the seismic traces at various frequencies. The approximate inversion procedure consists of two steps: first the local group velocities are determined at various frequencies by means of tomographic inversion of the group traveltimes, and then the local dispersion characteristics of the Love- or Rayleigh surface waves are inverted in the second step. In our investigations a robust version of the SIRT (Simultaneous Iterative Reconstruction Technique) method is used for tomography and an IRLS (Iteratively Reweighted Least Squares) algorithm using Cauchy weights is applied for the inversion of the group velocity data.

Keywords: wave dispersion, inversion

1. Introduction

In a discussion of the guided-wave seismic inverse problem KREY [1983] introduced the terms: 'vertical- and horizontal inversion'. He used the term 'vertical inversion' for the determination of the thicknesses and the petrophysical characteristics of the (one-dimensional) wave-guide structure by means of the frequency-dependent phase velocities and/or group velocities. A more compli-cated model with rapid thickness-changes along directions parallel to the coal seam was also discussed by KREY [1983] and the procedure giving the solution of the inverse problem for this case was called 'horizontal inversion'. We shall use

* University of Miskolc, Geophysics Department, H-3515 Miskolc–Egyetemváros

this latter term in a more general context: changes in both the geometrical (thickness) and petrophysical parameters are allowed.

1.1. The forward problem

The solution of the guided-wave seismic forward problem for horizontally layered, layerwise homogeneous wave-guide structure is well-discussed [SCHWAAB, KNOPOFF 1972, RÄDER et al. 1985, BUCHANAN 1987]. For direct calculation of the absorption-dispersion characteristics of Love-waves in a one dimensional wave-guide we use the algorithm presented by BUCHANAN [1987] with the modification that any dissipative properties of the medium will also be considered. In order to describe inelastic friction the constant Q model is used with the complex shear modulus $\mu = \mu_o[1 + i\varepsilon]$, (μ_0 is the real shear modulus; $\varepsilon = 1/Q$, Q being the quality factor). For a horizontally (weakly) inhomogeneous wave-guide with slowly changing (or constant) thickness the WKB method will be used to determine the absorption-dispersion characteristics [DOBRÓKA 1987, 1988]. A more general dispersion relation of [FANCSIK 1997] can also be applied; this author extended the use of the WKB method to the case of Rayleigh waves, too.

2. Vertical inversion of guided-wave dispersion data

If one solves the complex dispersion relation (for both Love- and Rayleigh waves) the frequency dependent phase velocity (V_{ph}^c), the group velocity (V_g^c), and the absorption coefficient a^c can be computed

$$V_{ph}^c = v_{ph}(\omega, \vec{m}) \qquad V_g^c = v_{gr}(\omega, \vec{m}) \qquad a^c = a(\omega, \vec{m})$$

where $\vec{m}$ is the vector of model parameters:

$$\vec{m} = \{\beta_1, \beta_2, \beta_3, \rho_1, \rho_2, \rho_3, \varepsilon_1, \varepsilon_2, \varepsilon_3\}^T$$

(for a three-layered model), where β denotes the shear velocity and ρ is the density (the superscript c refers to calculation). On forming a joint inversion algorithm one then introduces the combined response function

$$\vec{d}^c = \{V_{ph1}^c, ..., V_{phN_p}^c, V_{g1}^c, ..., V_{gN_g}^c, a_1^c, ..., a_{N_a}^c\}$$

with the kth coordinate

$$d_k^c = d\{\omega_k, \vec{m}\} \ .$$

Similarly, the combined vector of observations is introduced as

$$\vec{d}^{obs} = \left\{ V_{ph_1}^{obs}, \ldots, V_{ph_{N_p}}^{obs}, V_{g_1}^{obs}, \ldots, V_{g_{N_g}}^{obs}, a_1^{obs}, \ldots, a_{N_a}^{obs} \right\}$$

(the superscript *obs* refers to observation). In the inversion procedure the parameter vector is usually determined by minimizing the weighted norm

$$E = (\vec{e}, W\vec{e})$$

of the

$$\vec{e} = \vec{d}^{obs} - \vec{d}^c$$

vector. The W_{kk} weights are usually a priori given.

When the weight matrix is independent of the parameter vector, the linearized procedure of the weighted least squares leads to the normal equations

$$\underline{\underline{G}}^T \underline{\underline{W}} \, \underline{\underline{G}} \, \vec{x} = \underline{\underline{G}}^T \underline{\underline{W}} \, \vec{y}$$

where

$$y_k = \frac{d_k^{obs} - d_k^{(0)}}{d_k^{obs}}, \qquad G_{kj} = \frac{m_j^{(0)}}{d_k^{obs}} \left(\frac{\partial d_k^c}{\partial m_j} \right)_{\vec{m}_0}, \qquad x_j = \frac{\delta m_j}{m_j^{(0)}}.$$

Here $\vec{m}^{(0)}$ is the point in the model space around which the problem is linearized, $d_k^{(0)} = d\{\omega_k, \vec{m}^{(0)}\}$ and $\delta \vec{m}$ is the parameter correction.

In some cases the weight matrix contains the e_k residuals. For example the Cauchy weights are of the form

$$W_{kk} = \frac{s^2}{s^2 + e_k^2},$$

where s is the scale parameter. It was in order to save the linearity of the normal equations even in such cases that SCALES et al. [1988] introduced the Iteratively Reweighted Least Squares (IRLS) method. The resulting normal equation in the ith iterations of the IRLS procedure is

$$\underline{\underline{G}}^T \underline{\underline{W}}^{(i-1)} \underline{\underline{G}} \, \vec{x}^{(i)} = \underline{\underline{G}}^T \underline{\underline{W}}^{(i-1)} \vec{y} \qquad (1)$$

where $W^{(I-1)}$ is the Cauchy weight matrix containing the $e_k^{(I-1)}$ residuals of the previous step of iteration. In the following, this algorithm will be tested using synthetic data.

3. Horizontal inversion algorithms

The geological structure representing the seismic wave-guide often shows lateral inhomogeneities. If the inhomogeneity of the petrophysical parameters is weak and the change in the thickness is slow enough, the WKB method can be used to solve the forward problem. This gives the possibility of rapid calculation of the (local) phase- and group velocities as well as the absorption coefficients. The traveltime data belonging to various guided wave constituents can be calculated by (numeric) integration

$$t(\omega, \vec{m}) = \sum_i \frac{\Delta x}{V_{ph}(\omega, \vec{m}, x_i)}.$$ (2)

where the $\vec{m}$ parameter vector consists of the variables appearing in the vertical inverse problem and some further ones, depending on the discretization of laterally changing variables.

3.1. Exact inversion

The exact inversion algorithm was introduced by DOBRÓKA [1996]. Assuming a three layered wave-guide structure, the varying (x-dependent) thickness function can be approximated as a power series

$$H(x) = \sum_{j=1}^{P} B_j x^{j-1}$$ (3)

Here B_j are the unknown expansion coefficients. The parameter vector can be written in the form

$$\vec{m} = \{\beta_1, \beta_2, \beta_3, \rho_1, \rho_2, \rho_3, \varepsilon_1, \varepsilon_2, \varepsilon_3 . B_1, ..., B_p \}^T$$

when B_j-s are the coefficients of the (3) series expansion. In the formulation of the linearized inverse problem the $\underline{G}$ matrix can be computed as

$$G_{ij} = \frac{m_j}{t_i^{obs}} \left(\frac{\partial t_i}{\partial m_j} \right)_{\bar{m}_o}$$

and using a Cauchy-IRLS algorithm the normal equations can again be written in the form of Eq. (1). The exact horizontal inversion algorithm requires numerical integration in the forward modelling with the solution of the complex dispersion relation at all the x_i points (Eq. (2)). This results in relatively large computation times.

3.2. Approximate inversion

In order to reduce the computation time requirements an approximate inversion method was also developed in which the guided-wave seismic horizontal inverse problem is reduced to a (multiply solved) vertical inverse problem. To do this, as a first step in the approximate inversion procedure the local phase- and group velocities are determined at various frequencies by means of the tomographic method. The local absorption–dispersion characteristics given at different frequencies and positions are then inverted in a vertical joint inversion procedure. In our investigations the SIRT method (based on one-dimensional cells along the x-axis) was used for tomography and LSQ (Least Squares) or Cauchy-IRLS algorithms (IRLS method using Cauchy weights) were again applied for joint inversion of the phase- and group velocity as well as absorption coefficient data.

4. Numerical results

In order to test the horizontal inversion algorithms, synthetic data sets were generated. The petrophysical parameters of the model chosen for numerical investigations are the same as in *Table I*, with the thickness function

$$H_2(X) = d \ [1 + \exp(-X^2)], \quad X > 0, \tag{4}$$

where $\quad X = \dfrac{x}{20\,d} \quad$ and $d = 1$ (m).

H(m)	β (m/s)	α (m/s)	ρ (kg/dm³)	E
–	2000	3000	2.7	0.02
2	1000	1500	1.3	0.05
–	2500	3800	2.2	0.02

Table I. The model parameters
I. táblázat. A modellparaméterek

The theoretical traveltimes were calculated by means of Eq. (2) in the range of (150–750) Hz at 30 frequency points for all the receivers placed at the points x_j = $j\Delta x$ (j=1,...,10 and Δx=5 m). Random noise of Gaussian distribution was added: either 1% (data set I.) or 5% (data set II.). In order to simulate a data set containing outliers, data set III. is generated by adding 25% extra noise to a randomly selected 20 % portion of the data set I.

The thickness function found in the LSQ exact horizontal inversion is shown in *Fig. 1.* In the discretization of the thickness (Eq. (3)) we used P=5 which gives an acceptable approximation of the thickness function. The relative
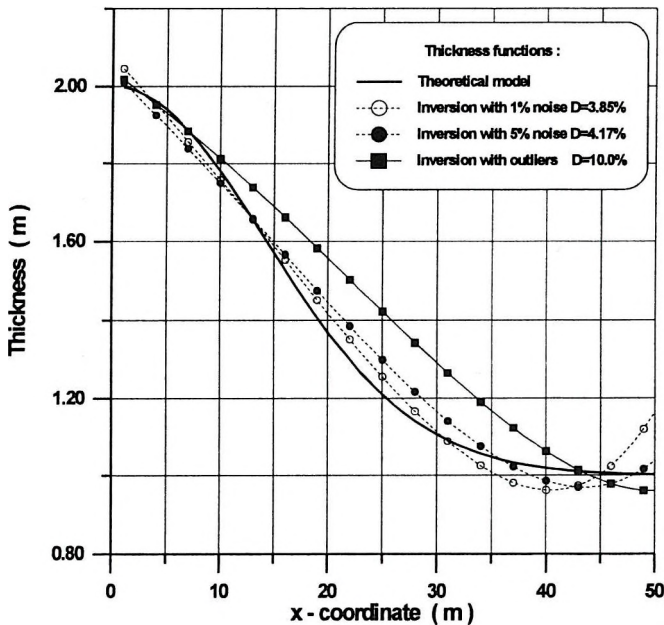
Fig. 1. Thickness function found in horizontal exact inversion
1. ábra. A horizontális egzakt inverzióban kapott vastagságfüggvény

distance between the $(H_o(x))$ exact and the $(H(x))$ estimated thickness is characterized by the scalar

$$D_H = \sqrt{\frac{1}{N} \sum_{i=1}^{N} \left(\frac{H(x_i) - H_o(x_i)}{H_o(x_i)} \right)^2}$$

The approximate inversion result is shown in *Fig. 2*. Both the exact and the approximate inversion of the synthetic dispersion (phase traveltime) data gave acceptable results. The quality of approximate inversion can appreciably be improved by joint inversion of various kinds of dispersion data.
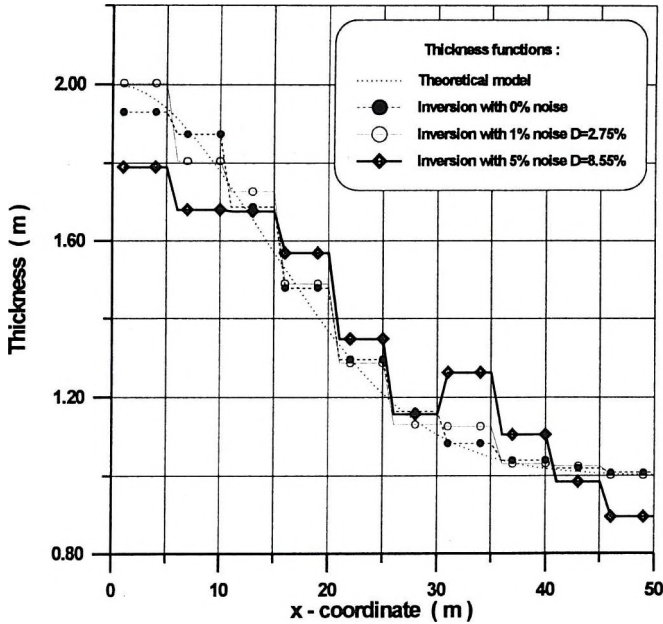

Fig. 2. Thickness function found in phase velocity approximate LSQ inversion
2. ábra. A fázissebesség adatok horizontális közelítő inverziójában kapott vastagságfüggvény

In order to test the approximate horizontal joint inversion algorithm the theoretical data were calculated by means of Eq. (2) and also

$$t_{gr}(\omega, \vec{m}) = \sum_i \frac{\Delta x}{V_{gr}(\omega, x_i)} \quad \text{.} \tag{5}$$

$$A(\omega, \vec{m}) = \sum_i a(\omega, x_i) \Delta x \quad . \tag{6}$$

in the range of (150–750) Hz at 30 frequency points for all the receivers located in any of the cells with their border defined at points $xj = j\Delta x$ ($j=1,...,10$ and $\Delta x=5$ m is the cell-size). Three data sets (I, II, and III) were again generated by adding noise in the same way as above. The joint inversion of phase- and group traveltimes results in *Fig. 3*, while the result of the phase velocity–absorption coefficient joint inversion is presented in *Fig. 4*. It can be seen that joint inversion gives more accurate parameter estimation.
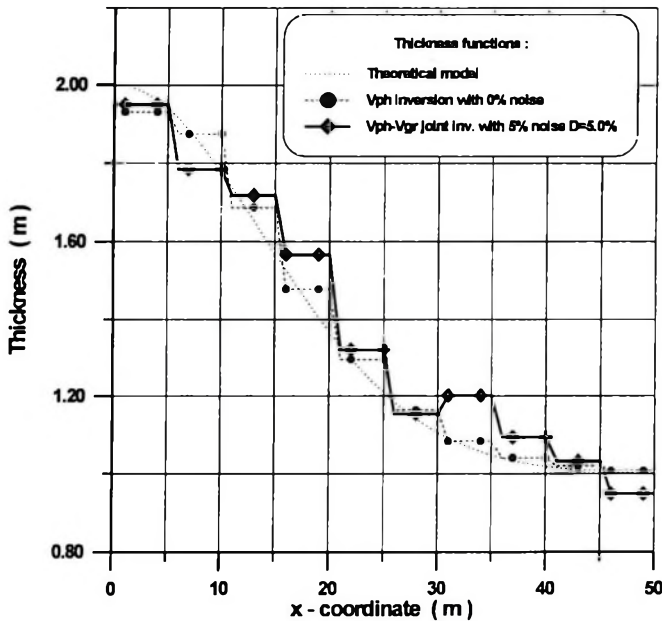
Fig. 3. Thickness function found in phase velocity–group velocity approximate joint inversion

3. ábra. A fázis- és csoportsebesség adatok horizontális közelítő együttes inverziójában kapott vastagságfüggvény

5. Field results

The horizontal inversion methods were also tested by means of in-situ measured surface wave data. The measurements were carried out in Borsod
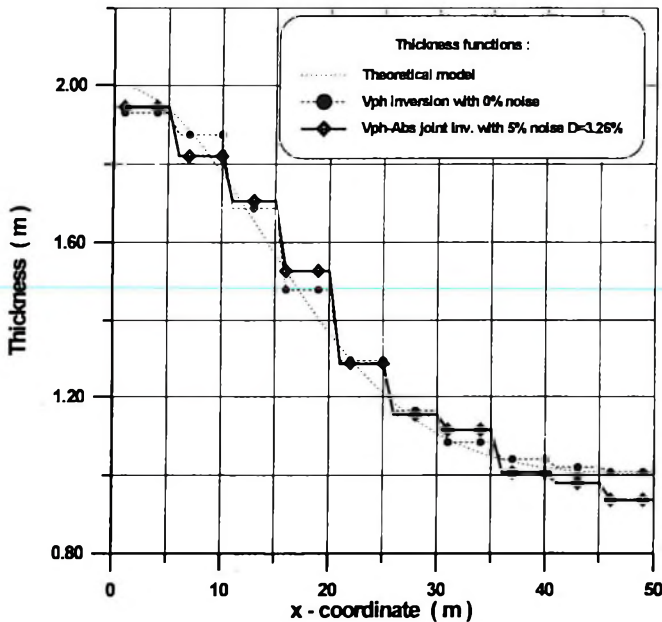
Fig. 4. Thickness function found in phase velocity–absorption coefficient approximate joint inversion

4. ábra. A fázissebesség és abszorpciós tényező adatok horizontális közelítő együttes inverziójában kapott vastagságfüggvény

County. The layout was similar to that assured in the generation of synthetic data. The seismic source and the five receivers were arranged along a straight line; the first receiver was 38 m apart from the source, the distance between receivers was 6 m. Horizontal displacements (perpendicular to the measurement line) were generated. 1 Hz Lennartz geophones were used to measure the displacements of the surface waves of the Love type. The measurement data were collected using the PC-regulated engineering seismic instrument ESS 03–24 of the Eötvös Loránd Geophysical Institute, Budapest.

The seismogram detected in the measurement (and filtered in the frequency range 2–35 Hz) is shown in *Fig. 5.* In order to find group slowness data from the filtered seismic traces the wavelet transform method was used with a Morlet-wavelet, as an analysing function. A typical result of the wavelet analyses — the amplitude as a function of the group traveltime and frequency — is shown in *Fig. 6* (belonging to the first receiver in the frequency range 0–15 Hz). For the sake of simplicity the basic mode group
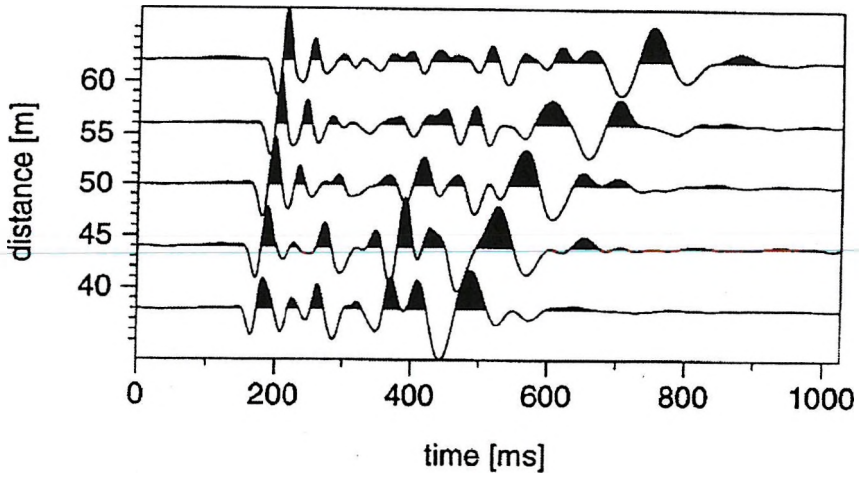
Fig. 5. The six seismic channels of the in-situ measurement

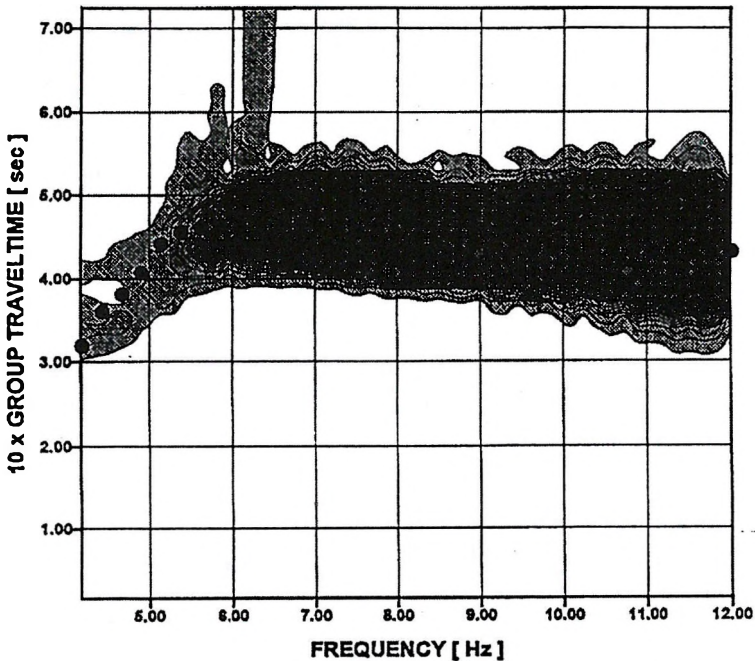5. *ábra.* A terepi mérésen regisztrált szeizmikus csatornák

Fig. 6. Dispersion analysis of the first seismic channel

6. *ábra.* Az 1. szeizmikus csatorna diszperzió analízisének eredménye

slowness data belonging to the maximum amplitudes in the 5–12 Hz frequency range were selected for inversion.

The group slowness data derived from the in-situ measured seismogram were used to test the approximate horizontal inversion algorithm. The start model was defined in agreement with the paper by MISIEK et al. [1997]. (In this work geoelectric- and seismic field data were measured at the same location and their joint inversion was discussed assuming a horizontally layered, layerwise homogeneous geological model. The parameters of the three-layered model given by this joint inversion procedure were chosen as the start model for the horizontal inversion.)

The one-dimensional cells required for the method were defined in agreement with the measurement layout: (0,38], (38,44], (44,50], (50,56], (56,62]. The local thickness and shear velocity values (in the first layer) were allowed to change cell by cell. The other model parameters of the wave-guide (H_2, VS_2, VS_3) were considered as common parameters of the inversion procedure. As a result of the approximate horizontal inversion procedure, the thickness- and shear velocity functions of the first layer are shown in *Fig. 7* and *Fig. 8* respectively. By means of the estimated model parameters, theoretical group traveltimes — as functions of the frequency — were also calculated at all geophone positions. As is shown by *Fig. 9*, the group traveltimes (calculated on the estimated model) are in relatively good agreement with those derived from the seismogram.

6. Conclusion

In order to demonstrate the accuracy and stability of approximate horizontal inversion, numerically simulated absorption–dispersion data were used. The inversion method was used to determine the lateral changes of the wave guide model for field measurements carried out in Borsod County. The relatively good fit between the observed and predicted group traveltime data (calculated on the model, given by horizontal inversion) proves that the approximate horizontal inversion method is sufficiently accurate for practical use.
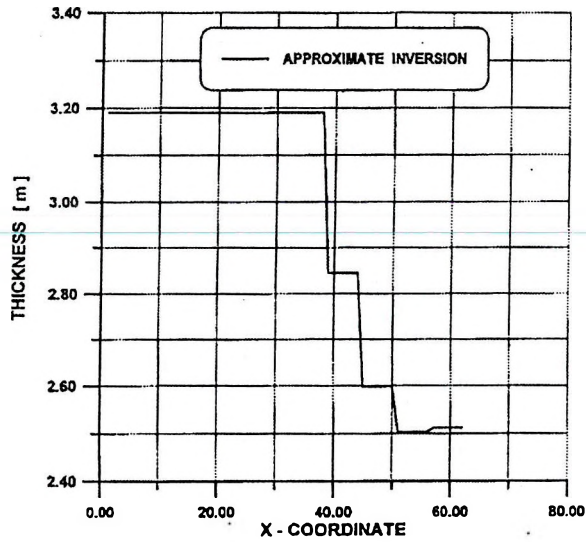
Fig. 7. Thickness function given by horizontal inversion

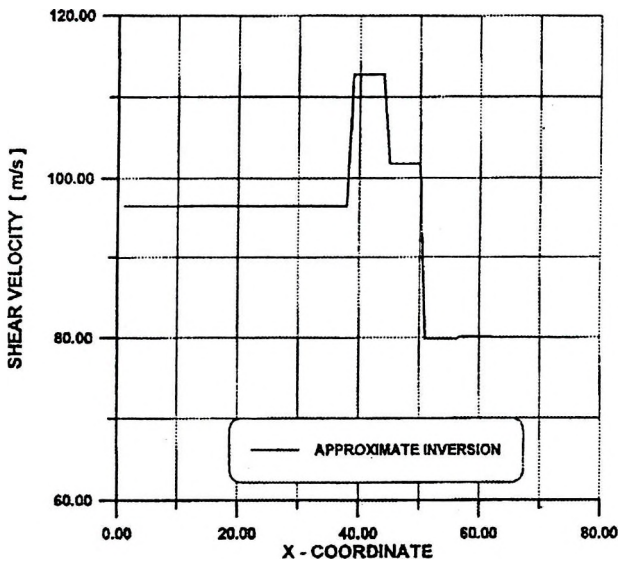*7. ábra.* A terepi adatok horizontális inverziójával kapott vastagságfüggvény

Fig. 8. Shear velocity function given by horizontal inversion

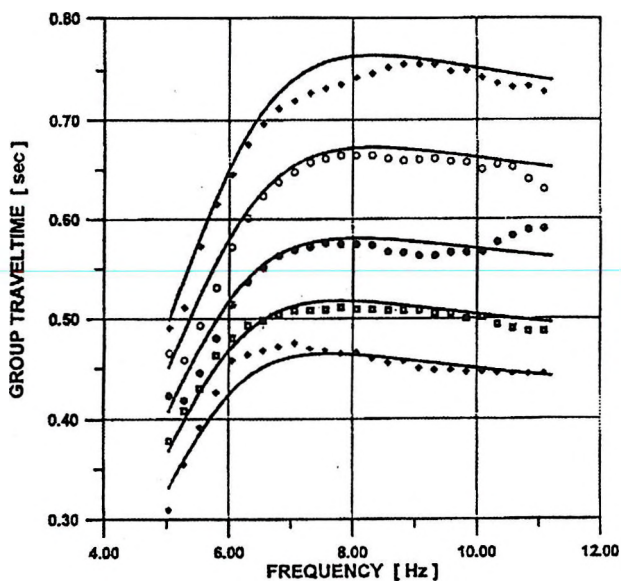*8. ábra.* A terepi adatok horizontális inverziójával kapott transzverzális sebességfüggvény

Fig. 9. Fit between the observed and predicted group traveltime data (calculated on the model given by horizontal inversion)

9. ábra. A mért és (a horizontális inverzió eredmény-modelljén) számított csoportsebesség adatok egyezése

7. Acknowledgements

REFERENCES

BUCHANAN D. J. 1987: Dispersion calculations for *SH* and *P–SV* waves in multilayered coal seams, Geophysical Prospecting **35**, pp. 62–70

DOBRÓKA M. 1987: Love seam-waves in a horizontally inhomogeneous three-layered medium. Geophysical Prospecting **35**, pp. 502–516.

DOBRÓKA M. 1988: On the absorption–dispersion characteristics of channel waves propagating in coal seams of varying thickness. Geophysical Prospecting **36**, pp. 318–331

DOBRÓKA M. 1996: Dispersion relation of Love waves propagating in inhomogeneous seismic waveguides with alternating layer thicknesses; inversion of the adsorption-dispersion characteristics. D.Sc. thesis, University of Miskolc

FANCSIK T. 1997: Investigation of the dispersion relations of Rayleigh waves propagating in waveguides characterized by slightly site-dependent parameters. Thesis, Budapest, 1997

HERING A., MISIEK R., GYULAI Á., ORMOS T., DOBRÓKA M., DRESEN L. 1995: A joint inversion algorithm to process geoelectric and surface wave seismic data. Part I. Basic Ideas. Geophysical Prospecting **43**, pp. 135–156

KREY Th. 1983: Some problems concerning the inversion of observed in-seam seismic dispersion data, presented at the 53rd SEG Meeting, Las Vegas, Expanded Abstracts, 55–68

MISIEK R., LIEBIG A., GYULAI Á., ORMOS T., DOBRÓKA M., DRESEN L. 1997: A joint inversion algorithm to process geoelectric and surface wave seismic data. Part II. Applications. Geophysical Prospecting **45**, pp. 65–85

RÄDER R., SCHOTT W., DRESEN L., RÜTER H. 1985: Calculation of dispersion curves and amplitude–depth distributions of Love channel waves in horizontally layered media. Geophysical Prospecting **33**, pp. 800–816

SCALES J. A., GERSZTENKORN A., TREITEL S., LINES L. R. 1988: Robust optimization methods in geophysical inverse theory. 58th SEG meeting, Anaheim, Expanded Abstracts, pp. 827–830

Vezetett hullám diszperziós adatok horizontális inverziója

DOBRÓKA Mihály

A vezetett hullámok fontos szerepet játszanak a felszín közeli szerkezetek kutatásában. Ismeretes, hogy csatornahullámok segítségével a széntelepes összletek tektonikai zavarai kutathatók. Ugyanakkor a vezetett hullámok információt hordoznak a hullámvezető szerkezet geometriai és anyagi jellemzőiről is, ezért a geofizikai inverzió módszereinek alkalmazásával ezek a paraméterek meghatározhatók a frekvenciafüggő fázis- és csoportsebesség ill. abszorpciós tényező adatok alapján.

A felszín közeli szerkezetek gyakran hullámvezetőként viselkednek, így a frekvenciafüggő diszperziós adatok inverziója révén a hullámvezető szerkezet jellemzői vizsgálhatók (HERING et al. 1994]. Ebből adódóan laterálisan változó hullámvezetők esetén mód van a hullámvezető szerkezet geometriai és anyagi jellemzői laterális változásának inverziós meghatározására is.

Ebben a dolgozatban felületi hullám diszperziós adatok inverziójával foglalkozunk. Az alkalmazott horizontális inverziós módszer bemeneti adatai a terepi szeizmikus csatornák diszperzió analízisével (különböző frekvenciákon) előállított csoportsebességek. A közelítő inverziós eljárás két lépésből áll:

1. lokális csoportsebességek előállítása (különböző frekvenciákon) a csoport-futási idő adatok tomográfiai inverziójával;

2. a lokális hullámvezető paraméterek meghatározása a lokálisan különböző frekvenciákon adott csoportsebességek (vertikális) inverziójával.

Vizsgálatainkban az ismert SIRT (Simultaneous Iterative Reconstruction Technique) módszer robusztifikált változatát [DOBRÓKA 1994] alkalmazzuk a tomográfiai rekonstrukcióban ill. az iteratív újrasúlyozás módszerével definiált (Cauchy súlyokat használó) eljárást alkalmazunk a diszperziós adatok vertikális inverziójában.

ABOUT THE AUTHOR

Mihály Dobróka received his M.Sc. in physics (1972) from Kossuth Lajos University (Debrecen). He obtained his university doctor's degree from the Eötvös Loránd University (Budapest) in 1976. The Hungarian Academy of Sciences awarded him his Candidate's degree (C.Sc.) in 1986 and his Doctor of Sciences degree (D.Sc.) in 1996. He has worked continuously at the University of Miskolc since 1972; at present he is professor of geophysics. His main fields of interest are geophysical inversion and tomography, seismic methods, and engineering geophysics.

2-D simultaneous inversion method to determine dipping geological structures

Ákos GYULAI[*]

A parameter estimation for a three-layer dipping structure through a field example by using the 2-D simultaneous inversion method is presented. In the inversion we solved the direct problem with an analytical procedure. In the simultaneous inversion the data in dip and in strike direction are presented together. Besides the local values of the layer thickness and the apparent resistivity we also determine the dipping of the layers from VES curves by using the L_2 inversion. The reliability of the estimated parameters is characterized by correlation and variance values. We compare the 2-D inversion results of the measured data in the dip-direction with the 1.5-D inversion results of measured data in the strike direction.

Keywords: inversion, dipping layers, VES

1. Introduction

In the investigation of simple dipping structures the local 1-D approach is often used. This approach results in only small errors up to a dip angle of 20 degrees, in the inversion of the Schlumberger VES data measured in the strike direction. In this method we do not use the characteristic feature that the structural changes are the most pronounced when the measurement is carried out in the dip direction [GYULAI 1995]. That is why, in practice, dip measurements are preferred as a means of determining the horizontal structure changes. It is done in spite of the fact that the interpretation of the data can be carried out only by using 2-D inversion. In these methods the a priori geological knowledge cannot be taken into consideration and the reliability of estimation is unsatisfactory even for simple structures.

For two-layer models with dipping layers CHASTANET de GERY, KUNETZ [1956] published analytical formulae to compute the potential in

* University of Miskolc, Geophysics Department, H–3515 Miskolc–Egyetemváros
Manuscript received (revised version): 11 September, 2001.

the case of a plane surface. For multi-layer models — starting from only one surface cross line — HMELEVSZKOJ and BONDARENKO [1989] published a solution to calculate the potential. For parallel dipping boundaries BERNABINI, CARDARELLI [1991] plotted apparent resistivity curves which were computed with the help of the so called Alfano integral equations. GYULAI [1995], making use of the potential equations of CHASTANET de GERY, KUNETZ [1956] and HMELEVSZKOJ, BONDARENKO [1989], determined the apparent resistivity equations for different arrays. To compute the resistivity, an algorithm was developed which made it possible to carry out simultaneous inversion on the basis of analytical forward modelling [GYULAI, ORMOS 1996].

Inversion can be realized with data of geophysical methods based on similar or different physical parameters. The former one is called simultaneous inversion, the latter joint inversion.

2. Solution of the direct problem

By simplifying the equations of GYULAI [1995], the potential of the first layer at the surface point M is:

$$U_M = \frac{I\rho_1}{2\pi} \left\{ \frac{1}{R} + \frac{2}{\pi} \int_0^\infty f_1(t)\,dt \int_0^\infty \frac{\cos ts}{\left[z^2 + r^2 + r_0^2 + 2rr_0 \cosh s \right]^{1/2}}\,ds \right\} \qquad (1)$$

where

r_0 is the distance of the source from the cross line of the surface and of the dip boundary,

r is the distance of the measuring point (M) from the cross line of the surface and of the dip boundary,

R is the distance of M from the source, and $R^2 = r^2 + z^2$,

α_1 is the angle of the dipping layer to the surface.

The function containing $f_1(t)$ layer parameters is:

$$f_1(t) = \frac{\rho_1 T(t)}{Y(t)} \qquad (2)$$

$$T(t) = -\sinh(\alpha_n - \pi)t + k_{21}\sinh(\alpha_n + \pi - 2\alpha_1)t + \\ + k_{32}\sinh(\alpha_n + \pi - 2\alpha_2)t - k_{21}k_{32}\sinh(\alpha_n - \pi + 2\alpha_1 - 2\alpha_2)t \tag{3}$$

$$Y(t) = -\sinh\alpha_n t - k_{21}\sinh(\alpha_n - 2\alpha_1)t - \\ - k_{32}\sinh(\alpha_n - 2\alpha_2)t + k_{21}k_{32}\sinh(\alpha_n + 2\alpha_1 - 2\alpha_2)t \tag{4}$$

where

$$k_{i,i-1} = (\rho_i - \rho_{i-1})/(\rho_i + \rho_{i-1})$$

and $I=1, ..., 3$. α_1, α_2 are the dip angles from the cross section of the layers computed from the horizontal; $\alpha_n = \pi$ if the surface is flat (*Fig. 1*); I is the inflow current to the rocks; $\rho_1...\rho_i$ is the resistivity of the layers.
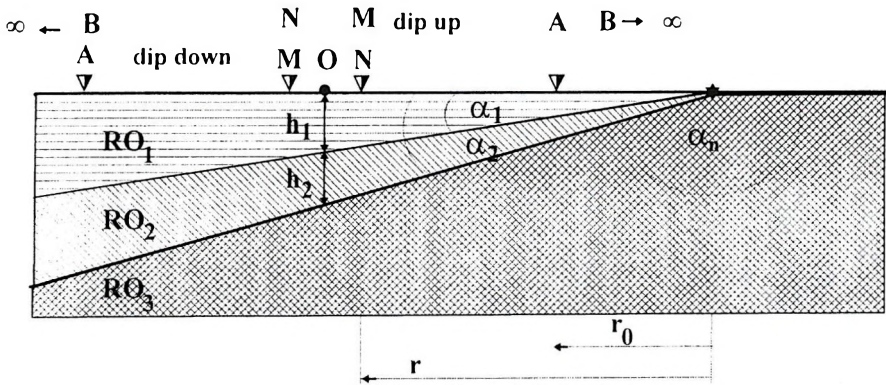
Fig. 1. Measuring array and model
1. ábra. Mérési elrendezés és a modell

Related to the horizontal layered case in the direct problem, the α_1, α_2 dip angles are new elements including the α_n cross and the point of the layer outcrop expressed by r_0 and the dip azimuth value expressed by r and z. These parameters of the dipping structure can be determined from the measured data, provided they have enough parameter sensitivity. For this investigation GYULAI [1995] introduced a new parameter sensitivity function for dipping structures.

Using Eqs. (1)–(4) the apparent resistivity function can be calculated for arbitrary measuring arrays, viz.

$$\rho_a = k \cdot \frac{\Delta U}{I} \tag{5}$$

where

$$\Delta U = \left(U_A^M - U_A^N \right) - \left(U_B^M - U_B^N \right) \tag{6}$$

I is the inflow current to the rock
k is the geometrical constant known in geoelectric practice.

With the help of Eqs. (1)–(6) the sounding theoretical data are generated:

$$\rho_a = \rho_a \left(r, \beta, \vec{p}_e \right) \tag{7}$$

where r is the measuring distance, β is the azimuth of the measuring direction (direction of the sounding compared to the N direction), $\vec{p}_e$ is the vector of electrical model parameters.

The vector of model parameters for a two layer structure is given by

$$\vec{p}_e = \left(h_1, \alpha_1, AZI, \rho_1, \rho_2 \right)^T \tag{8}$$

where h_1 is the local depth of the dipping layer at the reference point of soundings, AZI is the azimuth of dipping (clockwise direction from N), ρ_1 and ρ_2 are the apparent resistivities of the layers. The reference point for calculating local parameters in the case of pole-pole array represents the M electrode; in the case of three-electrode Schlumberger- and radial dipole arrays it represent the mid-point of M and the potential electrodes. With this kind of notation of reference points we differ from the conventional reference point used in apparent resistivity pseudosection studies. The reason for the difference is to ensure separation between dip down and dip up data at asymmetrical arrays.

The vector of the model parameter in the multi-layer case is:

$$\vec{p}_e = \left(RKIB, \alpha_1 ... \alpha_i, AZI, \rho_1 ... \rho_i \right)^T \tag{9}$$

where $RKIB$ is the distance of the common outcrop of dipping layers from the reference point of the sounding where

$\alpha_1 ... \alpha_i$ is the measure of dipping
AZI is the azimuth of the dipping

$\rho_1...\rho_i$ is the resistivity of the layers.

It is mentioned that it is useful to use different algorithms for two- and for multi-layer models. The solution of the direct problem is much simpler, faster and more precise in the case of two-layer models, as is demonstrated by GYULAI [1995].

3. Simultaneous inversion

In the case of dipping layers the number of unknown model parameters is larger than for the horizontally layered (1-D) case. Due to this, the single inversion of the unknown parameters does not give a reliable solution. At the same time the parameter sensitivity investigations [GYULAI 1995] show that the sensitivity for the same array is different in different measuring directions.

A similar phenomenon also occurs for different arrays. In view of the above, not only is it advisable but it is also necessary to apply such a simultaneous inversion method for the parameter estimation that uses the different directions and/or azimuth geoelectric sounding together.

If we use only geoelectric sounding the common parameter vectors of the soundings contain the same elements as each of the soundings would contain. If $\bar{X}$ is the simultaneous inversion parameter vector

$$\bar{X} = \vec{p}_e^{single} \tag{10}$$

In simultaneous inversion we estimate the same parameters as in single inversion but the data number is increased and we get more information about the model parameters. In the field case shown later we carried out the simultaneous inversion of a three-electrode (so-called half-Schlumberger) sounding measured in two azimuths. Let these measured data be

ρ_{aik}^{AZI1}, ρ_{aik}^{AZI2} . According to the notations used in DOBRÓKA et al. [1991] the theoretical apparent resistivity values are:

$$Y_{ik}^{cal} = Y\left(\vec{X}, \beta_k, r_{ik}\right) \tag{11}$$

where β_k is the azimuth of the kth measurement and r_{ik} is the ith sounding distance belonging to the kth azimuth.

Respectively relating the values of $Y_{ik}^{cal}\left(\vec{X},\beta_k,r_{ik}\right)$ to ρ_{aik}^{AZI1} values and to ρ_{aik}^{AZI2} values and solving the equation

$$\underline{\underline{G}}^T \cdot \underline{\underline{G}} \cdot x = \underline{\underline{G}}^T \cdot y \qquad (12)$$

[DOBRÓKA et al. 1991], we can estimate the model parameters of dipping layered models.

To qualify the results we use the relative data distance D, the relative model distance d (which shows the difference from the start model) defined by HERING et al. [1995], the matrix *cov* and the parameter reliability $\vec{\sigma}_p$ and the correlation matrix *corr* [SALÁT et al. 1982]. In order to get a reliable value for the whole estimation we also computed the

$$\vec{\sigma}_p = \left[\frac{1}{M}\sum_{j=1}^{M}\sigma_{pj}\right]^{1/2}$$

mean value, where M is the number of estimated model parameters.

4. Field case and parameter estimation with simultaneous inversion

The field surveys were carried out at the village of Korlát, Hungary. According to our former knowledge the geological structure can be approximated by a dipping layer geoelectric geophysical model, since on the deepening andesite and andesite tuff there is a gradually thickening clay layer as a cover. The synthetic inversion model studies show that the investigation of such structures can be carried out the most successfully by using asymmetric geoelectric arrays, e. g. three-electrode (so-called half-Schlumberger) surveys and the measurements should be made in at least two directions in order to obtain a reliable parameter estimation.

These two directions are, in practice, the dip down and the up ones, provided we know the azimuth of the dipping. The model and the array are shown in Fig. 1. It can be seen that the dip angles α start from the surface. The surface intersection of the layer boundaries has a specific role because the r and r_0 coordinates of electrodes start from here. Referring back to the fact that in Eq. (9), i.e. in the parameter vectors, it is the distance *RKIB* (the distance between the outcrop line and the point 0) that is represented and not the depths h_1 and h_2 which play a role. In view of this, we can calculate

the local depths h_1 and h_2 only indirectly from *RKIB* and dip angle α. Furthermore, the estimation errors can be calculated by error propagating law.

The three-electrode VES data can be seen in *Fig. 2*. At the starting (100 m) and ending (200 m) points of the profile we could only make measurements in the dip down or dip up directions due to some field constraints. At these sites, as the second measuring direction the strike direction (shown in Fig. 4) was used in the simultaneous inversion. At the inner points of the profile it can be seen that the VES data in the two directions
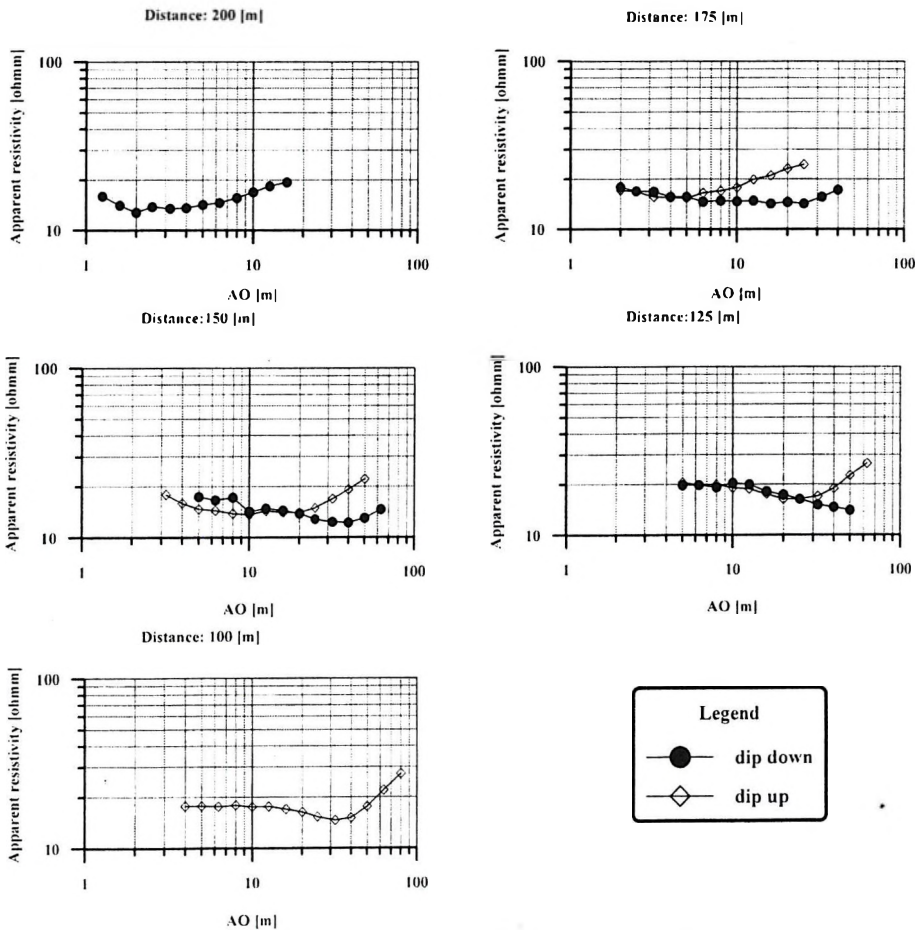
Fig. 2. Three-electrode (half-Schlumberger) VES sounding curves in dip directions
2. ábra. Háromelektródos (fél-Schlumberger) VESZ mérések dőlésirányban

differ significantly, and this fact forms the basis of the simultaneous inversion.

The 2-D simultaneous inversion result for VES stations is shown in *Fig. 3*. The ● denotes the local thickness and the local depth values of the layers. The shorter thick lines denote the estimated layer dipping at the VES stations. Connecting these elementary layers enabled us to determine the general slope of the dipping layers. At 150 m and 175 m a fault in the andesite is assumed with a faulting height of about 5 m. For better identification of the fault, we ought to have more data. The 35 ohm apparent resistivity of the andesite was considered as a fixed value along the whole length of the profile because the other VES surveys had been earlier carried out in the field. The results of 2-D inversion together with the reliability parameters are shown in *Table 1*.
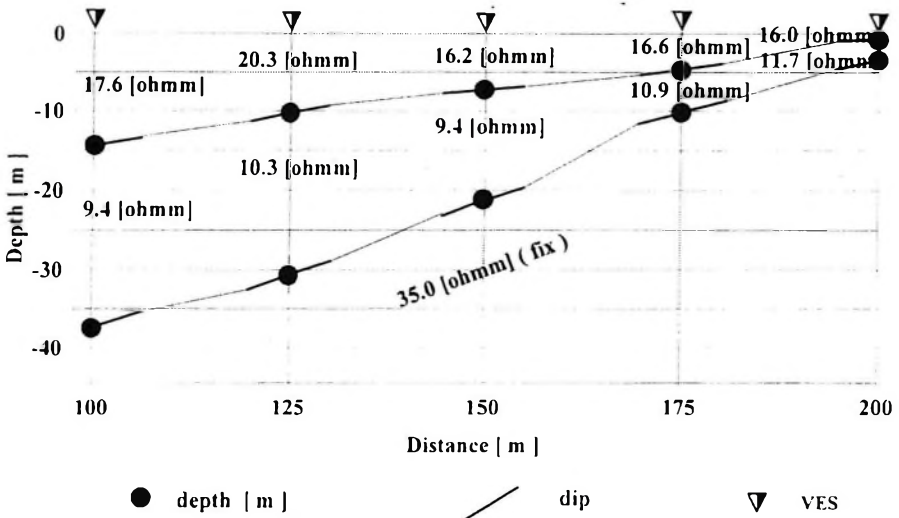
Fig. 3. Result of dip layered 2-D inversion for VES investigation
3. ábra. VESZ mérések dõlt réteges 2-D inverziójának eredménye

X/m	100	125	150	175	200
ρ_1 (ohmm)	17.6 (1%)	20.3 (1%)	16.2 (2%)	16.6 (2%)	16 (fix)
ρ_2 (ohmm)	9.3(63%)	10.3 (22%)	9.4 (37%)	10.9 (107%)	10.9 (22%)
ρ_3 (ohmm)	35 (fix)	35 (fix)	35 (fix)	35 (fix)	35 (fix)
α_1 (degree)	9.0 (35%)	8.1 (13%)	5.0 (36%)	7.6 (87%)	3.8 (44%)
α_2 (degree)	21.7 (47%)	23.3 (27%)	14.4 (36%)	17.0 (57%)	15.5 (13%)
h_1 (m)	14.4 (43%)	10.1 (21%)	7.3 (45%)	4.3 (92%)	0.6 (71%)
h_2(m)	22.0 (74%)	20.5 (46%)	13.8 (56%)	5.5 (47%)	1.8 (39%)
h_1+h_2 (m)	36.4	30.6	21.1	9.8	2.4
azimuth (degree)	180 (fix)	180 (fix)	180 (fix)	180 (fix)	180 (fix)
D (%)	3.3	1.9	5.8	4.8	2.2
$\vec{\sigma}_p$ (%)	50	26	39	74	43

Table I. Dipping flat layered 2-D simultaneous inversion result for VES stations

I. táblázat. Dőlt síkréteges, VESZ állomásonkénti együttes 2-D inverzió eredménye

The inversion procedure for the VES station of 125 m is shown in *Fig. 4*. We give the model distances represented by ▲ related to the start model, which data are shown in detail in *Table II*. The relatively low 19 % model distance and low iteration number result from our successful parameter estimation of the start model, by using 1-D inversion. The data distance of 1.8 % represents a good data fitting.
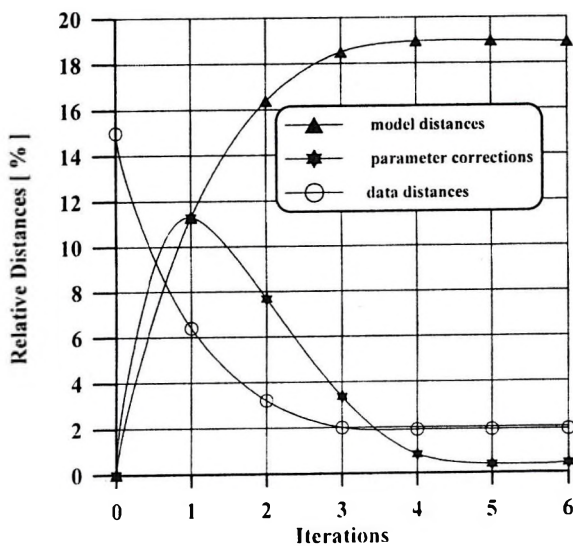
Fig. 4. The iterations, relative distances

4. ábra. Az iteráció menete, relatív távolságok

Start model		Exact model
ρ_1 (ohmm)	18	20.3
ρ_2 (ohmm)	15	10.3
ρ_3 (ohmm)	35	35
α_1 (degree)	10	8.1
α_2 (degree)	20	23.3
h_1 (m)	12	10.1
h_2(m)	30	20.5
h_1+h_2 (m)	42	30.6

Table II. 2-D dip flat layered inversion at 125 m VES point
II. táblázat. Dőlt síkréteges 2-D inverzió a 125 m-es VESZ pontban

In order to be sure about the reliability of the model parameter esti-
mation along the profile, we carried out independent Schlumberger VES
surveys in the strike-direction, too. The measured data are shown in *Fig. 5.*
We inverted these data both by single 1-D inversion and by 1.5-D joint in-
version. The results are shown in *Tables III.* and *IV.*

X	100	125	150	175	200
ρ_1 (ohmm)	17.3 (1%)	18.2 (1%)	17.2 (2%)	15.1 (1%)	15.1 (70%)
ρ_2 (ohmm)	7.9 (179%)	7.8 (105%)	9.8 (60%)	1.5 (125%)	11.9 (7%)
ρ_3 (ohmm)	35 (fix)	35 (fix)	35 (fix)	35 (fix)	35 (fix)
h_1 (m)	17.1 (59%)	12.7 (40%)	8.6 (43%)	5.6 (147%)	0.5 (231%)
h_2(m)	14.5 (235%)	13.0 (137%)	9.7 (93%)	4.8 (289%)	4.2 (40%)
h_1+h_2 (m)	31.6	25.7	18.3	10.4	4.7
D (%)	2.8	3.0	2.4	2.0	3.9
$\bar{\sigma}_p$ (%)	150	89	60	173	122

Table III. Result of 1-D single inversion
III. táblázat. Egyedi 1-D inverzió eredménye

Comparing Tables I, III, and IV, we can see that the reliability of the
2-D inversion for dipping layers (e.g. by comparison of the $\bar{\sigma}_p$ values) is
better than that of the 1-D single inversion, in spite of the greater number of
the unknowns. This is because of the simultaneous inversion. In *Fig. 6*, the
result of the 1.5-D joint inversion and those of the 2-D joint inversion can
be seen together at all VES points. The results of this latter inversion are
also shown in *Table V.* With the two inversions we got more or less the
same estimation. According to Table V the reliability values are higher in

the case of 1.5-D inversion. In spite of this we think that the great advantage of 2-D inversion for dipping layers is the fact that we can make a direct estimation about the dipping of the layers. Based upon the layer dipping the tectonic elements can also be determined, but for this purpose we need the exact estimation of local dip angles.
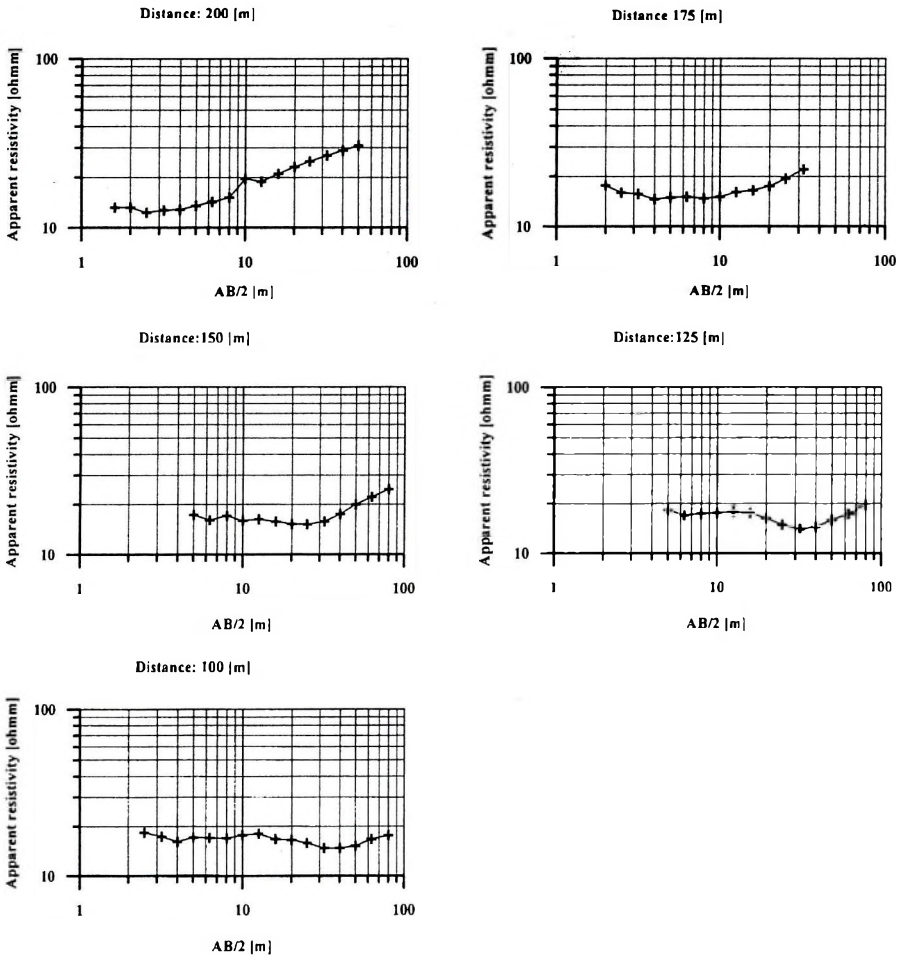

Fig. 5. Schlumberger VES investigations in strike direction

5. ábra. Schlumberger VESZ mérések csapásirányban

	α_1	α_2	ρ_1	ρ_2	RKB
α_1	1	−0.61	−0.72	−0.83	0.21
α_2	−0.61	1	0.43	0.94	−0.93
ρ_1	−0.72	0.43	1	0.52	−0.31
ρ_2	−0.83	0.94	0.52	1	−0.73
RKB	0.21	−0.93	−0.31	−0.73	1

	h_1	h_2	ρ_1	ρ_2
h_1	1	−0.99	−0.61	−0.99
h_2	−0.99	1	0.54	1.00
ρ_1	−0.61	0.54	1	0.54
ρ_2	−0.99	1	0.54	1

Table IV. Comparison of correlation matrices for the VES station at 125 m
IV. táblázat. Korrelációs mátrixok összehasonlítása a 125 m-es VESZ állomáson
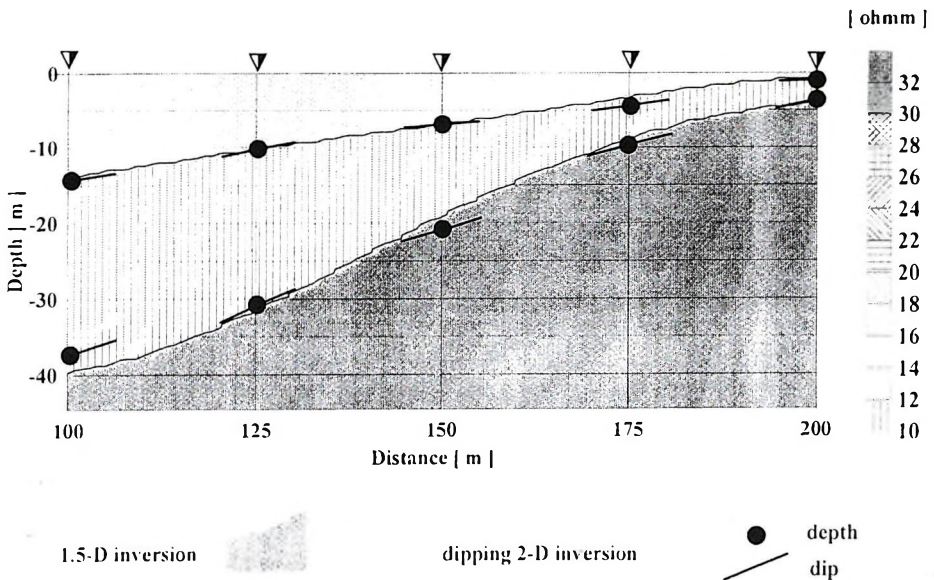
Fig. 6. Inversion result of VES investigations (comparison of dips 2-D and 1.5-D)
*6. ábra.*VESZ mérések inverziós eredménye (dőlt 2-D és 1,5-D összehasonlítás)

X (m)	100	125	150	175	200
ρ_1 (ohmm)	17.3 (24%)	18.1 (2%)	17.5 (2%)	16.3 (7%)	17.9 (29%)
ρ_2 (ohmm)	11.4 (13%)	11.4 (4%)	11.4 (4%)	11.4 (4%)	11.4 (4%)
ρ_3 (ohmm)	33.6 (7%)	33.6 (3%)	33.6 (3%)	33.6 (3%)	33.6 (3%)
h_1 (m)	13.8 (13%)	10.1 (11%)	6.9 (10%)	3.3 (24%)	0.5 (75%)
h_2 (m)	25.0 (3%)	21.7 (11%)	12.4 (10%)	5.7 (13%)	3.8 (34%)
h_1+h_2 (m)	38.8	31.8	19.3	9.0	4.2
D (%)	3	3.7	2.9	3.8	3.7
$\vec{\sigma}_n$ (%)	7	4	4	7	21

Table V. Result of 1.5-D simultaneous inversion

V. táblázat. 1,5-D együttes inverzió eredménye

Thanks to the former model investigations, the more reliable estimation of the layer dippings can be given by using simultaneous inversion of VES data measured in different directions and by using several array geometries.

5. Summary

The equations of the potential to solve the direct problem of dipping multi-layer models are known. Based upon the solutions, we set up an algorithm and a computer program in order to calculate the apparent resistivity [GYULAI 1995]. Based upon the analytical solution of the direct problem we elaborated a 2-D simultaneous inversion method for VES data. We carried out investigations on synthetic data in order to determine the parameter estimation reliability of dipping layers [GYULAI, ORMOS 1996]. Up till that time, no field testing had been carried out. Subsequently, however, field investigations proved successful so we now consider this method appropriate for such use.

Despite the fact that the cross line of the layer boundaries and the common outcrops can be considered as very strict requirements in field practice, our view is that such an approximation is allowable.

Acknowledgements

REFERENCES

GYULAI Á. 1995: Geoelectrical investigation of dipping beds with analytical forward modelling. Magyar Geofizika **36**, 1, pp. 40–46.

GYULAI Á., ORMOS T., 1996: Simultaneous inversion of geoelectric data for dipping beds based on analytical forward modelling. Magyar Geofizika **37**, 1, pp. 17–26.

CHATANET de GERY J., KUNETZ G. 1956: Potential and apparent resistivity over dipping beds. Geophysics **XXI**, 3, pp. 780–793.

HMELEVSZKOJ V. K., BONDARENKO V. M. 1989: Elektrorazvedka. Moskva, Nyedra 52–55.

BERNABINI M., CARDARELLI E. 1991: Geoelectrical surveys of dipping structures. Geophysical Prospecting **39**, pp. 953–966.

HERING A., MISIEK R., GYULAI Á., ORMOS T., DOBRÓKA M., DRESEN L. 1995: A joint inversion algorithm to process geoelectric and surface wave seismic data. Part I. basic ideas. Geophysical Prospecting **43**, 135–156.

DOBRÓKA M., GYULAI Á., ORMOS T., CSÓKÁS J., DRESEN L. 1991: Joint inversion of seismic and geoelectric data recorded in an underground coal mine. Geophysical Prospecting **39**, pp. 643–665.

SALÁT P., TARCSAI Gy., CSEREPES L., VERMES M., DRAHOS D. 1982: Statistical Methods in Geophysical Interpretation (University textbook: in Hungarian). Tankönyvkiadó, Budapest

Dőlt réteges földtani szerkezet meghatározása együttes 2-D inverziós módszerrel

GYULAI Ákos

A dolgozatban dőlt, háromréteges földtani szerkezet paramétereinek becslését mutatjuk be egy terepi példán 2-D együttes inverziós módszerrel. Az inverzióban a direkt feladatot analítikus módszerrel oldjuk meg. Az együttes inverzióban közösen szerepelnek a dőlés- és csapásirányú mérések adatai. A VESZ görbékből L_2 inverzióval a rétegvastagságok és fajlagos ellenállások lokális értékei mellett a rétegek dőlését is meghatározzuk. A becsült rétegparaméterek

megbízhatóságát a korreláció és a variancia értékekkel jellemezzük. Összehasonlítjuk a dőlésirányú mérési adatoknak 2-D inverziós módszerrel és az előbbiektől független csapásirányú geoelektromos mérési adatoknak 1,5-D inverziós módszerrel történő becslési eredményét.

ABOUT THE AUTHOR

Ákos Gyulai graduated as a geologist engineer at the Technical University of Heavy Industry, Miskolc, in 1968. He joined the Department of Geophysics at Miskolc University as a research associate in 1971 and since that time he has been a member of that department where he is currently professor. He has headed the Department of Mineralogy and Petrology since 2002. In 2002 he was awarded his D.Sc. by the Hungarian Academy of Sciences. His main interests are mining geophysics, lately engineering geophysics and environmental geophysics with emphasis on the development and application of inversion methods. He is a foundation member of the Mikoviny Earth Science Doctorate School. Since 2000 he has been the secretary of Geophysical Scientific Committee of the Hungarian Academy of Sciences. He is also a member of EAGE and the Association of Hungarian Geophysicists.

New geoelectric–seismic joint inversion method to determine 2-D structures for different layer thicknesses and boundaries

Ákos GYULAI[*] and Tamás ORMOS[*]

The basics of a new joint inversion method are presented. This new method is able to determine 2-D structures employing geophysical measurements based on various kinds of physical principles or arrays together, even for different layer boundaries for the different geophysical methods. The method was used on geoelectric and seismic refraction data. Applications are presented for synthetic computer-generated data and for a set of field data. It will be shown that the so-called function inversion method — by means of the appropriate conditional functions — also gives a good estimation for non-identical boundaries. This method also supports the view that joint inversion is a powerful means to investigate complicated geophysical and geological structures.

Keywords: geoelectrics, seismic methods, joint-inversion, thickness

1. Introduction

If one carries out only a single inversion of geophysical data it can often lead to model parameter estimation which is unreliable; this then appears in the value of the correlation coefficient near ± 1 and in the overall estimation error [INMAN, 1975, SALÁT et al. 1982]. This problem is particularly well-known in geoelectric measurements (VES), where quotient $h\circledR$ for S-type equivalence and $h\cdot\rho$ K-type equivalence are determined but the parameters separately are not [KOEFOED 1979].

Ambiguity of inversion estimation can be diminished by using one of the most important tools in data processing: joint inversion [VOZOFF, JUPP 1975, DOBRÓKA et al., 1991, GYULAI, ORMOS 1999].

* University of Miskolc, Geophysics Department, H–3515 Miskolc-Egyetemváros
Manuscript received: 5 March, 2001.

Joint inversion can be carried out with data of geophysical methods based on similar or different physical parameters. The former one is known as simultaneous inversion, the latter being the joint inversion method.

The hitherto known joint inversion methods are efficient (and can be called joint inversion) only if the different geological–(geo)physical models have at least one common parameter: the common parameter(s) is (are) usually the layer-thickness(es). The mutual correlation of the boundaries cannot always be carried out because they are not always identical to any other method. HERING et al. [1995] and MISIEK et al. [1997] developed a new joint inversion method which allows the boundary differences if there are other identical boundaries. The difference of the boundaries may already be considerably large when the application of the joint inversion method is already prohibited. The present joint inversion method developed by us enables joint inversion to be used for a real field model, when there are neither mutual geometrical nor (geo)physical parameters between the two geophysical models.

With this new method the joint inversion method can be used more widely.

2. Function inversion as a joint inversion method

The main idea of function inversion methods is to describe the layer-thicknesses (indirectly the boundaries) and (geo)physical parameters along the profile with functions expanded in series. At first, we determine the function coefficient by inversion and then we compute the local parameters of the model and use them point by point along the profiles.

Inversion for the function coefficients means joint- or simultaneous inversion as the coefficients refer to the whole length of the profile, and we use all the data observed in the geophysical measurement stations for their determination.

The idea of describing model parameters by functions and their application in a seismic inversion was first proposed in applied geophysics by DOBRÓKA [1996, 1997] and DOBRÓKA et al. [1995].

In function inversion, Fourier expansion is very often used to describe the changes of the model parameters [GYULAI, ORMOS 1999, GYULAI 2000, ORMOS et al. 1998] as follows

$$\rho_n(s) = \frac{1}{2}d_{n_0} + \sum_{k=1}^{K} d_{n_k} \cos k\frac{2\pi s}{S} + \sum_{k=1}^{K} d_{n_k}^{\bullet} \sin k\frac{2\pi s}{S}, \quad \text{where } n=1, \ldots, N$$

$$h_n(s) = \frac{1}{2}c_{n_0} + \sum_{l=1}^{L} c_{n_l} \cos l\frac{2\pi s}{S} + \sum_{l=1}^{L} c_{n_l}^{\bullet} \sin l\frac{2\pi s}{S}, \quad \text{where } n=1, \ldots, N{-}1$$

where function h_n is the thickness function of the nth layer-thickness, ρ_n is the resistivity function of the nth layer and $d_{n_k}, d_{n_k}^{\bullet}, c_{n_l}, c_{n_l}^{\bullet}$ denote the function coefficients. N is the number of layers, and s is the distance of the stations along the profile with length S.

To describe 'slow' change of model parameters the power functions can also be used successfully

$$\rho_n(s) = \sum_{p=1}^{P} a_{n_p} s^{(p-1)}, \quad \text{where } n = 1, \ldots, N$$

$$h_n(s) = \sum_{q=1}^{Q} b_{n_q} s^{(q-1)}, \quad \text{where } n = 1, \ldots, N{-}1.$$

The great advantage of using power functions is that we can successfully carry out the joint inversion even for 2 or 3 stations simultaneously.

2.1. Inversion of geoelectric measured data

We have developed a new inversion procedure, which we call the 1.5-D inversion method, for interpreting conventional VES measurements. This involves all the data of the VES stations measured in the direction of the structural strike of the section being linked in one joint inversion procedure [GYULAI, ORMOS 1997, 1999]. We used a 1-D solution of the direct problem at each VES station (i.e. local models) in the section. This procedure increases the extent of reliability of the parameter estimation compared to single inversion as will be shown by synthetic and field examples.

For investigating 2-D structures with parameters changing laterally 'quickly', new methods have been introduced which are different from the conventional VES method. The important element of these procedures is that the measurements are done with an electrode configuration which is a combination of horizontal profiling and vertical electric sounding in the

dip direction. The measured data are plotted in pseudo sections and are inverted by 2-D an inversion method [LOKE, BARKER 1996]. The reliability of the inversion results of pseudo sections can be increased by using a function inversion algorithm. The 1.5-D function inversion is one of these methods [GYULAI, ORMOS 1997, 1999] which can increase the reliability of the estimation in such a way that it can compensate the errors caused by 1-D forward modelling [ORMOS et al. 1999]. Another version of geoelectrical function inversion is the combined function inversion method. Here we realize a two-step inversion. At the beginning of the inversion we apply in the inversion algorithm the faster but less accurate 1-D forward modelling (1.5-D inversion), and then the slower but more precise 2-D forward modelling (e.g. finite difference method) [GYULAI 2000].

2.2. Inversion of time data of refracted waves

If the geometrical and (geo)physical model parameters change laterally slowly and continuously in the given 2-D structure, furthermore, conditions for using the refraction method are accomplished, the function inversion method can be applied for the kinematic inversion of refraction time data. BERNABINI et al. [1988] developed a method in which the layer boundaries are described by power functions and it is assumed that the layer velocities are horizontally non-variable. However, in practice it is not unusual for the layer velocities to change horizontally and that is why we developed a function inversion method for the refraction data that allows lateral changes of the physical parameters [ORMOS 2002].

A further advantage of this new method is that we can use several types of functions (e.g. Fourier expansion) in the same inversion procedure. Thus the method is suitable for estimating the parameters of real (complicated) field structures in a joint inversion process.

2.3. Joint inversion of geoelectric apparent resistivity and arrival time data of refracted waves

As we have seen in GYULAI and ORMOS's works [e.g. 1999] on synthetic and field geoelectric data, 1.5-D inversion (function inversion) can considerably reduce uncertainty in estimating the local layer parameters in the 2-D section. To increase the vertical and horizontal resolution of the inversion the information about the model from a single geophysical

method for enhancement might not always be enough: we need the joint inversion of data of several geophysical methods. If we do it with function inversion, it means — in practice — a double joint inversion procedure. In engineering and environmental geophysics one of the possibilities of this kind of inversion is the joint inversion of geoelectrical and refraction data for 2-D structures.

ORMOS et al. [1998] and KIS [1998] developed a joint inversion method to evaluate refraction and VES data located in the drift of the 2-D structure. DOBRÓKA et al. [1999] have developed a new, so-called hybrid joint inversion method to evaluate the joint inversion of dip refraction and drift VES data. The algorithm allows the change of either the geometrical or the physical parameters. Furthermore, these joint inversion methods assume that the geoelectric and seismic layer boundaries are the same.

3. Relative efficiency of the joint function inversion method

To characterize the uncertainty of the model parameters estimated by inversion we use the covariance matrix [SALÁT et al. 1982, DOBRÓKA et al. 1991] to compute the parameter error and the correlation matrix. One of the indices of the efficiency of function inversion is the error of the parameter estimation. We define it as:

$$
\sigma_{P_s} = \left[\frac{1}{M} \cdot \frac{1}{2N-1} \sum_{m=1}^{M} \sum_{n=1}^{2N-1} \sigma_{P_{mn}} \right]^{1/2},
$$

where M — number of measuring stations (local models),
  N — number of layers
  $\sigma_{P_{mn}}$ — error of nth parameters in the mth local model.

The first step in 1.5-D function inversion is to determine the function coefficients and their errors. From these we can compute the error of the nth parameter in the mth model based on error propagation law:

$$
\sigma_{P_{mn}} (\%) = 100 \cdot \frac{\sum_{i=1}^{J(n)} \sum_{j=1}^{J(n)} F_{mni} F_{mnj} (\Delta\sigma_{c_{ij}})^{1/2}}{P_{mn}},
$$

where $J(n)$ is the number of function coefficients for the nth layer ($1<n<N$).

In the case of 1.5-D function inversion, the joint inversion method is the most successful if we consider the geometrical parameters of the model (e.g. layer-thickness) or the physical (geophysical) parameters to be non-variable along the profile. It means that the model parameters are the zeroth elements of the function series (j=1). Let us define this special case of j as j^*. Real geophysical models often require that we allow horizontal changes of both types of parameters (thickness and physical parameters, too). In this case, we have to take it into consideration that the efficiency of joint inversion may be reduced. If the number of coefficients (for both parameters) reaches the number of measurement stations (local models) (j=M) along the profile, the joint inversion turns into sequences of single inversions [GYULAI, ORMOS 1999].

To extend the reliability of the parameter estimation let us define the relative efficiency of the function inversion. The relative efficiency of the function inversion is 100% if the geometrical or the (geo)physical parameters are non-variable along the profile so the number of function coefficients is j=1. The relative efficiency of joint inversion is 0 when at each parameter j=M is fulfilled. The relative efficiency is given by:

$$\eta(\%) = \frac{\sigma_{p_s}(\max) - \sigma_{p_s}(estimated)}{\sigma_{p_s}(\max) - \sigma_{p_s}(\min)} \cdot 100.$$

This definition may cause a distortion in the computation of efficiency at high σ_{p_s} values. With high σ_{p_s} values the efficiency improves; in other words, the greater the value of σ_{p_s}, the lower the physical value (it loses its error values) and it relates only to the large degree of uncertainty. This is because the deviation of parameters close to the estimation point are defined with the help of linearization (with the zeroth and first element of Taylor's expansion) so that the characterization of the extent of the confidence region is very inaccurate [SALÁT et al. 1982].

That is why we define the efficiency in another way, deriving it from the model distance

$$\eta^*(\%) = \frac{d(\max) - d(estimated)}{d(\max) - d(\min)} \cdot 100,$$

where d corresponds to the relative model distance [GYULAI, ORMOS 1999], such as the distance of the estimated model from the exact model. One of the problems of this definition is that it can only be used for known models (for investigating synthetic data) and we have to take into consideration that it also shows deviation because it is a probability parameter. We can expect that the relative efficiency determined in two ways is the same and gives similar values if σ_{p_s} is not too high ($\sigma_{p_s} < 50\%$) and the expected value of the model distances is estimated by a sequence of computer runs.

In *Figs. 1* and *2* we demonstrate the changing of the efficiency of joint inversion due to the number of unknown function coefficients. For these investigations we computed synthetic input data for lateral non-variable layer-thicknesses in the first case (Fig. 1), and in the second case for lateral non-variable resistivities (Fig. 2). In both cases we added errors to the synthetic data. During the inversion we allowed the change of the non-variable model parameters along the profile in the first case for the layer-thicknesses, in the second for the resistivities because of the error added to the data. During the test we used more than one coefficient to describe the model parameter mentioned above. (The first, i.e. zeroth, coefficient describes lateral non-variable model parameters.) With increasing number of these coefficients the degree of freedom of the inversion increases. We call them free coefficients. We made a series of inversions with a different number of free coefficients in both cases.

Figures 1 and 2 show the results of 1.5-D function inversions of apparent resistivity with added 3% Gaussian noise for 14 VES stations. VES data were calculated on a 2-D structure in the strike direction for logarithmically equidistant, AB/2=5–800 distances. In the joint inversion there were 14×23 data.

It can be seen from the figures that the increasing number of free coefficients leads to a decrease in the efficiency of inversion (the degree of efficiency), i.e. due to the data errors the estimated model parameters get farther from the theoretical values. In the figures summarizing the results we can also see that the relative model distances (differences from the theoretical models) are very close to the norm of the estimation errors in the case of a low number of free coefficients. With a high number of free coefficients — when the joint inversion turns into a single one — the model
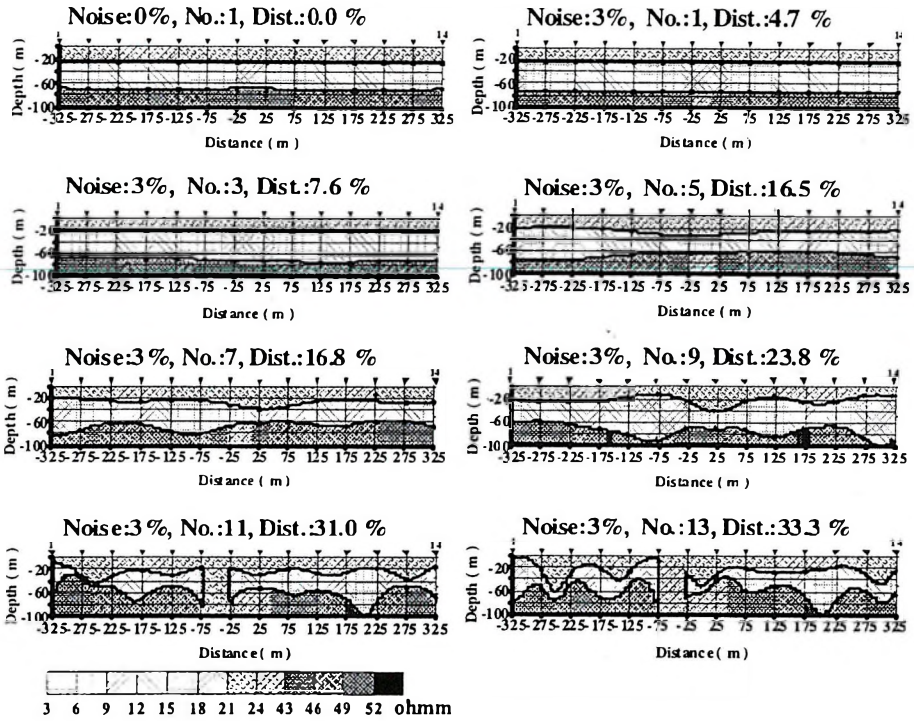
Noise:0%, No.:1, Dist.:0.0 %

Noise:3%, No.:1, Dist.:4.7 %

Noise:3%, No.:3, Dist.:7.6 %

Noise:3%, No.:5, Dist.:16.5 %

Noise:3%, No.:7, Dist.:16.8 %

Noise:3%, No.:9, Dist.:23.8 %

Noise:3%, No.:11, Dist.:31.0 %

Noise:3%, No.:13, Dist.:33.3 %
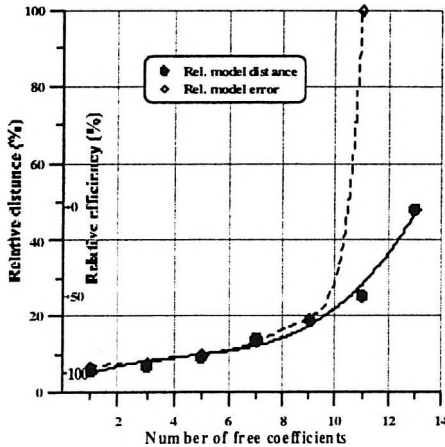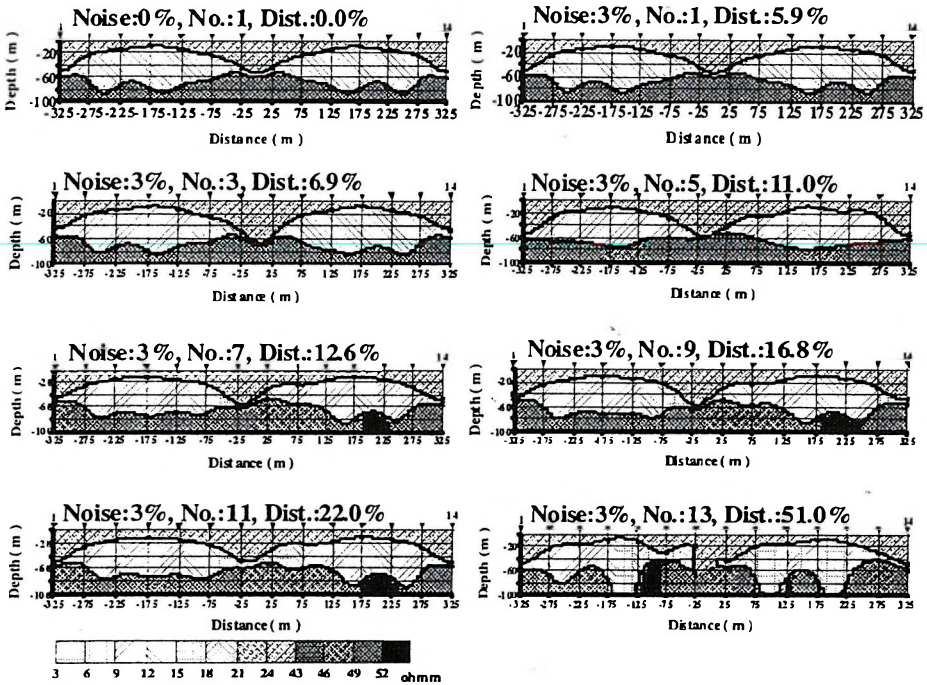
3 6 9 12 15 18 21 24 43 46 49 52 ohmm
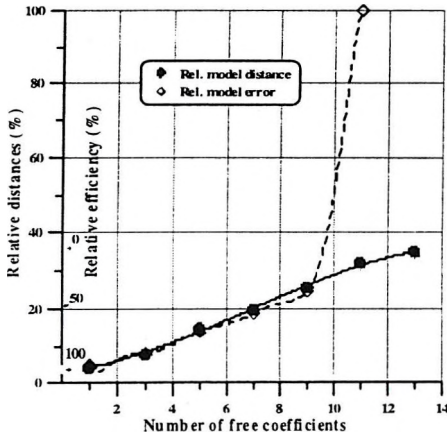
Fig. 1. Efficiency of function inversion for constant layer thickness and variable resistivity (No: number of free coefficients, Dist: distinctness between estimated model parameters and theoretical values)

1. ábra. A függvényinverzió hatékonysága konstans rétegvastagság, változó fajlagos ellenállás esetén (No: a szabad együtthatók száma, Dist.: a becsült és elméleti modell paraméterek közti eltérés)

parameter errors suddenly increase. The 'relative model error' curve separates from the model distance curve.

We have already referred to the fact that above a certain level the parameter estimation errors lose their physical values. In our example an

Fig. 2. Efficiency of function inversion for constant resistivity and variable layer thickness (No: the number of free coefficients, Dist: distinctness between estimated model parameters and theoretical values)

2. ábra. A függvényinverzió hatékonysága konstans fajlagos ellenállás, változó rétegvastagság esetén (No: a szabad együtthatók száma, Dist.: a becsült és elméleti modell paraméterek közti eltérés)

increase occurs in the estimation errors in the second layer which, in turn, causes a remarkable increase in the mean value of the whole model.

4. Joint inversion with different layer boundaries

Based on Figs. 1 and 2 we can make an important deduction: the changing of the relative efficiency based on model distance shows that the efficiency of the joint inversion is about 50% with half of the allowable coefficients. From this we can conclude that the joint inversion of different geophysical methods can also be carried out with different layer boundaries (with physical boundaries) by function inversion.

For joint inversion we do not need to demand the agreement of coefficients (mutual correlation of the boundaries) so that we can have free coefficients at different geophysical procedures. This may reduce the efficiency of joint inversion but the different geophysical layer boundaries are allowed to differ from each other.

To solve this problem we chose one of the simplest function inversion methods to describe the parameters by power functions

$$h_{e_j} = a_0 + a_1 s_1 + a_2 s^2 + a_3 s^3 + ... + a_n s^n,$$

where h_{e_j} is the thickness of the jth layer of the geoelectric model.

$$h_{s_j} = b_0 + b_1 s_1 + b_2 s^2 + b_3 s^3 + ... + a_n s^n$$

where h_{s_j} is the thickness of the jth layer of the seismic model, apart from the fact that the seismic direct problem is given for boundary depth. If the stations are located very close and

if $a_i = b_i$, $i=1,...,n$ the two boundaries are the same

if $a_0 \neq b_0$ and any other $a_i = b_i$ the parallel translation of the two layer boundary surfaces is allowed

if $a_1 \neq b_1$ and any other $a_i = b_i$ dip changes of the boundary are allowed

etc.

Describing the layer-thicknesses by Fourier expansion we can give the conditions for the similarities of the boundaries from the low or high frequency elements of amplitude spectrum besides the parallel translation of the boundaries. We composed the adjoint function for boundary conditions for linear inversion and we developed the inversion algorithm with it [GYULAI et al. 2000]. It is mentioned that there is a possibility to weight

the condition function for the coefficients. We made use of our a priori knowledge for the freedom of coefficients and the weighting of the adjoint auxiliary conditional equation.

4.1. 1.5-D joint inversion of synthetic geoelectric data

We generated synthetic VES data for a given geoelectric model (broken line in *Fig. 3a, b*). In order to simulate a moderately noisy measuring data system we added Gaussian noise of 3% to the calculated apparent resistivity values. In *Fig. 4* the dots denote this sounding data. We carried out the geoelectric joint inversion with 5×21 sounding data. We described the changes of the model parameters by power functions using 5,5,5 coefficients to describe the thickness and 5,3,3,3 coefficients to describe apparent resistivity in the inversion. The estimated model parameters are shown in Fig. 3 (continuous line). The data distance was 2.9% which is equal to 3% Gaussian error. The fitted data (between the theoretical curve and the data denoted by dots) can be seen in *Fig. 6*. The value of the model distance is 16.2%, which derives from the estimation error of the second layer thickness and the apparent resistivity of the second and the fourth layer. The mean of the model error is $\sigma_{p,} = 31.2\%$.

3.2. Function inversion of synthetic seismic refraction data

The geometrical parameters of the seismic model used by us differed from the geoelectric model so that we could investigate the joint inversion, (described later) for different layer boundaries.

The local parameter changes of the seismic model can be seen in *Fig. 5a, b* plotted by broken lines. We calculated seismic refraction arrival times for the estimated model for 80 geophones. The shot points were positioned equidistantly every 25 m with the first one on the zeroth point of the profile and the last one on its 200 m mark. To simulate field data we added errors to the calculated data. The errors were generated from source synchronizing deviations and high frequency model noise and the sum of Gaussian noise. The generated data system is shown in *Fig. 6* denoted by dots.

In 2-D seismic function inversion [ORMOS 1999] we described the layer-thicknesses by power functions with 4–4 degrees and the velocity by power functions with 6–3–2 degrees. The result of the inversion is shown
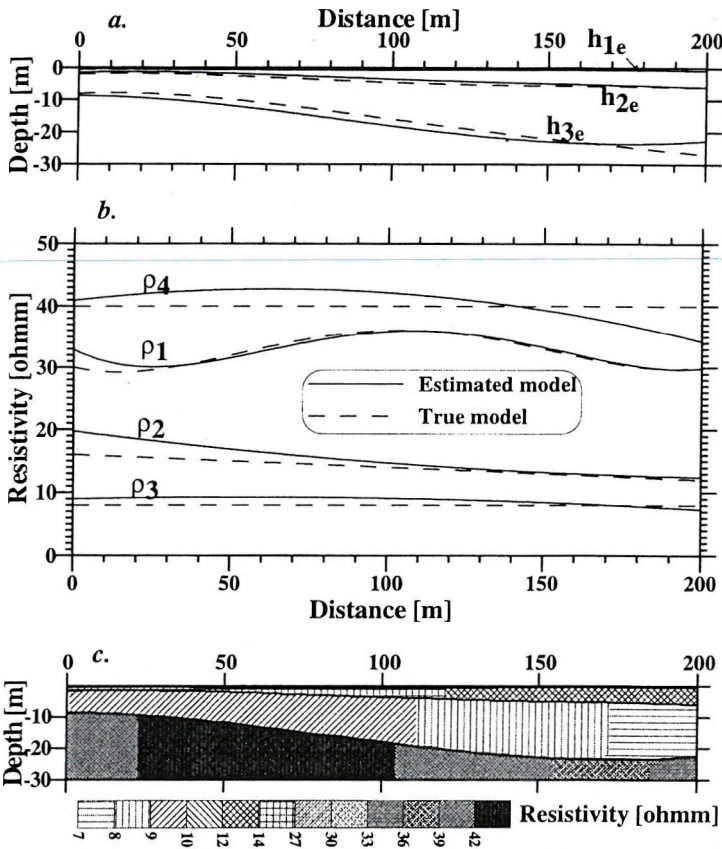
Fig. 3. Result of 1.5-D geoelectric inversion and the theoretical model parameters (plotted with broken line)

3. ábra. Az 1,5-D geoelektromos inverzió eredménye és az elméleti modell paraméterek (szaggatott vonallal rajzolt)

in *Fig. 5a, b* (continuous lines) and *Fig. 5c*. The data fitting error $D=6.8\%$, the model error $\sigma_{p_x} = 45.8\%$, and the model distance $d=17.5\%$ were obtained. In calculating the model distance and the value of the mean error (here and also in the joint inversion) we neglected the parameter data of the two ultimate points because at these points parameter estimation is very unstable due to the lack of refracted arrivals.
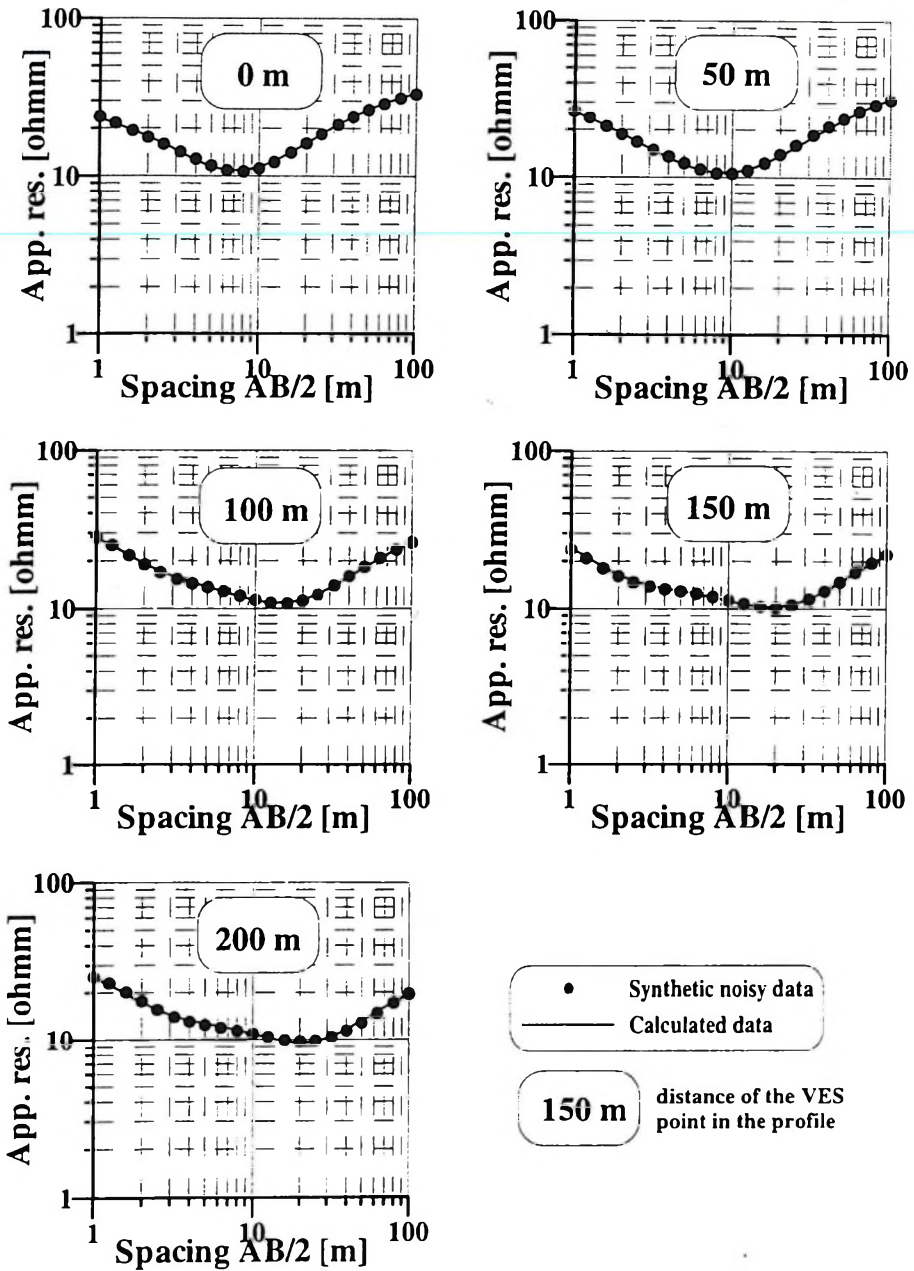
Fig. 4. VES sounding data with added Gaussian noise of 3% and the calculated theoretical curves for the model estimated by inversion

4. ábra. 3%-os Gauss hibával terhelt VESZ szondázási adatok, és a becsült modellből számított elméleti adatok
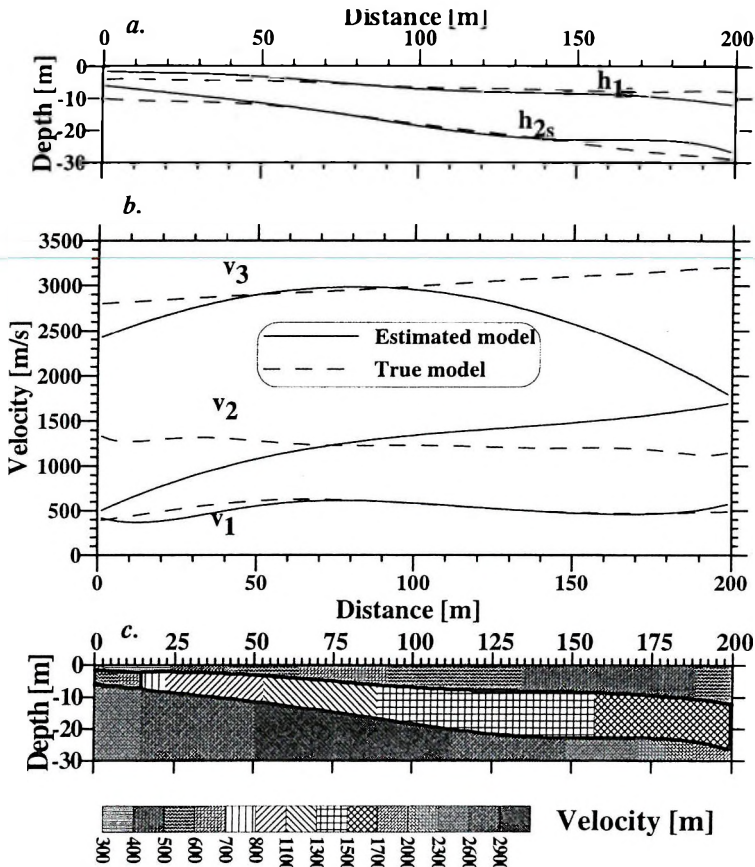
Fig. 5. Result of 2-D seismic inversion and the theoretical model parameters (plotted with broken line)

5. ábra. A 2-D szeizmikus inverzió eredménye és az elméleti modell paraméterek (szaggatott vonallal rajzolt)

4.3. Investigation of the joint inversion of synthetic geoelectric apparent resistivity and synthetic seismic refraction time data

As we have seen in Figs. 3a, b and 5a, b (dotted lines) the thicknesses of theoretical models in the joint inversion differ from each other and the geoelectric model is three-layered whereas the seismic model is two layered:

$$h_{e_1} + h_{e_2} = h_{s_1} - c,$$
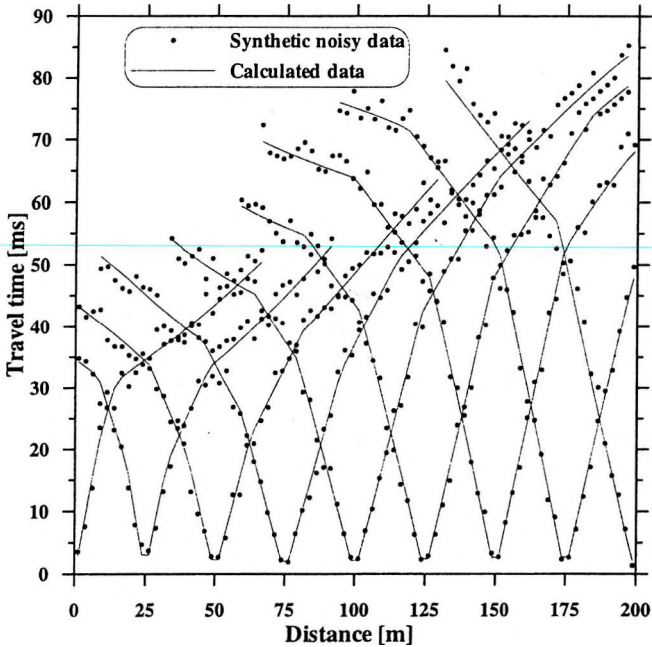
Fig. 6. Synthetic seismic refraction time data (with added noise) and the theoretical curves for the model estimated by inversion

6. ábra. Zajjal terhelt szintetikus refrakciós időadatok, és a becsült modellből számított elméleti görbék

$$h_{e_3} = h_{s_2}$$

where h is given in meters and c=2 m.

We carried out the joint inversion with the same thickness function inversion as described in geoelectric and seismic inversion. We would mention that in the joint inversion algorithm developed by us, the equality of the number of coefficients is not necessary as is shown in the latter field case.

The result of the joint inversion is shown in *Table I*, which contains the changes of the quality parameters as a function of c. It is obvious that during the inversion the theoretical value of $c \approx 2$ m changes due to the data errors. The average model distance minimum was obtained between c=2.2 and 2.4. The well-described model distance minimum shows that the unknown c value can be estimated by an appropriate inversion algorithm.

Geometric const. (c)[m]	Inversion of geoelectric data			Inversion of seismic data			Mean values
	data distance (D) [%]	model error σ_{p_e} [%]	model distance (d) [%]	data distance (D) [%]	model error σ_{p_s} [%]	model distance (d) [%]	model distance (d) [%]
2	2.9	25.3	12.6	7.0	11.9	9.9	11.25
2.2	2.9	25.5	12.4	7.0	11.7	9.2	10.80
2.4	2.9	24.8	12.1	7.1	11.7	9.3	10.70
2.6	2.9	23.9	13.3	7.1	11.3	11.0	12.15

Table I. Quality parameters of geoelectric–seismic joint inversion results, depending on geometrical parameter 'c'
I. táblázat. Geoelektromos–szeizmikus együttes inverzió eredményeinek minősítő paraméterei a „c" geometriai paraméter függvényében

	Inversion of geoelectric data			Inversion of seismic data		
	data distance (D) [%]	model error σ_{p_e} [%]	model distance (d) [%]	data distance (D) [%]	model error σ_{p_s} [%]	model distance (d) [%]
Individual	2.9	31.2	16.2	6.8	45.8	17.5
Joint	2.9	24.8	12.1	7.1	11.7	9.3

Table II. Comparison of quality parameters of geoelectric–seismic single and joint inversions (c=2.4 m)
II. táblázat. A minősítő paraméterek összehasonlítása geoelektromos–szeizmikus egyedi és együttes inverzió esetében (c=2,4 m)

Tables I and *II* show that the distance of the geoelectric model for 34% and the distance of the seismic model for 88% were reduced in the inversion, which results in an average of 61% reduction in model distance. It demonstrates that joint inversion increases the reliability of the parameter estimation for different layer boundaries as well. The result of the estimation by joint inversion is demonstrated along the profile (*Figs. 7, 8*). The relative distances during the iteration are shown in *Fig. 9* for joint
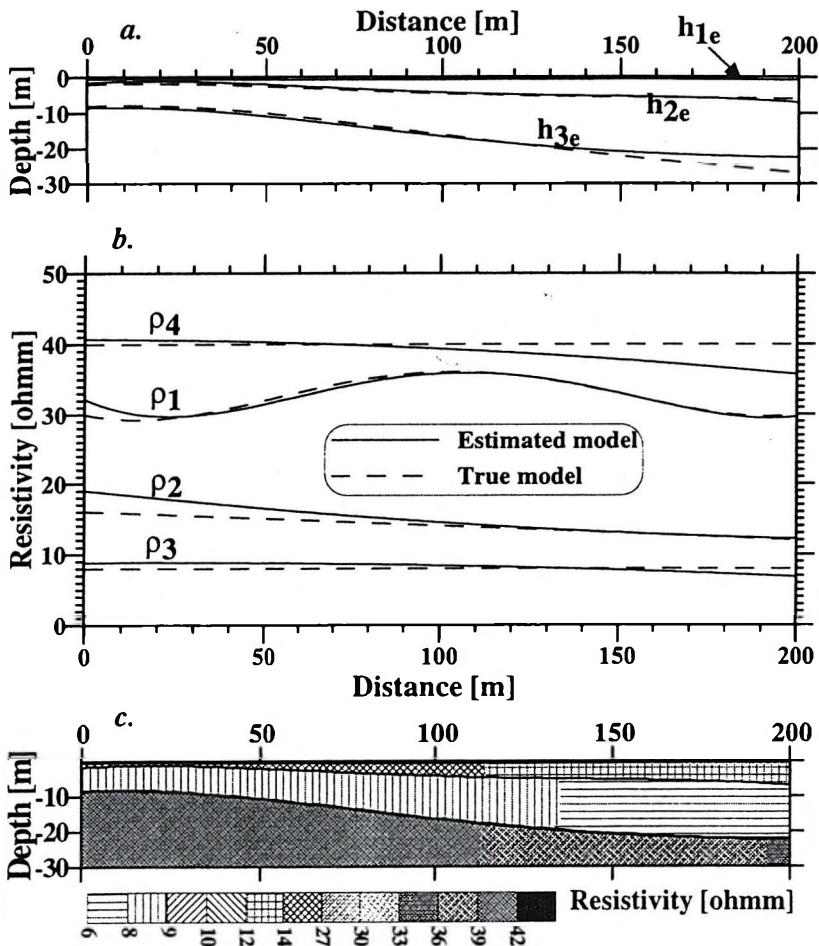
Fig. 7. Geoelectric model estimated by geoelectric and seismic joint inversion and the theoretical values (plotted with broken line)

7. ábra. Geoelektromos–szeizmikus együttes inverzióval becsült geoelektromos modell és az elméleti modell (szaggatott vonallal rajzolt)
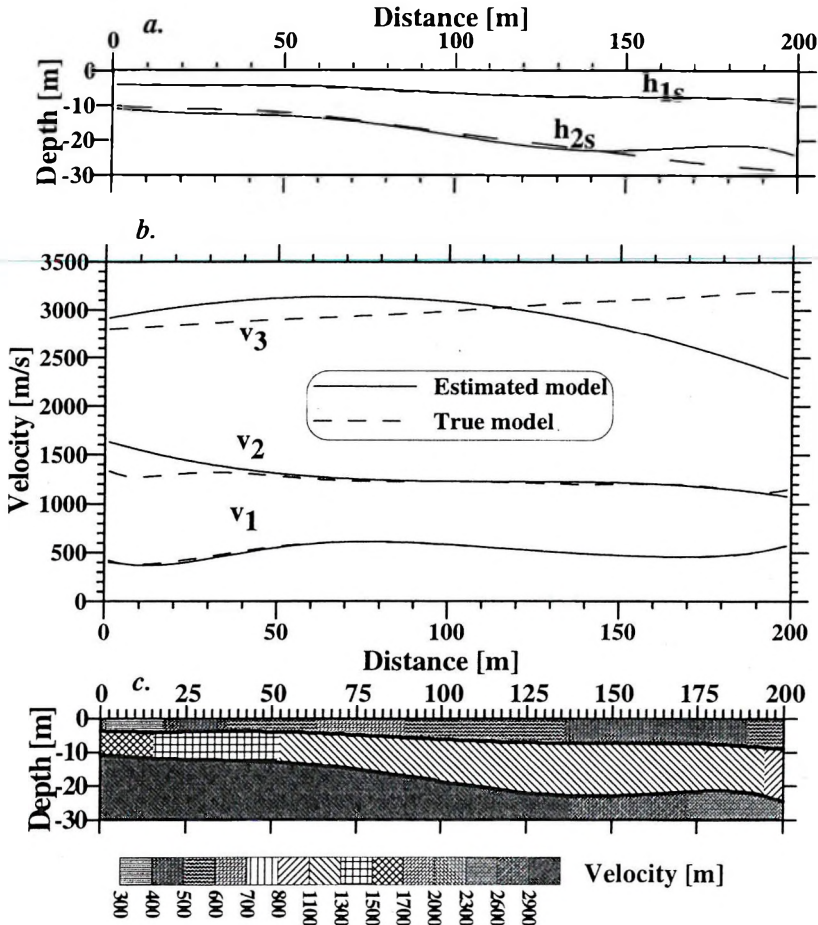
Fig. 8. Seismic model estimated by geoelectric and seismic joint inversion and the
theoretical values (plotted with broken line)

8. ábra. Geoelektromos–szeizmikus együttes inverzióval becsült szeizmikus modell és az
elméleti modell (szaggatott vonallal rajzolt)

inversion. It is noteworthy that besides the variability of the coefficient
correction the model correction changed little during the iteration.
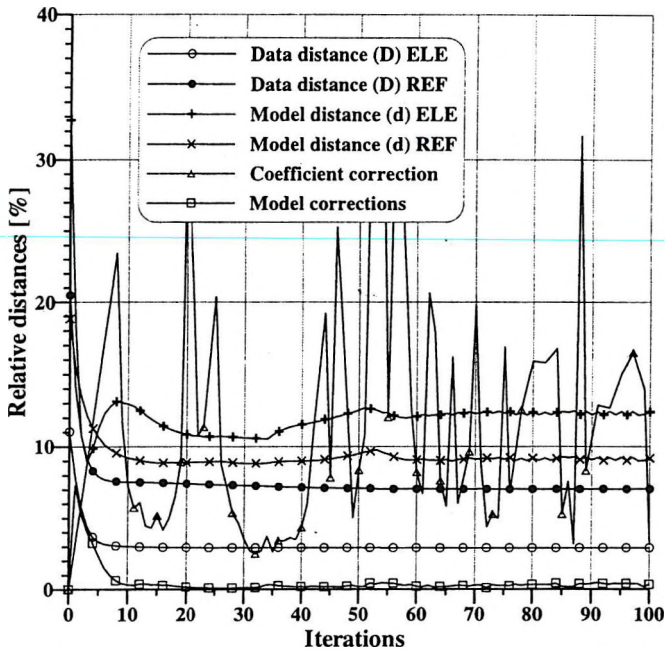
Fig. 9. Iterations of geoelectric and seismic joint inversion for synthetic data
9. ábra. A geoelektromos–szeizmikus együttes inverzió iterációs folyamata szintetikus adatokra

5. Inversion with different layer boundaries, a field study

The geophysical field observations were carried out in the village of Abaújszántó with the primary aim of investigating the positioning of cavities representing inhomogeneity, and not to explore rock stratification. The seismic investigation was planned for the exploration of surface waves and we got the relatively sparse refraction time data as its by-product.

5.1. 1.5-D inversion of geoelectric data

The geoelectric measurements were carried out along a 200 m profile. The 45–95 m long section for the inversion was extracted from this profile. We carried out the measurement using equidistant electrodes with electrode spacing of 2 m. We gained data in two configurations: axial dipole and pole-pole. In the former case the penetration depths were 2–3–4–5–6 m. We described the measured data in pseudosections (see *Fig. 10*). It can be seen clearly from the profile that the geological structure is layered and
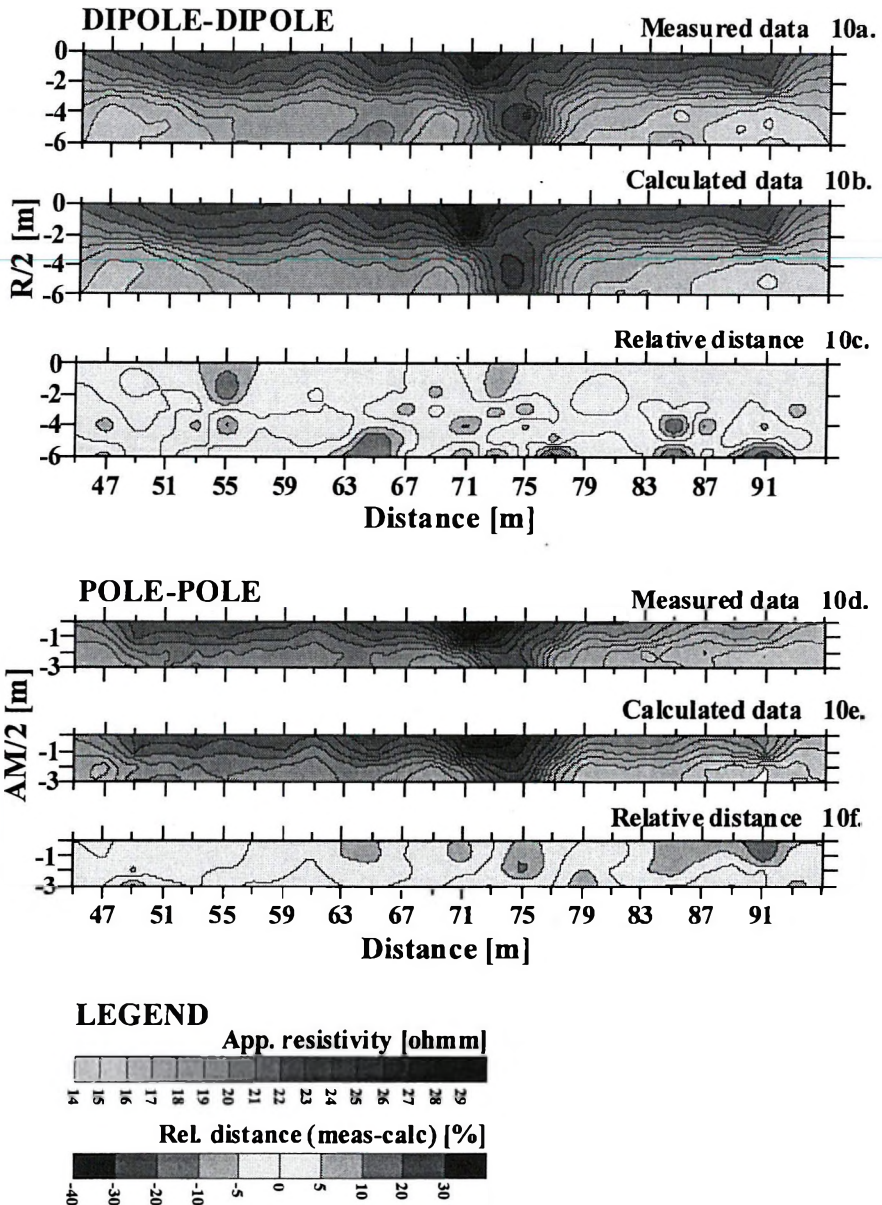
Fig. 10. Dipole-dipole and pole-pole pseudosections plotted with the results of field measurement, the theoretical values of the model estimated by inversion, and the relative distance between the data sets

10. ábra. Terepi dipól-dipól és pól-pól mérésekből, az inverzióval becsült modellből számított elméleti, valamint a kettő relatív eltéréséből számított látszólagos fajlagos ellenállás szelvények

at 75 m there is inhomogeneity related to cavity. In Fig. 10 we can also see the data of apparent resistivity in the form of a pseudosection for the model estimated by inversion and the difference of calculated and measured data.

Significant data errors were confined to individual points. In the inversion there were 216 apparent resistivity data, which realized 135 effective data by the MFV-algorithm used here [DOBRÓKA et al. 1991]. In the inversion the data distance was 2.8%, the mean model error $\sigma_{p_x} = 25.0\%$. The result section of the inversion is shown in *Fig. 11*. The 25% mean model error refers to an average model uncertainty which is due to the non-appropriate density of the data.
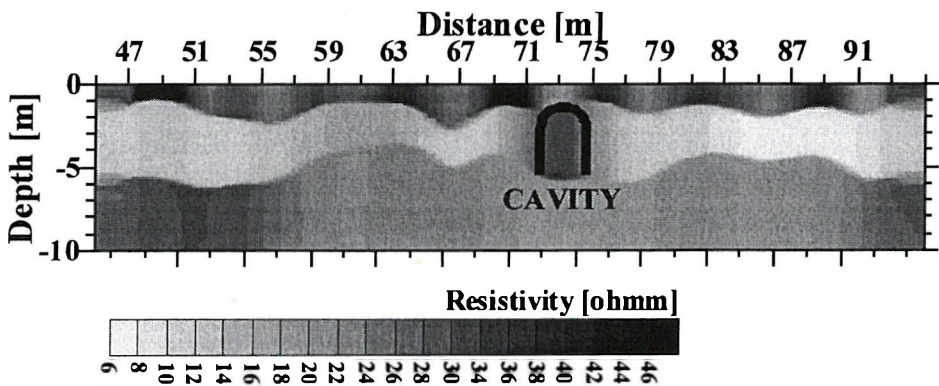
Fig. 11. Result of 1.5-D inversion from field data (interior part of Abaújszántó)
11. ábra. 1,5-D inverzió eredménye Abaújszántó belterületéről származó mérési adatokból

5.2. 2-D inversion of refraction data

Our refraction measurements were also carried out along a 200 m profile, but with 1 m geophone distances, where time data were obtained from 3 shot points. These data and the theoretical curves for the inversion model are shown in *Fig. 12*. We used the MFV-algorithm during the seismic inversion, too. The data distance is $D=6.8\%$, the $\sigma_p = 23.2\%$ value of the average model error refers to a 'moderately low' model estimation. This is due to the incomplete data sets as was already mentioned in the first part of section 4.2. The local values of estimated seismic model parameters are shown in *Fig. 13*.
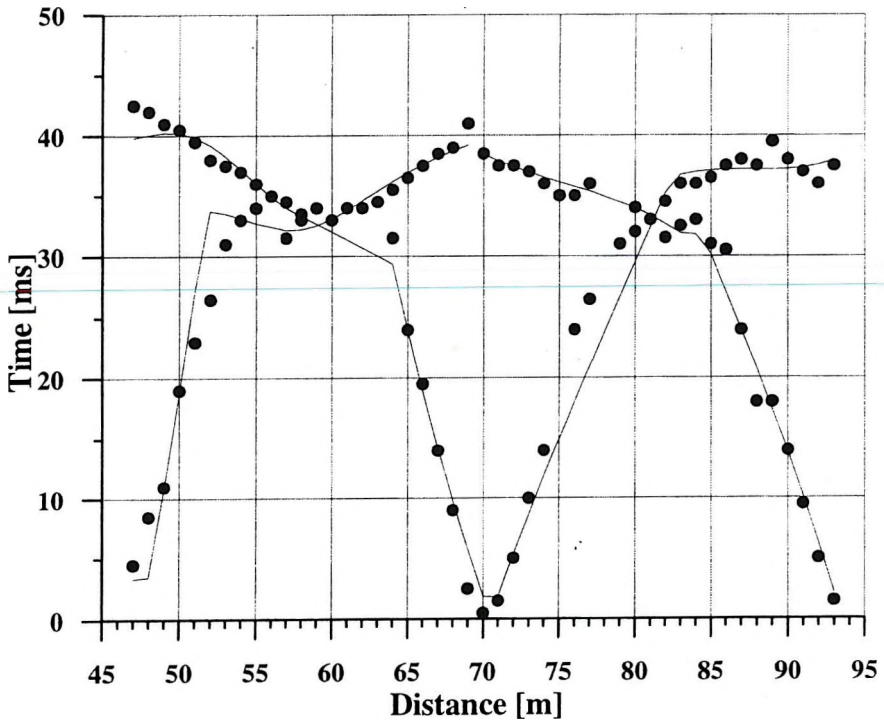
Fig. 12. Seismic refraction time data and the calculated theoretical curves estimated by inversion (Abaújszántó)

12. ábra. Szeizmikus refrakciós mért és az inverzióval becsült modellből számított elméleti időadatok (Abaújszántó)
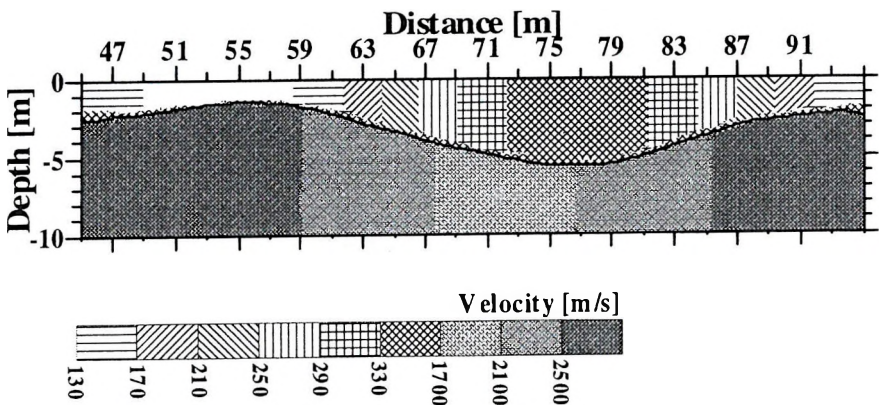
Fig. 13. Seismic field model estimated by 2-D seismic inversion (Abaújszántó)

13. ábra. A 2-D inverzióval becsült szeizmikus terepi modell (Abaújszántó)

5.3. Geoelectric and seismic joint inversion with different layer boundaries

As we can see from the geoelectric and seismic inversion results for the two methods, the boundaries are not identical. The geoelectric one is a three layer and the seismic one is a two layer model and they have not got the same boundary.

For joint inversion as well as in single inversion we used Fourier expansion in the function inversion. In the geoelectric inversion for the layer-thickness we used the expansion up to 9 and 4 harmonics and in seismic inversion up to 3 harmonics. In the joint inversion we assumed that the sum of the first and second geoelectric layer-thicknesses up to the third upper harmonic is the same as the seismic layer-thickness (here the first layer is created with a constant parallel shift). The relative freedom of layer boundaries is allowed by freedom of the further upper harmonics. We would mention that joint inversion failed (was not convergent) for identical geoelectric and seismic layer boundaries. The geoelectric and seismic model estimated by joint inversion is shown in *Fig. 14*. In the inversion the average estimation error of the geoelectric model was reduced from 25.0% to 11.1%; in the seismic model the mean estimation error was improved from 23.2% to 15.7% — which is rather efficient. The values of the S correlation norm — characterizing the correlations between the coefficients [GYULAI, ORMOS 1999] — is $S=0.296$ in geoelectric inversion, $S=0.406$ in seismic inversion, and $S=0.221$ in the joint inversion. The reduction of S in the joint inversion represents a better model parameter reliability than in the single inversion. The changing of the relative distances in the iteration can be seen in *Fig. 15*. The data distance values in joint inversion are practically equal to the values in single inversions.

5. Conclusions

Non-identical model boundaries are often one of the problems in the joint inversion of different geophysical methods. If the difference is significant for certain boundaries, we cannot efficiently use the known inversion methods to reduce the estimation errors. In contradistinction to what has just been said, the new joint inversion method developed by us makes it possible — as has been demonstrated in the synthetic and field examples. With this new procedure 1-D, 2-D, 3-D models can be used in
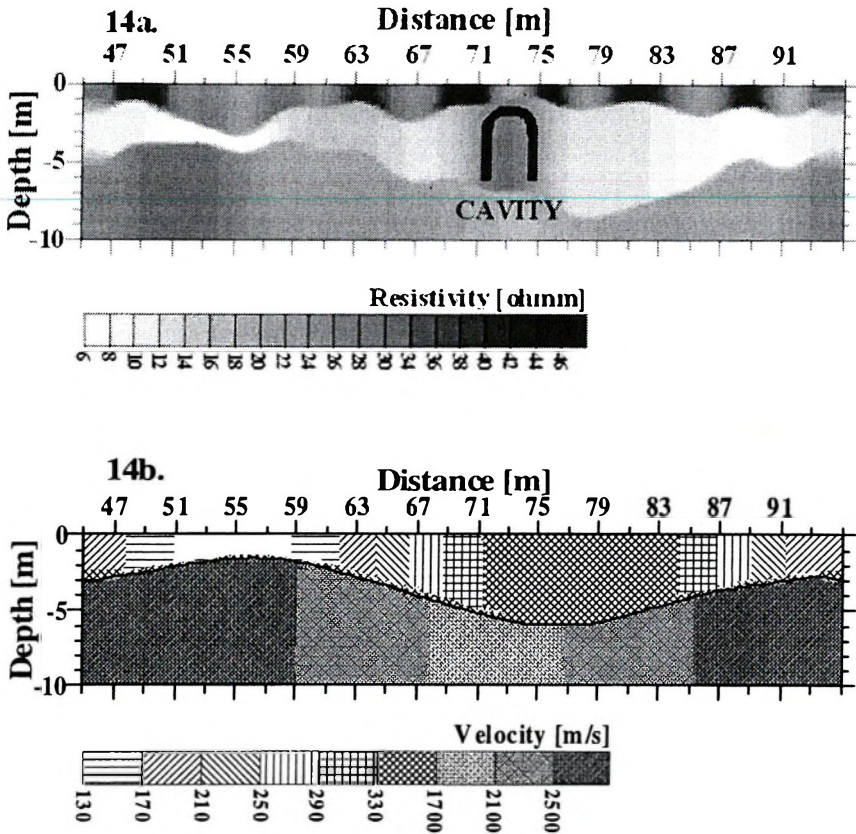
14a.   **Distance [m]**

Resistivity [ohmm]

14b.   **Distance [m]**

Velocity [m/s]

Fig. 14. Geoelectric and seismic models estimated by seismic and geoelectric joint inversion (Abaújszántó)

14. ábra. Geoelektromos és szeizmikus együttes iverzióval becsült geoelektromos és szeizmikus modellek (Abaújszántó)

joint inversion and with the use of the most appropriate geophysical method for a given type of model we can estimate the parameters of complex models more accurately. The new joint inversion method promises to be an efficient tool for interpreting geological, hydrogeological, and environmental investigations.
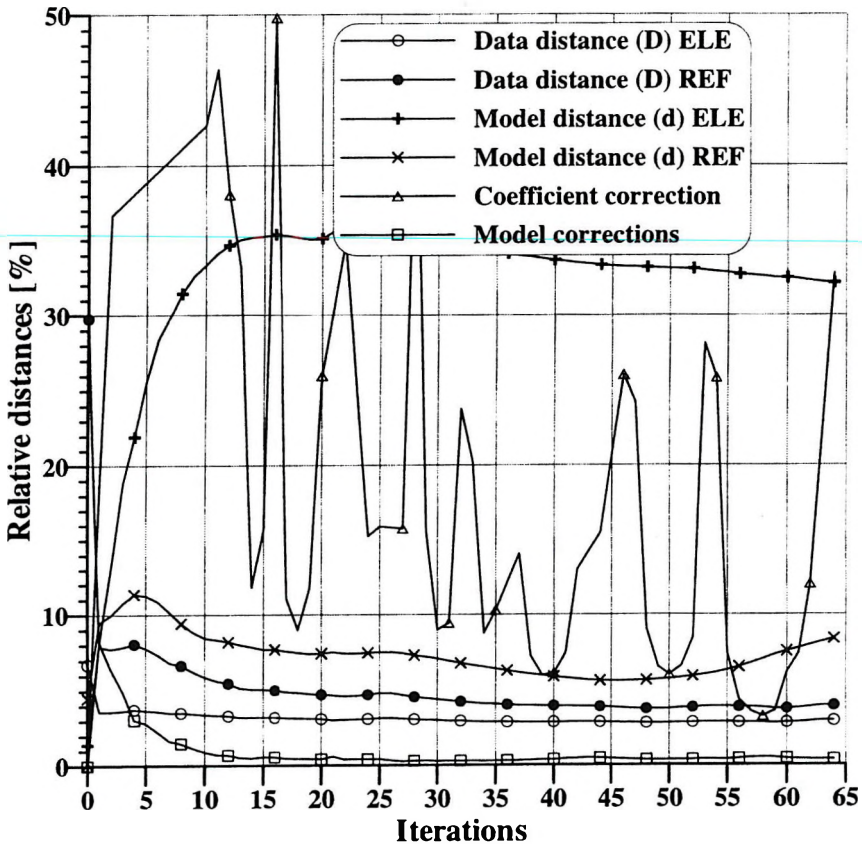
Fig. 15. Iterations of seismic and geoelectric joint inversion for field data (Abaújszántó)

15. ábra. A geoelektromos–szeizmikus együttes inverzió iterációs folyamata terepi adatokra (Abaújszántó)

Acknowledgements

REFERENCES

BERNABINI A., BRIZZOLARI E., CARDARELLI E. 1998: Interpretazione interattiva automatica di prospezioni sismiche a rifrazione. Atti del 7 Convegno Annuale de Gruppo Nazionale di Geofisica della Terra solida, Rome 30 novembre – 2 dicembre.

DOBRÓKA M., GYULAI Á., ORMOS T., CSÓKÁS J., DRESEN L. 1991: Joint inversion of seismic and geoelectric data recorded in an underground coal mine. Geophysical Prospecting 39, 643–665

DOBRÓKA M., FANCSIK T., AMRAN A. 1995: On the in seam seismic inverse problem. 57th EAEG Meeting, Glasgow, 29 May – 2 June

DOBRÓKA M. 1996: Dispersion relation of Love waves propagating in inhomogeneous seismic waveguides with alternating layer thicknesses; inversion of the adsorption–dispersion characteristics. D.Sc. thesis, University of Miskolc

DOBRÓKA M. 1997: Inversion of guided-wave dispersion data. EAGE 59th Conference and Technical Exhibition. Geneva 26–30 May. Extended Abstracts Vol. 1. p. 155

DOBRÓKA M., BERNABINI M., CARDARELLI E., NARDIS DE R. 1999: Quasi 2-D hybrid joint inversion of seismic- and geoelectric data. EAGE 61st Conference and Technical Exhibition, Helsinki, Finland, 7–11 June 1999, P 595 Poster

GYULAI Á., ORMOS T. 1997: Interpretation of vertical electrical sounding curves with the 1.5-D inversion method. Magyar Geofizika 38, 1, 25–29

GYULAI Á., ORMOS T. 1999: A new procedure for the interpretation of VES data: 1.5-D simultaneous inversion method. Journal of Applied Geophysics 41, 1–17

GYULAI Á. 2000: New geoelectrical inversion process for the determination of geological structures: Combined 2-D and 3-D function inversion. Magyar Geofizika 40, 4, 94–98

GYULAI Á., ORMOS T., DRESEN L. 2000: A joint inversion method to solve problems of layer boundaries, differently defined by seismics and geoelectrics. 6th EEGS Meeting, September 6–9. Bochum

HERING A., MISIEK R., GYULAI Á., ORMOS T., DOBRÓKA M., DRESEN L. 1995: A joint inversion algorithm to process geoelectric and surface wave seismic data. Part I: basic idea. Geophysical Prospecting 43, 135–156

INMAN J. R. 1975: Resistivity inversion with ridge regression. Geophysics 40, 798–817

KIS M. 1998: Investigation of near-surface structures by joint inversion of seismic and geoelectric data. Ph.D. thesis, University of Miskolc

KOEFOED O. 1979: Geosounding principles, resistivity sounding measurements. Amsterdam

LOKE M. H., BARKER R. D. 1996: Rapid least-squares inversion of apparent resistivity pseudosections by a quasi-Newton method. Geophysical Prospecting 44, 131–152

MISIEK R., LIEBIG A., GYULAI Á., ORMOS T., DOBRÓKA M., DRESEN L. 1997: A joint inversion algorithm to process geoelectric and surface wave seismic data. Part II: applications. Geophysical Prospecting 45, 65–85

ORMOS T., GYULAI Á., KIS M., DOBRÓKA M., DRESEN L. 1998: A new approach for the investigation of 2-D structures method development and case history. EAGE 60th Conference and Technical Exhibition, Leipzig, Germany, 8–12 June

ORMOS T., GYULAI Á., NYÁRI Zs. 1999: Cavity detection with resistivity and shallow seismic methods. 5th EEGS Meeting, September 6–9. Budapest, Proceedings VoP2

ORMOS T. 1999: Rekonstruktion von Refraktoren mittels Reihenentwicklung von Funktionen. 59. Jahrestagung der Deutschen Geophysikalischen Gesellschaft, Braunschweig, März 1999

ORMOS T. 2002: Inversion of refracted travel-times for near-surface investigation. EAGE 64th conference and Exhibition 27-30 May, 2002 Florence, Italy. Extended Abstracts D025
SALÁT P., TARCSAY GY., CSEREPES L., VERMES M., DRAHOS D. 1982: Statistical Methods in Geophysical Interpretation (University textbook; in Hungarian: A geofizikai interpretáció statisztikus módszerei) Tankönyvkiadó, Budapest.
VOZOFF K., JUPP D. L. B. 1975: Joint inversion of geophysical data. Geophysical Journal of the Royal Astronomical Society **42**, 977–991

Új geoelektromos–szeizmikus együttes inverziós módszer 2-D struktúrák meghatározására eltérő rétegvastagságok, illetve határfelületek esetére

GYULAI Ákos és ORMOS Tamás

A dolgozatban új együttes inverziós módszer alapjait mutatjuk be. Az inverziós módszer 2-D struktúrák meghatározására alkalmas különböző fizikai elven, vagy különböző mérési geometriájú geofizikai módszerek együttes alkalmazásával módszerenként eltérő réteghatárok esetében is. A módszert geoelektromos és szeizmikus refrakciós adatokra alkalmaztuk. Mind ismert modellekre számítógéppel generált adatrendszereken, mind terepi mérési adatokon mutatjuk be a módszer alkalmazását. Bemutatjuk, hogy az együttes inverziós módszerben alkalmazott úgynevezett függvényinverziós eljárás — az együtthatókra vonatkozó megfelelő feltételi egyenletek segítségével — nem identikus határfelületek esetén is jó becslést ad. Ez a módszer az együttes inverzió alkalmazásának az eddigieknél szélesebb lehetőségét teremti meg a bonyolult geológiai–geofizikai struktúrák kutatása területén.

ABOUT THE AUTHORS

Ákos Gyulai, for a photograph and biography, see this issue, p. 271.

Tamás Ormos (1948), graduated from the Technical University of Heavy Industry, Miskolc, as a geophysics engineer in 1972 and in the same year he joined the Department of Geophysics in Miskolc. He was awarded his doctorate in 1985, and his Ph.D. in 1995. His present post is assistant professor at the University of Miskolc. He has been giving lectures on seismics and engineering geophysics since 1972. His main scientific interests are mining geophysics, near surface seismics, and developing methods of inversion and joint inversion.

IP Data processing results from using TAU-transformation to determine time-constant spectra

Endre TURAI[*,**]

A generalization of the TAU-transform method [introduced by TURAI 1985] is presented. On combining the TAU transform method and the tools of inverse problem theory a general algorithm for determining the time-constant spectrum of polarizability data (deduced from time-domain IP measurements) is available for the general case of continuous spectra. Some results from interpreting field data collected over Hungarian waste sites are presented and — based on time-constant spectra — the main components of the contaminating material are characterized.

Keywords: IP data, TAU-transformation, time-constant spectra, waste disposal, Weighted Amplitude Value

1. Introduction

The induced polarization method is well known as an effective geophysical method of ore exploration [WAIT 1959; KELLER, FRISCH-KNECHT 1966; SUMNER 1976] because both the time-domain and frequency-domain IP measurements are capable of detecting even small amounts of metallic minerals. On the other hand, the metallic content is not the only factor resulting in polarizability of the medium: filtration- and membrane effects as well as electrochemical properties can also lead to similar phenomena. Induced polarization is a very useful geophysical method also in the detection of environmentally hazardous locations, particularly for waste sites.

2. TAU-transformation of time-domain IP curves

By means of time-domain IP data, apparent polarizability curves ($\eta_a(\tau)$) can be constructed. The strictly monotonically decreasing functions

---

* MTA-ME Research Group of Geophysical Inversion and Tomography, H– 3515 Miskolc–Egyetemváros
** University of Miskolc, Geophysics Department, H–3515 Miskolc–Egyetemváros

can generally be written as an integral transform of a function $w(\tau)$ [TURAI 1985]:

$$\eta_a(t) = \int_0^\infty w(\tau)\exp(-t/\tau)\,d\tau, \tag{1}$$

where t is the time and τ is the time-constant.

The function $w(\tau)$ will be called the spectrum of time-constants of the IP measurement, which can be normalized as

$$\int_0^\infty w(\tau)\,d\tau = 1.$$

Let us define TAU-transformation as a procedure generating the spectrum of time-constants from the polarizability curves:

$$v(\tau) = TAU\left[\eta_a(t)\right] \tag{2}$$

The IP effect of the rock is displayed by the $w(\tau)$ function: it represents all the important information (regarding the medium) contained by the time-domain IP data.

The two algorithms giving the TAU-transform for this case were developed by [TURAI 1985] based on a linear system of equations and Fourier transform.

3. General solution for the TAU-transform

In order to give the TAU-transform (Eq. (2)) for this general case we use the tools of inverse problem theory. In constructing a general algorithm to determine the TAU-transform [TURAI, DOBRÓKA 2001] we write the spectrum function in the form of a series expansion

$$w(\tau) = \sum_{q=1}^{Q} B_q\, \Phi_q(\tau) \;, \tag{3}$$

where Φ_q is the qth base function and B_q is the corresponding expansion coefficient. As base functions, we use Chebishev polynomials and interval-wise constant functions in our investigation. By inserting the discretized spectrum function into Eq. (1) we get

$$\eta_k = \sum_{q=1}^{Q} B_q \, S_{kq} \quad , \qquad S_{kq} = \int_0^{\infty} \Phi_q(\tau) \exp(-\frac{t_k}{\tau}) \, d\tau \qquad (4)$$

where t_k is the time point at which the kth IP data was detected. In the terminology of inverse problem theory Eq. (4) is the (linear) forward modelling formula for calculating theoretical polarizability data which can be written in matrix form as

$$\vec{\eta} = \underline{\underline{S}} \vec{B}.$$

Introducing the deviation between the measured and calculated data

$$\vec{e} = \vec{\eta}^{\,obs} - \vec{\eta}^{\,calc} \qquad (5)$$

we can reduce the TAU-transform problem to a simple inverse problem in which the unknown expansion coefficients are determined by minimizing a certain (L_2) norm of the vector given in Eq. (5). This leads to the well-known normal equation

$$\underline{\underline{S}}^T \underline{\underline{S}} \vec{B} = \underline{\underline{S}}^T \vec{\eta}.$$

By solving this linear set of equations, we can calculate the expansion coefficients and, by means of Eq. (3), determine the time-constant spectrum function (or in other words the TAU-transform problem has been solved). Depending on the noise contained by the measured data set, it may be necessary to use a more robust inversion method or to integrate new data sets into a joint inversion algorithm [DOBRÓKA et al. 1991]. The TAU-transform algorithm can easily be formulated also in such a case.

4. Results of time-domain IP measurements using TAU-transformation

TAU-transformation was applied in a TEMPUS project [No. JEP 1553, TURAI et al. 1992] and it was also tested above seven Hungarian waste sites (Nyékládháza—1997–99; Ráckeve—1997; Kecskemét—1997; Győröcske—1999, Pásztó—2000, Tokaj—2001 and Balmazújváros—2002). One of these waste sites (Kecskemét) was an industrial waste site

and the others were communal waste sites. Here we show some results of IP data measured above a waste site first near Győröcske, second near Pásztó, and third Tokaj.

Schlumberger electrode arrays were used for IP soundings. At each IP sounding point 16 discrete current electrode spacing points were used, the array parameters were $MN = 1$ m, $AB_{min} = 3,2$ m and $AB_{max} = 100$ m, where MN was the potential electrode spacing and AB was the current electrode spacing. At each current electrode spacing point the IP apparent polarizability values were measured at 5 discrete points of decay curves ($\eta_a(t = 0.1$ s), $\eta_a(t = 0.2$ s), $\eta_a(t = 0.4$ s), $\eta_a(t = 0.8$ s), and $\eta_a(t = 1.5$ s)). At each sounding point and at each current electrode spacing point the $w(\tau_n)$ time-constant spectra were calculated using the TAU-transformation described above. (Here τ_n denotes the nth discrete value of the time-constant.)

Let us see the Győröcske area first. Taking our field experiences into account we qualify the main types of polarization mechanisms by the τ_n time-constant values [TURAI, DOBRÓKA 2001]:

filtration polarization	$\tau_n < 0.4$ s,
membrane polarization	0.2 s $< \tau_n < 0.8$ s,
electrochemical or redox polarization	0.6 s $< \tau_n < 1.2$ s,
metallic or electrode polarization	1 s $< \tau_n$.

Table I. shows the sources of polarization:

type of polarization	source of polarization
filtration polarization	— porous soil and rocks with conductive fluid,
membrane polarization	— porous soil and rocks with disperse clay and water,
electrochemical polarization	— chemical agent with high reactivity for oxidation or reduction,
metallic polarization	— metallic components in porous rocks with conductive fluid.

Table I. Sources of polarization

I. táblázat. A polarizáció forrásai

The main components of contaminating material on a waste site are connected with the main types of polarization, so we can raise the effect of higher time-constants (connected with dangerous components — chemical and metallic) of the waste site and similarly we can reduce the lower

time-constant effect (connected with non-dangerous components — water and disperse clay) using a simple weighting procedure:

$$WAV\,(\tau_n) = \tau_n w(\tau_n).$$

The *WAV* (Weighted Amplitude Value) section shows the region of the more dangerous components. *Figure 1* presents a vertical *WAV* section. In terms of time-constant spectra, our results show that the polarization on the waste site near Győröcske is mainly of electrochemical *(Fig. 1.1)* and metallic *(Fig. 1.2)* origin. Where *WAV*s are high electrochemical and metallic polarization is to be found.
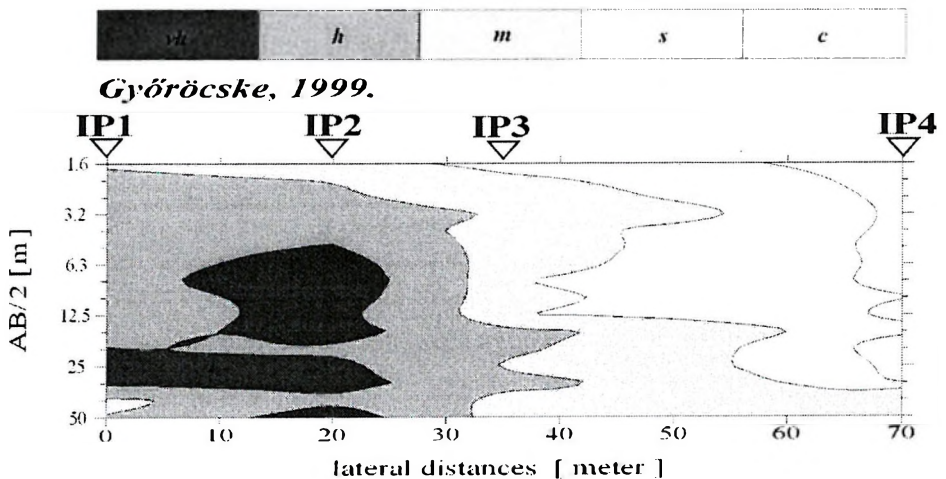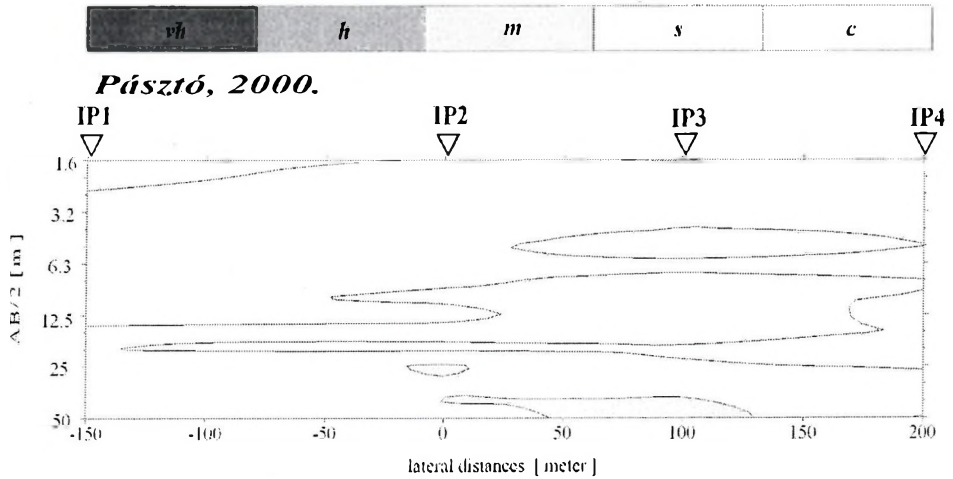

Fig. 1. Vertical *WAV* section near Győröcske. (*vh* — *WAV* is higher than 0.2; *h* — *WAV* is between 0.1 and 0.2; *m* — *WAV* is between 0.05 and 0.1; *s* — *WAV* is between 0.02 and 0.05; *c* — *WAV* is lower than 0.02.)

1. ábra. Vertikális *WAV* metszet Győröcske közelében. (*vh* — a *WAV* nagyobb, mint 0.2, *h* — a *WAV* 0.1 és 0.2 közötti, *m* — a *WAV* 0.05 és 0.1 közötti, *s* — a *WAV* 0.02 és 0.05 közötti, *c* — a *WAV* kisebb mint 0.02.)
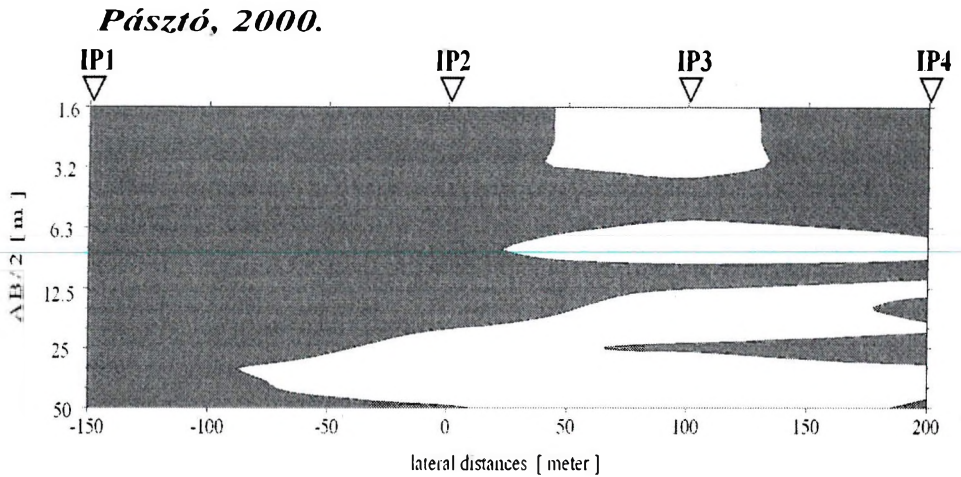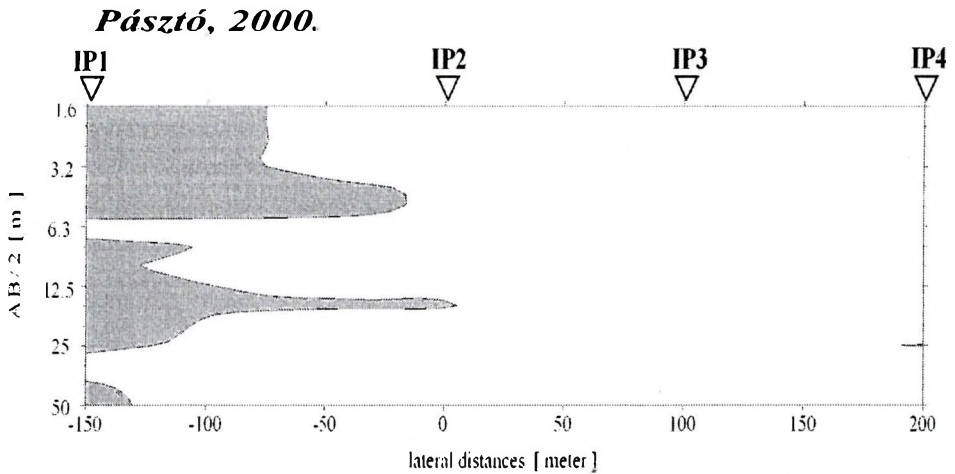
Győröcske, 1999.
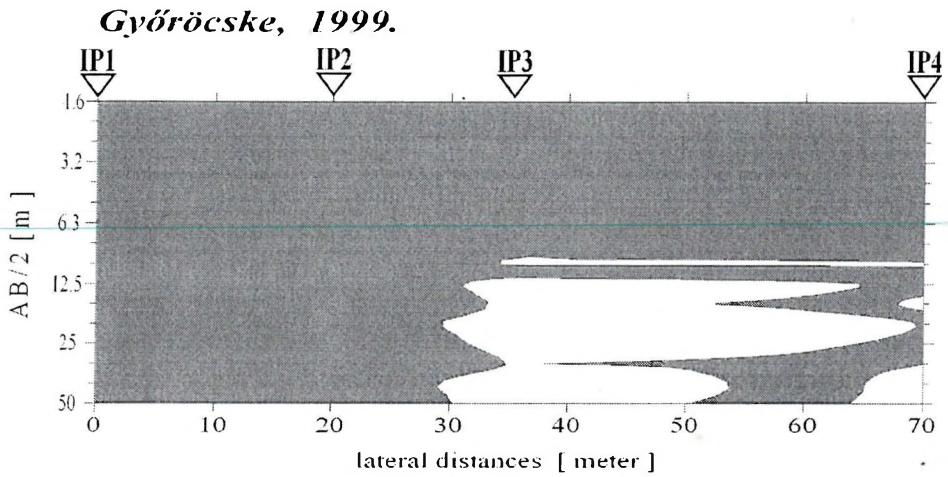
Fig. 1.1. Area of electrochemical polarization (time-constants are between 0.6 and 1.2 s)
1.1. *ábra.* Az elektrokémiai polarizáció területe (az időállandó 0.6 s és 1.2 s közötti)
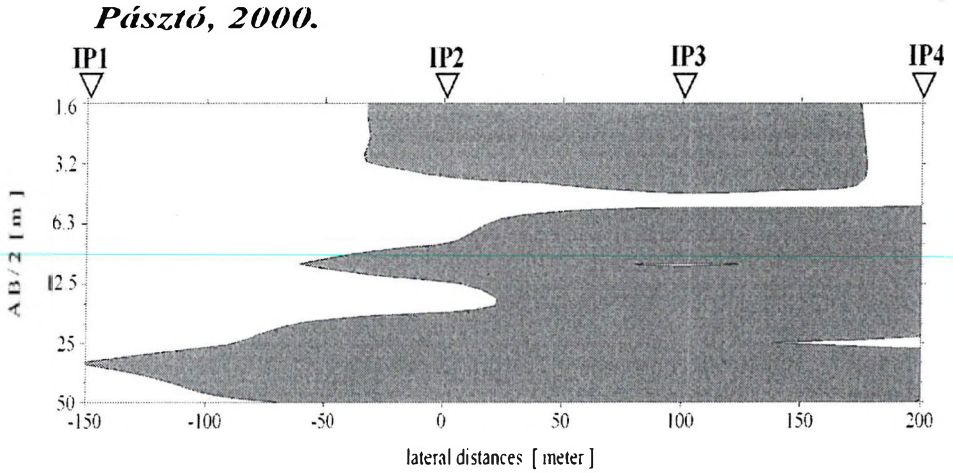
Győröcske, 1999.
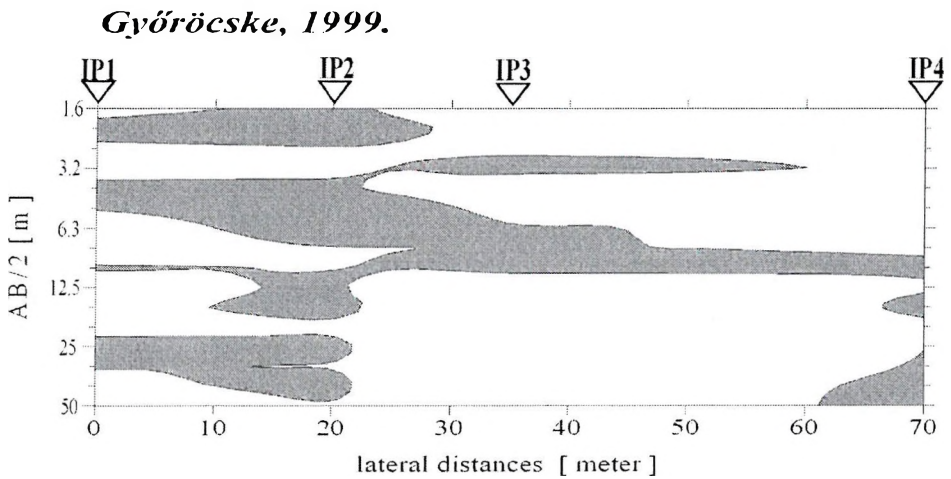
Fig. 1.2. Area of metallic polarization (time-constants are higher than 1 s)
1.2. *ábra.* A fémes polarizáció területe (az időállandó nagyobb mint 1 s)

The second waste site that was measured was near Pásztó; a *WAV* section from this site is shown in *Fig. 2.* Only small and medium *WAV*s are present near Pásztó. On analysing the type of polarization effect we found mainly membrane *(Fig. 2.1)*, electrochemical *(Fig. 2.2),* and metallic *(Fig. 2.3)* polarization. *Figure 3* presents a vertical *WAV* section over the Tokaj area. As can be seen, there are only small *WAV*s thereby indicating some dangerous regions under the surface. The polarization components are mainly electrochemical *(Fig. 3.1)* and metallic *(Fig. 3.2).*

Fig. 2. Vertical *WAV* section near Pásztó. (*vh* — *WAV* is higher than 0.2; *h* — *WAV* is between 0.1 and 0.2; *m* — *WAV* is between 0.05 and 0.1; *s* — *WAV* is between 0.02 and 0.05; *c* — *WAV* is lower than 0.02.)

2. ábra. Vertikális *WAV* metszet Pásztó közelében. (*vh* — a *WAV* nagyobb, mint 0.2; *h* — a *WAV* 0.1 és 0.2 közötti; *m* — a *WAV* 0.05 és 0.1 közötti; *s* — a *WAV* 0.02 és 0.05 közötti; *c* — a *WAV* kisebb mint 0.02.)

Pásztó, 2000.

Fig. 2.1. Area of membrane polarization (time-constants are between 0.2 and 0.8 s)
2.1. ábra. A membrán polarizáció területe (az időállandó 0.2 és 0.8 s közötti)
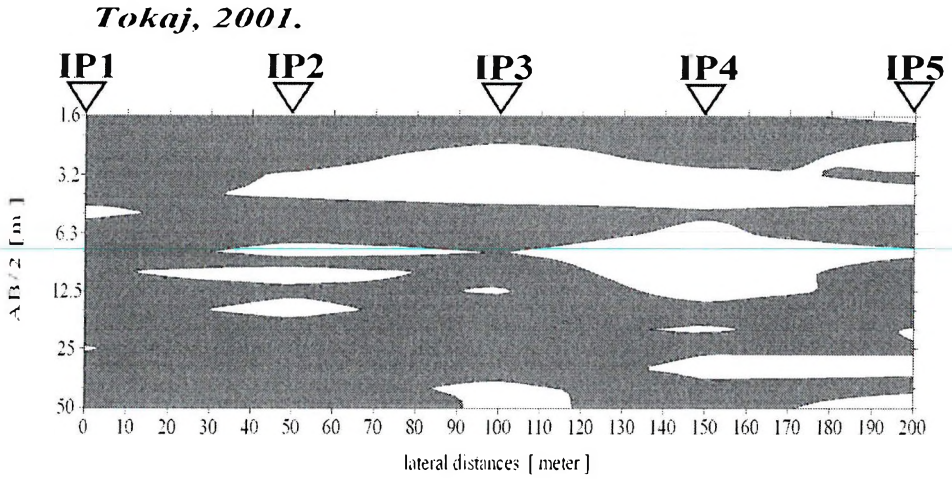
Pásztó, 2000.

Fig. 2.2. Area of electrochemical polarization (time-constants are between 0.6 and 1.2 s)
2.2. ábra. Az elektrokémiai polarizáció területe (az időállandó 0.6 és 1.2 s közötti)
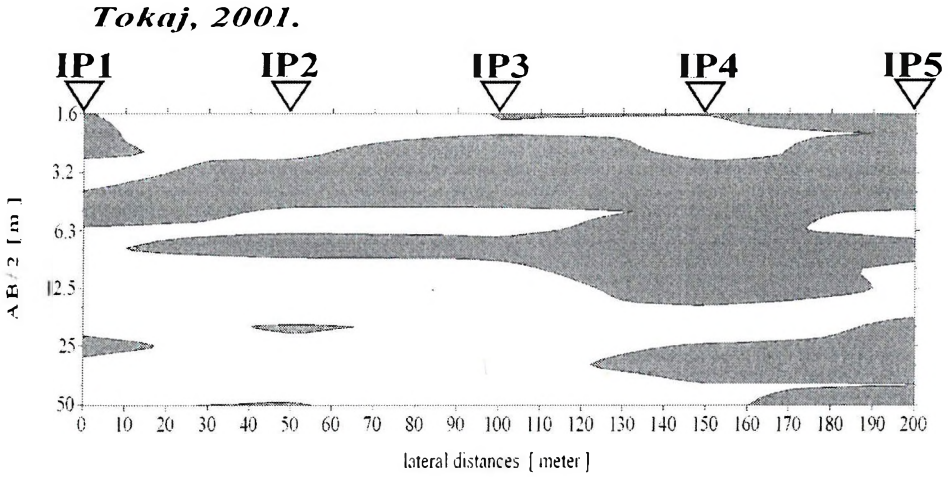
Pásztó, 2000.

Fig. 2.3. Area of metallic polarization (time-constants are higher than 1 s)

2.3. ábra. A fémes polarizáció területe (az időállandó nagyobb mint 1 s)
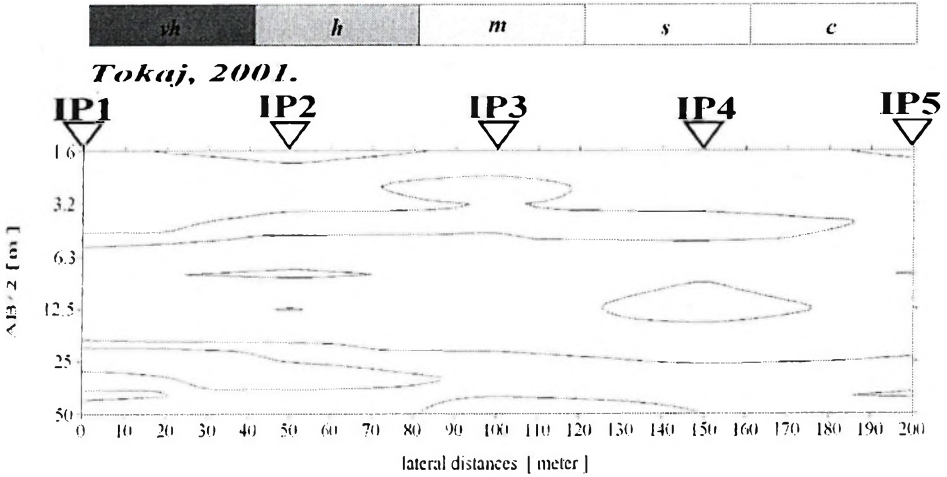
Fig. 3. Vertical *WAV* section near Tokaj. (*vh* — *WAV* is higher than 0.2; *h* — *WAV* is between 0.1 and 0.2; *m* — *WAV* is between 0.05 and 0.1; *s* — *WAV* is between 0.02 and 0.05; *c* — *WAV* is lower than 0.02)

3. ábra. Vertikális *WAV* metszet Tokaj közelében. (*vh* — a *WAV* nagyobb mint 0.2; *h* — a *WAV* 0.1 és 0.2 közötti; *m* — a *WAV* 0.05 és 0.1 közötti; *s* — a *WAV* 0.02 és 0.05 közötti; *c* — a *WAV* kisebb mint 0.02)

Tokaj, 2001.

Fig. 3.1. Area of electrochemical polarization (time-constants are between 0.6 and 1.2 s)

3.1. ábra. Az elektrokémiai polarizáció területe (az időállandó 0.6 s és 1.2 s közötti)

Tokaj, 2001.

Fig. 3.2. Area of metallic polarization (time-constants are higher than 1 s)

3.2. ábra. A fémes polarizáció területe (az időállandó nagyobb mint 1 s)

Acknowledgements

, GEOELECTRIC DATA RECORDED IN AN UNDERGROUND COAL MINE. GEOPHYSICAL PROSPECTING **39**,   PP. 643–665

KELLER G. W., FRISCHKNECHT F. C. 1966: Electrical Methods in Geophysical Prospecting. Pergamon Press, Oxford

SUMNER J. S. 1976: Principles of Induced Polarization for Geophysical Exploration. Elsevier, Amsterdam

TURAI E. 1985: TAU-Transformation of Time-Domain IP Curves. ANNALES Univ. Scien. Budapestinensis de Rolando Eötvös Nom., Sectio Geophysica et Meteorologica, Tomus I–II., pp. 182–189

TURAI E., ELSEN R., LIMBROČK K. 1992: Analysis of IP Time-Domain Data Measured above a Waste Site near Offheim using TAU-Transformation of IP Chargeability Curves, JEP 1553–92. TEMPUS project report, DMT-Bochum

TURAI E., DOBRÓKA M. 2001: A New Method for the Interpretation of Induced Polarization Data — the TAU-Transform Approach. 63rd EAGE Conference, Amsterdam, pp. 049/1–049/4

WAIT J. R. 1959: Overvoltage Research and Geophysical Applications, Pergamon Press, London

Az IP adatok feldolgozásának eredményei, a TAU-transzformáció időállandó spektrum meghatározási célú alkalmazásával

TURAI Endre

A dolgozat a TURAI [1981] által közzétett TAU-transzformációs módszer általánosítását mutatja be. A TAU transzformációs módszer és az inverziós elmélet eszközeinek ötvözésével folytonos spektrumok esetére egy olyan általános algoritmust tudunk létrehozni, amellyel az időtartománybeli Gerjesztett Polarizációs (GP) mérések polarizációs adataihoz tartozó időállandó spektrum meghatározása lehetséges lesz. A dolgozat magyarországi hulladéklerakók fölött mért terepi adatok időállandó spektrumon alapuló értelmezésének néhány eredményét mutatja be a főbb polarizálódó összetevők súlyozott időállandókkal történő jellemzésével.

ABOUT THE AUTHOR

Endre Turai received his M.Sc. (1978) in geophysical engineering from the Technical University of Heavy Industry (Miskolc). He obtained his university doctor's degree from the same university in 1984. In 1994 he was awarded his Candidate's degree (C.Sc.) by the Hungarian Academy of Sciences. He graduated as an engineer-economist at the University of Miskolc in 1993, and received his Ph.D. in Applied Earth Sciences from the same university. Currently, he is an associate professor at the University of Miskolc. His main fields of interest are geophysical data processing and interpretation, electric and electromagnetic methods, economics of geophysical explorations, and geoinformatics.

Global inversion of well log data

Péter Norbert SZABÓ[*]

A global optimization method for solving the nonlinear geophysical well-logging inverse problem is presented. At first a conventional point by point inversion method using local response equations is applied to estimate, separately, the petrophysical parameters (effective porosity, water saturation, shale and matrix contents) at different depths. In addition, I introduce the so-called interval inversion procedure, which uses all the data in a greater depth-interval in a joint inversion process. To test and compare the inversion methods synthetic and field well log data are inverted. The results show that the interval inversion algorithm is more powerful and yields more accurate petrophysical parameters than the local point by point inversion method. The former results in much more accurate and reliable parameter estimation and also gives an estimate for the layer-thicknesses as an additional item of geological information that up till now could not have been treated as an unknown in geophysical well-logging inversion.

Keywords: optimization, inverse problem, petrophysical parameters

1. Introduction

The role of geophysical well-logging is to inform us about the geometrical position and petrophysical properties of the rocks traversed in the borehole. To determine these parameters modern inversion methods can be used with the application of up-to-date informatics. The unknowns of the nonlinear inverse problem are characteristic petrophysical values, where a few parameters have a constant value in a layer, and several parameters are invariable in the zone investigated. The layer-thicknesses might also be treated as unknowns, but the conventional point by point inversion technique, which uses the well log data set separately, cannot handle this problem. Thus the layer boundary-coordinates can be determined only in a pre-inversion procedure. In practice, point by point inversion is generally used to interpret the measured data. Most point inversion procedures are based on linearized optimization methods and give a weighted least squares (LSQ) solution. If we have satisfactory a priori information about the

• University of Miskolc, Geophysics Department, H–3515 Miskolc–Egyetemváros
Manuscript received: 22 October, 2002.

petrophysical model, they work as a very quick and effective algorithm. However, being gradient methods if extensive inversion problems arise they can probably assign the solution to a local optimum of the objective function. This problem is solved by the global optimization methods that search the absolute extremes of the objective function with much higher probability than linearized optimization methods. The most preferred global optimization procedures are Simulated Annealing and Genetic Algorithms.

2. The forward problem

In formulating the forward problem let us introduce the column vector of the petrophysical model parameters at a certain depth-point as

$$\vec{m} = \{POR, SX0, SW, VSH, VSD, VLM\}^T \quad , \tag{1}$$

where POR denotes the effective porosity, $SX0$, SW denote the water saturation in the invaded and the virgin zone, VSH, VSD, VLM denote the specific volume of shale, sandstone and limestone. To determine the model parameters we utilize logs measured in the borehole that record various parameters of natural and induced physical fields as a function of depth. The following transposed vector contains the observed data of a possible combination of well logs at a certain depth

$$\vec{d}^{(obs)} = \{SP, GR, PORN, DEN, AT, RMLL, RLLD\}^T \quad , \tag{2}$$

where SP [mV] represents the spontaneous potential, GR [API] denotes the natural gamma-ray, $PORN$ [p.u. (porosity unit)] denotes the neutron porosity, DEN [gcm^{-3}] denotes the bulk density, AT [μsm^{-1}] denotes the acoustic traveltime, and $RMLL$, $RLLD$ [ohmm^{-1}] denote the micro- and deep laterolog resistivity data. The measured data reflect the immediate vicinity of the borehole. The SP, GR logs are mainly sensitive to the lithology, $PORN$, DEN, AT logs indicate the porosity, and $RMLL$, $RLLD$ data are primarily influenced by the water saturation. Since the measurement is carried out in relatively complicated borehole surroundings we need to create a petrophysical model of the formation of interest on the basis of the corrected observed data set and the available a priori information. In the next step we calculate data by means of the petrophysical parameters of the relevant model by certain petrophysical relationships. These latter are

called response functions and they connect the model parameters with the well log data used for solving the direct problem. Through the set of response functions there is a connection between the predicted model parameter vector and the calculated data vector, viz.

$$\vec{d}^{(calc)} = \vec{g}(\vec{m}, \vec{c}) \quad , \tag{3}$$

where $\vec{c}$ denotes the vector of textural constants and zone parameters. The choice of the response functions depends on the depth and the petrophysical properties of the formation investigated. (The interpreter can find many kinds of detailed empirical equations in handbooks). In forward modelling we substitute the initial (and later the estimated) values of the model parameters of Eq. (1) into Eq. (3), then the data obtained are compared with the observed data set to make a prediction for the petrophysical model by an inversion method. Obviously, the set of response equations is nonlinear with regard to the model parameters, but we can transpose the direct problem relatively quickly to other geophysical problems that have generally simple structured equations. Thus it is advantageous to solve the inverse problem by means of a global optimalization method.

3. Inversion algorithms

To solve the nonlinear geophysical well-logging inverse problem a point by point inversion method is conventionally used, which utilizes the data set of a certain depth-point to determine the petrophysical model parameters for the given point. Under the procedure we consider the adjacent depth-points to be independent from each other using local response equations to calculate the theoretical well log data. Therefore we cannot determine the layer-thicknesses by this method. The inverse problem can be solved by the minimization of the error between the observed and the calculated data having a marginally overdetermined system.

The theoretical data at the depth-point are calculated by means of a local set of response equations of Eq. (3). The calculated vector data of the jth log can be written in a general form as

$$d_j^{(calc)} = g_j(m_1, \ldots, m_M) \tag{4}$$

where M denotes the number of model parameters at the point.

Since the number of observed data is slightly more than the number of unknown model parameters at the point, the accuracy and the reliability of

the estimations are relatively limited. For Eqs. (1) and (2) there are 6 petrophysical parameters against 7 well log data, so it is worth inverting data of a greater interval jointly in one inversion procedure. The so-called interval inversion algorithm is based on the series expansion of the petrophysical parameters, which develops depth-dependent layer characteristic parameters [DOBRÓKA 1995]. With appropriate series expansion the relation in Eq. (4) modifies to a response function interpreted in a depth-interval. The synthetic data calculated from the jth log at depth z is

$$d_j^{(calc)}(z) = g_j\left(B_1^{(1)},...,B_{Q_1}^{(1)},......,B_1^{(M)},...,B_{Q_M}^{(M)},Z_1,...,Z_n,z\right), \qquad (5)$$

where B denotes the unknown discretization coefficients with Q number of discretization coefficients required for the development of any model parameter, and Z_1, ..., Z_n represent the layer boundary co-ordinates that can be chosen as unknown model parameters. By interval inversion we can determine the B coefficients in order to approximate the petrophysical model parameters in Eq. (1) along the whole observed interval.

4. Global optimization method – Simulated Annealing

Linearized inversion methods are the most used for inversion, because for an initial model that is near to the solution they are very quick and effective algorithms and are also capable of checking the quality of the estimated model parameters. But as they are not absolute minimum searching methods, they generally assign the solution to a local optimum of the objective function. This problem is solved by the Simulated Annealing (SA) method, which performs the global optimization of the objective function by random walking in the parameter space. SA was first proposed by METROPOLIS et al. [1953] to model the thermal equilibrium state of solids.

In metallurgy the removal of the effect of work-hardened solids is realized by a slow cooling process from the temperature of the liquid alloy. This process reduces progressively the kinetic energy of a large number of atoms with high thermal mobility before crystallization. Theoretically, the perfect crystal grating, which has minimal overall atomic energy is produced by an infinitely slow cooling process. This is analogous to the stabilization in the global optimum of the objective function of a geophysical inverse problem. A quicker cooling operation for that causes grating de-

fects, where the solid freezes in an imperfect grid with a higher energy state. It is similar to the stagnation of the inversion process at a local minimum of the objective function (generally known as energy function). However, atoms may escape from this higher energy state owing to a special annealing process and after that — by means of slow cooling — the optimal crystal grating can be achieved. The SA-method uses this procedure to search for the global optimum of the energy function.

The MSA-algorithm (SA based on the Metropolis algorithm) modifies the components of the relevant model parameter vector in every iteration step. The modification of the *j*th model parameter can be performed by means of

$$m_j^{(new)} = m_j^{(old)} + b$$

where *b* denotes an actual perturbation term. This small number can be varied between $[b, b_{max}]$, where b_{max} is generally decreased by

$$b_{max}^{(new)} = b_{max}^{(old)} \cdot \varepsilon$$

after a specified number of iteration steps ($0 \leq \varepsilon \leq 1$). During the random walk in the parameter space the energy function of the relevant model is calculated and compared with the previous one in every iteration step. The acceptance probability *(P)* of the new model depends on the Metropolis criterion

$$P(\Delta E, T) = \begin{cases} 1 & , \; if \; \Delta E \leq 0 \\ \exp(-\Delta E / T) & , \; if \; \Delta E > 0 \end{cases}$$

where *T* denotes a temperature which must be reduced by *T(new)*=T(*old*) / ln(*actual iteration step*) during the search to achieve the global optimum [GEMAN, GEMAN 1984]. It is clear that if the energy is lower in the new step than in the previous one, we always accept the new model. Otherwise if the energy of the new model had been increased, there would also be a probability of acceptance depending on the value of the energy needed to escape from the local minimum. If $P(\Delta E) \geq \alpha$ is fulfilled (where α is generated with uniform probability from $[0,1]$), then the new model parameters are accepted otherwise we reject them. The convergence of the inversion is largely influenced by the cooling process applied. We must avoid too rapid cooling because the solution can be frozen at a local minimum, but neither should there be too slow cooling because of unnecessarily increasing the CPU time.

4.1. Global point by point inversion

Let us define the objective function, i.e. energy function of the inverse problem. If our data are charged with Gaussian noise we can choose optimally to minimize

$$E_2 = \frac{1}{L} \sum_{i=1}^{L} \left(\frac{d_i^{(obs)} - d_i^{(calc)}}{d_i^{(obs)}} \right)^2 \rightarrow \min \tag{6}$$

which is based on the principle of the LSQ-method. The quality of inversion results are characterized separately at every depth-point by the following relative model and data distances [DOBRÓKA et al. 1991]

$$Ddata = \sqrt{\frac{1}{L} \sum_{j=1}^{L} \left(\frac{d_j^{(obs)} - d_j^{(calc)}}{d_j^{(obs)}} \right)^2} \cdot 100[\%] \tag{7}$$

$$Dmod = \sqrt{\frac{1}{M} \sum_{k=1}^{M} \left(\frac{m_k^{(est)} - m_k^{(exact)}}{m_k^{(exact)}} \right)^2} \cdot 100[\%]$$

Determination of the reliability of the estimated parameters for global optimization methods is different from the event of linearized optimization. To get useful information about the statistics of the model parameters determined it is nowadays a problem of several orders of magnitude longer computational run time. Here I did not deal with this problem, but we are working on a new technique to solve it.

4.2. Global interval inversion

The energy function of the interval inversion problem is the following for Gaussian data noise

$$E_2 = \frac{1}{DP \cdot L} \sum_{h=1}^{DP} \sum_{i=1}^{L} \left(\frac{d_{hi}^{(obs)} - d_{hi}^{(calc)}}{d_{hi}^{(obs)}} \right)^2 \rightarrow \min , \qquad (8)$$

where DP denotes the number of depth points in the processed interval. If we also have outliers in the data set it is better to choose the following norm for optimization, which is equivalent to the known Least Absolute Deviations (LAD) method

$$E_1 = \frac{1}{DP \cdot L} \sum_{h=1}^{DP} \sum_{j=1}^{L} \left| \frac{d_{hj}^{(obs)} - d_{hj}^{(calc)}}{d_{hj}^{(obs)}} \right| \rightarrow \min . \qquad (9)$$

The inverse problem is now largely overdetermined, therefore we can also determine the co-ordinates of the formation boundaries automatically by the interval inversion algorithm based on Eq. (5). The petrophysical and the geometric parameters of the formations can be obtained by optimizing Eq. (8). The quality of the inversion results is characterized in the whole depth interval processed by the following relative model and data distances

$$Ddata = \sqrt{\frac{1}{DP \cdot L} \sum_{h=1}^{DP} \sum_{j=1}^{L} \left(\frac{d_{hj}^{(obs)} - d_{hj}^{(calc)}}{d_{hj}^{(obs)}} \right)^2} \cdot 100[\%]$$

$$Dmod = \sqrt{\frac{1}{R \cdot M} \sum_{r=1}^{R} \sum_{k=1}^{M} \left(\frac{m_{kr}^{(est)} - m_{kr}^{(exact)}}{m_{kr}^{(exact)}} \right)^2} \cdot 100[\%] \qquad (10)$$

where R denotes the number of layers in the interval involved in the inversion. In the computation, a layer-wise homogeneous model is assumed.

5. Numerical results

In order to test and compare the inversion algorithms based on the Simulated Annealing method, noisy synthetic well log data were generated as quasi-measured input data. After processing them optimal petrophysical

parameters were estimated and the diagnostic values of Eqs. (7) and (10) were calculated to characterize the algorithms from the point of view of accuracy. Furthermore, measured well log data collected in a Hungarian borehole were also interpreted in order to prove that the global inversion methods can be utilized for real geological structures as well.

5.1. Generation of synthetic data sets

To invert noisy synthetic well log data a series of strata that consists of four homogeneous sedimentary layers was defined. The petrophysical parameters of the model are shown in *Table 1*, where *H* denotes the layer thickness [m], *POR* denotes the effective porosity [fraction], *SX0* denotes the water saturation in the flushed zone [fraction], *SW* denotes the water saturation in the virgin zone [fraction], *VSH* denotes the shale content [fraction], *VSD* denotes the sand content [fraction], and *VLM* denotes the limestone content [fraction].

H (m)	POR	SX0	SW	VSH	VSD	VLM
8.0	0.2	1.0	1.0	0.1	0.7	0
5.0	0	1.0	1.0	0.9	0.05	0.05
10.0	0.3	0.8	0.5	0	0.7	0
6.0	0.1	1.0	1.0	0.5	0.3	0.1

Table I. Four-layered petrophysical model
I. táblázat. Négyréteges kőzetfizikai modell

Synthetic data were calculated for this four-layered model. In *Fig. 1a, b* synthetic well logs can be seen from Eq. (2) charged with 5 per cent Gaussian noise. In addition to the 25 per cent of these data, random noise was added to simulate well logs charged with outliers. In Fig. 1a, b the curves with outliers are represented by a grey line in the same diagram.

5.2. Inversion of synthetic data sets

The petrophysical parameters estimated by point by point inversion based on the MSA method were determined by the optimization of Eq. (6) for fixed layer boundary-coordinates. At this point there were only 7 data against 6 model parameters. In *Fig. 2*, it can be seen that very different values of the model parameters were obtained in the same layer because of the narrow type of overdetermination and the noise propagated from the data space to the model space. Petrophysical parameters estimated by the
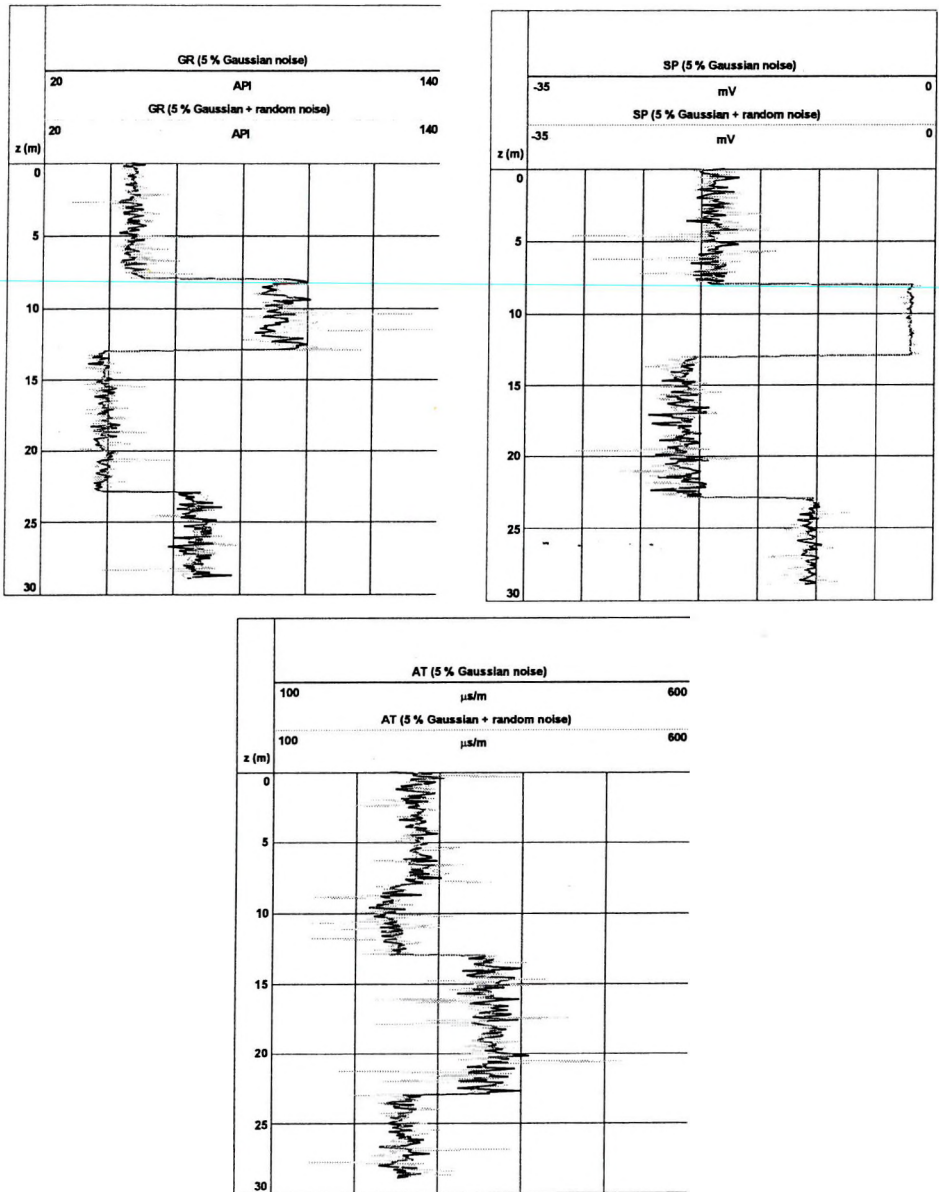
Fig. 1a. Synthetic data set charged with 5% Gaussian noise and 5% Gaussian plus random noise. GR: natural gamma ray log; AC: acoustic traveltime log; SP: spontaneous potential log

1a. ábra. 5% Gauss zajjal és 5% Gauss + véletlen zajjal terhelt szintetikus karotázs szelvények. GR: természetes gamma szelvény; AC: akusztikus terjedési idő szelvény; SP: természetes potenciál szelvény
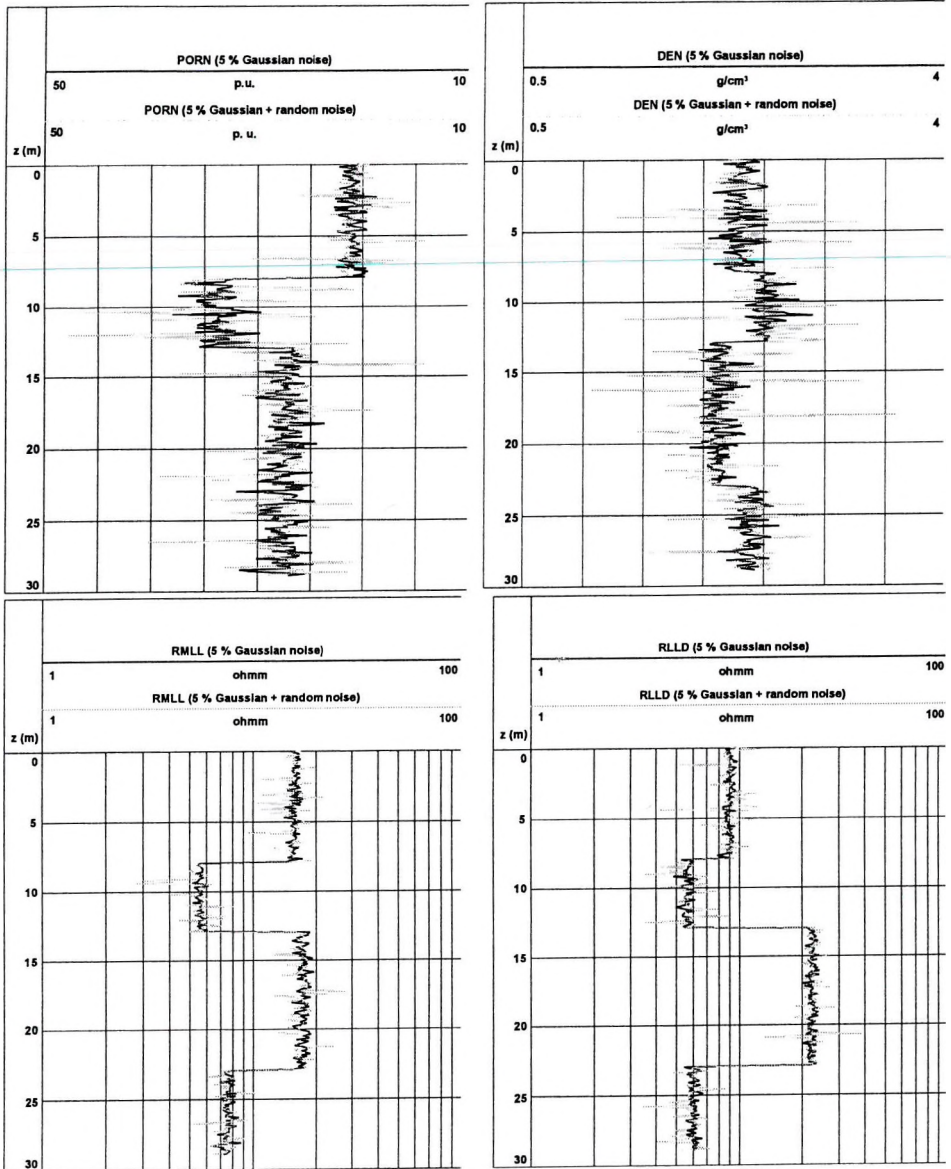
Fig. 1b. Synthetic data set charged with 5% Gaussian noise and 5% Gaussian plus random noise. PORN: neutron porosity log; DEN: density log; RMLL: microlaterolog; RLLD: deep laterolog

1b. ábra. 5% Gauss zajjal és 5% Gauss + véletlen zajjal terhelt szintetikus karotázs szelvények. PORN: neutron-porozitás szelvény; DEN: sűrűség-szelvény; RMLL: mikrolaterolog szelvény; RLLD: mélybehatolású laterolog szelvény

point by point inversion method are loaded with relatively high uncertainty, which is not a very advantageous feature concerning the estimation of the moveable hydrocarbon saturation ($SCHM=SX0-SW$) in the third bed ($SCMR=1-SX0$ means hydrocarbon saturation that cannot be produced). The relative data and parameter distances from Eq. (7) can be found in *Table II*, where 'o' means that there are outliers in the data set. The MSA-procedure always gave initial model independent and convergent solutions. In comparison with the linearized LSQ-method, which was also tested on this model (and gave 10.52 per cent for *Ddata*, and 5.69 per cent for *Dmod*), it was found that global optimization improves the accuracy of the estimated model.

Well log data (noise)	Inversion algorithm	Layer-thickness	Energy function	*Ddata* (%)	*Dmod* (%)
Synthetic (5%)	Separated	Fixed	E_2	5.65	9.65
Synthetic (5%)	Interval	Fixed	E_2	5.03	1.89
Synthetic (5% + o)	Interval	Fixed	E_2	13.41	6.62
Synthetic (5% + o)	Interval	Fixed	E_1	7.54	2.75
Synthetic (5%)	Interval	Unknowns	E_2	5.11	2.20
Measured	Separated	Fixed	E_2	4.82	—
Measured	Interval	Fixed	E_1	5.98	—
Measured	Interval	Unknowns	E_1	6.06	—

Table II. Accuracy of inversion results estimated by MSA inversion methods

II. táblázat. MSA inverziós módszerrel becsült inverizós eredmények pontossága

Besides constant layer-thicknesses the interval inversion can also be found in Table II. For the determined model there were 2030 data against 24 unknowns in the total inverted depth-interval. Thus over-determination was highly increased in comparison with point by point inversion. It can be seen in Fig. 2 that interval inversion resulted in much more accurate parameter estimation with better stability. Relative data and model distances used are formulated by Eq. (10).

With regard to interval inversion it is pointed out that there is a five times better result compared with point by point inversion, which implies a very accurate and reliable algorithm. On the other hand, the linearized LSQ
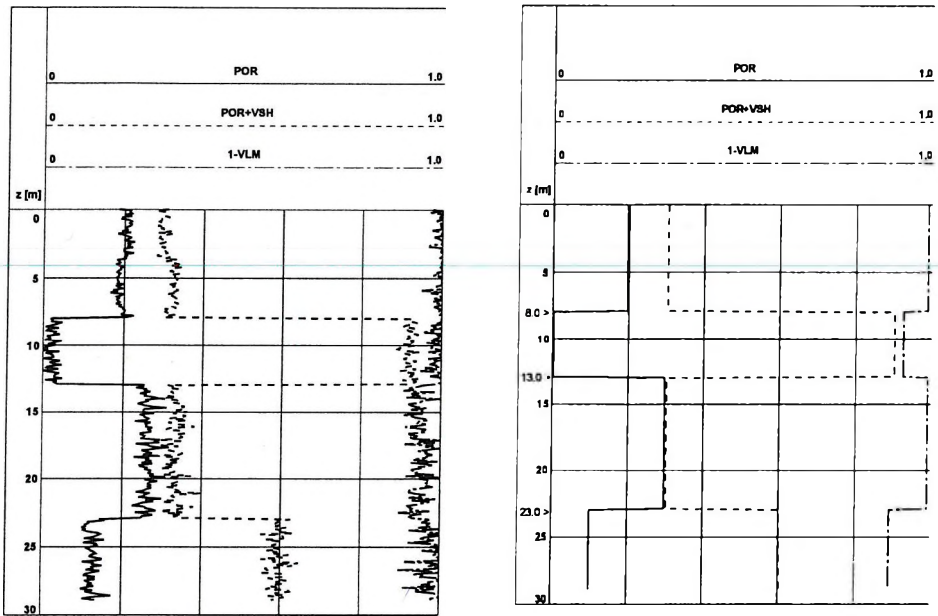
Fig. 2. Point by point and interval inversion results. On the right the estimated
layer-boundary co-ordintaes are also represented in depth scale
2. ábra. Mélységpontonkénti és intervallum inverziós eredmények. A jobb oldali ábra
mélységskáláján a becsült réteghatár-koordináták szerepelnek

interval inversion method was also tested (giving 2.27 per cent for *Dmod*)
and proved less powerful than the global interval inversion procedure.
Moreover, in practice it is possible that there are outliers in the well-log
data set. Let us analyse the interval inversion of synthetic data charged with
outliers. At first let us optimize the energy function (Eq. (8)) and then apply
Eq. (9), which is well known for its resistance against outliers. The data
distance is also defined in Eq. (9). From Table II it can be seen that there are
adequate results despite the existence of outliers. Thus it can be stated that
the MSA technique can be made resistant by way of selecting the objective
function based on Eq. (9).

Let us take layer-thicknesses into account as unknown model
parameters in the interval inversion process. In Table II, it can be seen that
the accuracy of model parameter estimation is quite as good as interval in-
version given that there are fixed layer boundary-coordinates. These re-
sults are still four times more accurate than those from point by point inver-
sion. The interval inversion procedure was stable and resulted in very

accurate parameter estimation for both the layer thicknesses and the petrophysical parameteres. It is also important to mention that the layer thicknesses as unknown model parameters converged primarily to their expected values. The exact layer-thickness values of the inversion model were achieved approximately in the 3000th iteration step, where the total number of iteration steps was 200000. They were followed by the petrophysical model parameters giving a very accurate solution of the interval inversion problem. As a consequence, the MSA interval inversion method is able to estimate more accurate hydrocarbon saturation than the linearized point by point inversion method; this feature is highly important in petrophysical practice.

6. In-situ results

To invert in-situ well log data 6 logs measured in a Hungarian borehole were chosen. Four unconsolidated sedimentary layers were investigated, where the sand bed in between was a water-bearing formation with a relatively high porosity and a little amount of shale. Supposing a simple lithology *POR, VSD, VSH* volumetric petrophysical parameters were treated as unknowns for the fixed values of *SX0* and *SW*. The input data set was composed of the corrected values of *SP, GR, DEN, RMLL, CNC* (compensated neutron), *RILD* (deep induction) well logs. The data set can be seen in *Fig. 3a, b*, and the results of point by point and interval inversion in case of unknown layer-thicknesses are given in *Fig. 4*.

For point by point inversion there were 3 unknowns against 6 data per depth point. Altogether there were data from 195 points. In the case of interval inversion we had to determine 12 volumetric petrophysical parameters and a further 3 boundary-coordinates of the formations. Table II shows that the fitting in data space is satisfactory and the tendency is analogous with that of the inversion of synthetic data. From the point of view of forward modelling more accurate parameters can be obtained by choosing more appropriate response functions and textural constants. Interval inversion can be developed by making a more suitable series expansion, which better describes the vertical changes of the petrophysical parameters in the computed interval. Lastly, the interval inversion method has a considerable advantage over point by point inversion as it determines automatically the layer-thicknesses. The layer boundary-coordinates were

obtained at 8.1, 13.5 and 16.5 meters (the depth-coordinates were transformed as the top of the first layer could be at zero level) as can be seen in Fig. 4.

7. Conclusions

It was shown that the global inversion of well log data based on the MSA method results in a correct solution that is independent of the initial model. However, it is important to emphasize that the convergence of the global optimization process is largely influenced by the setting of control parameters of the Simulated Annealing algorithm (e.g. initial temperature, cooling process) and choosing a proper fitting function to minimize.

A disadvantage is that MSA requires more computer time than linearized optimization methods.

It was shown that it is more advantageous to use the interval inversion method by determining the layer-thicknesses than point by point inversion. It utilizes more information from the observed data and can be improved by
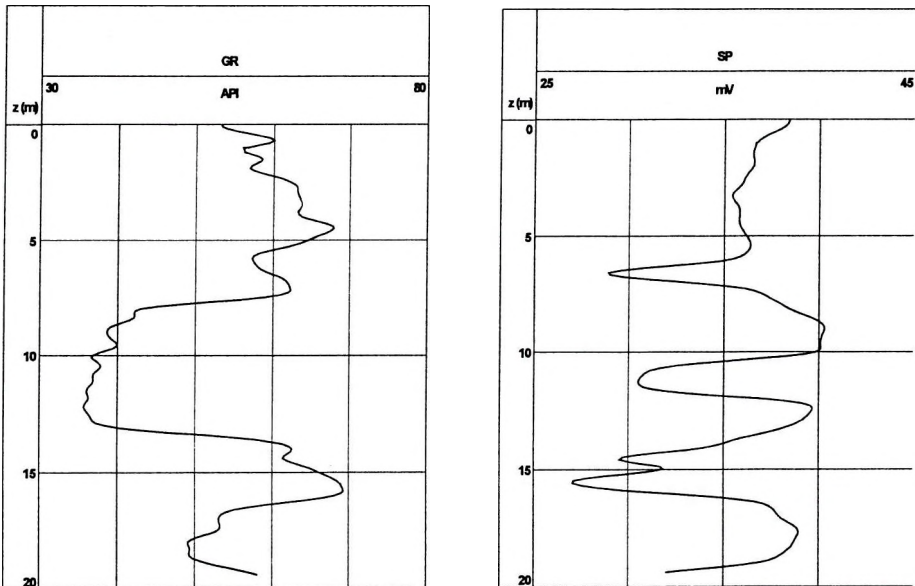
Fig. 3a. Measured well log data inverted. GR: natural gamma ray log;
SP: spontaneous potential log

3a. ábra. Terepi mérési szelvények. GR: természetes gamma szelvény, SP: természetes
potenciál szelvény
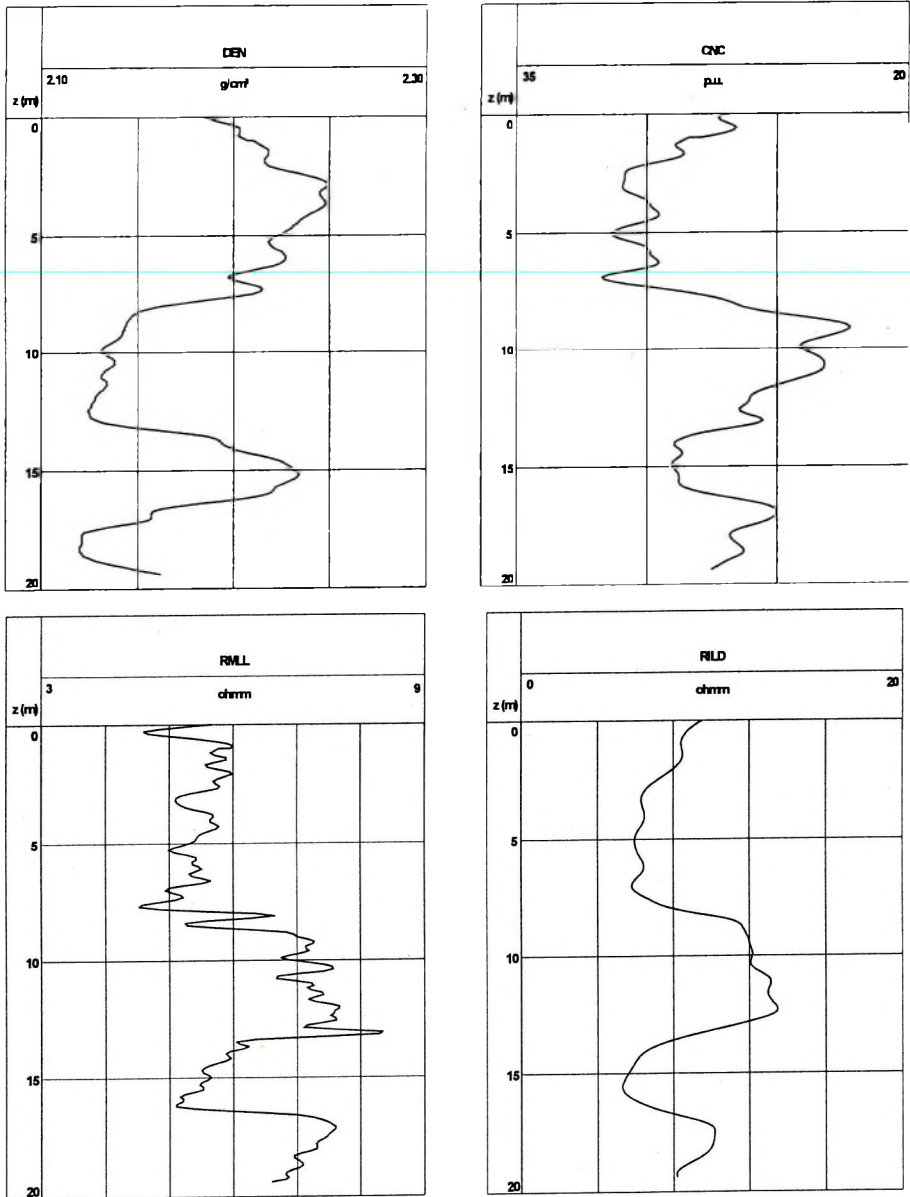
Fig. 3b. Measured well log data inverted. DEN: density log; CNC: compensated neutron porosity log; RMLL: microlaterolog; RILD: deep induction log

3b. ábra. Terepi mérési szelvények. DEN: sűrűség szelvény; CNC: kompenzált neutron-porozitás szelvény; RMLL: mikrolaterolog; RILD: mélybehatolású indukciós szelvény
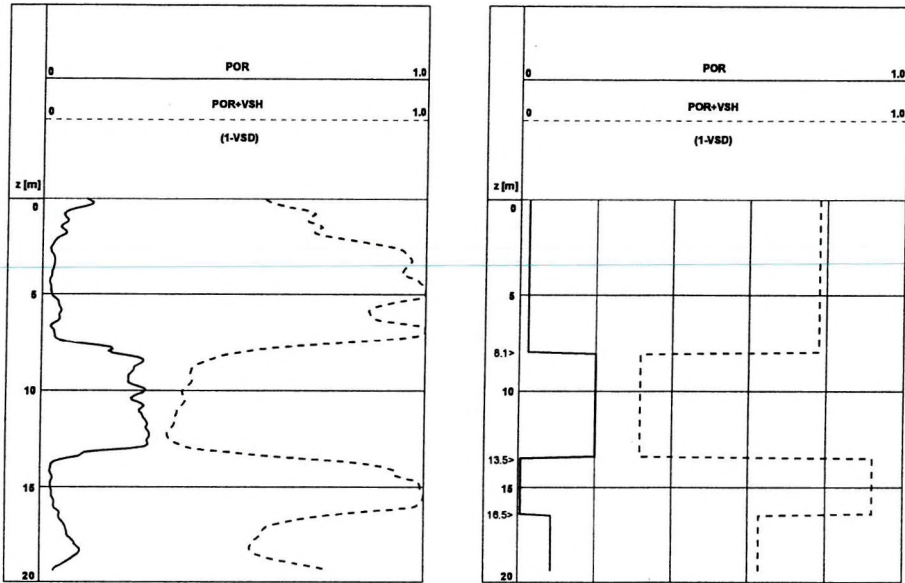
Fig. 4. MSA point by point and interval inversion results

4. ábra. MSA mélységpontonkénti és intervallum inverzió eredmények

choosing more suitable basis functions in the series expansion of petrophysical model parameters. The vertical changes of porosity, saturation, shale and matrix volumes can be derived in one inversion procedure by appropriate series expansion. Moreover the interval inversion procedure is able to give an estimate for the layer thicknesses. Thus it offers much greater promise in terms of yielding more geological information about the geological structure investigated in the borehole.

REFERENCES

DOBRÓKA M., GYULAI Á., ORMOS T., CSÓKÁS J., DRESEN L. 1991: Joint inversion of seismic and geoelectric data recorded in an underground coal mine. Geophysical Prospecting **39**, pp. 643–665

DOBRÓKA M. 1995: Introduction of joint inversion algorithms to the geophysical well logging interpretation. Study, Univ. of Miskolc

DOBRÓKA M., SZABÓ P. N. 2001: The inversion of well log data using Simulated Annealing method. Geosciences, Publications of the University of Miskolc, Series A, Mining **59**, pp. 115–137

GEMAN S., GEMAN D. 1984: Stochastic relaxation, Gibbs distributions, and the Bayesian restoration of images. EEE Trans. Pattern analysis and Machine Intelligence, **6**, 6

METROPOLIS N. 1953: Equation of state calculations by fast computing machines. J. Chem. Phys. **21**, pp. 1087–7092

Mélyfúrási geofizikai adatok globális inverziója

SZABÓ Péter Norbert

A nemlineáris mélyfúrási geofizikai inverz probléma megoldására globális optimalizációs módszert mutatunk be. Először lokális válaszegyenleteken alapuló hagyományos mélységpontonkénti (szeparált) inverzióval becsüljük meg a pontbeli kőzetfizikai paraméterek (effektív porozitás, víztelítettség, agyagtartalom, kőzetmátrix fajlagos térfogat) értékeit. Ezután bevezetjük az ún. intervallum inverziós eljárást, mely egy nagyobb mélységintervallum adatrendszerét egyetlen együttes inverziós eljárásban értékeli ki. Az inverziós algoritmusok tesztelése és összehasonlítása céljából szintetikus és terepi adatrendszereket invertálunk. Az inverziós eredmények rámutatnak arra, hogy az intervallum inverzió hatékonysága és a becsült petrofizikai paraméterek pontossága nagyobb, mint lokális pontonkénti inverzió esetén. Az intervallum inverziós módszer igen stabil és megbízható paraméterbecslés tekintetében, és képes meghatározni a rétegvastagságokat, melyek eddig nem szerepeltek ismeretlenként a hagyományos mélyfúrási geofizikai inverzió problémakörében.

ABOUT THE AUTHOR

Péter Norbert Szabó was born in Miskolc in 1976 and attended the Avasi Secondary Grammar School in Miskolc from 1990–1994. He graduated as a geophysical engineer from the University of Miskolc in 1999 after which he participated in the Ph.D. education program on geophysics in the Faculty of Earth Science and Engineering at the University of Miskolc and was awarded his Ph.D. in 2002. He was offered a post as an assistant lecturer in Miskolc University's Department of Geophysics where he has been since January 2003. He is interested in borehole geophysics and geophysical inversion. Since 2002 he has been closely involved in the work of the Association of Hungarian Geophysicists as a member of the Juvenile Delegation. He has taken part in many meetings and conferences both at home and abroad.

Copyright